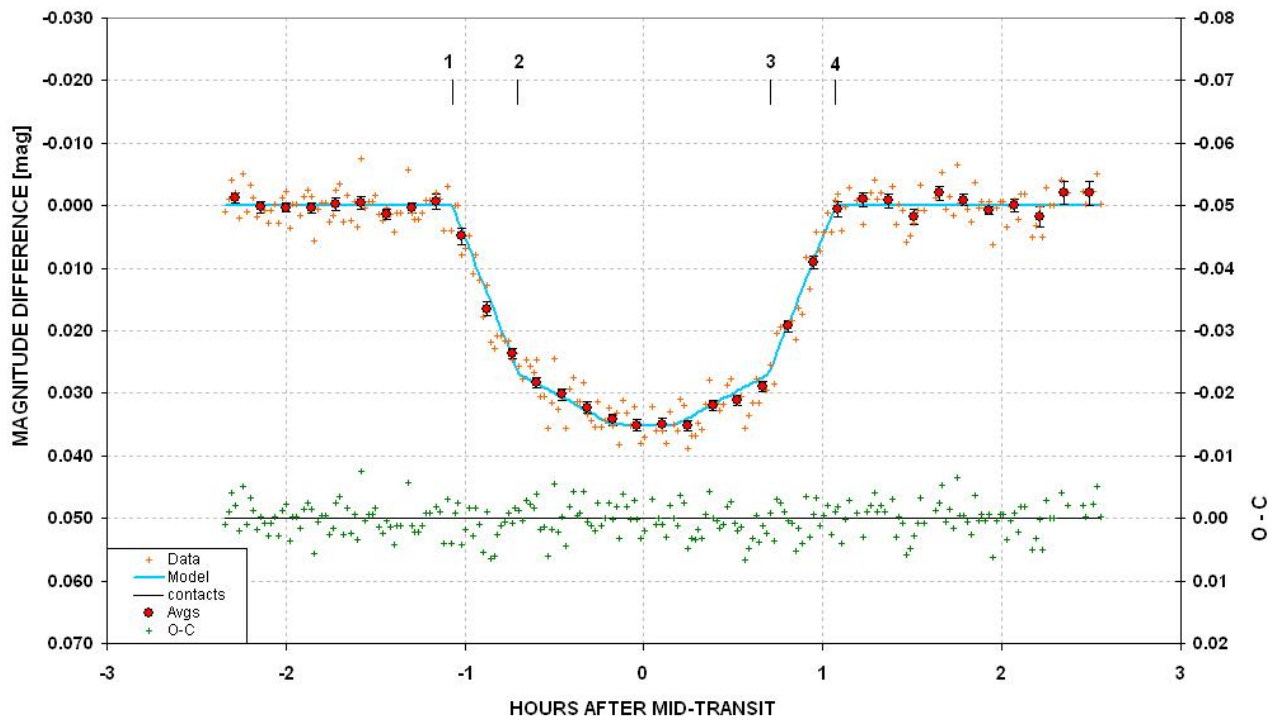
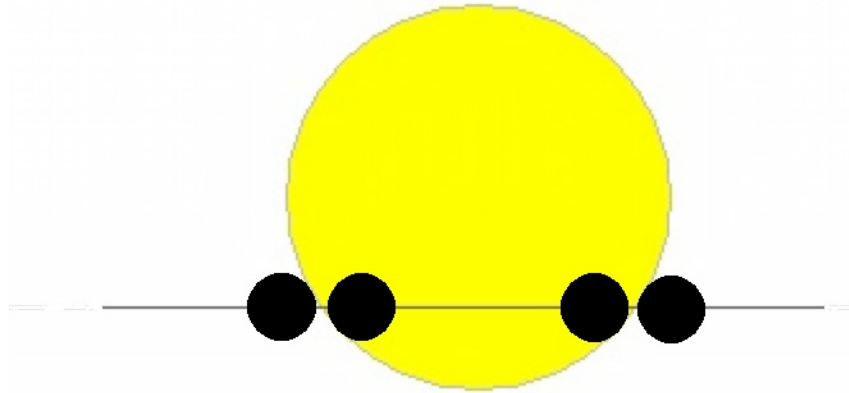


EXOPLANET OBSERVING FOR AMATEURS

Second Edition (plus)



Bruce L. Gary

Books by Bruce L. Gary

ESSAYS FROM ANOTHER PARADIGM, 1992, 1993 (Abridged Edition)

GENETIC ENSLAVEMENT:

A CALL TO ARMS FOR INDIVIDUAL LIBERATION, 2004, 2006, 2008

THE MAKING OF A MISANTHROPE: BOOK 1, AN AUTOBIOGRAPHY, 2005

A MISANTHROPE'S HOLIDAY: VIGNETTES AND STORIES, 2007

EXOPLANET OBSERVING FOR AMATEURS (First Edition), 2007

QUOTES FOR MISANTHROPES: MOCKING HOMO HYPOCRITUS, 2007

EXOPLANET OBSERVING FOR AMATEURS

THIRD EDITION

Bruce L. Gary

Reductionist Publications, d/b/a
5320 E. Calle Manzana
Hereford, AZ 85615

Bruce L. Gary
5320 E. Calle Manzana
Hereford, AZ 85615; SA
axa@brucegary.net

Cover Illustration: WASP-10 light curve, 2008 November 14, by the author, using a 14-inch Meade LX200 telescope and an SBIG ST-8XE CCD, unfiltered. The sketch is a scale-accurate depiction of exoplanet WASP-10b transiting in front of its parent star, WASP-10a.

Copyright 2010 by Bruce L. Gary

All rights reserved except for brief passages quoted in a review. No part of this book may be reproduced, stored in a retrieval system, or transmitted in any form and by any means: electronic, mechanical, photocopying, recording or otherwise without express prior permission from the publisher. Requests for usage permission or additional information should be addressed to:

“Bruce L. Gary” <axa@brucegary.net>

or

Reductionist Publications, d/b/a
5320 E. Calle Manzana
Hereford, AZ 85615

Second Edition (plus): 2010 October 22 (typo and other corrections)

Second Edition: 2009 November 10

First edition: 2007 August

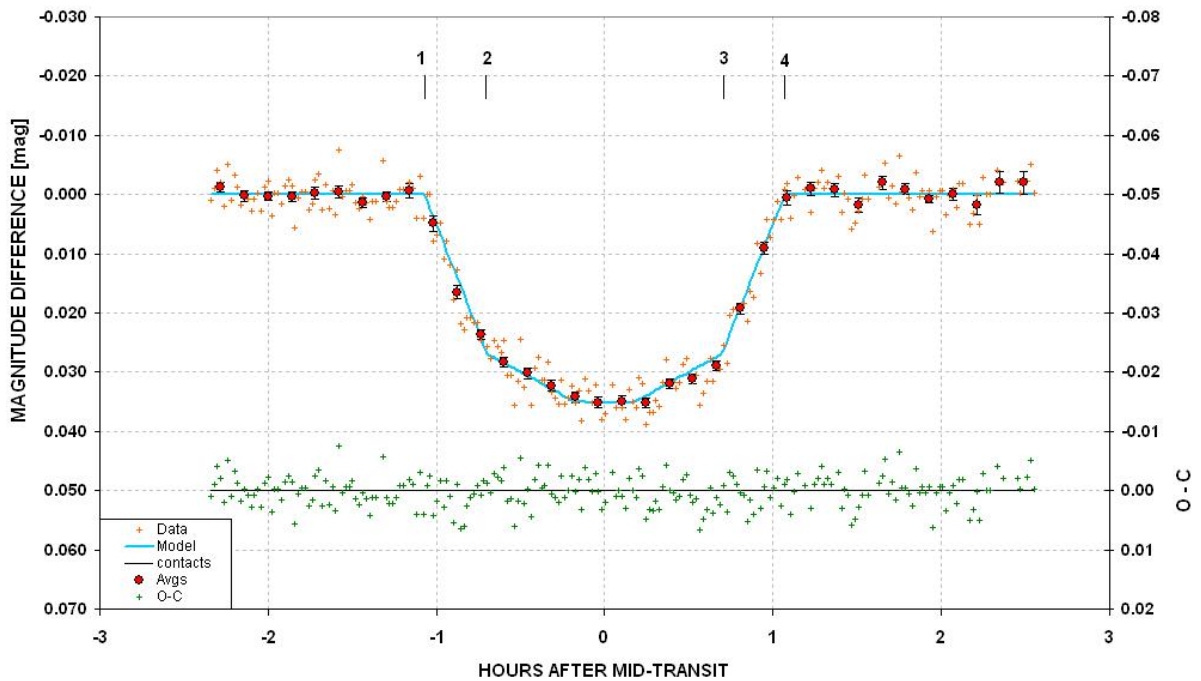
Printed by Mira Digital Publishing, St. Louis, MO

ISBN 978-0-9798446-3-8

Dedicated to the memory of

Carl Sagan

A giant among men, who would have loved the excitement of exoplanet discoveries, which
would have further inspired him to speculate about
life in the universe.



Author’s amateur exoplanet light curve of WASP-10 made November 14, 2008 with a 14-inch Meade LX200 telescope and no filter. Exoplanet WASP-10b moves in front of the star during contact 1 to 2, is obscuring $\sim 3.6\%$ of the star’s disk between contacts 2 and 3, and is moving off the star during contacts 3 to 4. The smooth variation between contact 2 and 3 is produced by stellar “limb darkening.” The lower plot is the differences between individual measurements (one per image) and a simple model, showing that systematic variations are too small to notice, implying that the model fit is an adequate representation of the measurements for the purpose of inferring mid-transit time, transit length and transit shape. WASP-10 is similar in brightness ($V\text{-mag} = 12.7$) to other exoplanet stars ($V\text{-mag} = 11.2$) and is slightly redder than most ($B-V \sim 1.1$ versus 0.63).

CONTENTS

Preface to Second Edition	1
Preface to First Edition	3
Introduction	7
1 Could I Do That?	10
2 Observatory Tour	17
3 Exoplanet Projects	23
4 BTE List	28
5 Planning the Night	33
6 Atmosphere Tutorial	40
7 Filter Choice	48
8 Flat Fields	56
9 Dark Frames	64
10 Exposure Times and Defocusing	65
11 Focus Drift	71
12 Autoguiding	76
13 Photometry Aperture Size	78
14 Photometry Pitfalls	83
15 Image Processing	86
16 Three Photometry Methods Previewed	91
17 Spreadsheet Processing - Comp/Chk and Ensemble	96
18 Spreadsheet Processing - Artificial Star	106
19 Star Colors	117
20 Stochastic SE Budget	126

21 Exoplanet Stars are Not Variable Stars	137
22 Archiving Amateur Data and Searching for Anomalies	144
23 The Optimum Observatory	149
24 The Joy of Exoplanet Observing	152
Appendix A – Flat Field Evaluation	155
Appendix B – Selecting Target from Candidate List	163
Appendix C – Air Mass from JD	166
Appendix D - Planet Size Model	167
Appendix E – Measuring CCD Linearity	188
Appendix F – Measuring CCD Gain	198
Appendix G – Plotting Light Curve Data	200
Appendix H – Comparing Filters	202
Appendix I – Transit Model and Fitting Procedure	213
Appendix J – Amateur Spectroscopy	220
Abbreviations	221
Glossary	225
Astronomy Hardware Company Contact Info	234
Acknowledgements	237
References	238
Index	240

PREFACE

To Second Edition

Two years ago I wrote the First Edition of this book. At that time there were 15 Bright Transiting Exoplanets, BTEs; now there are 46. At the same time that I published the First Edition I began a web-based archive for amateur observations submitted to me, called the Amateur Exoplanet Archive, AXA. After the first year the AXA contained 178 amateur-submitted light curves; today it has 666. A lot has happened in the last two years.

Even though I'm using the same hardware and software now, my image processing and data analysis of image readings is considerably improved. This has been another surprise to me after I began writing the Second Edition. Most of the advice I offered in the First Edition is still basically valid, but it is not optimum. Several changes in observing strategy and data analysis are presented in this edition. For example, I used to recommend an R-band filter; now I recommend observing with a "clear with blue-blocking" filter (i.e., CBB-band). Even a clear filter (or no filter) is usually better than using an R-band filter, assuming your telescope aperture isn't greater than about 16 inches. Another example, something that never occurred to me until other amateurs reported good results with it, is the strategy of "defocusing" when observing bright stars (e.g., V-mag < 10). I have seen the benefits of defocusing, to the point of producing donut shapes, for such stars.

Occasionally an AAVSO observer wanting to observe exoplanet transits would ask why there weren't any "comp stars" in the finder charts on the AXA web page devoted to each exoplanet. Since I made the transition from AAVSO observing to exoplanets a few years ago I understood the question, so I devote a chapter to explaining why having "comp" stars, with calibrated magnitudes, are not relevant for exoplanet observing.

This Second Edition also describes the "big picture" for archiving amateur exoplanet data for use by professionals. A year ago I began collaboration with Caltech to transfer AXA data files and their transit fit solutions to Caltech's IPAC computer for inclusion in the NStED archive (IPAC = Infrared Processing and Analysis Center; NStED = NASA/IPAC/NEExSci Star and Exoplanet Database). This is where the professionals go to see what's available in the public domain about their favorite exoplanet system. Having amateur data at the same site, and in the same data download format, is an important step in bridging the professional/amateur divide in a way that benefits both groups. In the past year the Czech Astronomical Society has created an archive for amateur data submissions, called the Exoplanet Transit Database, ETD. My two year old AXA has become so "successful" that I can't keep up with data submissions if I continued to update plots of transit properties (such as mid-transit time versus date, transit length versus date, etc). I have therefore discontinued routine updates of the plots, which has given me free time for observing, and I look forward to the ETD taking over AXA's role. These new developments are described in the Second Edition.

Another change in this edition is a slightly larger page size. This means figures can be wider and therefore presented in higher quality. An expensive improvement is the use of a color printer for all pages; this means it's not necessary to search through a central insert section to see what a figure looks like in color, which was necessary in the First Edition.

PREFACE – Second Edition

The activity level of amateurs in observing exoplanets has grown pretty much as I expected two years ago. The AXA, for example, has 48 regular contributors. Interestingly, only six of these are in the United States; 41 are in Europe. None are in California or Arizona, which are two very active places for AAVSO observing. Exoplanets seem to have a greater appeal in Europe, which still puzzles me. However, I predict that amateurs in California, Arizona and other USA states, plus the Chinese, Indians, Japanese, will join the ranks of avid amateur observers of exoplanet transits in due time.

The First Edition was printed and sold at cost until I ran out of copies. A PDF-document version of the book was available at a web site for free downloads. During the first two months approximately 2000 downloads were logged. This high number of downloads still puzzles me, since there aren't that many amateurs observing exoplanets. The free PDF of the First Edition will remain available, at http://brucegary.net/book_EOA/x.htm. This Second Edition was for exclusive sale by Adirondack Astronomy until that company went out of business (summer of 2010). A few copies of the Second Edition are for sale by Starizona, one of the finest astronomy stores in America (starizona.com/acb/). A free PDF download of the Second Edition (Plus) is available at brucegary.net/book_EOA/x.htm.

PREFACE

To First Edition (Updated)

The search for planets orbiting other stars is interesting to even my daughters and neighbors. Why the public fascination with this subject? I think it's related to the desire to find out if we humans are "alone in the universe." This would explain the heightened interest in exoplanet searchers to find **Earth-like** planets. NASA and the NSF are keenly aware of this, and they are currently formulating a "vision" for future funding that is aimed at Earth-like exoplanet discoveries.



The author's favorite telescope, a Meade RCX400 14-inch on an equatorial wedge.

The public's interest in planets beyond our solar system may also account for *Sky and Telescope* magazine's interest in publishing an article about the XO Project, a professional/amateur collaboration that found a transiting exoplanet XO-1 (since then four more discoveries have been announced by this project). The above picture, from the *Sky and Telescope* article (September, 2006), helps make the point that amateur telescopes are capable of providing follow-up observations of candidates provided by professionals using wide-field survey cameras. The XO Project is a model for future professional/amateur collaborations.

PREFACE – First Edition

Astronomers, ironically, have traditionally tried to remain aloof from things that excited the general public. I recall conversations in the Jet Propulsion Laboratory cafeteria in the 1970s where I defended Carl Sagan’s right to communicate his enthusiastic love for astronomy to the public. There was a “pecking order” in astronomy at that time, which may still exist to some extent, in which the farther out your field of study the higher your status. Thus, cosmologists garnered the highest regard, and those who studied objects in our solar system had the lowest status. My studies were of the moon, which was about as low a status as possible. Some would say that at that time there was only one level lower than mine: those who speculated about other worlds and the possibilities for intelligent life on them.

How things change! We now know that planets are everywhere in the galaxy. Billions upon billions of planets must exist! This is the message from the tally of ~ 400 extra-solar planetary systems (as of mid-2009). Among them are 60 exoplanets that transit in front of their star (46 that are brighter than 14th magnitude), and the number is growing with a doubling time of 1.1 years.

It is important to realize that bright **transiting** exoplanets are far more valuable than faint exoplanets, or any of the non-transiting ones! The bright transits allow for an accurate measure of the planet’s size, and therefore density; and spectroscopic investigations of atmospheric composition are also possible. Studies have even been made of transiting exoplanet atmospheric temperature fields.

Part of the explosion of known transiting exoplanets can be attributed to the role played by amateur astronomers. Five of the 45 bright transiting exoplanets were discovered by the XO Project, which includes a team of amateurs. During the past few decades, when professional observatories have become more sophisticated and plentiful, amateur observatories have also become more capable - due to the introduction of affordable CCD cameras suitable for astronomical use, better telescopes and sophisticated computer programs for controlling hardware and processing images. We amateurs have therefore continued to make useful contributions. The discovery of exoplanets is one of the most fruitful examples!

Not only are amateurs capable of helping in the discovery of exoplanets through collaborations with professionals, but amateurs are well-positioned to contribute to the discovery of **Earth-like** exoplanets and their moons! This is explained in Chapter 22.

How can this be? After all, the professionals have expensive observatories at mountain tops, and they use very sophisticated and sensitive CCD cameras. But with this sophistication comes expensive operation on a “per minute” basis! With telescope time so expensive, these highly capable facilities can’t be used for lengthy searches. Moreover, big telescopes have such a small field-of-view (FOV) that there usually aren’t any nearby bright stars within an image for use as a “reference.” I will argue that the optimum size telescope for most ground-based exoplanet studies has an aperture between 25 and 50 inches, as explained in Chapter 23. Although few amateurs can afford telescopes in this optimum size range, telescopes with 8 to 14 inch apertures are capable of producing scientifically useful observations for most of the known bright transiting exoplanets. Thousands of these telescopes are in use by amateurs today.

This book is meant for amateurs who want to observe exoplanet transits, and who may eventually want to participate in exoplanet discoveries. There are many ways for amateurs to have fun with exoplanets; some are “educational,” some could contribute to a better understanding of exoplanets,

PREFACE – First Edition

and others are aimed at new discoveries. The various options for exoplanet observing are explained in Chapter 3.

The advanced amateur may eventually be recruited to become a member of a professional/amateur team that endeavors to discover exoplanets. This might be the ultimate goal for some readers of this book. Let's review how this works. A professional astronomer's wide-field survey camera, consisting of a regular telephoto camera lens attached to an astronomer's CDD, monitors a set of star fields for several months before moving on to another set of star fields. When a star appears to fade by a small amount for a short time (e.g., <0.030 magnitude for ~ 3 hours), and when these fading events occur at regular intervals (~ 3 days, typically), a larger aperture telescope with good spatial resolution must be used to determine if the brightest star in the survey camera's image faded a small amount or a nearby fainter star faded by a large amount (e.g., an eclipsing binary). Amateur telescopes are capable of making this distinction since they can quickly determine which star fades at the predicted times and how much it fades. As a bonus the amateur observations can usually characterize the shape of the fading event, whether it is flat-bottomed or V-shaped. If the star that fades has a depth of less than ~ 30 milli-magnitudes (mmag), and if the shape of the fade is flat-bottomed, there is a good chance that a transiting exoplanet has been identified. Armed with this information the professionals are justified in requesting observing time on a large telescope to measure radial velocity on several dates, and thereby determine the mass of the secondary. If the mass is small it must be an exoplanet.

As more wide-field survey cameras are deployed by the professionals in a search for transiting candidates there will be a growing need for amateur participation to weed out the troublesome "blended eclipsing binaries." This will allow the professionals to focus on only the good exoplanet candidates for big telescope spectroscopic radial velocity measurements.

The role amateurs can play in this exploding field is exciting, but this role will require that the amateur learn how to produce high-quality transit light curves. A background in variable star observing would be helpful, but the exoplanet requirements are more stringent, because the variations are so much smaller, that a new set of observing skills will have to be mastered by those making the transition. Image analysis skills will also differ from the variable star experience. This book explains the new and more rigorous observing and image analysis skills needed for partnering with professionals in exoplanet studies.

The reader is entitled to know who I am, and my credentials for writing such a book. I retired from 34 years employment by Caltech and assigned to work at the Jet Propulsion Laboratory (JPL) for studies in three fields: planetary radio astronomy, microwave remote sensing of the terrestrial atmosphere, and airborne sensing of the atmosphere for studies of stratospheric ozone depletion. I have about 62 peer-reviewed publications in various fields, and four patents on aviation safety using microwave remote sensing concepts and an instrument that I developed. I retired in 1998, and a year later resumed a childhood hobby of optical astronomy. I was one of the first amateurs to observe an exoplanet transit (HD209458, in 2002).

I have been a member of the XO Project's extended team (ET) of amateur observers from its inception in 2004. The XO Project was created by Dr. Peter McCullough, a former amateur, but now a professional astronomer at the Space Telescope Science Institute, STScI. The XO project has announced the discovery of five exoplanets, XO-1b, XO-2b, XO-3b, XO-4b and XO-5b. All members of the XO team are co-authors of the announcement publications in the *Astrophysical Journal*. I have

PREFACE – First Edition

worked with fellow ET members for 4.5 years, and I am familiar with the issues that amateurs face when changing from variable star observing to exoplanet transit observing. The XO Project is currently the only professional/amateur collaboration for exoplanet discovery. It is my belief that it will soon become generally recognized that the XO Project model for involving amateurs is a cost-effective and very productive way to achieve results in the discovery and study of exoplanets.

I want to thank Dr. Steve Howell (National Optical Astronomy Observatory, Tucson, AZ) for writing an article for *The Planetary Society* (Howell, 2002) after the discovery of HD209458b, the first transiting exoplanet to be discovered (Charbonneau, 1999). In Howell's article he explained how accessible exoplanet transit observing is for amateurs, and this led to my first successful observation of an exoplanet transit.

I also want to thank Dr. Peter McCullough for inviting me to join the XO ET in December, 2004. ET membership grew from the original four in 2005 and 2006 to a current list of seven (names of the original ET are in bold): **Ron Bissinger**, Mike Fleenor, Cindy Foote, Enrique Garcia-Melendo, **Paul Howell**, Joao Gregorio and **Tonny Vanmunster** (I resigned in 2009). Thank you all, for this wonderful learning experience and the fun of being part of a high-achieving team.

INTRODUCTION

This book is intended for use by **amateur** astronomers, not the professionals. The distinction is not related to the fact that professional astronomers understand everything in this book; it's related to the fact that the professionals don't **need** to know most of what's in this book.

Professionals don't need to know how to deal with telescopes with an imperfect polar alignment (because their telescopes are essentially perfectly aligned). They don't have to deal with telescopes that don't track perfectly (because their tracking gears are close to perfect). They don't have to worry about focus changing during an observing session (because their "tubes" are made of low thermal expansion materials). They don't have to worry about CCDs with significant "dark current" thermal noise (because their CCDs are cooled with liquid nitrogen). Professionals don't have to worry about large scintillation noise (because it's much smaller with large apertures). Professionals can usually count on sharp images the entire night with insignificant changes in "atmospheric seeing" (because their observatories are at high altitude sites and the telescope apertures are situated well above ground level). Professionals also don't have to deal with large atmospheric extinction effects (again, because their observatories are at high altitude sites).

If a professional astronomer had to use amateur hardware, at an amateur site, they would have to learn new ways to overcome the limitations that amateurs deal with every night. There are so many handicaps unique to the amateur observatory that we should not look to the professional astronomer for help on these matters. Therefore, amateurs should look for help from each other for solutions to these problems. In other words, don't expect a book on amateur observing tips to be written by a professional astronomer; only another amateur can write such a book.

I've written this book with experience as both a professional astronomer and a post-retirement amateur. Only the first decade of my professional life was in astronomy, as a radio astronomer. The following three decades were in the atmospheric sciences, consisting of remote sensing using microwave radiometers. Although there are differences between radio astronomy and optical astronomy, and bigger differences between atmospheric remote sensing with microwave radiometers and optical astronomy, they share two very important requirements: 1) the need to optimize observing strategy based on an understanding of hardware strengths and weaknesses, and 2) the need to deal with stochastic noise and systematic errors during data analysis.

This book was written for the amateur who may not have the background and observing experience that I brought to the hobby 10 years ago. How can a reader know if they're ready for this book? Here's a short litmus test question: do you know the meaning of "differential photometry"? If so, and if you've done it, then you're ready for this book.

Lessons Learned

One of the benefits of experience is that there will be many mistakes and "lessons learned," and these can lead to a philosophy for the way of doing things. One of my favorite philosophies is: **KNOW THY HARDWARE!** It takes time to learn the idiosyncrasies of an observing system, and no

INTRODUCTION

observing system works like it might be described in a text book. There usually are a myriad of little things that can ruin the best planned observing session. Only through experience with one particular observing system can these pitfalls be avoided. I therefore encourage the serious observer to plan on a long period of floundering before serious observing can begin. For example, during the floundering phase try different configurations: prime focus, Cassegrain, use of a focal reducer, placement of focal reducer, use of an image stabilizer, etc. During this learning phase try different ways of dealing with finding focus, tracking focus drift, auto-guiding, pointing calibration, etc. Keep a good observing log for checking back to see what worked.

One of my neighbors has a 32-inch telescope in an automated dome, and it's a really neat facility. But as he knows, I prefer to use my little 11-inch telescope for the simple reason that I understand most of the idiosyncrasies of my system, whereas I assume there are many idiosyncrasies of his system that I don't understand.

At a professional observatory the responsibility for "know thy hardware" is distributed among many people. Their staff will include a mechanical engineer, an electrical engineer, a software control programmer, an optician to perform periodic optical alignment, someone to perform pointing calibrations and update coefficients in the control software, a telescope operator, a handy man for maintaining utilities and ground-keeping and a director to oversee the work of all these specialists. Therefore, when an astronomer arrives for an observing session, or when he submits the specifics of an observing request for which he will not be present, all facets of "know thy hardware" have already been satisfied.

In contrast, the amateur observer has to fill all of the above job responsibilities. He is the observatory "director," he does mechanical and electrical calibration and maintenance, he's in charge of programming, pointing calibration, scheduling and he's the telescope operator – and the amateur is also his own "funding agency." Thus, when the amateur starts an observing session he has removed his mechanical engineer hat, his programmer's hat, and all the other hats he wore while preparing the telescope system for observing, and he becomes the telescope operator carrying out the observing request of the astronomer whose hat he wore before the observing session began. The admonition to "know thy hardware" can be met in different ways, as illustrated by the professional astronomer many-man team and the amateur astronomer one-man team.

I once observed with the Palomar 200-inch telescope, and believe me when I say that it's more fun observing with my backyard 11-inch telescope. At Palomar I handed the telescope operator a list of target coordinates, motion rates and start times, and watched him do the observing. I had to take it on faith that the telescope was operating properly. With my backyard telescope I feel "in control" of all aspects of the observing session; I know exactly how the telescope will perform and I feel comfortable that my observing strategy is a good match to the telescope system's strengths and weaknesses. Based on this experience I will allege that **amateur observing is more fun!**

Another of my philosophies is: GOOD DATA ANALYSIS IS JUST AS IMPORTANT AS GETTING GOOD DATA. It is customary in astronomy, as well as many observing fields, to spend far more time processing data than taking it. A single observing session may warrant weeks of analysis. This is especially true when using an expensive observing facility, but the concept also can apply to observations with amateur hardware.

INTRODUCTION

One last Philosophy I'll mention is: WHEN YOU SEE SOMETHING YOU DON'T UNDERSTAND, WHILE OBSERVING OR DURING DATA ANALYSIS: STOP, DON'T PROCEED UNTIL YOU UNDERSTAND IT. This one is probably difficult to making a convincing case for unless you've ignored the advice and wasted time with fundamentally flawed data or analysis procedure. This advice is especially true if you're writing a computer program to process data, because program bugs are a part of every programming experience. A corollary to this advice might be: Never believe anything you come up with, even if it makes sense, because when there's a serious flaw in your data or analysis it may show itself as a subtle anomaly that could easily be ignored.

These are some of the themes that will be a recurring admonition throughout this book. Some readers will find that I'm asking them to put too much work into the process. My advice may seem more appropriate for someone with a professional dedication to doing things the right way. If this is your response to what I've written, then maybe you're not ready yet for exoplanet transit observing. Remember, if it's not fun, you probably won't do a good job. If you don't enjoy floundering with a telescope and trying to figure out its idiosyncrasies, then you probably won't do a good job of learning how to use your telescope properly. This hobby should be fun, and if a particular project seems like work, then consider a different project! Astronomy is one of those hobbies with many ways to have fun, and I dedicate this book to those advanced amateurs who like having fun with a challenging task like exoplanet transit observing.

Chapter 1

”Could I do that?”

“Could I do that?” was my reaction 7 years ago to an article claiming that amateurs could observe exoplanet transits (Howell, 2002).

The article stated that transits of HD209458 had even been measured with a 4-inch aperture telescope. Could this be true, or was it hype for selling magazines? The article appeared in The Planetary Society’s *The Planetary Report*, which is a reputable magazine. I had a Meade 10-inch LX200 telescope and a common CCD camera which I had just begun to use for variable star observing.

“Why not?” I decided, with nothing to lose for trying.

My First Transit Observation in 2002

Before the next transit on the schedule I e-mailed the author of the article, Dr. Steve Howell, and asked if he had any advice. He suggested using a filter, such as V-band (green), and “keep the target near the center of the image.”

On the night of August 11, 2002, I spent about 9 hours taking images of HD209458 with a V-band filter. The next day I processed the images and was pleasantly surprised to see a small “dip” in my plot of brightness versus time that occurred “on schedule” (Fig. 1.01). The depth was also about right, but since my observations were “noisy” they were really a “detection” instead of a measurement. Nevertheless, it felt good to join a club of about a half-dozen amateurs who had detected an exoplanet transit.

By today’s standards my CCD was unimpressive (slow downloads, small chip size) and my telescope was average. The only thing advanced was my use of MaxIm DL (version 3.0) for image processing. Even my spreadsheet was primitive (Quattro Pro 4.0). Today there must be 1000 amateurs with better hardware than I had 7 years ago, based on membership numbers of the AAVSO (American Association for Variable Star Observers).

I recall thinking “If only there was a book on how to observe exoplanet transits.” But there couldn’t be such a book since the first amateur observation of HD209458 had been made 2 years earlier by a group in Finland led by Arto Oksanen (http://www.ursa.fi/sirius/HD209458/HD209458_eng.html). Besides, this was the only known transiting exoplanet at that time. Moreover, not many amateurs had a 16-inch telescope like the one used by Oksanen’s team. The idea of amateurs observing an exoplanet transit was a “novelty.” But that was then, and this is now!

I’ve figured out how to observe exoplanet transits since those early days. To see what a difference that makes look at the next figure.

CHAPTER 1 – COULD I DO THAT?

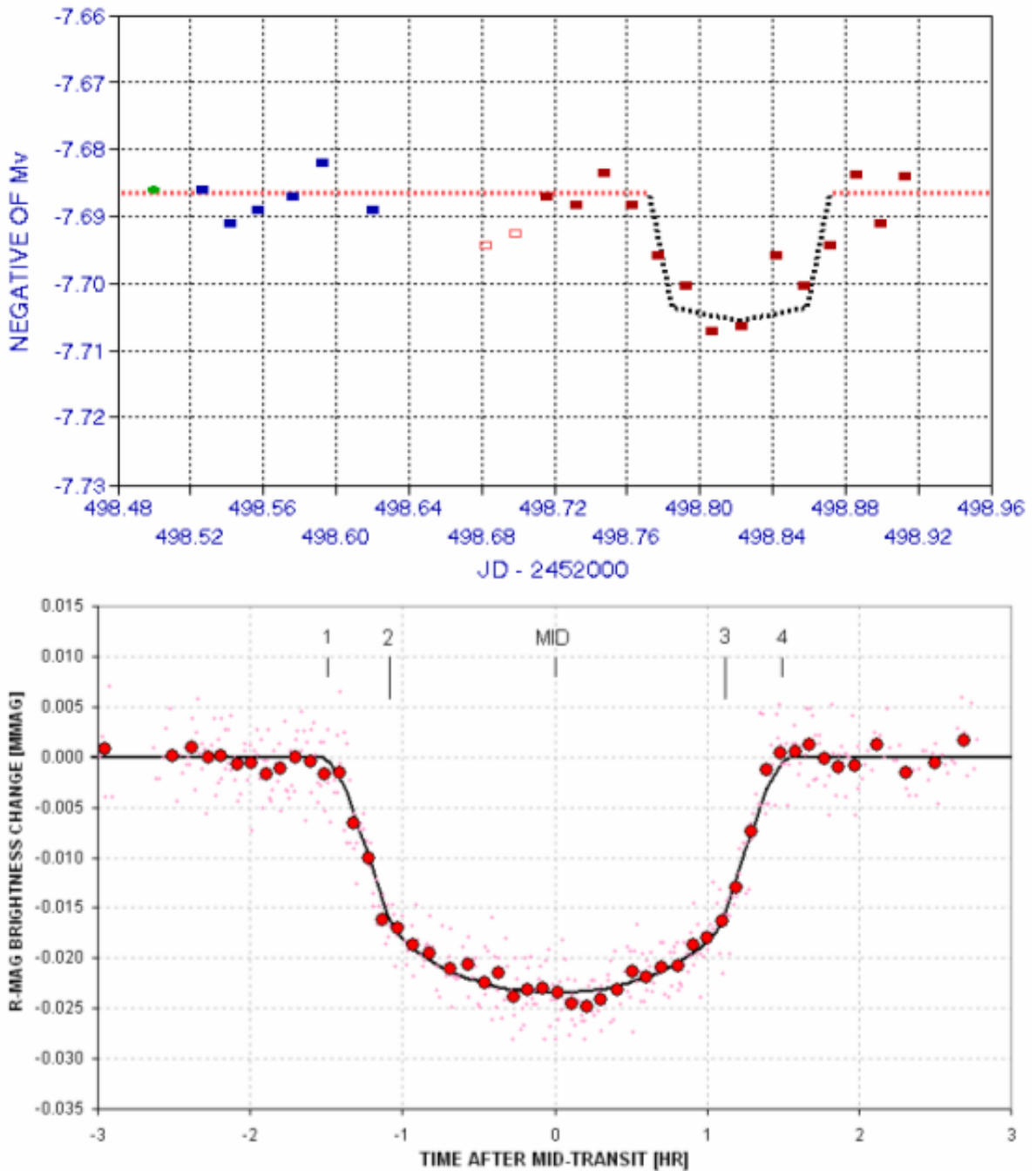


Figure 1.01. *Knowing what to do makes a difference. Upper panel: my first light curve of HD209458, made 2002 August 12. Lower panel: a recent light curve of XO-1 made in 2006 (average of March 14 and June 1 transits).*

During the past 7 years my capability has improved more than 10-fold, and most of this is due to improved technique. Although I now use 14- and 11-inch telescopes, if I were to use the same 10-inch that I used 7 years ago for my first exoplanet transit I could achieve in one minute what took me

CHAPTER 1 – COULD I DO THAT?

15 minutes to do back then. Some of this improvement is due to use of a slightly improved CCD, and some is from use of a tip/tilt image stabilizer, but most of the improvement is due to improved techniques for observing, image processing and spreadsheet analysis. These are things that can be shared with other amateurs in a book. That's the book I wanted 7 years ago. You are now holding such a book. It is based on 7 years of floundering and learning. It can save you from lots of time with "trial and error" observing and processing ideas, and give you a 15-fold advantage that I never had for my first exoplanet transit observation.

Minimum Requirements for Exoplanet Transit Observing

You don't have to live on a mountain top to observe exoplanet transits. My 2002 transit observation was made from my backyard in Santa Barbara, CA, located only 200 feet above sea level. Dark skies are also not even a requirement; my Santa Barbara residence was within the city, and my skies didn't even resemble "dark" until after midnight. For pretty picture imaging, where dark skies matter more, I disassembled my telescope and put it in my car trunk for a drive to the nearby mountains. I now live in Arizona, but my darker skies are only a bonus, not a requirement.

What about "seeing"? Good atmospheric seeing is nice, but again it's not a requirement. I actually had more moments of good seeing in Santa Barbara than here in Arizona, at a 4660 foot altitude site. In fact, some of the sharpest images of planets come from Florida and Singapore, both sea level sites. Seeing is mostly influenced by winds at ground level, and the height of the telescope above ground. My median seeing in Arizona is ~3.0 "arc for typical exposure times (30 to 60 seconds).

Telescope aperture matters, yes, but an 8-inch aperture is adequate for the brighter transiting exoplanets (10th magnitude). For most transiting exoplanets a 12-inch aperture is adequate. Since the cost/performance ratio increases dramatically for apertures above 14 inches, there are a lot of 14-inch telescopes in amateur hands. I've never owned anything larger, and everything in this book can be done with this size telescope. My present telescope is an 11-inch Celestron CPC 1100 (My 14-inch Meade LX200 GPS has been "in repair" for most of the past year). You'll need an "equatorial wedge" for equatorial mounting; alt-az mounts are unsuitable for exoplanet observing (as explained later).

CCD cameras are so cost-effective these days that almost any astronomical CCD camera now in use should be adequate for exoplanet observing. If you have an old 8-bit CCD, that's a real handicap. You should upgrade to a 16-bit camera. For a bigger field-of-view, consider spending a little more for a medium-sized chip CCD camera. My CCD is a Santa Barbara Instrument Group (SBIG) ST-8. You may want to buy a color filter wheel for the CCD camera, but that's certainly not a requirement. In fact, I sometimes observe unfiltered to maximize signal-to-noise. Large aperture telescopes are in the best position to benefit from the use of a filter.

Autoguiding is essential for achieving quality exoplanet transit light curves. I used to recommend use of a tip/tilt image stabilizer, such as SBIG's AO-7, because as a bonus it provided fast adjustments that made better use of good "seeing" conditions. However, I now autoguide using the standard method of adjusting the telescope drive motors.

Software! Yes, software is a requirement and your choice can be important. I've been using MaxIm DL/CCD for 8 years, and it's an impressive program that does everything! MDL, as I'll refer to it, controls the telescope, the telescope's focuser, the CCD, the color filter wheel, the image stabilizer if

CHAPTER 1 – COULD I DO THAT?

you have one, and a dome if you have one of them. It also does an excellent job of image processing, and after it performs a photometry analysis you may use it to create a text file for import to a spreadsheet. Other exoplanet observers use AIP4WIN, and it also does a good job. CCDSoft might do the job, but I find it lacking in user-friendliness and capability. Many European amateurs use FotoDif for photometric analysis of image sets.

Spreadsheets are an important program you'll probably want to use. Every computer with a Windows operating system comes with Excel, and even though Excel seems constructed to meet the needs of an executive who wants to make a pie chart showing sales, it also is a powerful spreadsheet for science. I've moved all my spreadsheet work to Excel. That's what I assume you'll be using in Chapter 16-18.

Previous Experience

Whenever an amateur astronomer considers doing something new it is natural to ask if previous experience is adequate, especially if there is no local astronomy club with experienced members who can help out with difficult issues. Some people prefer to learn without help, and I'm one of them. The astronomy clubs I've belonged to emphasized the eyepiece "Wow!" version of amateur astronomy, so help on serious matters was never available locally. This will probably be the case for most amateurs considering exoplanet observing. Being self-taught means you spend a lot of time floundering! Well, I like floundering! I think that's the best way to learn. Anyone reading these pages who also likes to flounder should consider setting this book aside, with the intention of referring to it only when floundering fails. For those who don't like floundering, then read on.

The best kind of amateur astronomy experience that prepares you for producing exoplanet light curves is variable star observing using a CCD. "Pretty pictures" experience will help a little, since it involves dark frame and flat frame calibration. But variable star observing requires familiarity with "photometry," and that's where previous experience is most helpful.

One kind of photometry of variable stars consists of taking an image of stars that are known to vary on month or longer time scales, and submitting measurements of their magnitude to an archive, such as the one maintained by the AAVSO. Another kind of variable star observing, which requires more skill, is monitoring variations of a star that changes brightness on time scales of a few minutes. For example, "cataclysmic variables" are binaries in which one member has an accretion disk formed by infalling gas from its companion. The stellar gas does not flow continuously from one star to the other, but episodes of activity may occur once a decade, approximately. An active period for gas exchange may last a week or two, during which time the star is ~100 times brighter than normal. The cataclysmic variable rotates with a period of about 90 minutes, so during a week or more of heightened activity the bright spot on the accretion disk receiving gas from its companion will rotate in and out of view, causing brightness to undergo large "superhump" variations every rotation (90 minutes). The amplitude of these 90-minute variations is of order 0.2 magnitude. Structure is present that requires a temporal resolution of a couple minutes.

Any amateur who has observed cataclysmic variable superhumps will have sufficient experience for making an easy transition to exoplanet observing. Amateurs who have experience with the other kind of observing, measuring the brightness of a few stars a few times a month, for example, will be able to make the transition to exoplanet observing, but it will require learning new skills. Someone who

CHAPTER 1 – COULD I DO THAT?

has never performed photometry of any stars may want to consider deferring exoplanet observing until they have some of the more traditional photometry experience.

I'll make one exception to the above required experience level description. Anyone with work experience making measurements and performing data analysis, regardless of the field, is likely to have already acquired the skills needed for exoplanet monitoring, even if they have never used a telescope. For example, before retiring I spent two decades making measurements and processing data as part of investigations within the atmospheric sciences. I think that experience alone would have been sufficient background for the astronomy hobby that I started 10 years ago. I'll agree that my amateur astronomy experience when I was in high school (using film!) was helpful. And I'll also agree that my decade of radio astronomy experience 4 decades ago was also helpful, but the differences between radio astronomy and optical astronomy are considerable. For anyone who has never used a telescope, yet has experience with measurements and data analysis, I am willing to suggest that this is adequate for "jumping in" and starting exoplanet observing without paying your dues to the AAVSO conducting variable star observations! The concepts are straightforward for anyone with a background in the physical sciences.

What are the "entry costs" for someone who doesn't own a telescope but who has experience with measurements and data analysis in other fields? Here's an example of what I would recommend as a "starter telescope system" for such a person:

- \$3000 Celestron 11-inch telescope (CPC 1100)
- \$2000 monochrome 16-bit CCD
- \$ 450 equatorial wedge for polar mounting
- \$ 450 MaxIm DL/CCD

Total cost about \$6000

Meade telescopes are another option, but they have a way of needing frequent repairs. The Meade brand has something unique in its favor, however, and that's their commitment to fork mounts for apertures as large as 14 inches. The largest fork-mounted Celestron Schmidt-Cassegrain (currently sold) is the 11-inch CPC. The smaller aperture telescopes in the CPC series have a smaller "visual back" hole (1.5 versus 2 inch diameter), but they can still be used for exoplanet observing with normal optical back-end optics (e.g., no AO-7). Celestron sells a 14-inch Schmidt-Cassegrain telescope, but it's on a German equatorial mount (GEM). It's possible to use a GEM for exoplanet observing, but the meridian flips invariably produce shifts in the exoplanet light curve, and this can be annoying. I recommend Celestron's CPC 1100 (11-inch aperture) model for exoplanet observing.

There's a cheaper option if you'll be satisfied with observing only the brightest few transiting exoplanets, those brighter than 10th magnitude, for example (of which there are 9 known, as of this writing). For them you may use a digital single-lens reflex (DSLR) camera with a telephoto lens mounted piggy-back to any equatorially-mounted telescope with a sidereal drive. For example, Gregor Srdoc, of Croatia, produced a transit light curve of 10.7 V-magnitude XO-4 using a 64-mm (2.5-inch) aperture telephoto lens and a 12-bit DSLR camera. Most amateur astronomers already have hardware similar to this, so why not give this set-up a try? Another bright BTE option is to use an astronomical grade CCD (12- to 16-bit depth) with an ordinary camera lens, piggy-backed to an equatorially-mounted telescope with a sidereal drive. Such a system is more expensive than the DSLR

CHAPTER 1 – COULD I DO THAT?

option because astronomical-grade CCD cameras are more expensive than DSLR cameras. Here's an example of what can be achieved using such a system.

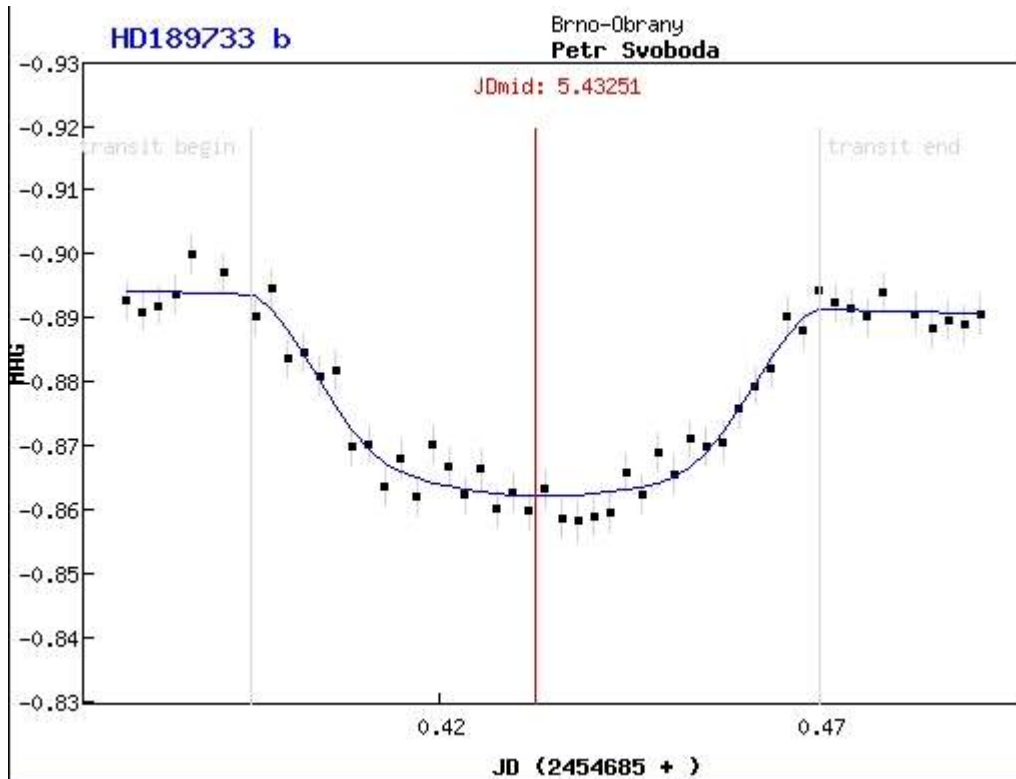


Figure 1.02. Light curve of a 7.7 magnitude exoplanet transit using a 34-mm (1.33-inch) camera lens and SBIG ST-7 CCD, by Czech Republic amateur Petr Svoboda.

The cheapest way to achieve a large aperture telescope is to buy a Dobsonian. For example, it's possible to buy a new 16-inch Dobsonian for under \$2000. So what's wrong with these telescopes for exoplanet observing? They're all mounted to an alt-az platform, and during an observing session the star field will rotate with respect to a CCD pixel field. The problem with this is that the target star, and all reference stars, will move through a field of pixels with slightly different flat field corrections. No flat field is good enough to assure that systematic errors will be removed during the flat-field calibration to a level required for exoplanet light curves, where flat field error variations of ~ 0.005 magnitude can be disastrous! Image "derotators" can be used to keep the star field more-or-less fixed with respect to the CCD pixel field, but then it's necessary to make flat fields for the entire range of image rotation settings that will occur during an observing session, and this can be laborious. I haven't seen any amateurs who have succeeded in using a Dobsonian telescope system for exoplanet transit observing. The professionals have managed to observe exoplanet transits using large alt-az telescopes, on occasion, so it is possible; but until its feasibility has been demonstrated using amateur hardware and software I advise against trying it with a Dobsonian telescope.

It has been estimated that tens of thousands of astronomical CCD cameras have been sold during the past two decades, and most of these were sold to amateur astronomers. The number of telescopes bought by amateurs is even higher. Many of these amateur systems are capable of observing

CHAPTER 1 – COULD I DO THAT?

exoplanet transits. Amateur astronomy may not be the cheapest hobby, but there are many hobbies even more expensive. With the growing affordability of CCD cameras and telescopes, and a consequent lowering of the \$6000 entry level, the number of amateurs who may be tempted by exoplanet observing in the near future may be in the thousands.

Imagine the value of an archive of exoplanet transit observations with contributions from several hundred amateurs. The day may come when every transit of every known transiting exoplanet will be observed (except for those faint OGLE, CoRoT, Kepler and very faint HST ones). Changes of transit shape and timings are possible, and these can be used to infer the existence of new planets, smaller and more interesting ones, as well as moons of the known exoplanet. The job is too large for the small number of professional observatories, and the cost of using them for this purpose is prohibitive.

If you are considering a hobby that's fun and scientifically useful, and if you're willing to learn new observing skills and spend time processing a night's images, then a community of almost 100 amateur exoplanet observers who have already made the transition are there to welcome you to this exclusive club.

Chapter 2

Observatory Tour

Since I will be using real data to illustrate systematic errors it will be useful to describe my observing systems. Note the use of the word "systems" in the plural form. Even with one telescope it will matter whether you are configured Cassegrain or prime focus, and whether a dew shield is used, or whether a focal reducer lens is used, and where it's inserted. Every change of configuration will change the relative importance of the various systematic error sources. During the past five years I have had three different telescopes, so I am aware of issues related to telescope design differences - such as the problems produced by meridian flips (i.e., 14-inch Celestrons). Most of these telescopes have had 14-inch apertures, and all have had catadioptric (folded) optics : Celestron CGE-1400, Meade RCX400, Meade LX200GPS and (currently) Celestron CPC-1100. These are typical telescopes now in use by advanced amateurs for exoplanet transit observations.

I use a sliding roof observatory (SRO) and an 8-foot dome observatory. Both enclosures are located in the backyard of my Southern Arizona residence, at an altitude of 4660 feet. The skies are dark and seeing can be as good as 1.8 "arc, though it is typically 2.5 to 3.5 "arc.

All control functions are performed by a computer in my house, using 100-foot cables in buried conduit (the control room is shown as Figs 2.04 and 2.05). Separate conduits are used for a power cable and command/data cables in order to prevent the power cable from interfering with command and data signals. An identical pair of buried conduit cabling connects to the sliding roof observatory.



Figure 2.01. *Sliding roof and dome observatories, HAO and HAO#2.*

CHAPTER 2 – OBSERVATORY TOUR



Figure 2.02 *The author next to the “Hereford Arizona Observatory” 8-foot diameter ExploraDome.*

I’ll describe my current hardware, which was recently moved from the SRO to the dome observatory. The telescope is a Celestron CPC-1100 on an equatorial mount. I used to use an SBIG AO-7 tip/tilt image stabilizer but I recently removed the AO-7 and discovered that optical quality improved. I attribute this improvement to a better match of the focal reducer’s location to its design distance to the CCD focal plane. I now accomplish autoguiding with the CCD’s second chip, a TC-237, using drive motor nudging. Following the focal reducer is a 5-position color filter wheel (CFW), which is attached to an SBIG ST-8XE CCD. I use the following filters: CBB (clear with blue-blocking), NIR (near infra-red), g’, r’ and i’. This configuration provides a “plate scale” of 0.86 ”arc/pixel (without binning). Since my “atmospheric seeing” FWHM is usually 2.5 to 3.5 ”arc for typical exposure times (30 to 60 seconds) there are ~ 3 to 4 pixels per FWHM, which is above the 2.5 pixel per FWHM requirement for precision photometry. The FOV for this configuration is 22 x 15 ’arc.

The Celestron CPC-1100 comes with only a manual focusing knob, so I attached a wireless Crayford-style motorized focuser to the CPC-1100’s 2-inch “visual back” (the focal reducer attaches to the motorized focuser). The wireless focuser communicates with a local control unit mounted to my office window having a clear line-of-sight to the dome. Since the dome is made of UV-stabilized polyethylene it is transparent to the wireless focuser’s radio signal.

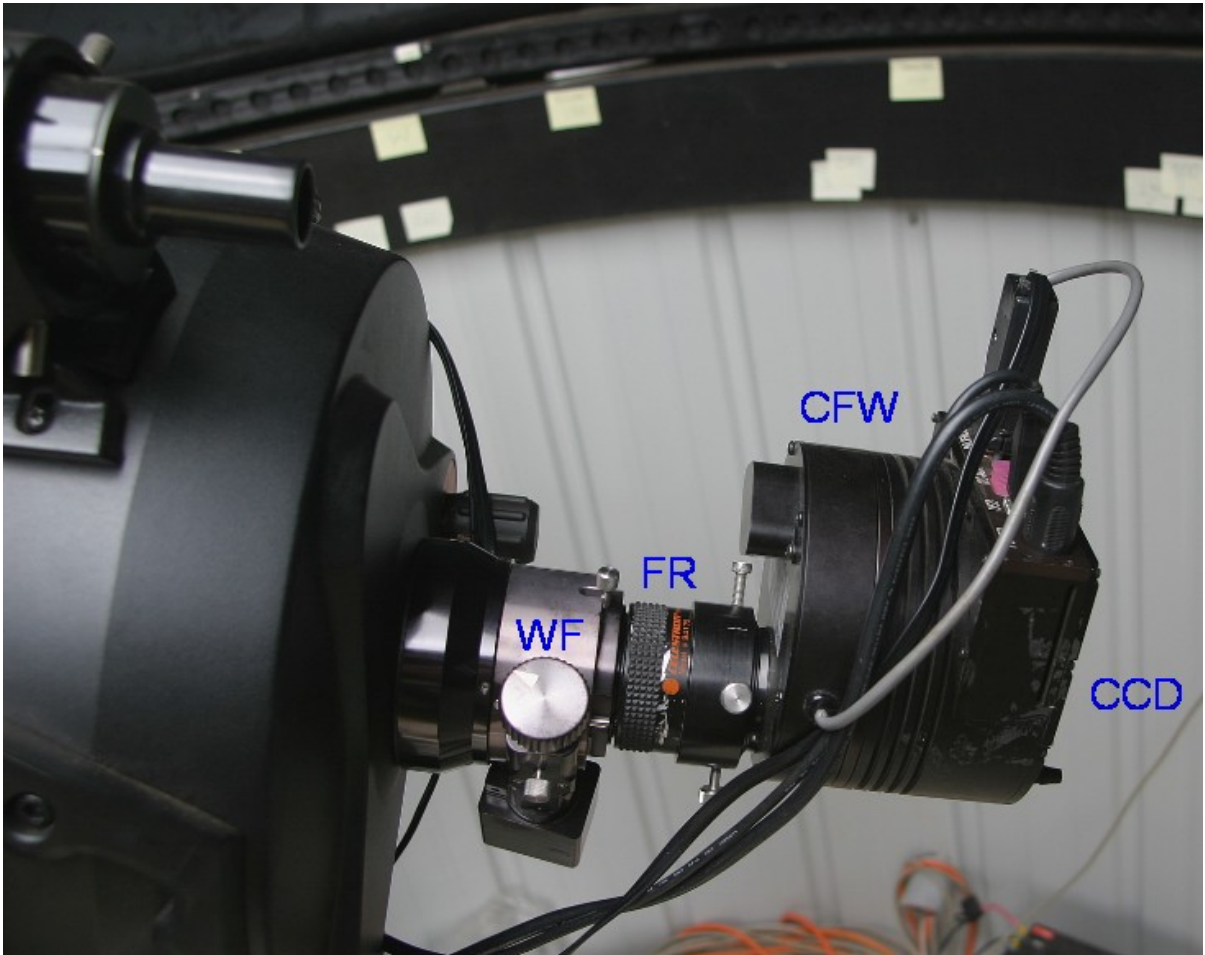


Figure 2.03. *My current optical backend configuration: Craycroft-style wireless focuser (WF), focal reducer (FR), CFW and CCD (SBIG ST-8XE). The telescope is a Celestron CPC-1100 (11-inch aperture) Schmidt-Cassegrain, $f/10$ (without the focal reducer).*

I also have a wireless weather station, with the sensors at the top of a 10-foot pole located near the sliding roof observatory (shown in Fig. 8.01). The pole is wood and the communications are wireless because lightning is common during our summer “monsoon season” (July/August). The weather station is a Davis Vantage Pro 2, supplemented by their Weather Link program for computer downloads from a data logger. This program produces graphical displays of all measured parameters: outside air temperature, dew point, barometric pressure, rain accumulation, and wind maximum and average (for user-specified intervals, which I’ve chosen to be 5 minutes). I find the graphs of wind and temperature to be very useful during an observing session.

What used to be a “master bedroom” is just the right size for everything needed in an observatory control room. The main computer is connected to the telescope via 100-foot cables in buried conduit. The computer has a video card supporting two monitors, one for MaxIm DL and the other for TheSky/Six and other supporting programs (labeled “Monitor #2” in the next figure).

CHAPTER 2 – OBSERVATORY TOUR

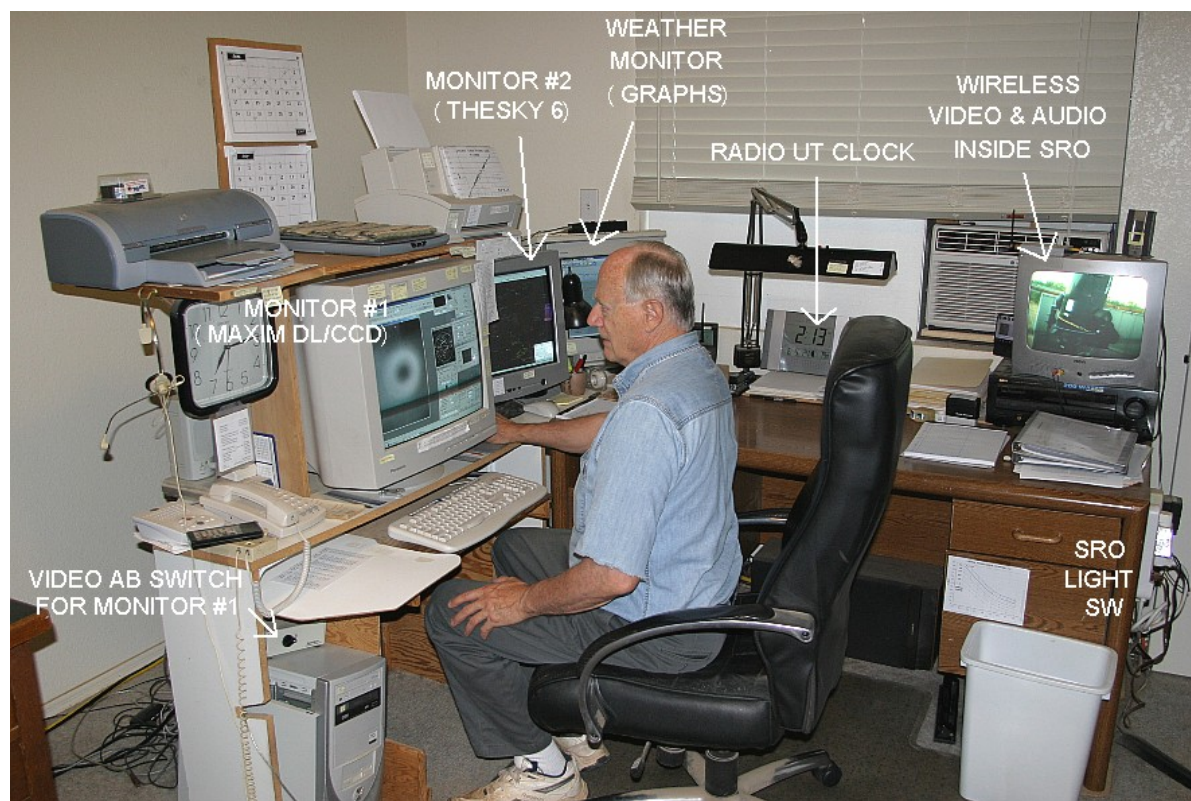


Figure 2.04. The author is shown manning the control room at the beginning of an observing session (making flat fields). Equipment is described in the text.

Another computer is dedicated to running the Davis Weather System program that downloads readings from the data logger and displays them as graphs on its own monitor. The Davis Weather System also has a real-time display panel; I find this useful for quick readings of wind speed, wind direction, temperature and dew point temperature when recording outside conditions in the observing log.

A radio controlled UT clock is synchronized with WWVB radio time signals every night. When accurate time-tagging of images is important I visually compare the radio controlled clock with the main computer's clock, which is synchronized using internet queries by a program (AtomTimePro) at 3 hour intervals.

Above Monitor #1 is a flat bed scanner with a small blanket. This is where the cat sleeps, and occasionally wakes, stretches, and reminds me about observing strategies.

On the desk (behind my chair) is another monitor for display of a wireless video sensor in the observatory. It shows a view of the telescope when a light is turned on by a switch (right side of desk). It also has an audio signal that allows me to hear the telescope drive motors, the sound of the wind as well as barking coyotes. (My two dogs observe with me, on the floor, and they get excited whenever coyote sounds come over the speaker.)

CHAPTER 2 – OBSERVATORY TOUR

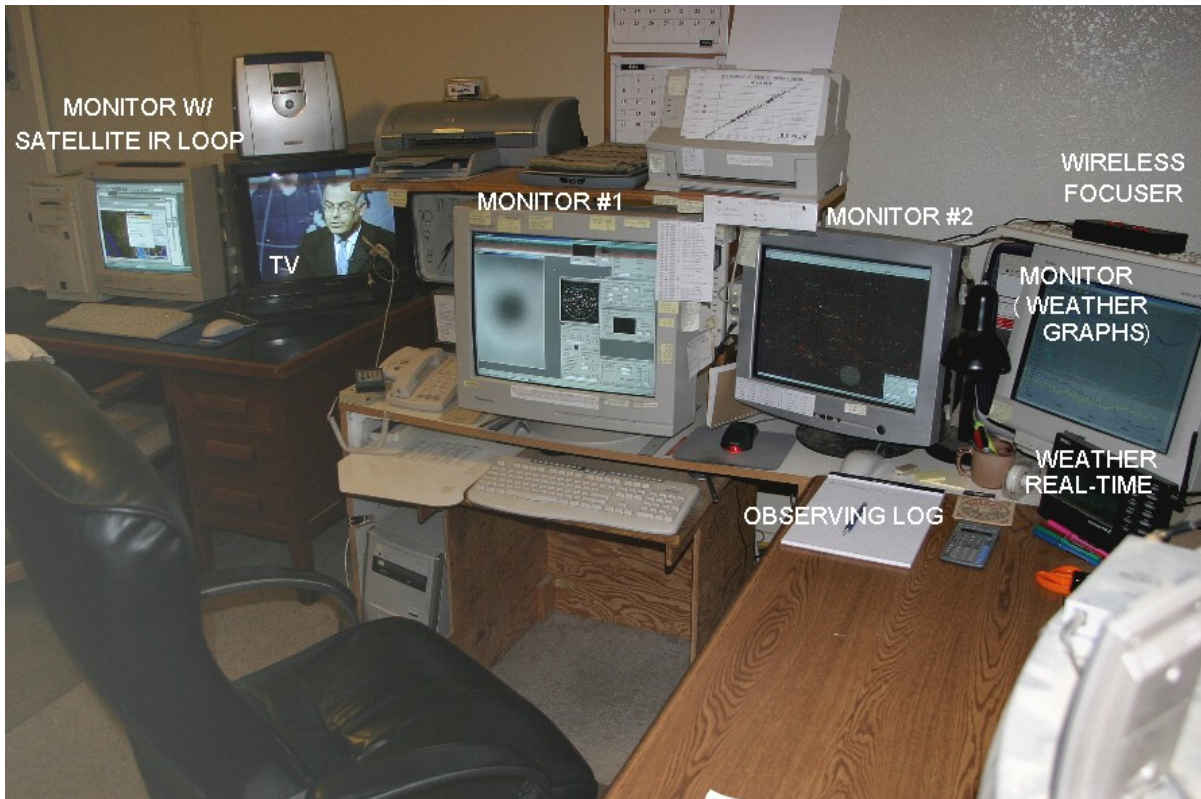


Figure 2.05. *Another view of control room.*

Below the wireless video display monitor is something found in practically every observatory: a “hi fi” for observing music. Since my area is remote, with no FM radio signals, I have a satellite radio (Sirius) receiver with an antenna on the roof and channel selector next to the wireless monitor.

Sometimes I have to take flat frames while a favorite program is on TV (e.g., “60 Minutes” seems to be the usual one), so I have a second TV on a desk to my left (Fig. 2.05). The remote control for it sits on a headphone switch box (next to the phone). It displays a satellite TV signal that comes from a receiver in the living room.

At the left end of the table in Fig. 2.05 is a secondary computer used to display IR satellite image loops that show when clouds are present. It also offloads computing tasks from the main computer (such as e-mail notices of GRB detections) to minimize the main computer’s competition for resources. The secondary computer has a LAN connection with the primary computer, which allows downloading images from the main computer for off-line image analysis without interfering with the main computer’s resources.

On top of the main computer (below table, to left) is a video AB switch for sending the main monitor’s video signal to another monitor in my living room. This allows me to “keep track of tracking” from my living room chair, while reading or watching TV. The remote monitor in the living room is on a swivel that allows me to keep track of it from my outdoor patio chair. Comfort is important when a lot of hours are spent with this all-consuming hobby.

CHAPTER 2 – OBSERVATORY TOUR

Charts are taped to every useful area. On one printer is a graph for converting J-K to B-V star colors. On the side of the main monitor is a list of currently interesting exoplanet candidates, with current information from other XO Project observers. Charts are readily visible for estimating limiting magnitude, simplified magnitude equation constants, and a quick way to predict maximum transit length from an exoplanet's star color and period (same as Fig. B.01). Post-its are used to remind me of handy magnitude equations, site coordinates, local to UT time conversion and nominal zenith extinction values.

Chapter 3

Exoplanet Projects

Exoplanets can be thought of as belonging to three categories:

- 1) bright transiting exoplanets, BTEs (46 known, as of mid-2009)
- 2) faint transiting exoplanets, FTEs (16 known)
- 3) exoplanets not known to undergo transits, NTEs (311 known)

Those in the first category are by far the most important. This is because transits of “bright transiting exoplanets” (BTEs) allow investigations to be made of the exoplanet’s atmospheric composition and temperature. Atmospheric composition is investigated using large, professional telescopes with sensitive spectrographs. Atmospheric temperature is inferred from thermal infrared brightness changes as the exoplanet is eclipsed by the star. These investigations can only be done with bright (nearby) exoplanets. In addition to permitting atmospheric studies, the BTEs permit a determination to be made of their size. Since the exoplanet’s mass is known from radial velocity measurements (with professional telescopes) the planet’s average density can be derived. The size and average density allow theoreticians to construct models for the planet’s density versus radius, which lead to speculations about the presence of a rocky core. All of these measurements and models can be used to speculate on the formation and evolution of other solar systems. This, in turn, can influence speculation on the question of “life in the universe.” The rate of discovery of BTEs, shown on the next page, is growing exponentially. Therefore, projects for BTEs that are described in this chapter can be done on a fast-growing list of objects.

The “faint transiting exoplanets” (FTEs) can’t be studied for atmospheric composition and temperature, but they do allow for the determination of exoplanet size and density since transit depth can be measured. Most FTEs are near the galactic plane, near the center, and this makes them especially difficult to observe with amateur telescopes. Although hardware capability improves with time, for both amateurs and professionals, I have adopted the somewhat arbitrary definition of V-mag = 14 for the FTE/BTE boundary. At the present time most amateurs are incapable of measuring transit properties when V-mag > 14.

The many “non-transiting exoplanets” (NTEs) should really be described as not being known to exhibit transits. Of the 311 known a statistical argument can be made that probably 15 to 20 of them actually are transiting but observations of them are too sparse to have seen the transits. As more amateurs observe NTEs the BTEs among them will hopefully be identified. This is what happened to GJ 436, which languished on the TransitSearch.org web site list for years before it was observed at the right time and found to undergo 6 milli-magnitude deep transits by a team of amateur observers (Gillon *et al*, 2007). This underscores the potential value of NTEs for the amateur observer.

For those NTEs that are truly NTE, which is probably 95% of them, we’ll never know the inclination of the exoplanet’s orbit accurately enough to establish more than a lower-limit constraint on mass. Since transits for them cannot be observed the exoplanet’s size will remain unknown, which means

CHAPTER 3 – EXOPLANET PROJECTS

the planet's density can't be established. Atmospheric composition and temperature can't be determined either since transits don't occur.



Figure 3.01. Cumulative number of known BTEs versus date. The blue symbols are for the northern celestial hemisphere, and the green symbols are for the southern celestial hemisphere. The curves are sigmoid fits with a doubling time of ~ 1.1 year. A total trace suggests that within a decade there will be about 100 known BTEs, with few additional ones left to be discovered after that.

All categories of exoplanets are worth considering for a night's observing session. It's understandable that the beginning observer will want to start by observing a few "easy" transits. Once the excitement of this has worn off, however, there may be interest in other observing projects, such as those described next.

A "starspot," analogous to a sunspot, will produce a small brightening anomaly during a transit (the interval Contact 2 to Contact 3). If a feature is seen on one light curve it may not be seen on others unless the period of exoplanet orbit and period of rotation at the sunspot's latitude are related by an integer multiple. Therefore the best strategy for amateurs to detect starspots is to coordinate observing

CHAPTER 3 – EXOPLANET PROJECTS

so that two or more light curves of the same transit show the same brightening feature. The BTE CoRoT-2 has already been shown by one observer to have exhibited a starspot feature.

If an exoplanet has a **debris system** in the same orbit (*e.g.*, volcanic ejecta surrounding and perhaps following the "hot Jupiter" planet) the debris particles will "forward scatter" and produce brightness enhancements before ingress and after egress. The shape of the pre-ingress and post-egress brightening features may be different, and only one might be present. This effect is likely to be too small for detection using amateur observations but unusually large, transient ejection events should not be ruled out.

If an exoplanet has a **ring system** the ring particles will also "forward scatter" and produce a brightening before ingress and after egress that can last several minutes. In 2004 Joe Garlitz and I independently noticed that amateur light curve (LC) observations of TrES-1 showed a small brightening (~5 mmag) after egress, lasting ~10 minutes. Ron Bissinger did an exhaustive statistical analysis of many TrES-1 LCs and concluded that the feature was statistically significant. Subsequent HST observations failed to confirm the feature so we are left to assume that the apparent brightenings were a statistical fluke. All exoplanets should be inspected for such a feature even though the effect is probably going to be much smaller than amateur observations could detect (< 0.3 mmag according to Barnes and Fortney, 2004).

One of my favorite projects is to monitor a known BTE's "**out-of-transit**" (OOT). If no other exoplanets are present in the BTE's solar system then the observed OOT LCs will be a very uninteresting plot with constant brightness for the entire observing session. However, if another exoplanet exists in the BTE's solar system its orbit is likely to be in the same plane as the known BTE, and it may produce its own transits on a different schedule from the BTE. Since the known BTE was based on a data base of wide field survey camera observations the transits produced by the BTE will be the easiest to detect. Therefore, an observer searching for a second exoplanet in a BTE solar system should be prepared for a transit that's more difficult to detect. The second exoplanet's transit depth will probably be much shallower, and it could either last longer or be shorter, and it will come at times that differ from the BTE transit.

Before selecting an exoplanet to observe extensively in the OOT mode check its "impact parameter." This is the ratio of the "transit chord's closeness to star center" divided by star radius. If the impact parameter is close to 1.0 then it's a close to grazing transit; this means that any outer planets in that system would not transit. An impact parameter of zero corresponds to a transit that goes through the star's center; this means that all other planets in the system are likely to transit. As you may have guessed, BTEs have impact parameter values ~0.4, typically. Exoplanets in orbits that are twice the size of the known exoplanet are likely to produce transits in such systems. Given that a planetary system exhibits orbital periods that are proportional to orbital radius raised to the 1.5 power, a second exoplanet in an orbit that is twice the size of a hot Jupiter will have a period of 2.8 times that of the hot Jupiter.

There's a variant of the OOT observing project type, which could be called "**looking for Trojans.**" This project is based on the presence of Trojan asteroids in our solar system. Jupiter is accompanied by swarms of asteroids in approximately the same orbit as Jupiter but preceding and following by 60 degrees of orbital position. These locations are gravitationally stable and are referred to as Lagrangian points L4 and L5. There are about 1100 Trojans, and none of them are large (exceeding 370 km). If they were lumped together in one object it would have a diameter ~1% that of Jupiter. In solar

CHAPTER 3 – EXOPLANET PROJECTS

systems with a Jupiter-sized planet orbiting close to its star, the so-called “hot Jupiter” that most BTEs resemble, the BTE would have to be accompanied by a much larger Trojan companion to produce observable transits. As far as I know these larger Trojan companions cannot be ruled-out by present theories for solar system formation and evolution, so they are worth an amateur’s attention as a special project. The search strategy is straight-forward: simply observe at times that are 1/6 of a BTE period before and after the BTE’s scheduled transit.

Another exoplanet project is “**transit timing variations**” (TTV). The goal is to detect anomalies in mid-transit times caused by the gravitational influence of another planet in a resonant orbit, as described in more detail in Chapter 22. Although this is something one person could do alone it is more appropriate to combine mid-transit timings by many observers in a search for anomalies. The magnitude of the anomalies can be as much as 2 or 3 minutes and the time scale for sign reversals is on the order of a year. Only BTE objects are suitable for this project.

Searching for an “Exomoon” is an exciting new thing to look for in amateur transit observations, as pointed out by David Kipping (*Sky & Telescope*, July 2009, pg 30-33; also described at the author's web site: <http://www.homepages.ucl.ac.uk/~ucapdki/exomoons.html>). The concept is simple: a moon of an exoplanet will cause it to move around the parent star with a varying orbital velocity, causing detectable TTV. It will also cause transit length variations, TDV (Transit Duration Variations). TTV effects for an Earth mass moon could be as large as 2 minutes, and the TDV effect could be as large as 1 minute, according to David Kipping’s calculations. Effects as large as these could be measured by amateurs! The main challenge to exomoon searches is the fact that the moon’s orbital period is likely to be much shorter than the exoplanet’s orbit around the star. Thus, if a search is to be made it will have to involve a complicated hypothesis testing approach, such as showing that an exomoon period of X days causes TTV with a multiple of X day anomalies. So far this has not been done.

Transit length and depth could exhibit secular (non-cyclic) changes if the exoplanet is close to grazing (impact parameter close to 1.0). Such changes could occur if there’s another planet in a resonant orbit causing gravitational tugs to accumulate in a way that causes the exoplanet’s orbital inclination to change. At least one such exoplanet is suspected of exhibiting transit length changes.

A somewhat more challenging observing project is to refine “**transit depth versus wavelength.**” Again, this can only be done with BTEs. As the name implies, it consists of observing a BTE at known transit times with different filters. If you have a large aperture (larger than 14 inches) you could alternate between two filters throughout an event. The goal is to further refine the solution for the planet’s path across the star and simultaneously refine the star’s limb darkening function. As explained later, an exoplanet whose path passes through star center will have a deeper depth at shorter wavelengths whereas if the path is a chord that crosses farther than about 73% of the way to the edge at closest approach (impact parameter $b > 0.73$) the opposite depth versus color relationship will be found. Constraining the path’s geometry and star limb darkening will lead to an improved estimate for planet size and this is useful for theoreticians studying planetary system formation and evolution.

Every amateur should consider **observing nominally NTE** exoplanets at times they’re predicted to have possible transits. These observations can determine whether or not they really are an NTE instead of a BTE that is “waiting” to be discovered. As stated above, GJ 436 is one example of an exoplanet that was nominally identified as an NTE which in fact was discovered to exhibit transits by an amateur group that changed it to a BTE. Another famous example is HD 80606, which was first

CHAPTER 3 – EXOPLANET PROJECTS

observed by Greg Laughlin with the Spitzer infrared telescope to undergo eclipses of the exoplanet by the star (when it was near periastron, in an eccentric orbit close to the star). A few months later amateurs helped establish that primary transits were also occurring. The list of nominally NTE exoplanets can be found at TransitSearch.org, which is maintained by Greg Laughlin. Times favorable for transits, if they occur, are given on this web site, as well as likely transit depth.

Finally, some exoplanet observers who exhibit advanced observing skills may be invited to join a group of amateurs supporting professionals conducting wide field camera surveys that are designed to find exoplanet transits. So far only the XO Project makes use of amateurs this way, in a systematic way, but other wide field survey groups may recruit a similar team of advanced amateurs for follow-up observations. The main task of these observers is to observe a star field on a list of interesting candidates, at specific times, to identify which star is varying at the times when the survey cameras detect small fades from a group of stars in the camera's low-resolution photometry aperture. If a star is found that varies less than ~ 30 mmag it may be an exoplanet, and spectroscopic observations of radial velocity on several dates would then be required to establish the secondary's mass. It is very unlikely that amateur spectroscopy will ever be precise enough to distinguish between the masses of a planet and star (e.g., brown dwarf). This task is best performed using professional telescopes. A low mass for the secondary (< 13 times Jupiter's mass) almost assures that it is an exoplanet, although careful additional observations and model fitting will have to be done by professionals to confirm this. If you're on the team of amateur observers contributing to follow-up observations that lead to an exoplanet discovery, you will be smiling for days with a secret that can't be shared until the official announcement is made. Appendix B is included for amateurs on a team charged with wide field camera follow-up observations.

Whenever the night sky promises to be clear and calm the amateur observer will have many observing choices. I suspect that amateur exoplanet observers will eventually form specialty groups, with some specializing in each of the following possible areas:

- Starspots search
- Ring or debris system brightenings search
- Exomoon search
- OOT searches for new exoplanets
- Trojan transit searches
- TTV produced by another exoplanet in resonant orbit
- Transit depth versus filter band
- Search for transits by nominal NTEs
- Wide field camera candidate follow-up

The next chapter demonstrates how to determine when any of the known BTEs can be observed for any observing site and date. This information can be useful in planning observing sessions for days and weeks ahead, so as not to miss an important event for whichever category is most interesting to you.

Chapter 4

BTE List

All observing projects start with a list of candidate objects. Here's a BTE list.

Object	RA	Dec	V-mag	B-V	HJDo	Period [days]	Depth [mmag]	Length [hours]	b	Season [Month]
46	WASP-17	15:59:51 -28:03.7	11.6	0.50	4559.18102	3.7354417	20.3	4.37	0.35	05.8
45	WASP-16	14:18:44 -20:16.5	11.3	1.22	4584.42878	3.118601	12.4	1.87	0.80	05.0
44	HAT-P-13	08:39:32 +47:21.1	10.62	0.73	4779.92979	2.916260	8.	3.23	0.67	01.9
43	WASP-13	09:20:25 +33:52.9	10.42	?.??	4491.6161	4.35298	8.4	3.8	0.??	02.3
42	HAT-P-12	13:57:33 +43:29.6	12.84	?.??	4419.19556	3.2130598	20.	2.34	0.21	04.6
41	WASP-15	13:55:43 -32:09.6	10.9	?.??	4584.6982	3.75217	11.5	3.5	0.57	04.6
40	HD80606	09:22:38 +50:36.2	8.5	?.??	4987.7842	111.43740	11.5	11.64	0.77	02.2
39	WASP-6	23:12:38 -22:40.4	11.9	?.??	4596.43267	3.3610060	26.4	2.61	0.26	09.4
38	HAT-P-11	19:50:50 +48:04.9	9.59	1.05	4605.89132	4.8878162	4.2	2.30	0.35	07.7
37	WASP-12	06:30:33 +29:40.3	11.69	0.42	4508.9760†	1.091422†	16.5	2.95	0.36	01.0
36	CoRoT-4	06:48:47 -00:40.4	13.7	0.??	4141.36416	9.20205	14.0	4.42	0.??	01.0
35	CoRoT-3	19:28:13 +00:07.3	13.29	0.91	4283.1383	4.25680	5.2	3.77	0.55	07.1
34	CoRoT-1	06:48:19 -03:06.1	13.6	0.57	4159.4532	1.5089557	24.8	2.46	0.??	01.0
33	HAT-P-8	22:52:10 +35:26.8	10.26	0.47	4437.67582	3.076331†	8.5	3.75	0.32	09.2
32	WASP-11	03:09:29 +30:40.4	11.89	0.??	4729.90631	3.7224690	22.4	2.59	0.24	11.5
31	HAT-P-9	07:20:40 +37:08.4	12.30	0.50	4417.9077	3.92289	14.0	3.3	0.52	01.3
30	WASP-10	23:15:58 +31:27.8	12.7	0.??	4790.84014†	3.0927255†	35.2	2.15	0.58	09.4
29	WASP-14	14:33:06 +21:53.7	9.75	0.46	4465.81963	2.243756	11.7	2.78	0.51	05.1
28	XO-5	07:46:52 +39:05.7	12.13	0.84	4485.6664	4.187732	13.8	3.05	0.55	01.5
27	XO-4	07:21:34 +58:16.0	10.67	0.57	4485.9322	4.12502	09.7	4.58	0.18	01.4
26	WASP-7	20:44:10 -39:13.5	9.51	0.??	3985.0149	4.954658	10	3.67	0.08	08.1
25	HAT-P-7	19:28:59 +47:58.2	10.5	?.??	4667.7382	2.2047215†	7.2	3.84	0.37	07.4
24	CoRoT-2	19:27:07 +01:23.0	12.57	?.??	4237.53562	1.7429964	35.2	2.27	?.??	07.4
23	WASP-5	23:57:24 -41:16.6	12.26	?.??	4373.99598	1.6284279	12.5	2.37	0.31	09.8
22	WASP-4	23:34:15 -42:03.7	12.5	?.??	4383.313070	1.3382324	34	2.12	0.06	09.7
21	WASP-3	18:34:32 +35:39.7	10.64	?.??	4605.55915	1.846834	12.2	2.71	0.51	07.0
20	HAT-P-6	23:39:06 +42:28.0	10.54	0.34	4035.67575	3.8529978†	9.8	3.43	0.60	09.7
19	HAT-P-5	18:17:37 +36:37.3	12.03	0.62	4241.77663	2.7884747†	15.2	3.01	0.42	06.9
18	HD17156	02:49:45 +71:45.2	08.17	0.64	4671.86311†	21.2163540†	06.5	3.06	0.55	11.3
17	HAT-P-4	15:19:58 +36:13.8	11.21	0.57	4245.8154	3.056536	09.6	4.2	0.01	05.6
16	TrES-4	17:53:13 +37:12.7	11.34	0.48	4230.9054†	3.553930†	13.5	3.52	0.75	07.2
15	HAT-P-3	13:44:22 +48:01.7	11.86	0.8	4566.72741†	2.8997405†	16.0	2.01	0.49	04.5
14	XO-3	04:21:53 +57:49.0	09.80	0.45	4449.8672†	3.1915228†	09.8	2.87	0.70	12.0
13	GJ 436	11:42:11 +26:42.4	10.68	1.52	4280.78148	2.643904	08.1	0.95	0.92	03.5
12	XO-2	07:48:08 +50:13.2	11.18	0.82	4147.74902	2.6158605†	14.2	2.67	0.16	01.5
11	TrES-3	17:52:07 +37:32.8	12.40	0.71	4185.9107†	1.306186†	27.2	1.29	0.82	06.7
10	HAT-P-2	16:20:36 +41:02.9	08.71	0.41	4212.8559	5.63341	05.5	3.46	0.54	06.0
09	XO-1	16:02:12 +28:10.2	11.19	0.66	3887.74733†	3.94150242†	23.4	2.91	0.73	05.9
08	WASP-2	20:30:54 +06:25.8	11.98	1.02	3991.5138†	2.1522221†	19.5	1.74	0.39	08.0
07	WASP-1	00:20:40 +31:59.4	11.65	0.54	3151.486	2.519955†	14.6	3.67	0.3	10.0
06	TrES-2	19:07:14 +49:19.0	11.41	x.xx	3957.6372†	2.470600†	17.1	1.71	0.83	07.3
05	HAT-P-1	22:57:47 +38:40.5	10.4x	0.6x	4363.94656	4.4652934	14	2.65	0.70	09.3
04	HD189733	20:00:43 +22:42.7	07.67	1.08	3988.8051†	2.2185629†	29.0	1.70	0.66	07.7
03	HD149026	16:30:30 +38:20.8	08.16	0.56	4327.37211	2.8758887	03.0	3.31	0.45	06.0
02	TrES-1	19:04:10 +36:38.0	11.79	0.78	3898.87330†	3.0300703†	25.1	2.47	0.76	07.3
01	HD209458	22:03:11 +18:53.1	07.65	0.63	2826.628521	3.52474859	18.0	2.97	0.48	08.8

Figure 4.01. List of BTEs (most recently discovered BTEs at top). HJDo is Heliocentric Julian Date for a reference mid-transit, P is the orbital period of the BTE; together they constitute an ephemeris for calculating future mid-transit times. Impact parameter “b” shows whether the transit chord is close to grazing (1.0) versus central (0.0). “Season” is the month when the object transits at local midnight. (Screen capture from Amateur Exoplanet Archive home page.)

CHAPTER 4 – BTE LIST

This section describes how to calculate when BTE transits occur in order to plan days or months ahead. I like to maintain observing calendars for at least a month in advance so that especially important transits won't be "missed" by committing to other plans for those important dates.

Information on exoplanets is maintained on many archives. The one shown above is from the Amateur Exoplanet Archive, AXA (maintained by the author of this book). This archive was designed two years ago for the express purpose of guiding the amateur in deciding which exoplanet to observe on specified nights. A similar archive is maintained by the Czech Republic Astronomical Society that created the "Exoplanet Transit Database," ETD, with a web site URL address of <http://var2.astro.cz/ETD/>. The ETD web site accepts data file submissions. The AXA archives amateur data that are submitted to a special e-mail address (axa@brucegary.net). More information about these sites are given in a later chapter. A more extensive list of exoplanet information is maintained by Jean Schneider at <http://exoplanet.eu/catalog-transit.php>. This web site is always current, but it is not as user-friendly to the amateur observer because it does not list transit depth, transit length, observing season, how many amateur observations already exist, etc.

One thing to notice about the above table is that most of the BTEs are in the northern celestial hemisphere. This is due to a "selection effect" since wide field camera surveys were installed first in the Earth's northern hemisphere. Now that the SuperWASP survey is operational in the southern hemisphere the number of BTEs in the southern celestial hemisphere is expected to eventually grow faster than those in the northern celestial hemisphere.

Another thing to notice about this table is that most of the BTEs are best observed in the 5 summer months, May through September (61%, or 28 of 46). I'm still puzzled by this. It is unfortunate that the northern hemisphere summer is also the time when nights are shortest, and is therefore the least favorable time for observing a complete transit. (For my site there's an additional handicap: Southern Arizona has a monsoon season from July to September, and most of these nights are overcast with a residual of the afternoon's thunderstorms.)

What's the table in Fig.4.01 good for when planning an observing session for an upcoming clear night? You may use this table by first noting which objects are "in season." An object with a Season matching an observing date will transit at local midnight on that date, and will therefore offer a longer observing session than for other dates. "Season" begins approximately 3 months before "opposition" and ends 3 months afterwards. On those dates the object transits at 6 AM and 6 PM, respectively. An object may be observed "outside" the season, but observing intervals will be limited (the amount will depend on site latitude and object declination).

You'll want to be able to calculate when transits can be observed before any observing planning can begin. This can be done using a spreadsheet that I maintain and make available at the following web site: http://brucegary.net/book_EOA/xls.htm. It has an input area on the first worksheet for observing site coordinates, as well as date (if different from current date). All known BTEs with transits that can be observed are then displayed on any night of interest (also selectable if different from current date). Additional information is displayed about the BTE (UT for ingress, mid-transit and egress, elevation for these events, depth, length, RA and DE coordinates, etc). Figure 4.02 illustrates the spreadsheet's main display worksheet.

CHAPTER 4 – BTE LIST

A	B	C	D	E	F	G	H	I	J	K	L	M	N	O	P	Q	R	S	T	U	V	W	X	Y
1			Darkness UT range	1.6	to	12.8																		
2	Today's Date	10/28/2009	UT																					
3	Offset (days)	5																						
4	Target Date:	11/3/2009	UT	Eve of	Elon:																			
5			Local date at sunset:	11/2/2009																				
6	Exoplanet	UT Date	lng	Mid	Egr	tot	lng	Mid	Egr	EL	EL	EL	LHA	V-mag	D	L	RA	DEC				# in archive	AXA Priority	Period [days]
7	CoRoT-1	11/3/2009			7.54	61	0	0	2	-4	12	27	-4.9	12.6	35.2	2.27	06:48:19.2	-03:06:08				2	2	1.5
8	CoRoT-2	11/3/2009	2.86	3.99		43	2	1	0	40	26	12	4.0	12.6	35.2	2.27	19:27:06.9	01:23:00				19	1	1.7
9	CoRoT-3	11/3/2009	4.27			56	1	0	0	22	-2	-26	6.1	13.29	5.2	3.77	19:28:13.2	00:07:19				1	2	4.3
10	CoRoT-4	11/3/2009				0	0	0	0															
11	GJ 436	11/3/2009				0	0	0	0															
12	HAT-P-1	11/3/2009				0	0	0	0															
13	HAT-P-2	11/3/2009				0	0	0	0															
14	HAT-P-3	11/3/2009				0	0	0	0															
15	HAT-P-4	11/3/2009				0	0	0	0															
16	HAT-P-5	11/3/2009				0	0	0	0															
17	HAT-P-6	11/3/2009				0	0	0	0															
18	HAT-P-7	11/3/2009				0	0	0	0															
19	HAT-P-8	11/3/2009				0	0	0	0															
20	HAT-P-9	11/3/2009				0	0	0	0															
21	HAT-P-11	11/3/2009	2.76	3.91	5.06	80	2	2	2	58	47	35	3.6	9.59	4.2	2.30	19:50:50.1	48:04:51				3	1	4.9
22	HAT-P-12	11/3/2009				0	0	0	0															
23	HAT-P-13	11/3/2009				0	0	0	0															
24	HD 149026	11/3/2009				0	0	0	0															
25	HD 189733	11/3/2009				0	0	0	0															
26	HD 17156	11/3/2009		2.94	4.45	214	0	1	3	30	38	44	19.7	8.17	6.5	3.02	02:49:45.0	71:45:11				10	9	21.2
27	HD 209458	11/3/2009	7.20			37	2	0	0	26	8	-10	6.2	7.65	18.1	2.94	22:03:10.8	18:53:04				12	1	3.5
28	HD 80606	11/3/2009				0	0	0	0															
29	TrES-1	11/3/2009				0	0	0	0															
30	TrES-2	11/3/2009		2.10	2.95	49	0	2	2	65	57	49	2.5	11.41	17.1	1.71	19:07:13.9	49:18:59				44	1	2.5
31	TrES-3	11/3/2009				0	0	0	0															
32	TrES-4	11/3/2009				0	0	0	0															
33	WASP-1	11/3/2009				0	0	0	0															
34	WASP-2	11/3/2009	2.68	3.55	4.42	77	2	2	2	56	47	36	2.5	12	19.5	1.74	20:30:54.1	06:25:46				25	1	2.2
35	WASP-3	11/3/2009				0	0	0	0															
36	WASP-4	11/3/2009				0	0	0	0															
37	WASP-5	11/3/2009				0	0	0	0															
38	WASP-6	11/3/2009				0	0	0	0															
39	WASP-7	11/3/2009				0	0	0	0															
40	WASP-10	11/3/2009				0	0	0	0															
41	WASP-11	11/3/2009				0	0	0	0															
42	WASP-12	11/3/2009		5.42	6.88	53	0	1	3	4	20	38	-5.5	11.69	17.2	2.92	06:30:32.8	29:40:20				7	1	1.1
43	WASP-13	11/3/2009				0	0	0	0															
44	WASP-14	11/3/2009				0	0	0	0															
45	WASP-15	11/3/2009				0	0	0	0															
46	WASP-16	11/3/2009				0	0	0	0															
47	WASP-17	11/3/2009				0	0	0	0															
48	XO-1	11/3/2009				0	0	0	0															
49	XO-2	11/3/2009				0	0	0	0															
50	XO-3	11/3/2009				0	0	0	0															
51	XO-4	11/3/2009				0	0	0	0															
52	XO-5	11/3/2009	9.47	10.98	12.49	85	3	3	1	56	73	82	-1.3	12.14	13.7	3.02	07:46:51.8	39:05:40				14	1.5	4.2

Figure 4.02. Sample Excel spreadsheet showing which BTEs can be observed on a specific UT date for a specific observing site (the authors). Other details are explained in the text.

In this figure it can be seen that 10 transit events can be observed on the UT date 2009.11.03 from the author’s observing site. A “figure of merit” column (H) shows that the “most important” BTE to observe, according to a subjective algorithm, is HD 17156. This BTE’s transit can only be observed from mid-transit through egress, with elevations shown in columns M and N. The depth and length for this BTE’s transits is shown, as are the RA and Declination. Column W shows how many amateur observations are archived in the AXA (at some recent date), and column X is my subjective assessment of the scientific merits of studying each BTE.

Other worksheets in this spreadsheet are devoted to individual BTEs. If an observer is especially interested in a specific BTE these other pages are useful. For example, suppose you want to know other dates when HD 17156 can be observed. From the above figure we already know that HD 17156 can be observed on 2009.11.03 (from the observing site of interest). The next figure is from the same spreadsheet, and shows details of 39 consecutive transits starting with those close to the date of interest.

CHAPTER 4 – BTE LIST

	A	B	C	D	E	F	G	H	I	J	K	L	M	N	O	P	Q	R	S	T	U	V	W	X	Y	Z	AA		
1	HD17156	Transit Times											57.30	7.19	5.6					UT times are JD (if RA & Dec are entered)									
2		Tc [HJD]	4459.6994	day	8.17	V-mag							2009	7.2															
3		P	21.216451	hr	6.5	Depth								1.6	UT (darkness starts)														
4		L	3.02	hr										12.8	UT (darkness ends)														
5		RA	2.83	hr									308	308	11.1	Season[Mo#]													
6		Dec	71.8										DOY	18						ELmin									
7			5136			ing	ing	Mid	Mid	egr	egr	ing	Mid	egr	ing	Mid	egr	ing	Mid	egr	ing	Mid	egr	ing	Mid	egr	ing	Mid	egr
8	Try	31	HJD ing	HJD mid	HJD egr	Year	Mo	Day	Mo	Day	Mo	Day	UT	UT	UT	EL	EL	EL	fr day	fr day	fr day	UT hr	UT hr	UT hr	UT hr	UT hr	UT hr	UT hr	
9																													
10	HD17156	31	5117.346	5117.409	5117.472	2009	10	12.85	10	12.91	10	12.97				13	14	17	0.35	0.41	0.47	-3.69	-2.18	-0.67	20.3	21.8	23.3		
11	HD17156	32	5138.563	5138.626	5138.689	2009	11	3.06	11	3.13	11	3.19		2.94	4.45	30	38	44	0.56	0.63	0.69	1.51	3.02	4.53	1.4	2.9	4.5		
12	HD17156	33	5159.779	5159.842	5159.905	2009	11	24.28	11	24.34	11	24.41	6.62	8.13	9.64	49	46	40	0.78	0.84	0.91	6.70	8.21	9.72	6.6	8.1	9.6		
13	HD17156	34	5180.996	5181.059	5181.122	2009	12	15.50	12	15.56	12	15.62	11.82			24	18	15	1.00	0.06	0.12	11.90	-10.59	-9.08	11.8	13.3	14.8		
14	HD17156	35	5202.212	5202.275	5202.338	2010	1	5.71	1	5.78	1	5.84				15	19	25	0.21	0.28	0.34	-6.91	-5.40	-3.89	17.0	18.5	20.0		
15	HD17156	36	5223.429	5223.492	5223.555	2010	1	26.93	1	26.99	1	27.05				41	47	50	0.43	0.49	0.55	-1.71	-0.20	1.31	22.2	23.8	1.3		
16	HD17156	37	5244.645	5244.708	5244.771	2010	2	17.15	2	17.21	2	17.27	3.47	4.98	6.49	43	36	29	0.65	0.71	0.77	3.48	4.99	6.50	3.5	5.0	6.5		
17	HD17156	38	5265.862	5265.925	5265.987	2010	3	10.36	3	10.42	3	10.49				16	14	13	0.86	0.92	0.99	8.68	10.19	11.70	8.7	10.2	11.7		
18	HD17156	39	5287.078	5287.141	5287.204	2010	3	31.58	3	31.64	3	31.70				22	29	36	0.08	0.14	0.20	-10.13	-8.62	-7.11	13.9	15.4	16.9		
19	HD17156	40	5308.295	5308.357	5308.420	2010	4	21.79	4	21.86	4	21.92				49	50	47	0.29	0.36	0.42	-4.93	-3.42	-1.91	19.1	20.6	22.2		
20	HD17156	41	5329.511	5329.574	5329.637	2010	5	13.01	5	13.07	5	13.14		1.86	3.37	32	25	19	0.51	0.57	0.64	0.26	1.77	3.28	0.3	1.9	3.4		
21	HD17156	42	5350.727	5350.790	5350.853	2010	6	3.23	6	3.29	6	3.35			8.56	13	15	18	0.73	0.79	0.85	5.46	6.97	8.48	5.5	7.1	8.6		
22	HD17156	43	5371.944	5372.007	5372.070	2010	6	24.44	6	24.51	6	24.57	10.73	12.24		33	40	46	0.94	0.01	0.07	10.65	-11.84	-10.33	10.7	12.2	13.8		
23	HD17156	44	5393.160	5393.223	5393.286	2010	7	15.66	7	15.72	7	15.79				49	44	38	0.16	0.22	0.29	-8.15	-6.64	-5.13	15.9	17.4	18.9		
24	HD17156	45	5414.377	5414.440	5414.503	2010	8	5.88	8	5.94	8	6.00				22	17	14	0.38	0.44	0.50	-2.96	-1.45	0.06	21.1	22.6	0.1		
25	HD17156	46	5435.593	5435.656	5435.719	2010	8	27.09	8	27.16	8	27.22		3.75	5.26	16	21	27	0.59	0.66	0.72	2.24	3.75	5.26	2.2	3.8	5.3		
26	HD17156	47	5456.810	5456.873	5456.936	2010	9	17.37	9	17.43	9	17.44	7.41	8.92	10.43	43	48	50	0.81	0.87	0.94	7.43	8.94	10.45	7.4	8.9	10.4		
27	HD17156	48	5478.026	5478.089	5478.152	2010	10	8.53	10	8.59	10	8.65	12.57			41	34	27	0.03	0.09	0.15	-11.37	-9.86	-8.35	12.6	14.1	15.6		
28	HD17156	49	5499.243	5499.305	5499.368	2010	10	29.74	10	29.81	10	29.87				15	13	14	0.24	0.31	0.37	-6.18	-4.67	-3.16	17.7	19.3	20.8		
29	HD17156	50	5520.459	5520.522	5520.585	2010	11	19.96	11	20.02	11	20.08			1.95	24	31	38	0.46	0.52	0.58	-0.98	0.53	2.04	22.9	0.4	2.0		
30	HD17156	51	5541.675	5541.738	5541.801	2010	12	11.18	12	11.24	12	11.30	4.13	5.64	7.15	49	49	45	0.68	0.74	0.80	4.21	5.72	7.23	4.1	5.6	7.1		
31	HD17156	52	5562.892	5562.955	5563.018	2011	1	1.39	1	1.45	1	1.52	9.34	10.85		30	23	18	0.89	0.95	0.02	9.41	10.92	-11.57	9.3	10.8	12.4		
32	HD17156	53	5584.108	5584.171	5584.234	2011	1	22.61	1	22.67	1	22.73				13	15	20	0.11	0.17	0.23	-9.40	-7.89	-6.38	14.6	16.1	17.6		
33	HD17156	54	5605.325	5605.388	5605.451	2011	2	12.82	2	12.89	2	12.95				35	42	47	0.32	0.39	0.45	-4.20	-2.69	-1.18	19.8	21.3	22.8		
34	HD17156	55	5626.541	5626.604	5626.667	2011	3	6.04	3	6.10	3	6.17		2.51	4.02	47	42	36	0.54	0.60	0.67	0.99	2.50	4.01	1.0	2.5	4.0		
35	HD17156	56	5647.758	5647.821	5647.884	2011	3	27.26	3	27.32	3	27.38	6.22			20	16	13	0.76	0.82	0.88	6.19	7.70	9.21	6.2	7.7	9.2		
36	HD17156	57	5668.974	5669.037	5669.100	2011	4	17.47	4	17.54	4	17.60				18	23	29	0.97	0.04	0.10	11.38	-11.11	-9.60	11.4	13.0	14.5		
37	HD17156	58	5690.191	5690.254	5690.316	2011	5	8.69	5	8.75	5	8.82				45	49	49	0.19	0.25	0.32	-7.43	-5.92	-4.41	16.7	18.2	19.7		
38	HD17156	59	5711.407	5711.470	5711.533	2011	5	29.91	5	29.97	5	30.03				39	32	25	0.41	0.47	0.53	-2.23	-0.72	0.79	21.9	23.4	0.9		
39	HD17156	60	5732.624	5732.686	5732.749	2011	6	20.12	6	20.19	6	20.25				14	13	15	0.62	0.69	0.75	2.96	4.47	5.98	3.0	4.6	6.1		
40	HD17156	61	5753.840	5753.903	5753.966	2011	7	11.34	7	11.40	7	11.47	8.23	9.74	11.25	26	33	40	0.84	0.90	0.97	8.16	9.67	11.18	8.2	9.7	11.2		
41	HD17156	62	5775.056	5775.119	5775.182	2011	8	1.56	8	1.62	8	1.68				50	48	44	0.06	0.12	0.18	-10.65	-9.14	-7.63	13.4	14.9	16.4		
42	HD17156	63	5796.273	5796.336	5796.399	2011	8	22.77	8	22.84	8	22.90				28	21	17	0.27	0.34	0.40	-5.45	-3.94	-2.43	18.6	20.1	21.6		
43	HD17156	64	5817.489	5817.552	5817.615	2011	9	12.99	9	13.05	9	13.12			2.74	14	17	21	0.49	0.55	0.62	-0.26	1.25	2.76	23.7	1.2	2.7		
44	HD17156	65	5838.706	5838.769	5838.832	2011	10	4.21	10	4.27	10	4.33	4.89	6.40	7.91	37	44	48	0.71	0.77	0.83	4.94	6.45	7.96	4.9	6.4	7.9		
45	HD17156	66	5859.922	5859.985	5860.048	2011	10	25.42	10	25.49	10	25.55	10.06	11.57		46	40	33	0.92	0.99	0.05	10.13	11.64	-10.85	10.1	11.6	13.1		
46	HD17156	67	5881.139	5881.202	5881.265	2011	11	15.64	11	15.70	11	15.76				19	15	13	0.14	0.20	0.26	-8.67	-7.16	-5.65	15.2	16.8	18.3		
47	HD17156	68	5902.355	5902.418	5902.481	2011	12	6.86	12	6.92	12	6.98				19	25	32	0.36	0.42	0.48	-3.48	-1.97	-0.46	20.4	21.9	23.5		
48	HD17156	69	5923.572	5923.634	5923.697	2011	12	28.07	12	28.13	12	28.20	1.64	3.15	4.66	46	49	49	0.57	0.63	0.70	1.72	3.23	4.74	1.6	3.2	4.7		

Figure 4.03. Details for a specific BTE (HD 17156) for 39 consecutive transits at the author’s observing site.

This worksheet shows the information of the previous figure in row 11. It shows that the next transit, on 2009.11.24, is a better one since ingress can be included in an observing session in addition to mid-transit (with the cursor over a cell showing 8.13 UT) and egress.

This specific example illustrates how a long-term observing project for a specific BTE can be planned. An observer with several BTEs of special interest may want to create an “observing calendar” a month ahead, or longer, so that important events won’t come as a surprise, or won’t be missed due to social engagements.

Not all exoplanet projects are this straightforward. Trojan searches, for example, require that 1/6th of a period be added and subtracted from mid-transit time for making an observing schedule. I leave it to the reader interested in this to figure out how to do this.

As described in the previous chapter, there are many observing projects for amateurs interested in contributing to the study of exoplanets. Once basic skills have been “mastered” the simplest project is to choose a BTE and observe it every clear night regardless of when it is expected to undergo transit (OOT observing). This will provide a wealth of data for assessing systematic errors affecting light curve behavior with air mass and hour angle. It may also turn up an unexpected transit produced by a second exoplanet in the far off solar system. This observing strategy could also produce the discovery

CHAPTER 4 – BTE LIST

of a Trojan exoplanet. I recommend OOT observing for anyone who has the required patience and interest in understanding their telescope system, but I especially recommend it during the learning process (after doing a real transit, just for that emotional satisfaction).

Each person will have a favored observing style, and trying out the ones described in this and the previous chapter is a way to find which one is your favorite. Enjoy!

Chapter 5

Planning the Night

This chapter may seem “tedious” to someone new to exoplanet observing. However, keep in mind that the requirements for observing exoplanets, with a precision goal of ~ 0.002 magnitude, is significantly more challenging than observing variable stars, with precision requirements that are more relaxed by a factor of 10 or 20. Any amateur who masters exoplanet observing is working at a level somewhere between amateur and professional. Naturally more planning will be involved for such a task.

Probably all amateurs go through a phase of wanting to observe many objects each night. Eventually, however, the emphasis shifts to wanting to do as good a job as possible with just one object for an entire night’s observing. Exoplanets should be thought of this way.

This chapter describes ways to prepare for a night’s observing session. The specifics of what I present are less important than the concepts of what should be thought about ahead of time. Observers who are unafraid of floundering are invited to begin with a total disregard of the suggestions in this chapter since floundering “on one’s own” is a great learning experience. I encourage floundering; that’s how I’ve learned almost everything I know. You might actually conclude that what you learn first-hand agrees with my suggestions.

If you don’t like floundering, then for the rest of this chapter imagine that you’re visiting me in Southern Arizona for an instructive observing session. Together, we’ll plan observations that illustrate decisions that have to be made for a typical exoplanet transit. Let’s assume that it’s June 18, 2010 (local time) and you’ve asked me to show you how to observe an exoplanet transit.

In the afternoon we begin an “observing log.” This is an essential part of any observing session, and starting it is the first step for planning a night’s observations. We begin the log by noting the time for sunset. A table of sunset and sunrise times for any observing site can be created at a web site maintained by the U. S. Naval Observatory: http://aa.usno.navy.mil/data/docs/RS_OneYear.html. Moonrise and set times are also available at this site. CCD observing can begin about 55 minutes after sunset (at my latitude of 31 degrees). Sky flats are to be started at about sunset. The exact time for taking flats depends on the filters that are to be used, the telescope’s f-ratio, binning choice and whether a diffuser is placed over the aperture (treated in the next chapter). Filter and binning choices can’t be made until the target is chosen. That’s what we’ll do next.

Choosing a Target

Since we’re going to spend 6 or 8 hours observing, it is reasonable to spend a few minutes evaluating the merits of various exoplanet candidates. I will assume that you are not privy to one of those secret lists of possible exoplanet candidates maintained by professional astronomers using wide field survey cameras. (If you are such a member, then Appendix B was written for you.)

CHAPTER 5 – PLANNING THE NIGHT

We want to observe a *known* transiting exoplanet system, which means we’ll be checking the “bright transiting exoplanet” (BTE) list that was described in the previous chapter. If none are transiting tonight then we could either perform out-of-transit (OOT) observations of a BTE or observe an exoplanet system where transits *might* be occurring. This “might transit” category includes exoplanets currently on the NTE list (at TransitSearch.org), BTE Trojan searches and undiscovered second exoplanets in resonant orbits that produce shallow transits at unknown times (these categories are described in Chapter 3). Since you’ve asked to observe a transit we’ll be consulting the spreadsheet that I described in the previous chapter, called BTE_ephem.xls, that includes all 46 known BTEs (downloadable at http://brucegary.net/book_EOA/xls.htm). The second worksheet lists all transits available from my observing site for today’s date. Here’s some of what it shows for my observing site on the local time date of June 18, 2010:

A	B	C	D	E	F	G	H	I	J	K	L	M	N	O	P	Q	R	S	T	U	V	W	X
1			Darkness UT range	3.5	to	11.2																	
2	Today's Date:	6/17/2010	UT																				
3	Offset (days)	0																					
4	Target Date:	6/18/2010	UT																				
5			Local date at sunset:	6/17/2010																			
6	Exoplanet	UT Date	Ing	Mid	Egr	tot	Ing	Mid	Egr	EL	EL	EL	LHA	V-mag	D	L	RA	DEC			# in archive	AXA Priority	
7	1 CoRoT-1	6/18/2010				0	0	0	0													CoRoT-1	2 2
8	2 CoRoT-2	6/18/2010				0	0	0	0													CoRoT-2	14 1
9	3 CoRoT-3	6/18/2010				0	0	0	0													CoRoT-3	0 2
10	4 CoRoT-4	6/18/2010				0	0	0	0													CoRoT-4	0 2
26	20 HD 17156	6/18/2010				0	0	0	0													HD 17156	10 9
27	21 HD 209458	6/18/2010				0	0	0	0													HD 209458	7 1
28	22 HD 80606	6/18/2010				0	0	0	0													HD 80606	1 10
29	23 TrES-1	6/18/2010				0	0	0	0													TrES-1	28 1
30	24 TrES-2	6/18/2010	8.31	9.16	10.02	134	6	5	3	72	71	67	0.5	11.41	17.1	1.71	19:07:13.9	49:18:59			TrES-2	41 1	
31	25 TrES-3	6/18/2010				0	0	0	0													TrES-3	61 1
32	26 TrES-4	6/18/2010				0	0	0	0													TrES-4	9 2
33	27 WASP-1	6/18/2010				0	0	0	0													WASP-1	14 1
34	28 WASP-2	6/18/2010				0	0	0	0													WASP-2	23 1
35	29 WASP-3	6/18/2010				0	0	0	0													WASP-3	22 2
36	30 WASP-4	6/18/2010				0	0	0	0													WASP-4	1 3
37	31 WASP-5	6/18/2010				0	0	0	0													WASP-5	0 2
38	32 WASP-6	6/18/2010				0	0	0	0													WASP-6	0 1
39	33 WASP-7	6/18/2010				0	0	0	0													WASP-7	0 3
40	34 WASP-10	6/18/2010				0	0	0	0													WASP-10	9 3
41	35 WASP-11	6/18/2010				0	0	0	0													WASP-11	3 2
42	36 WASP-12	6/18/2010				0	0	0	0													WASP-12	7 1
43	37 WASP-13	6/18/2010				0	0	0	0													WASP-13	0 1
44	38 WASP-14	6/18/2010				0	0	0	0													WASP-14	9 1
45	39 WASP-15	6/18/2010				0	0	0	0													WASP-15	1 2
46	40 WASP-16	6/18/2010				0	0	0	0													WASP-16	0 2
47	41 XO-1	6/18/2010	5.92	7.37	8.83	296	8	5	3	84	66	47	1.8	11.19	23.4	2.91	16:02:11.6	28:10:11			XO-1	54 8	
48	42 XO-2	6/18/2010				0	0	0	0													XO-2	35 1
49	43 XO-3	6/18/2010				0	0	0	0													XO-3	23 1
50	44 XO-4	6/18/2010				0	0	0	0													XO-4	9 2
51	45 XO-5	6/18/2010				0	0	0	0													XO-5	14 1

Figure 5.01. Partial screen capture of BTE_ephem.xls for the author’s observing site on evening of 2010.06.17, showing that XO-1 will undergo a complete transit on this night (June 18, UT).

The “Figure of Merit” (column H) calls our attention to a full transit of XO-1. Ingress occurs at 5.92 UT (10:55 PM, local) when the target is at an elevation of 84 degrees. Egress occurs at 8.83 UT (1:50 AM, local), when elevation is 47 degrees. We note that the mid-transit depth is 23.4 mmag, and the object’s V-band magnitude is 11.19. The RA/DE coordinates for this object are conveniently displayed. The sky is clear, the wind is calm, and one of the easiest exoplanets is transiting tonight. Life is good!

Choosing a Filter

The subject of what filter to use is more complicated than most amateur exoplanet observers realize. There’s a well-established tradition of just using R-band for all observations, and I regret that I probably contributed to this belief in the First Edition of this book. I now recommend using a “clear

CHAPTER 5 – PLANNING THE NIGHT

with blue-blocking” filter, CBB filter, as the default choice. A few exceptions warrant using another filter, such as the “near infra-red” NIR filter, or a V-band or Ic-band filter. This is such an important topic that I have devoted an entire chapter to it (the next one). For now, just assume that you’ll be using a CBB filter. If you don’t have a CBB filter then use of a “clear” filter (or observe unfiltered).

Planetarium Program

TheSky/Six from Software Bisque is my favorite “planetarium program” (an unfortunate name, but that’s what these sky map display programs are called). We will use the program’s display of the night sky to find out the elevation of XO-1 during the night, and specifically during the predicted transit. We need to allow for acceptable elevations for the entire transit, from about an hour before ingress to about an hour after egress. Transits of “hot Jupiters” (large exoplanets orbiting close to their star) have transit lengths similar to XO-1, ~3 hours. The best observing situation is for mid-transit to occur at local midnight, but this rarely happens. We need to study XO-1’s elevation versus time for the 5 hours centered on mid-transit in order to be sure it is above the local horizon (e.g., trees).

Sunset occurs at 7:28 PM, so quality observing could start at ~8:23 PM (lower quality observations could start somewhat earlier). When quality observing can begin XO-1 will be at 60 degrees elevation, and rising. If observing began at 8:23 PM, 2.5 hours of data could be obtained before ingress. That’s good because it’s more than the one hour that we need. When XO-1 comes out of transit at 1:50 AM it will be at 48 degrees elevation; after another hour it will be at 36 degrees, and two hours after egress it will be at 24 degrees. Although observations should extend to at least an hour after egress, two hours is even better, so let’s plan on observing 2 hours after egress to be safe. Observations of XO-1 will therefore end at ~3:50 AM. TheSky/Six tells us that we will be able to obtain plenty of pre-ingress and post-egress data for establishing an out-of-transit baseline.

At this point in the planning process we have chosen a target, but reference star options have to be considered. This is the subject of the next section.

Deciding FOV Placement

Field-of-view (FOV) placement can be established before observing begins. My CCD (ST-8XE) has a second chip devoted to autoguiding, so it is important to determine which main chip FOV placement provides for a bright star within the autoguider’s FOV. This is where TheSky/Six is very helpful, as the next figure illustrates. It is a screen capture (inverted) of TheSky/Six with my main chip’s FOV centered on XO-1. (By the way, my FOV assumptions are based on Meade repairing my 14-inch LX200 telescope and returning it before they file for bankruptcy protection.) There are no bright stars in the autoguider’s FOV, so this positioning is unacceptable. By moving slightly to the right a sufficiently bright star can be used for autoguiding (V-mag = 11.3 according to TheSky). This improved positioning is shown in Fig. 5.03.

The next consideration is “what stars can serve as reference for XO-1?” There’s a bright star in the upper-left corner, but can it serve as a good reference star? To be a “good” reference star it should be about the same color as XO-1. Using TheSky/Six, a click of the mouse on XO-1, then a click on the star in the upper left, leads to the answer: XO-1’s J-K = 0.412 and the bright star’s J-K = 0.218. The bright star is bluer than XO-1 by $\Delta J-K = 0.194$. The bright star is also 1.38 magnitude brighter

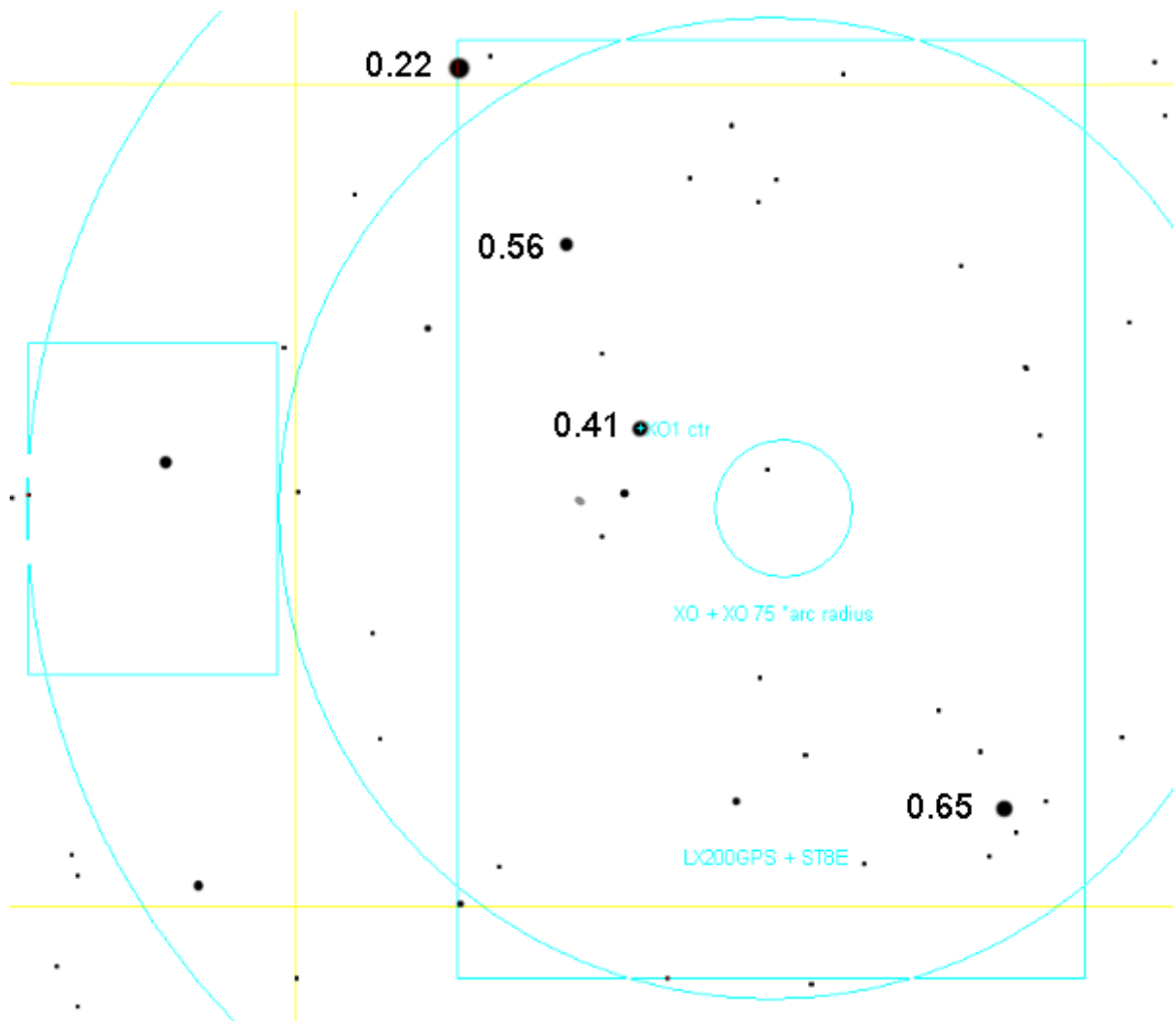


Figure 5.03. Colors (*J-K*) of *XO-1* and possible reference stars.

When there's a choice between using two reference stars versus using one, it is better to use two. Why? Mostly because of something called “scintillation” that is described in Chapter 20. The average of two stars will have root-2 smaller scintillation fluctuations than a single star, regardless of its brightness. Using 4 stars for reference is even better, as their average flux will exhibit $\frac{1}{2}$ the scintillation noise of a single star. So at this stage in our planning we should strive to position the FOVs in order to have as many stars as possible that are similar in brightness (and color) to the BTE.

We are fortunate that suitable reference stars are close to *XO-1*. What if the only stars near the target had greatly different colors? What options would we have for minimizing “star color” extinction effects (Chapter 19)? V-band and R-band would become slightly more attractive alternatives to CBB-band or clear (or unfiltered) in this case because of their narrower bandpasses. The narrower the bandpass, the smaller “star color extinction” effects are. Since *XO-1* is in a “friendly” star field we don't have to change our filter choice.

CHAPTER 5 – PLANNING THE NIGHT

At this stage in formulating a plan for the night we have decided on a target (exoplanet), we've decided on an exact placement of the CCD FOV on the star field, and we've tentatively adopted a filter (CBB). We need to save the exact FOV placement so that it is easily found when the observing session begins. This can be done by either screen capturing TheSky/Six's display for the chosen FOV placement (e.g., Fig. 5.03) or by creating a new "object" in TheSky/Six "User Defined Data" list using RA/Dec coordinates for the FOV center.

Binning

At this point in planning we know an air mass range, so an inference can be made about the sharpest "atmospheric seeing" during the observing session. We next consult the ClearSkyClock at <http://www.cleardarksky.com/> to learn that "average seeing" is expected for the night. In order to know if it is safe to observe with 2x2 binning (instead of 1x1) we need to calculate the sharpest seeing expected during the observing session. At my site FWHM is typically 2.5 "arc at zenith. XO-1 passes overhead, close to zenith, so the smallest air mass is ~1.0. For this case it is not necessary to make use of the relationship that FWHM is proportional to $\text{AirMass}^{1/3}$ (cf. Chapter 10), because we already know that 2.5 "arc seeing can be expected during the observing session. Since this is a median seeing near zenith there will be images that are sharper, so we must accommodate seeing as good as maybe 2.0 "arc. A plate scale of 0.8 "arc or smaller could be used without serious degradation to photometry precision (referring to the rule of thumb that there should be at least ~ 2.5 pixels per FWHM in order to assure high precision light curves). Since my 1x1 plate scale is 0.67 "arc we can't bin 2x2. We note in the observing log that we plan on 1x1 binning.

Why try to observe 2x2 instead of 1x1? There are two reasons. Modern CCD chips perform "on-chip" binning, and they have less "read noise" for 2x2 binned images than unbinned images. The component of "readout" noise is reduced by a factor two for 2x2 binning. This can be explained by recognizing that since there is only one readout for a 2x2 reading versus 4 readouts for reading the same 4 individual pixels; since noise grows as the square-root of the number of readouts the single reading versus 4 readings means there is half the readout noise for the 2x2 image. The second benefit for 2x2 binning is that download times are 4 times faster (e.g., 2 seconds instead of 8 seconds), and this improves the percentage of time spent collecting photons during an observing session (cf. Chapter 20-). Knowing whether binning is going to be used affects when flat frame exposures of the twilight sky can begin. If 2x2 binning is chosen for the night's observing, scheduling of flat frames would have to be made later than for the case of unbinned imaging (as explained in Chapter 8).

Finalized Plan

In the observing log we note that the goal for the night is an XO-1 transit and we include the ingress and egress times. We note that a CBB-band filter will be used, and binning will not be employed. We don't know when to start flat fields yet, but we know it will be close to sunset. No configuration changes were made since the previous observing session, and that's noted in the observing log.

We have time before observing begins, so how about joining me for dinner at Delio's Pizza, a few miles from my place. Besides, every observing session can benefit from pizza snacks, a dark beer and observing music!

CHAPTER 5 – PLANNING THE NIGHT

There are two more things we have to decide before we can go to dinner, however: the filter choice reassessment, and scheduling flat field observations. Reassessing our default choice of a CBB-band filter is the subject of the next two chapters.

Chapter 6

Atmosphere Tutorial

You are probably wondering why an entire chapter is devoted to the atmosphere. It provides a background that serves two purposes: it will help in selecting a filter to use for a specific observing session, and it will be referred to in a later chapter that describes the importance of selecting “same color” reference stars.

The “atmosphere spectrum” of zenith extinction and sky brightness (without moonlight) is a good starting place.

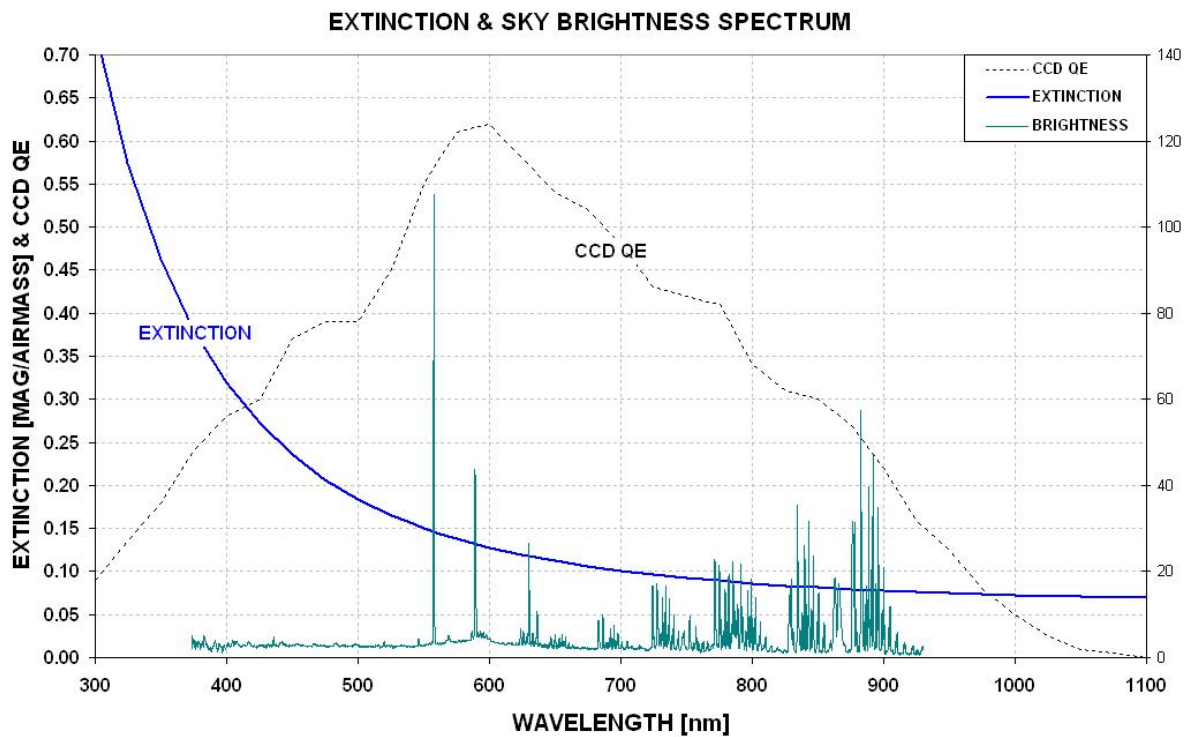


Figure 6.01. Extinction (thick blue trace) has constant and Rayleigh components that cause greater amounts of absorption at short, blue wavelengths. For a typical CCD (KAF1602E, found in the SBIG ST-8XE) quantum efficiency (QE) peaks at about 600 nm. Atmospheric emission (aqua trace) has a wealth of “sharp” emission lines produced mostly by molecules in the upper atmosphere (airglow), which combine with other broad spectral sources produce a “sky brightness” spectrum, which is plotted using an arbitrary scale on the right (based on monitoring measurements on moonless nights at Kitt Peak and Mount Hopkins, published by Massey, Gronwall and Pilachowski, 1990, and modified here to have units of flux per wavelength interval).

Let’s consider the difference between atmospheric absorption (extinction) and sky brightness, both of which ground-based astronomers try to avoid. The atmosphere has three principal extinction components (in the visible region): 1) Rayleigh scattering by molecules (that are smaller in size than

CHAPTER 6 – ATMOSPHERE

light wavelengths, so they scatter short wavelengths much more strongly), 2) Mie scattering by aerosols (dust) that is approximately constant for all wavelengths (since most particles are larger than light wavelengths, so they just block and reflect light), and 3) resonant molecular absorption (by oxygen, ozone and water vapor). The first two components are more important than the third. The thick blue trace in the above figure is an empirical fit to absorption, also called extinction, at my observing site (at 4670 feet altitude).

If a flashlight is pointed upward the sky brightens, but it doesn't become more absorptive. This may help explain why the air can glow at a specific wavelength, due to some chemical reaction between two molecules, yet light from stars at the same wavelength won't be absorbed any more than at nearby wavelengths. Some features of the "sky brightness" trace in the previous figure are due to molecules that both absorb and emit. For example, oxygen molecules absorb and emit at 558 nm. This accounts for the brightest, sharp line feature in the sky brightness trace (Fig.6.01). At about 595 nm, however, is a broad feature due to high-pressure sodium lamps from nearby towns. This component of light doesn't contribute to absorption but it is something to be avoided in the interest of minimizing the sky background level in CCD readings.

The next figure shows where the standard filter passbands are located with respect to the atmospheric absorption and emission spectrum.

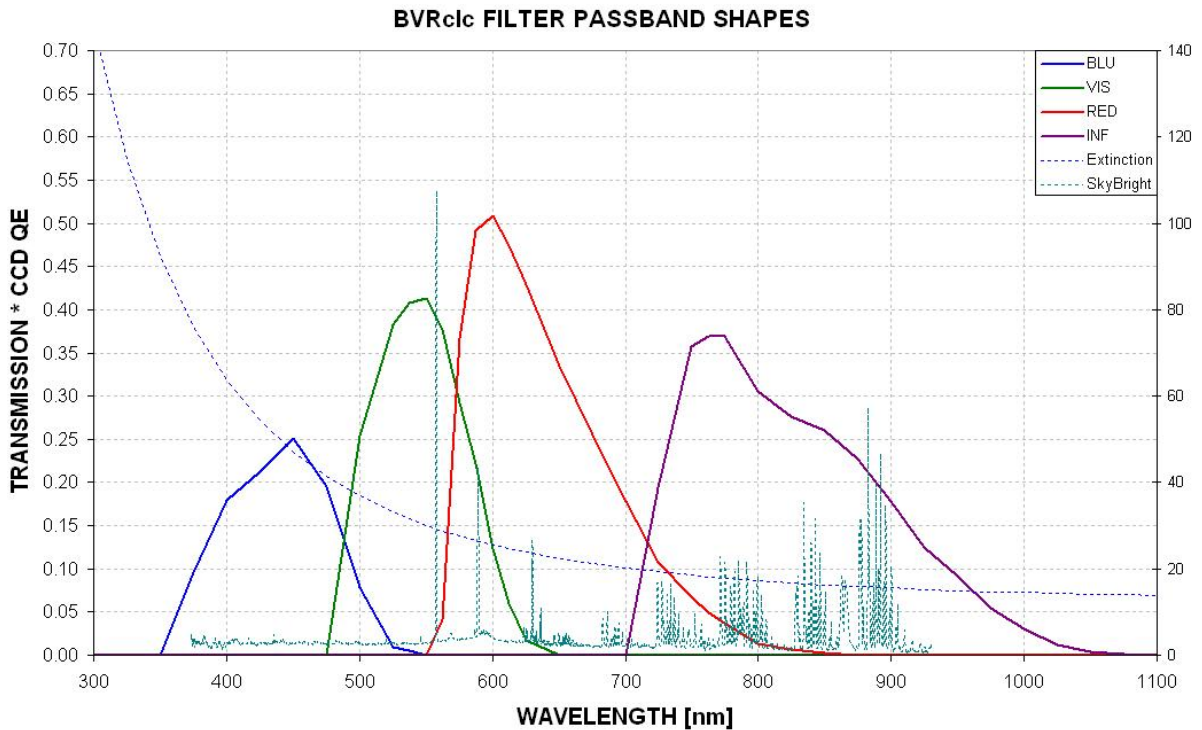


Figure 6.02. Filter response functions, multiplied by a typical CCD's *QE* function.

This plot shows, for example, that high pressure sodium lamps (broad feature at 595 nm) will affect the sky background level when using an R-band filter, which is something to keep in mind if you live near one of these lamps. The same lamps also affect V-band observations since both V-band and R-band overlap this annoying emission feature. The bright oxygen emission at 558 nm is within the V-

CHAPTER 6 – ATMOSPHERE

band region, but it's so narrow that it doesn't contribute significantly to the sky background level or to extinction. The I-band region contains many small air glow emissions, mostly from OH molecules.

This book promotes the use of a blue-blocking filter. The corresponding response function is what I shall refer to as CBB-band (“clear with blue-blocking”), shown in the next figure.

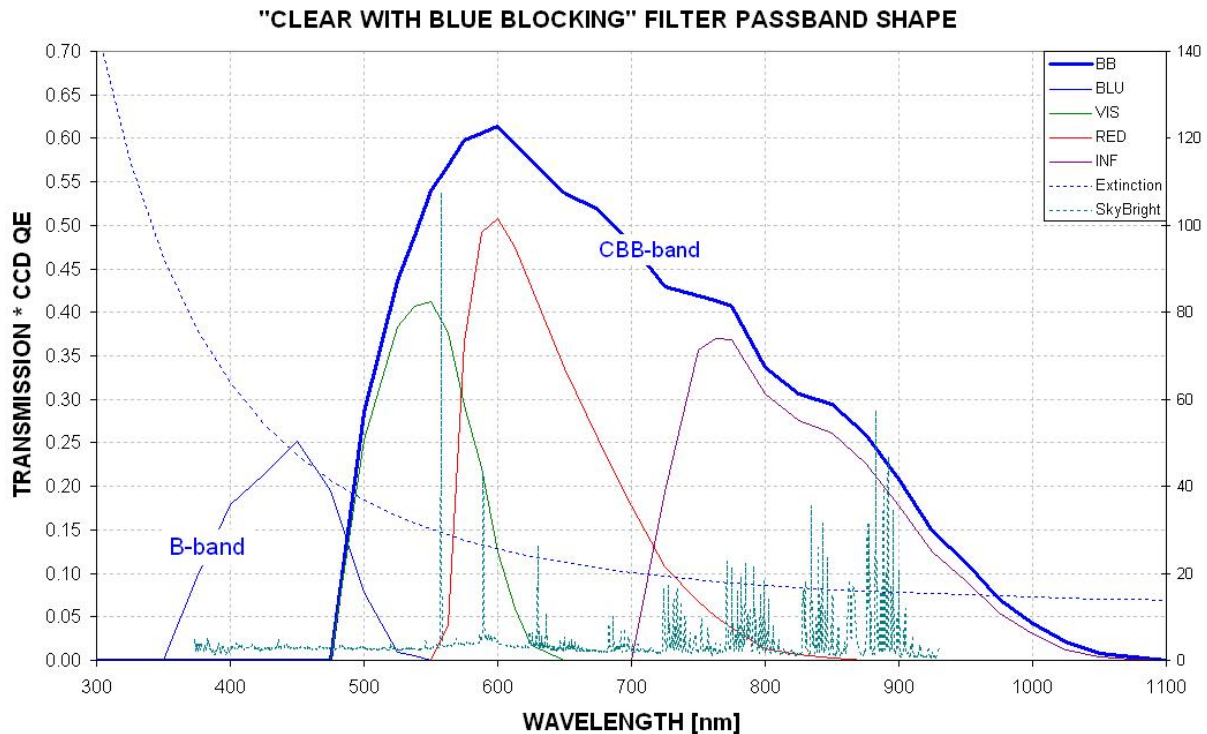


Figure 6.03. A clear filter with blue blocking (CBB-band) response function including CCD quantum efficiency function. A CBB filter “turns on” at the same wavelength as the V-band filter, but it then continues to transmit photons at all longer wavelengths. In other words, CBB-band merely blocks most of the B-band photons.

CBB-band has the advantage that it experiences much less atmospheric absorption than a clear filter (or no filter) while sacrificing only a small amount of total flux that could be registered by the CCD. For a typical star the loss of flux is only $\sim 7\%$. As will be explained in a later (Chapter 19) the CBB-band has an additional advantage, related to the desire to use stars for reference that have different colors similar to the target star.

Atmospheric extinction is a more important consideration for amateurs than sky brightness. This is due partly to the fact that amateurs don't cool their CCDs to the same cold temperatures achieved by professionals (who use liquid nitrogen). Amateurs, therefore, deal with noise levels dominated by thermal emission by the CCD, and sky background is usually less important (except during bright, moonlit nights – to be discussed later). Because atmospheric extinction is more important than sky brightness, let's consider Rayleigh scattering and aerosol absorption in greater detail.

Rayleigh scattering is proportional to the total number of molecules along a line-of-sight (since saturation doesn't occur), so this component of atmospheric extinction should vary with observing site altitude (as well as air mass). The following figure shows what can be expected for zenith extinction due only to Rayleigh scattering at three observing altitudes.

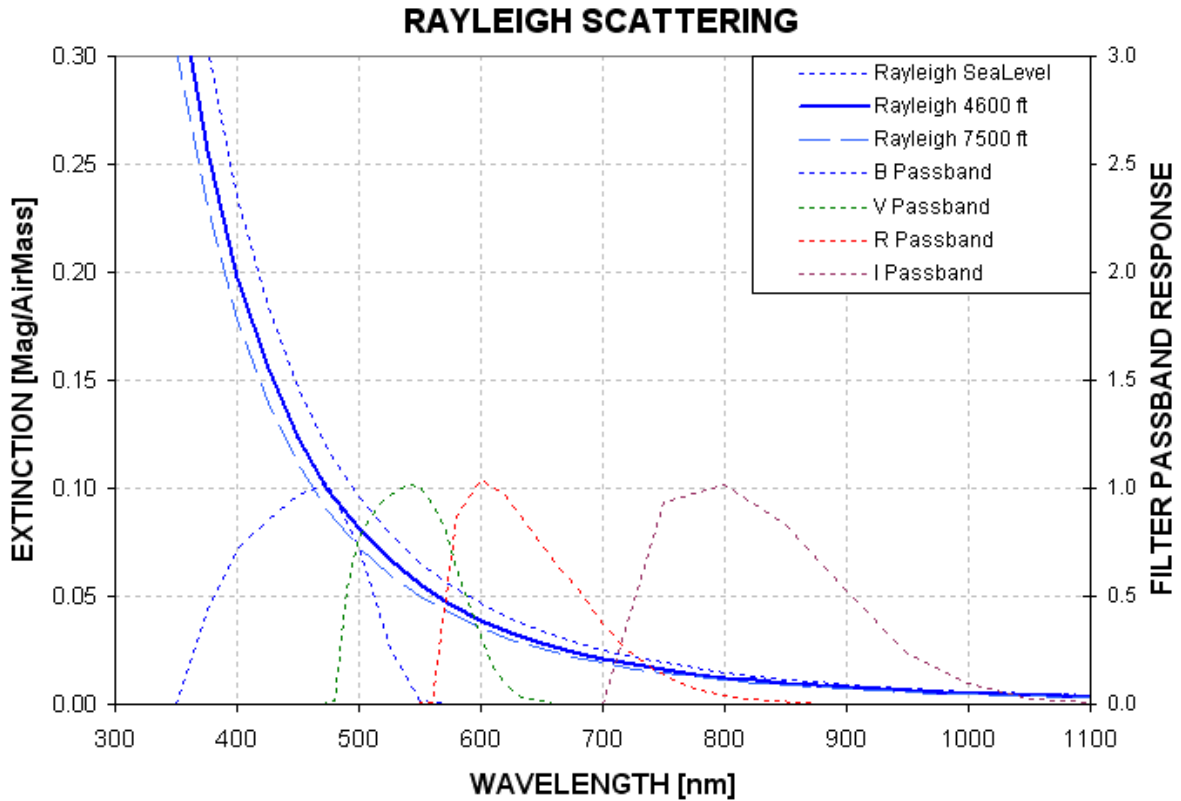


Figure 6.04. Atmospheric Rayleigh scattering at wavelengths where CCD chips are sensitive for three observing site altitudes. Filter spectral response shapes are shown for B, V, R and I (Custom Scientific BVRcIc filters and KAF1602E CCD chip, normalized to 1). The Rayleigh scattering model is based on an equation in Allen's *Astrophysical Quantities*, 2000.

Notice how much Rayleigh scattering varies throughout the B-filter response region; the greatest scattering (at 350 nm) is 5 times the smallest (at 550 nm)! High altitude observing sites have only slightly lower values of Rayleigh scattering than typical amateur sites.

What about the aerosol (dust) component of extinction. The following figure shows aerosol Mie scattering versus altitude for three wavelengths. (It is customary for "Mie scattering" to refer to the situation of the particle circumference being much greater than wavelength). A model fit to this data allows for the conversion to scattering versus wavelength for specific altitudes. Dust has a much greater dependence upon observing site altitude than Rayleigh scattering. This is clearly seen in Fig. 6.06, which also includes the Rayleigh scattering component. It should be noted that for B-band both scattering components are about the same. For I-band the only scattering component that's important is aerosol Mie scattering.

CHAPTER 6 – ATMOSPHERE

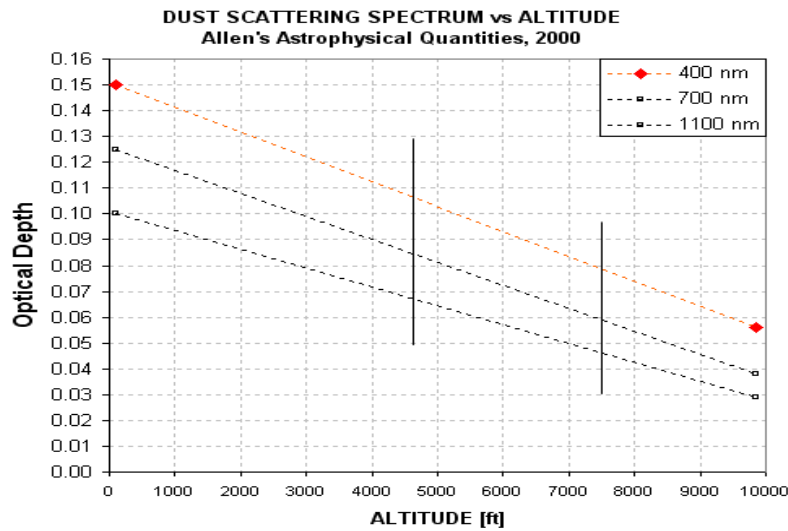


Figure 6.05. Atmospheric aerosol (dust) Mie scattering versus observing site altitude for three wavelengths (based on a global model by Toon and Pollack, 1976, cited in Allen’s Astrophysical Quantities, 2000).

In Fig. 6.06 the amplitude of the aerosol component was adjusted slightly to provide a fit to measurements made at my 4670-foot altitude observing site.

Atmospheric pressure at a given observing site varies within a narrow range of $\pm 2\%$, typically, and the Rayleigh component at each site should vary within this same narrow range. Aerosol burdens vary by much larger amounts, so day-to-day changes in total extinction are driven mainly by aerosol changes. Seasonal extinction patterns are mostly determined by seasonal patterns of aerosol burden. Volcanic ash lofted to the stratosphere, where it will reside for many months, can produce large temporary aerosol scattering events.

It should be possible to use I-band extinction to infer extinction at the shorter bands. The opposite is less true since it’s difficult to infer I-band extinction from a B-band extinction measurement (since B-band extinction is dominated by Rayleigh scattering).

Observers at different altitudes will have different levels for both Rayleigh and aerosol scattering. This is shown in Fig. 6.07 using a model for both atmospheric pressure and seasonal-average aerosol burden versus altitude. Going from sea level to 7500 feet, for example, the long wavelength total extinction decreases by a factor two. The B-band extinction changes is less dramatic because aerosol scattering, which changes by large percentages, is a minor component of total extinction and the Rayleigh scattering component changes by only 24%.

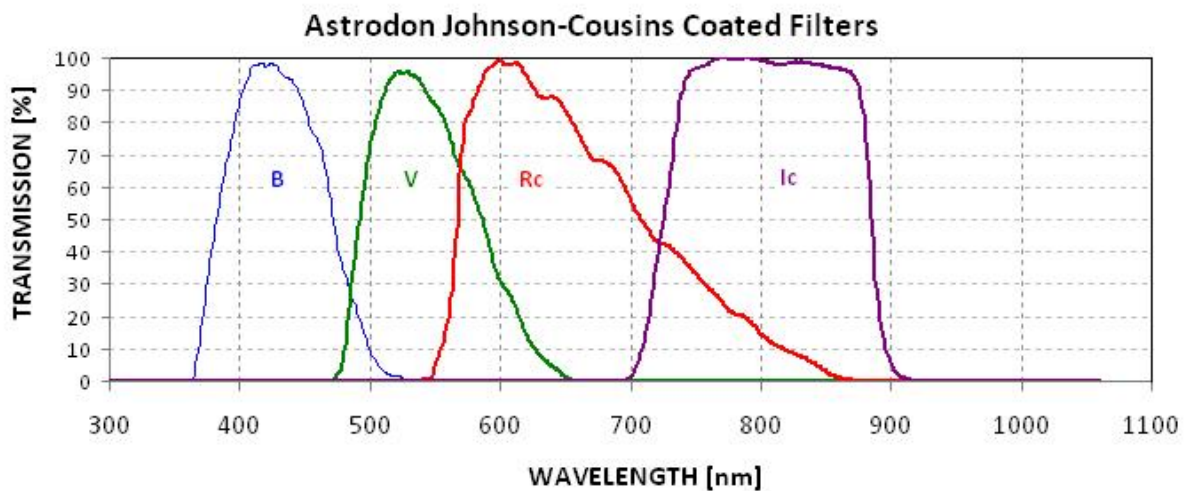
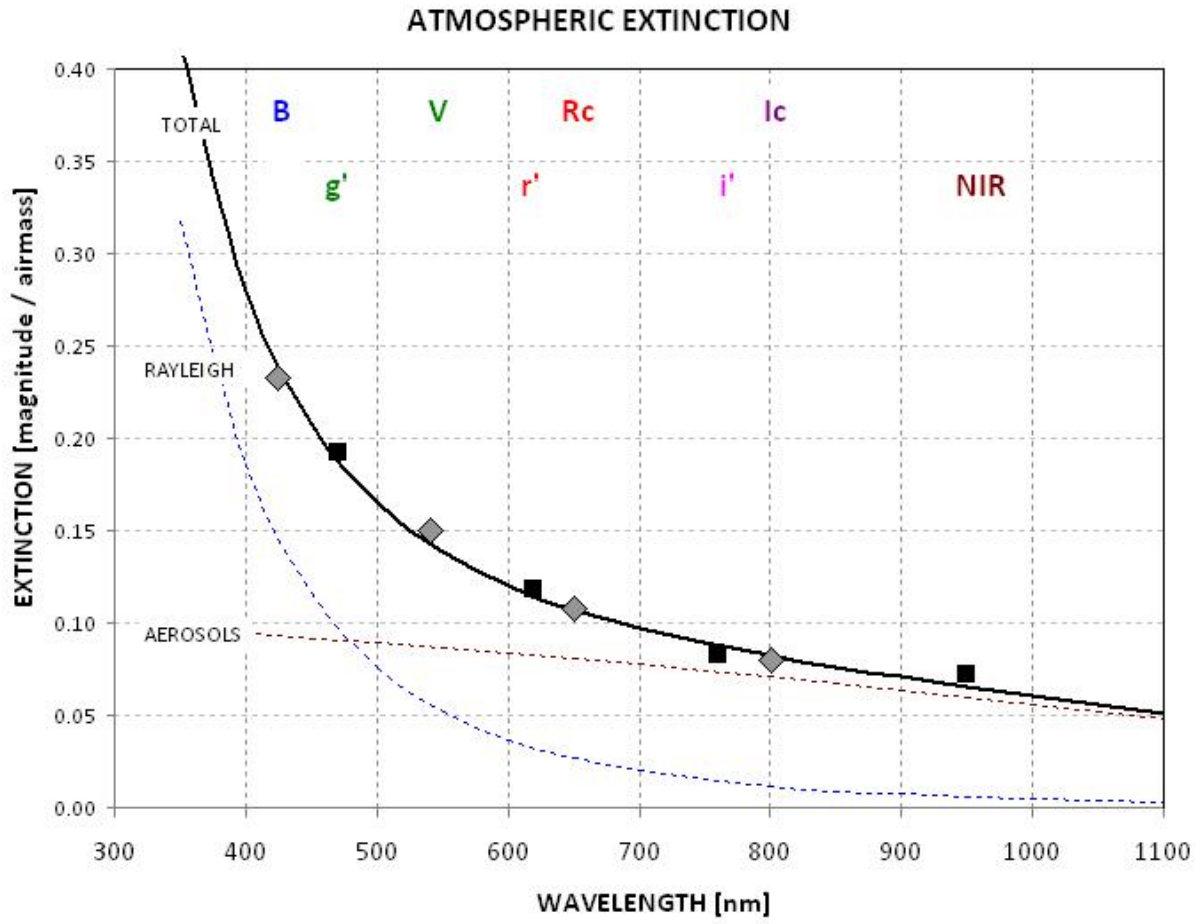


Figure 6.06. Atmospheric extinction (Rayleigh plus aerosol components) compared with measurements using BVRcIc, g'r'i' and NIR filters (top panel) at my observing site (4670 feet altitude). Lower panel shows transmission functions for the Astrodon BVRcIc filter set.

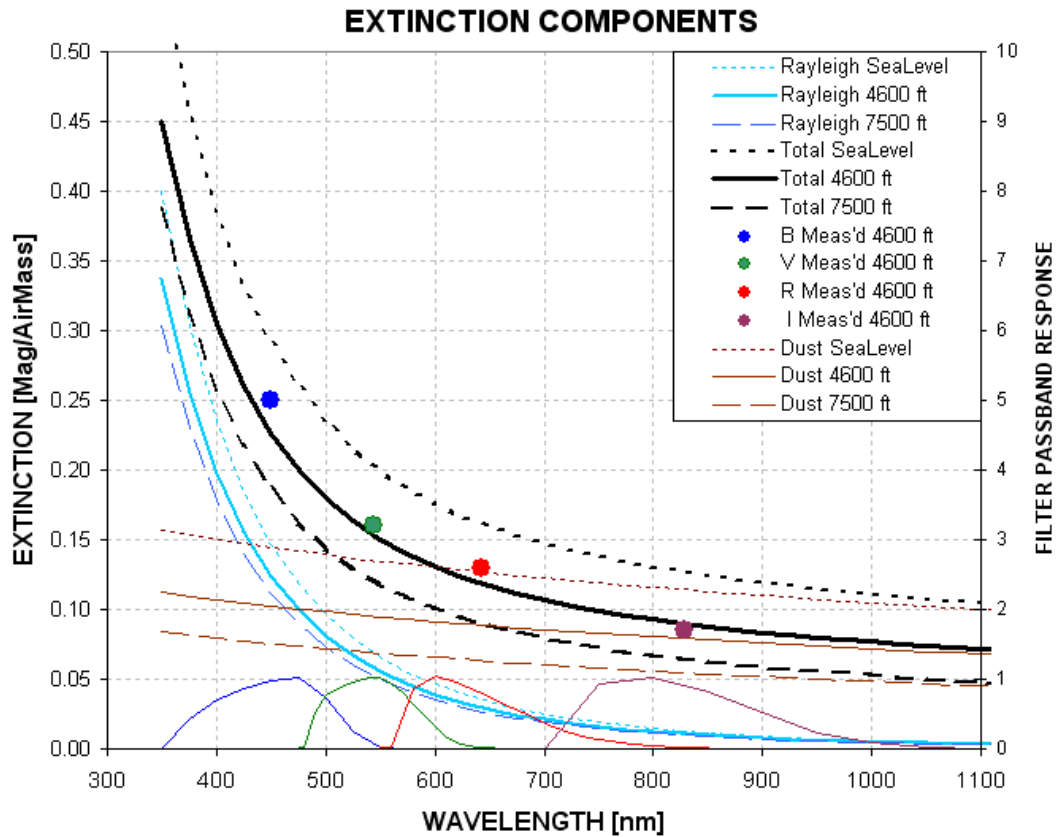


Figure 6.07. Atmospheric total extinction components (Rayleigh scattering and aerosol scattering) for a selection of altitudes. Typical measured extinction coefficients for BVRcIc at my site are shown as large filled circles (seasonal average).

It should be noted that the smooth extinction traces in these two plots do not include a few narrow-band molecular absorption lines. For example, water vapor has a moderately strong absorption at 935 nm (from 895 to 980 nm), but the equivalent width of the feature (at airmass = 2, mid-latitudes) is less than 4% of the width of some Ic-band filters (and is excluded by the Astrodon Ic-band filter). These absorption lines are within the z' and NIR-band filters, but the equivalent width is again small in comparison to the entire bandpass of those filters and is unlikely to produce noticeable effects for amateur observers. Oxygen has a narrow absorption feature at 760 – 766 nm, but the equivalent width is small in relation to the Rc and Ic bandpasses and the absorption is fairly constant with time.

Imagine changes in only the aerosol component and the effect these changes will have on total extinction at the various filter bands. Total extinction for all bands will move up and down together, and these movements will be slightly larger at short wave bands than long ones. This is illustrated in Fig. 6.08, where it is shown how a g'-band extinction can be used to predict extinction at other bands.

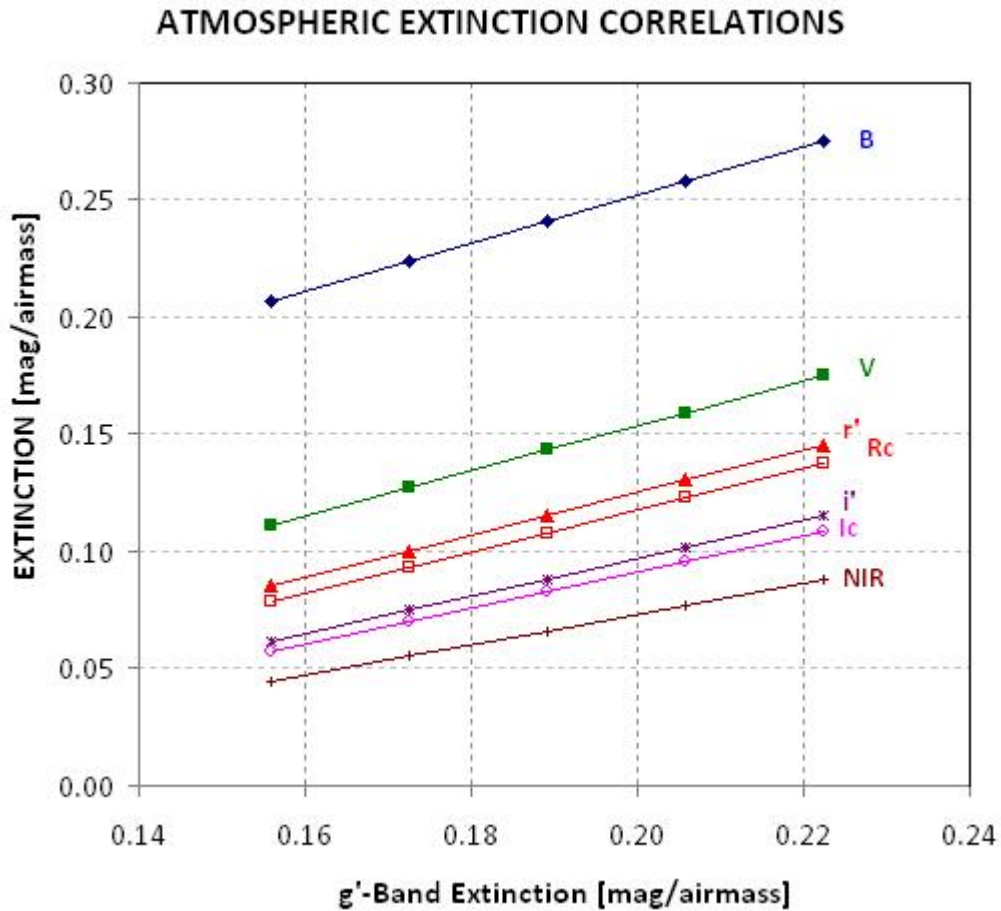


Figure 6.08. When only aerosol scattering changes it is possible to predict extinction at other bands than the one being measured, which is g' -band for this illustration.

My several-year records of extinction measurements with BVRcIc filters show a similar (though noisier) pattern like the ones in Fig. 6.08. One of my future goals is to determine how reliable the method is for using one filter band's extinction to predict the others. Since my site has the highest extinction in June, just before the monsoon “cleans the atmosphere,” this figure can have month notations along the x-axis to facilitate extinction estimations when no observations are available.

This chapter's background on the atmosphere is needed for the next chapter's discussion of selecting a filter before observing begins.

Chapter 7

Filter Choices

You are probably wondering why an entire chapter is devoted to the matter of which filter to use for a specific observing session. Until recently the most common filter choices were B, V, Rc and Ic, whose transmission functions are shown in the top panel of the following figure.

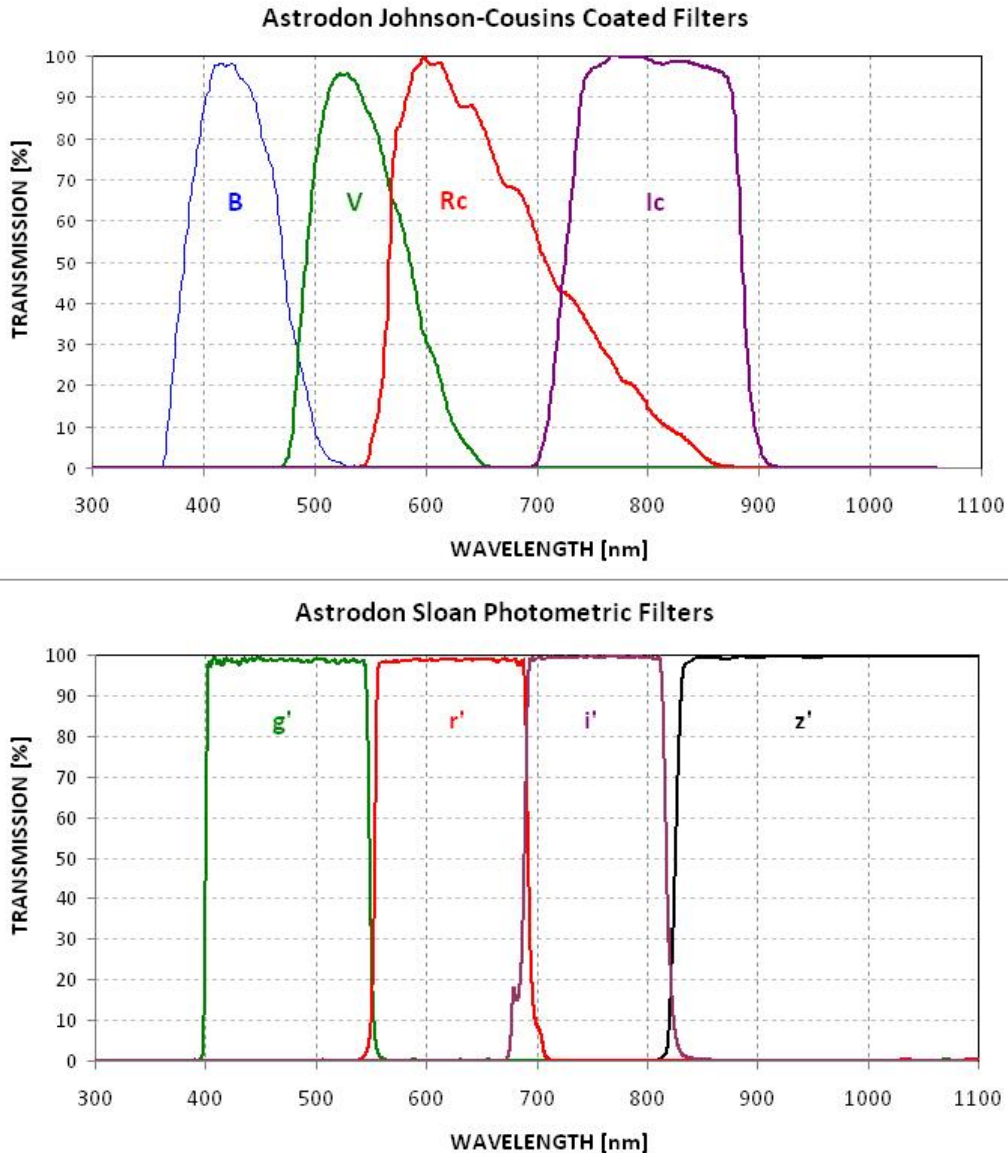


Figure 7.01. Filter transmission for the two main filter set choices (transmission functions were kindly provided by Don. S. Goldman, PhD, Astrodon Imaging, Orangevale, CA).

CHAPTER 7 – FILTERS

Most amateur observers now use an R-band filter for all their exoplanet transits, and they produce good quality light curves. So what’s wrong with just adopting R-band for all exoplanet observing? The simple answer is that “it’s not optimum for most situations.”

Now we have the additional filter choices of g' , r' , i' and z' . This is the so-called SDSS filter set because they were designed on behalf of the Sloan Digital Sky Survey. Passband responses for the SDSS filter set are shown in the lower panel of Fig. 7.01.

Two more filters should be considered for exoplanet observing: CBB and NIR. The spectral transmission shapes for these filters is shown in Fig. 7.02. (The CBB filter is manufactured and sold by Custom Scientific; a CBB is also manufactured by Astrodon and sold by Adirondack Astronomy with a product name XOP-BB, www.astrovid.com). The CBB filter is similar to a clear filter because it passes about 93% of a typical star’s light, but it has a “turn-on” wavelength of about 480 nm, the same as a V-band turn-on. The NIR filter (Near Infra-Red Luminance, manufactured by Astrodon) is similar, as it passes wavelengths longer than ~ 710 nm, but only about 32% of a typical star’s light is at these long wavelengths. Both CBB and NIR are useful for two main reasons: 1) they block blue light, thus reducing sky background levels when the moon is up, and 2) the light they pass has smaller atmospheric extinction than a clear filter, thus enabling an observing period to be extended to times when elevations are very low.

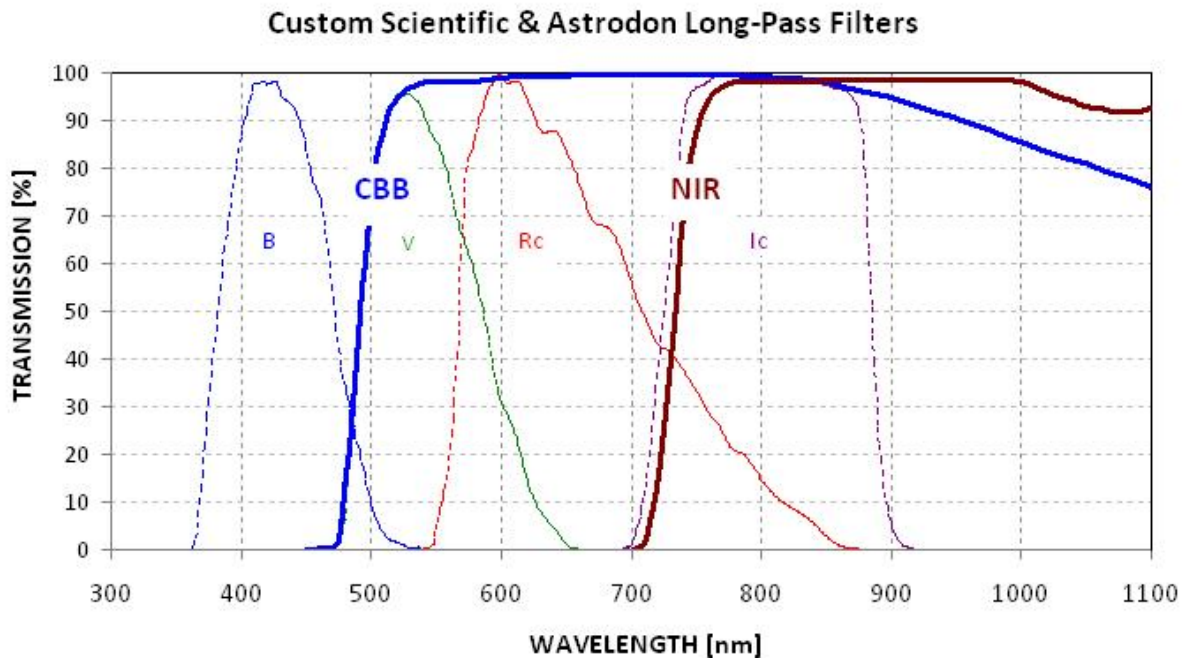


Figure 7.02 Long pass filter transmission functions. The Custom Scientific CBB passes longward of ~ 480 nm and the Astrodon “NIR Luminance” filter passes longward of ~ 710 nm.

My first exoplanet transit observation was made with a V-band filter because that’s what a professional astronomer recommended. I didn’t give much thought to the matter, until maybe a year later when I noticed that R-band produced light curves with better SNR. R-band then became my default filter choice. I had a “clear” filter (parfocal with the others), but I only used it for the faintest

CHAPTER 7 – FILTERS

BTEs. My thinking at the time was that R-band had fewer systematic effects than the clear filter but for very faint BTEs systematic effects were less important than the need to simply “detect” the transit.

Two years ago, when I wrote the First Edition of this book, I included (in Chapter 14 of that edition) a demonstration of the effect of using reference stars that were redder or bluer than the target star for images made with a clear filter. In one case the light curve was “bowed” upward, symmetric about transit, and in the other case the bowing was downward. The measured “air mass curvature” effect was consistent with the explanation that without a filter the effective wavelength of a star could shift enough to cause blue stars to exhibit larger atmospheric extinction than red stars. I concluded that it was “dangerous” to observe exoplanet transits unfiltered (or with a clear filter).

Calculations (described in the First Edition) showed that a filter that blocked blue light should have significantly smaller “air mass curvature” since most of the blue star’s greater extinction was due to just the blue component of its light. I therefore recommended use of a blue-blocking filter, or CBB filter, which “turned on” at the same wavelength as a V-band filter (~ 480 nm) and never “turned off” at longer wavelengths. By not filtering out long wavelength light the CCD’s reduced response at longer wavelengths determined the spectral response function of the filter/CCD combination. CBB-band, as I refer to it, removed only about 7% of a typical star’s light, yet my calculations showed that it should reduce systematic effects by about a factor of 7.

At the time I wrote the First Edition I hadn’t verified with observations the merits of using a CBB filter, and I mistakenly allowed the impression to exist that the R-band filter should be the default choice for exoplanet observing. During the last two years I have seen the merits of observing with a CBB filter (and also unfiltered, when I was “forced” into a backend optical configuration that couldn’t accommodate a CFW) and this caused me to revive interest in the CBB-band option, as well as NIR as a new option. I am now able to make the following statement:

**A “clear with blue-blocking” filter (CBB)
should be an amateur’s default choice for exoplanets.**

And I will expand on this by also stating that:

**A “near infra-red” filter (NIR)
should be used when observations at low elevations are necessary
or when a nearly full moon is above the horizon.**

The CBB filter has most of the high SNR advantages associated with unfiltered observing, yet it has most of the reduced systematics advantages associated with V-band and R-band observing. For most BTEs (those fainter than 10th magnitude), and for most telescopes (smaller in aperture than ~ 16 inches), I recommend that CBB-band be the first filter that you consider using. The most important exceptions are when a complete transit requires observing at low elevations or when a nearly full moon is causing bright sky backgrounds, for which the NIR filter is to be preferred.

So why would a professional astronomer recommend observing exoplanets with a V-band filter (or I-band, or even the longer wavelength of z-band)? It’s because they use large aperture telescopes that afford plenty of photons, and even with a narrow band filter their SNR is large. For the professionals, therefore, the SNR loss associated with a filter as narrow as V-band is a small penalty that’s worth the

CHAPTER 7 – FILTERS

benefit of reduced systematics. I am frequently reminded that professional astronomers take for granted the large collecting area that their large aperture telescopes afford, and they forget the plight of us amateurs trying to work with maybe 5% of their photon plenitude.

When the question of what filter to use is addressed by observers experienced with AAVSO type observations it is natural for them to think in terms of which filter affords the best possibility for inter-comparison between observers, as if two or more observers will be needed to create an exoplanet transit light curve. I know of only one case where this has been a valid concern in the past: the 2009.02.13 transit of HD 80606, which lasted ~ 12.6 hours and therefore required more than one observer's data for piecing together a transit light curve. With a standard filter, such as V-band, adjustments can be made for telescope system star color systematics (i.e., CCD transformations) so that each observer can present their portion of the transit light curve using a standard magnitude system to facilitate comparison with data from other observers.

Before you conclude that using V-band (or R- or I-band) filters are a good idea because it allows many observers to combine their portions of a light curve, consider the following. This BTE has a period of 111 days, the longest for any known transiting exoplanet. No other exoplanet has such a long transit (with so few opportunities for characterizing transit properties), so this is a rare example of when special attention should be paid to the use of standard filters. Note that among the 5300 transits that occur during a typical year, only 3 of them (0.06%) are by HD 80606. Of the 46 known BTEs all except HD 80606 have transit lengths less than 4.6 hours. The median transit length of the presently known 46 BTEs is 2.91 hours, and the median interval between transits is 3.08 days. Single observing sessions can produce data for a complete transit on many occasions each year for 98% of the known BTEs. The AXA has very few transit events that were observed simultaneously by two or more observers at significantly different longitudes. The need for inter-comparing data from many observers is essentially non-existent, so the argument for using standard filters (BVRcIc) that can be "CCD transformed" to standard magnitudes has negligible validity for observers of exoplanet transits.

Another argument that has been presented for using one of the standard filters instead of a broad bandpass filter (such as clear or CBB or NIR) is that the broad bandpass filters have large "throughputs" (lots of photons), and this requires short exposures, which in turn mean that each short exposure image will suffer from large scintillation noise. This complaint is baffling since the effect of scintillation on the average of 10 short exposures is the same as the scintillation of one exposure 10 times as long. The scintillation argument is frequently misunderstood, as it is also used to argue for the benefits of defocusing – which I will address in a later chapter (it's a false argument). Scintillation needs to be considered in terms of its effect on a "per observing session unit of time" basis, not its effect on single exposures, so whenever you hear about the need for something on the basis of scintillation, pause and ask yourself if the argument makes sense.

Another argument for sticking with V-band is that R-band filters, as well as CBB and clear, include H-alpha emission from stars, which has been found to vary for some stars. Recall that H-alpha emission occurs at 656 nm, and its ~ 0.1 nm wide (i.e., it constitutes 0.05% of the R-band width, and < 0.02 % of the CBB and clear filter width).

A statistical analysis of the Amateur Exoplanet Archive, which now has over 640 entries by amateurs, shows a preponderant preference for the R-band filter. 53% of the AXA data submissions employed an R-band filter, and 26% use a clear filter (or CBB filter, or are unfiltered). In other words, 83% of

CHAPTER 7 – FILTERS

observers chose either an R-band or clear type filter (all of which include the H-alpha emission line), while only 11% chose a V-band filter. (Ironically, the V-band observations at AXA have the greatest percentage of poor quality light curves.) V-band filters may serve the professionals well, but amateurs have shown a preference for using R-band as a first choice (and C or CBB for second choice), and there can be little doubt that these choices have produced a wealth of useable exoplanet transit light curves.

Not every observing situation is best served by using the CBB and NIR broadband filters that I recommend as default choices. These exceptions will call for use of one of the standard filters (BVRcIc) or even a SDSS i' or z' filter. Here's my list of those exceptional situations:

- 1) One is when the BTE is very bright, such as V-mag ~ 7.7 (HD 209458 and HD 189733). These stars are so bright that SNR is actually “too high” for apertures greater than ~ 4 inches, requiring very short exposures, which cause poor duty cycles (described later). For these bright stars amateurs should consider using one of the standard filters, such as V, Ic or z' . Among these alternatives my favorite is the z' filter. An alternative to changing filters is to observe defocused, which is discussed in Chapter 9.
- 2) Another situation for not using a CBB filter is when the BTE is very red, or very blue, leading to the probable situation that reference stars can't be found that have a star color similar to the BTE. The reddest BTE is GJ 436 (B-V = +1.52), and the bluest is HAT-P-6 (B-V = +0.34). These would be BTEs for which the CBB filter may not be as good as one of the following (provided the star is sufficiently bright): NIR, V, R or Ic-band, or g' , r' and i' .
- 3) The third situation for using a different filter from CBB (or clear) has already been mentioned: when a nearly full moon is above the horizon causing the sky background to appear to be bright. Notice that I used the word “appear.” At night we can't notice that a bright full moon sky is actually blue, just like the daytime sky (only less bright). Using a long wavelength filter, such as Ic, i' or NIR, should be considered for all nights when a nearly full moon is above the horizon, and especially when it is near the target.
- 4) High air mass observing should be done with one of the long wavelength filters: Ic, i' , z' or NIR. Atmospheric extinction is lowest at z' -band, and even quite low at NIR-band. If the target star is faint then CBB may still be preferred because of its greater “throughput” (flux).
- 5) As stated above, HD 80606 has transits longer than any single observing session, which means that data from two or more observers have to be combined to characterize a full transit. For this one BTE it is recommended that one of the standard filters be used, so that CCD Transformations Equation corrections can be applied to produce magnitudes on a standard scale. These are rare events, occurring no more often than three times per year.

I will mention a couple rare situations that are best handled by using a filter other than the CBB filter. Shortly after discovery of an exoplanet there is value in knowing whether or not transit depth decreases or increases with wavelength. This information provides a constraint on the geometry of the transit chord with respect to the star's disk. When the transit chord has a closest approach to the star center that is less than ~ 0.7 times the star's radius (which is the case for most exoplanets) transit depth will decrease with wavelength. When the chord is farther from star center, such as for a grazing

CHAPTER 7 – FILTERS

transit, transit depth will increase with wavelength. This pattern is due to limb darkening being greater at shorter wavelengths. For this case transit depth should be measured using a wide spacing of wavelengths, such as B and Ic, or g' and i'.

The other situation calling for a filter other than CBB or unfiltered is when the goal is to monitor transit timing variations, TTV. The purpose for producing high-quality TTV might be to search for anomalies produced by another planet in a resonant orbit, or to search for an exomoon of the known exoplanet. TTV can be done best when there are sharp transitions from OOT (out-of-transit) to ingress and from egress to OOT. Referring to the light curve on the cover of this book, the desire for “sharp” transitions means we want the brightness change at contact 2 and 3 to be as deep as possible, thus causing the slopes to be steeper. This occurs when limb darkening is small (when the star’s brightness is almost as great near the limb as at the center). And for a typical star this is the situation at long wavelengths. Therefore, the “sharpest” ingress/egress transitions are observed with such filters as (listed in order of improved sharpness): I-band, i'-band, NIR-band or (best of all) z'-band.

In support of item 4, above, I once observed an exoplanet transit with an I-band filter until it abruptly set behind a nearby mountain at an elevation angle of 7 degrees (air mass = 8). The light curve showed no evidence of distortion due to this rare observing condition. Using z'-band would be even better when the need calls for high air mass observing, especially when the observing site is near sea level.

For all other situations it is possible to achieve good quality light curves using CBB or NIR filters, or even a clear filter. The light curve on the cover of this book was obtained unfiltered, and the reason for its success is that the target was high in the sky for the entire observing session. The light curve is for the exoplanet system WASP-10. This star is somewhat fainter than the median for BTEs (V-mag = 12.7, versus 11.20 median), it is somewhat redder (B-V ~ +1.1, versus +0.63 typical). The median color for stars that can be used for reference, based on the 1259 stars in the Landolt list, is B-V = +0.64. Thus, observing WASP-10 unfiltered might seem risky since few nearby stars are likely to have the same redness as the target star. In a later chapter I'll describe a procedure that I use for dealing with this situation. For now let the cover light curve stand for the notion that although unfiltered observations may produce light curve systematics there are data analysis ways for dealing with them (described in Chapter 18). The payoff for this approach is that clear filter observing provides the highest SNR, which for amateurs is almost always very important.

Probably few observers factor-in the need for a bright autoguider star when they choose a filter for a specific observing session. To minimize systematic errors it is important to keep the star field fixed with respect to the pixel field (to minimize systematics related to an imperfect flat field), and it's therefore important to have a sufficiently bright autoguider star to assure quality autoguiding. When all autoguider star candidates are faint it may be better to use a CBB filter than any of the others, merely to permit good autoguiding.

Occasionally a very faint star is to be observed using a small aperture telescope. This situation forces the use of a CBB (or clear) filter. If systematics are present using such a broad bandpass they probably won't be noticed since the light curve will be too noisy for the defects to show.

If you're fortunate to own a large aperture telescope (e.g., larger than 16 inches), observations can be made alternating between filters. One accomplished observing team, using a 24-inch aperture (Jerry

CHAPTER 7 – FILTERS

and Cindy Foote), routinely make 3-color light curves of medium bright exoplanets. Deciding which filter will be optimum is an easier task when you have sufficient SNR to alternate between several filters. Large aperture observers will rarely need to use the CBB or NIR filters since they pass too much light; the larger the aperture the greater is the payoff for using such narrow-band filters as V-band and z'-band.

Occasionally I am surprised about something unusual done by an advanced amateur that turns out “better than it should.” One of the most interesting was an observation submitted to the AXA by Colin Littlefield, of Indiana. He observed HD 189733 with an ordinary DSLR camera attached to an 8-inch telescope. He processed the 3-color images by first separating the R, G and B images from each RGB image, then producing a light curve for each color. All 3 light curves are good quality and scientifically useful. One of them is shown here.

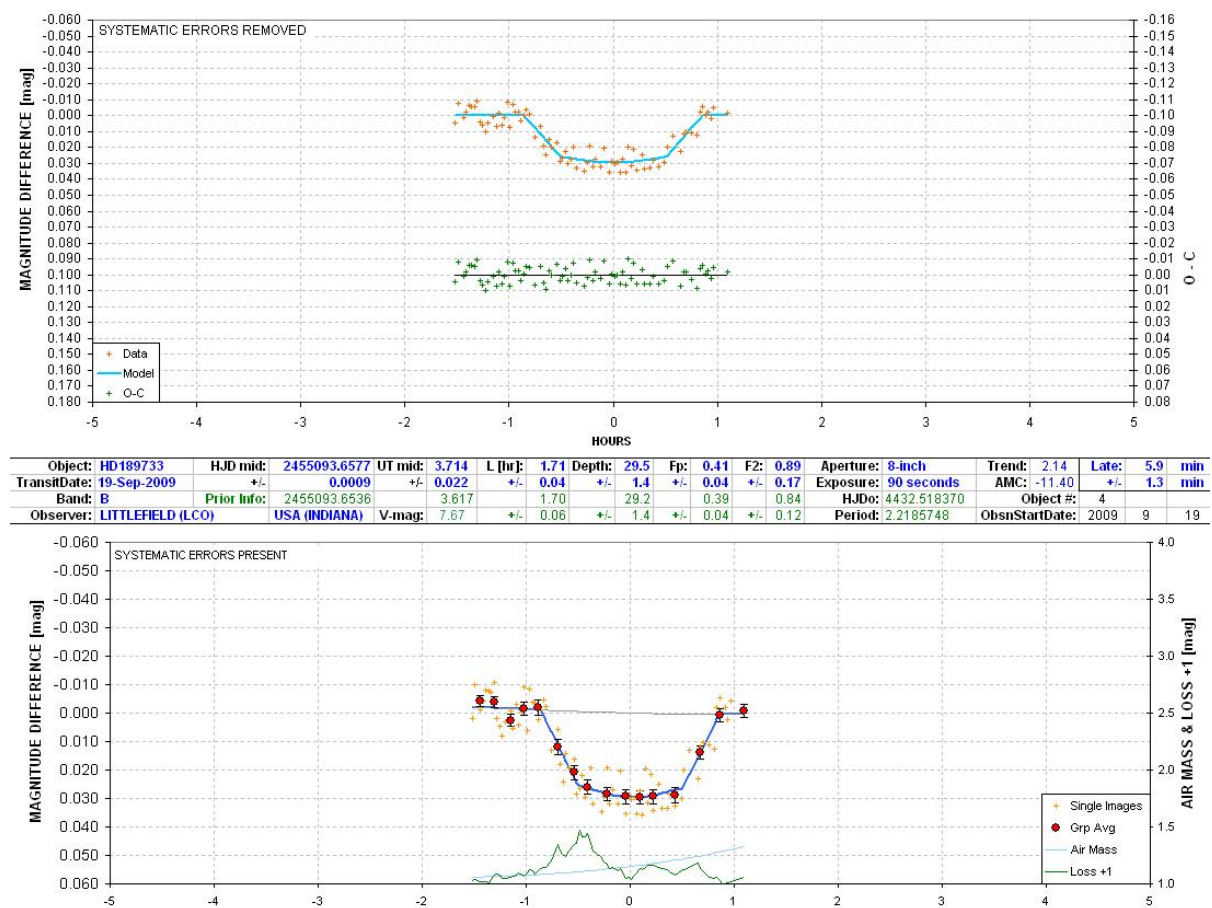


Figure 7.03. Light curve by Colin Littlefield using a regular DSLR camera. B-images were extracted from RGB images to produce this blue band light curve. Other light curves of similar quality for green and red bands were also produced from the same set of RGB images.

Finally, the question often arises “What are the differences between observing unfiltered, using a clear filter and using a luminance filter?” Unfiltered is what it says, and photons of all wavelengths that the telescope optics pass make it to the CCD. “Pretty picture amateurs” may want to brighten the

CHAPTER 7 – FILTERS

final color image by adding a less filtered image (that shows fainter stars). If this is to be done unfiltered, when the color filter wheel rotates to the unfiltered position the focus setting will have to be adjusted (since filters change focus plane location). If a clear filter is used, however, and providing it is “parfocal” with the other filters (same focus setting for all filters), then a focus change would not be needed. A “luminance” filter blocks UV and infra red (IR), passing essentially B, V and R. Removing UV and IR can lead to a sharper image since the optics ahead of the filter wheel (focal reducer and corrector plate) are designed to produce the sharpest images in the BVR region, which means the optical designer may decide to sacrifice image quality at UV and I bands in order to be best for B, V and R bands. A similar situation may arise for an exoplanet observer, such as when a “bright” image is needed to see if background stars are present at locations that could produce problems with precision photometry using a standard filter.

It’s possible to construct a decision “flow chart” for choosing a filter. I have not yet done so for my personal use, but the day I feel compelled to optimize observing to the highest level I may rely upon a formalized decision flow chart. It’s better for you, dear reader, to think about the material in this chapter and devise your own filter choosing procedure. It will be intuitive at first, and with experience it may become rigorously defined. Exceptions to any rules that apply in most situations will always exist (e.g., XO-2 has an equally bright companion nearby, with the same color, so some of the above guidelines don’t apply). So many factors can influence the choice of filter that my advice is to try out various “filter philosophies,” evaluate the results and use the one that you like – even if it is V-band!

For those who want “data based evidence” that the CBB and NIR filters are good choices for a typical exoplanet, I have included in Appendix H the results of an observational project to evaluate 5 filter choices by observing with all of them in alternation. I found that the best performing filters for the exoplanet chosen for this case study (CoRoT-3) were CBB, NIR, R, i’ and V – in that order!

The question we ended Chapter 5 with can now be answered: what filter should be used for an observation of XO-1 on the night of June 18, 2010. Recall that ingress, mid-transit and egress occur near midnight at elevations within the range 47 to 84 degrees! One hour before ingress the moon will be at an elevation of 81 degrees, and one hour after egress it will be at 35 degrees. This is an unusually favorable observing situation, so we can relax in considering atmospheric extinction. There is no need for the NIR filter’s small atmospheric extinction feature. The CBB filter will afford a greater SNR than the NIR filter without any penalties related to extinction. But where’s the moon during transit? According to TheSky/Six the first-quarter moon is at 14 degrees elevation, and setting, at ingress. It will be 70 degrees from XO-1. The sky background will therefore only be slightly brighter than without a moon, so the CBB filter is still a good choice.

What a lot of work just to decide on using the CBB filter for the observations of XO-1 on June 18, 2010! Before we can take a break for dinner we need to answer one more question: “When should flat fields begin?”

Chapter 8

Flat Fields

It would be nice if CCDs responded to a uniformly bright source, such as the daylight sky, by producing the same output counts for all pixels. This does not happen for two reasons: pixels differ slightly in their efficiency at converting photons to photo-electrons (and converting photo-electrons to counts during readout), and a uniformly bright sky does not deliver the same flux of photons to all CCD pixels due to such optical effects as vignetting and shadowing by dust particles on optical surfaces close to the CCD (*i.e.*, “dust donuts”).

For amateur telescopes the shape of the vignette function will differ with filter band. The amount of these differences will depend on f-ratio and the presence of a focal reducer (and its placement).

Flat field corrections are supposed to correct for all these things. Alas, in practice, flat fields correct for only most of them.

Sometimes I think the art of making quality flat fields could be a hobby, all by itself! It could take so much time that there would be no time left over for using the knowledge gained. There must be a dozen procedures in use for making a master flat, and the sorry truth is that none of them are as good as the user imagines them to be.

Some observers use “light boxes” placed over the front aperture. If the light source is “white” this can produce reasonable flats for all filters. However, it is difficult to attain uniform illumination of the surface facing the telescope aperture – which is where my attempts with this method have always failed.

Another method is to use a white light source to illuminate a white board, which in turn illuminates a second white board that is viewed by the telescope. The use of two white boards reduces specular reflections, which can be troublesome for “shiny” white boards. The trick with this method is to provide a uniform illumination of the white board viewed by the telescope, and within the confines of a small sliding roof observatory or dome this can be difficult. One of my problems with this approach is that wind often blows one of the white boards out of place. I always thought I obtained good results from this method, but it’s too cumbersome to use routinely.

Sometimes master flats are produced by median combining a large number of images of different star fields (“night sky flats”). For pretty picture work at least a dozen images are needed. For exoplanet observing you would need hundreds of images for median combining in order to reduce residual star effects to the required smoothness needed for mmag precision. I don’t recommend this method.

The twilight sky overhead is a convenient way to produce flat fields. For most telescopes these images can be taken when the sky is bright and exposure times are short enough that stars do not appear in any of the images. The telescope can either be stationary or tracking (stationary is better). Master flats produced this way are acceptable for most uses, but for precision exoplanet monitoring the presence of even faint stars in the master flat are unacceptable. A diffuser placed over the aperture

CHAPTER 8 – FLAT FIELDS

can eliminate stars in the flat field images. That's the method I've adopted, which I'll describe after two detour discussions: stray light and star colors.

All flat field procedures can be degraded by "stray light." For example, an open tube telescope that does not have sufficient baffling in front of the CCD camera may register light from the ground or other locations not within the CCD's FOV. For another example, I once noticed that my AO-7 image stabilizer was allowing light to leak through the joint formed by the two outer mounting cases. This leak was blocked by simply applying black electrician's tape around the joint. Light leaks from all "back end" components can be reduced by wrapping a dark cloth around them while exposing flat frames.

Stray light that occurs during an observing session is unimportant for exoplanet monitoring. For example, if there's a bright star near the exoplanet it may reflect off internal structures and produce rings of light at the same location on all images where the FOV is offset the same amount from the bright star. The nearby moon can produce large brightness gradients in images. Don't worry about these stray light artifacts. They would ruin pretty picture taking, but photometry is usually unfazed by stray light in photometry images.

If all stars were the color of the sun, for example, which we can think of as white for now, then the best light source for producing flat fields would also be white. But some stars are blue, and some are red. If we had a light source that was blue, and another that was red, we could make flat fields for these colors as well, and we'd see that the three master flats differed slightly. A proper processing of images would then involve performing calibrations three times, using the master flats for red, white and blue. Each star's flux could then be measured using each of the three calibrated image sets and the flux to be used for subsequent analyses would depend on the star's color. This little exercise illustrates some of the futility of expecting to obtain a "perfect" flat field.

It's worth noting that flat field corrections wouldn't be necessary for exoplanet observing if the star field could be positioned at the exact same pixel location for an entire observing session. If that could be accomplished the only errors for neglecting to correct for flat field effects would be limited to a constant bias for the target star, and since these biases would be the same for all images they would not alter the shape or depth of an exoplanet transit light curve.

Keeping the star field fixed with respect to pixels requires not only that the autoguider work perfectly, it also requires that the polar axis be aligned perfectly. Consider observing a source at 60 degrees declination with a polar axis alignment error of only 0.1 degree. During a 6-hour observing session the image would rotate as much as 0.2 degree. The effect is greater for higher declinations. If the autoguider is located 20 'arc from the center of the main chip, for example, then stars in the middle of the FOV will move 7 ''arc during the observing session, and stars near the corners farthest from the autoguider will move even more. Since no flat field correction is perfect these movements will cause systematic variations in each star's flux as it moves across the pixel field. The vignette response function is usually "steep" near the edges, so this is where small inaccuracies in the flat field can produce errors with systematic trends. If a 2 'arc polar alignment error is present then these effects would probably be too small to correct for, but perfect autoguiding would still be required. Although it's a worthy goal for amateurs to achieve a perfect polar alignment, and to achieve perfect autoguiding, flat field corrections are a prudent safeguard and must be performed.

CHAPTER 8 – FLAT FIELDS

I'll use my telescope system to illustrate how the scheduling of flat frames can be done at about sunset. I point the telescope at zenith well before sunset and place a "double T-shirt" diffuser over the aperture, illustrated in the next figure. The two white T-shirts diffuse sky light, and by using it I never see star trails in my flats. Since the T-shirts let only a fraction of the incident light enter the telescope the sky flat exposures have to begin sooner than if the T-shirt diffuser were not used. Use of the double T-shirt diffuser affords the unexpected bonus of allowing for a more relaxed flat frame observing session. This is due to the fact that the diffuser's reduction of light entering the telescope requires that flat field exposures begin sooner, when sky brightness changes more slowly.



Figure 8.01. *Double T-shirt diffuser is being placed on top of the telescope aperture for obtaining flat fields. (A wireless Davis Weather Station is in the background.)*

As mentioned in a previous chapter the time to start exposing flat fields depends on the filter (and binning choice). A photometric B-band filter passes much less light than any of the other filters, so it requires longer exposures for the same sky brightness. A common practice is to keep exposure times within the 1 to 10 second range (explained below). If flat fields are needed for all filters the sequence for exposing flats should start with B-band, and be followed by V-band, I-band, R-band, CBB-band and finally clear. For the g'r'I'NIR filter set, for example, the sequence is i'r'g'NIR and CBB.

Exposure times shorter than ~1 second can produce slightly unequal actual exposure times at different locations on the CCD. For example, consider a shutter that opens and closes like the old style cameras. As the shutter opens it would begin exposing the CCD center first, and as it closed the center would be the last to have incoming light shut off. This would produce a non-uniform pattern of

CHAPTER 8 – FLAT FIELDS

center-to-edge actual exposure time. The shorter the exposure time the greater the percentage disparity between the center and edge. Few CCDs use this type of shutter, but it illustrates a concept. Rotating shutters are better, but they too have a greater likelihood of producing different actual exposure times at different locations on the CCD for short exposures. CCD camera shutters differ, but exposures longer than ~1 second are generally considered to be unaffected by this problem.

Exposures that are too long are simply inconvenient, and they interfere with making flat field exposures with other filters. Hence, the goal is to schedule the flat field exposures so that they all are within the range of 1 to 10 seconds.

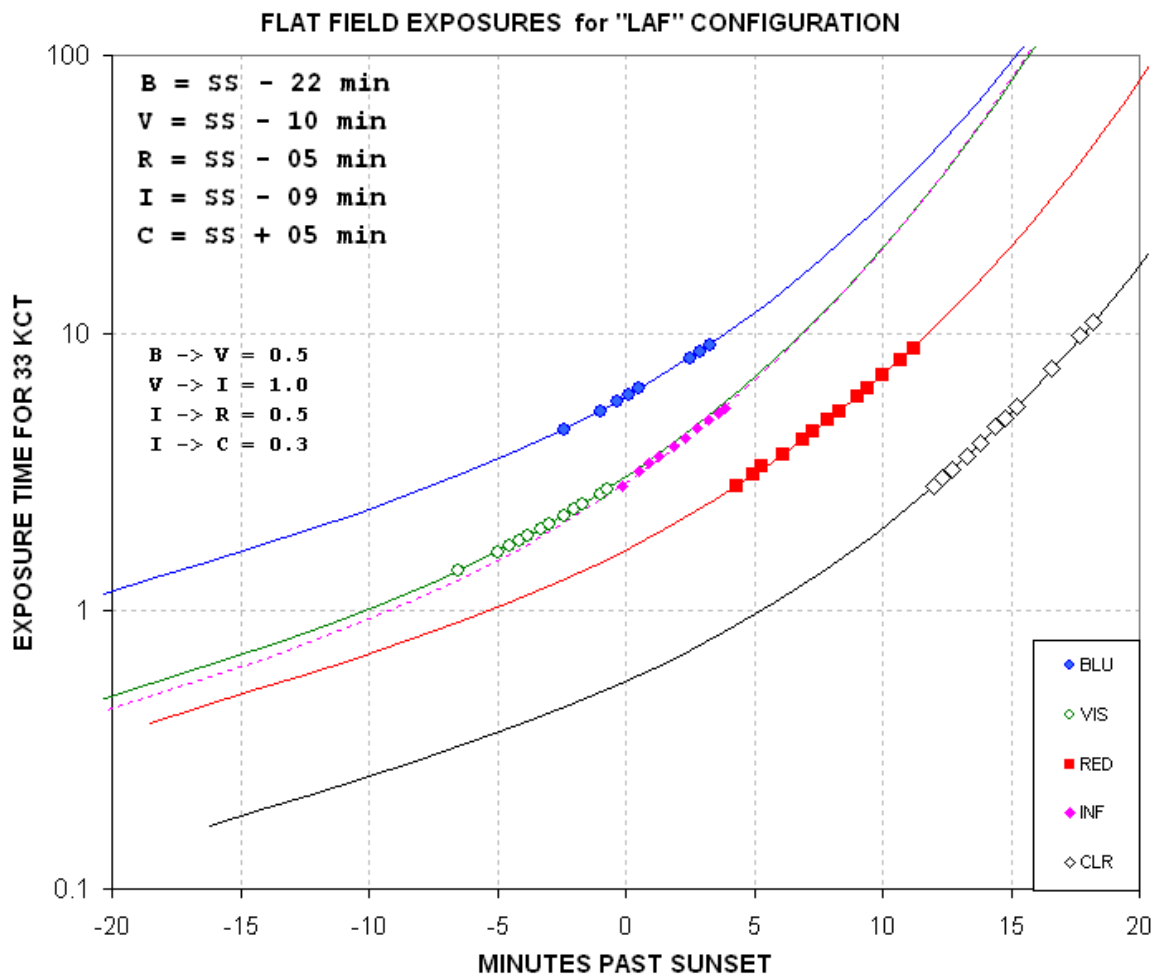


Figure 8.02. Exposure time versus time after sunset for various filters for an $f/8$ telescope system (binned 1×1) and use of a “double T-shirt” diffuser.

This figure shows that for my B-band filter I can start flat field exposures ~20 minutes before sunset but no later than about 5 minutes afterwards (assuming my binning is 1×1). At 10 minutes before sunset I can start the V-band flat frames. Next are the I-band, R-band and finally the clear filter flat fields. Since the clear filter flats can be made as late as 20 minutes after sunset the entire flat frame series can take 40 minutes, assuming all filters are to be used on that night’s observing session.

CHAPTER 8 – FLAT FIELDS

Figure 8.02 assumes that no binning will be used (i.e., 1x1 “binning,” or “full-resolution”). If 2x2 binning is planned then flat fields will have to be made later than the times in this graph. Since the CCD’s analog-to-digital converter will be dealing with 4 times the voltage for a specific sky brightness (produced by 4 times as many photo-electrons) we can estimate a time to observe from Fig. 8.02 by choosing the 4-second to 40-second exposure time region; at these times the actual exposures required for the desired counts will be within the range 1 second to 10 seconds.

My sliding roof observatory is usually opened about a half hour before sunset. I immediately start cooling the CCD to something close to 0 C. The flats can be taken at any temperature; according to SBIG they don’t have to be taken at the same temperature as the light frames later in the night. The reason for achieving some amount of cooling is to reduce dark current “thermal” noise.

In making flats it is sometimes stated that dark frame subtractions are optional. This is not true for precision photometry. I strongly recommend the use of dark frame subtraction for every flat frame exposure. When exposing flats of the sky near zenith after sunset, exposure times have to be increased every few minutes to assure that the maximum count is within a range of values that is slightly below values where non-linearity and other versions of saturation occur. For 16-bit CCDs “A/D converter saturation” occurs at 65,535 counts (“counts” and “ADU” are the same thing). The “conventional wisdom” is to keep the maximum flat field counts within the range 30,000 to 35,000, the latter value being where many observers believe non-linear effects can be expected. Images with maximum counts lower than 30,000 can be used, but the noise component for these images is a greater percentage of the signal component and they may reduce the quality of the combined flat images (the “master flat”). Every time the exposure time is changed a new dark frame has to be taken for use with that flat and those following with the same exposure. This can slow things down, but that’s a fair price to pay for the assurance of minimizing the effects of bad pixels later. Incidentally, by automatically using a dark exposure calibration of each flat frame there is no need to worry about bias corrections (since the dark and light frames share the same bias field).

My CCD is linear up to 59,000 counts, and I suspect that the “common wisdom” of avoiding exposures that produce counts above ~35,000 is out of date for modern CCDs. Each observer will want to measure their CCD’s linearity range in order to know how to be guided on setting flat field exposure times, as well as for setting exposure time for star fields. Measuring linearity is described in Appendix E.

When I first started using a CCD I would combine several flat field images and then smooth the resultant image to reduce “noise.” Don’t do this! Every pixel has a slightly different behavior (QE, bias, gain) from its neighbors and this behavior must be preserved in the master flat field image. Moreover, small dust donuts can have sharp gradients and these shouldn’t be changed by smoothing.

I also used to produce a master flat by median combining individual flats (specifying use of the background level for “normalize”). I’ve had a few bad experiences with improper results using the “normalize” setting, which I attribute to the use of flats with too much variation in average level. Because sky brightness is changing fast near sunset it’s difficult to adjust exposure times to produce similar count levels in all images. I now favor the averaging of individual flat frames. The only reason to median combine is to remove cosmic ray defects. I rarely see this, but nevertheless it is wise to do a cursory visual inspection of the flats before averaging them to make a master flat.

CHAPTER 8 – FLAT FIELDS

The longer I try to improve flat fields the more I've come to believe that perfect flat fields are fundamentally impossible. Even the meaning of a flat field, or the task it is to perform, seems more vague and impossible the more I think about it. I now believe that even the idea of a perfect flat field is theoretically impossible unless it is for an extremely narrow filter. Instead of trying to achieve the perfect flat field it might be better to spend more effort learning to live with imperfect ones.

Consider flats taken at zenith near sunset. Since the sky is blue the flats we're getting this way are meant for use with blue stars, as described above. Since the sky becomes slightly bluer as the sun sinks below the horizon, flats taken shortly after sunset will differ from flats taken late after sunset. In essence, the early and late flats are meant for stars of different blueness. Red stars deserve flats taken with a red sky, but this is not easily achieved. Using a red filter with a blue sky just means the effective wavelength is weighted to the blue side of the filter's bandpass. It's not feasible to use a different flat for each star, depending on its color, which in most cases we don't know. The narrower the filter the less these troublesome effects will be. Unfiltered flats correcting unfiltered images of a star field can therefore be expected to exhibit the worst systematic errors.

When a diffuser cover is not used there is risk of introducing brightness gradients in flat frames if the sky itself has a brightness gradient within the FOV. For this reason it is sometimes recommended to point the telescope at a location slightly off of zenith, away from the sun, where the sky does not have brightness gradients. This is also the darkest (and bluest) part of the sky. If you want a whiter part of the sky for dark frames it's inviting to point close to the horizon, but of course that's where brightness gradients are greatest. With a diffuser, however, this is possible since spatial gradient information is smeared away. Sometimes I actually point the telescope halfway to the western horizon in order to get a whiter sky, which is possible only when using a diffuser cover.

An upper limit for the size of these subtle effects can be estimated from all-sky measurements of Landolt star fields using all-sky photometry procedures. When I evaluate telescope constants for all-sky equations for a specific telescope configuration I always have larger residuals for converting unfiltered star fluxes to CV and CR magnitudes than for the observations using a filter (converting B-filter fluxes to B-magnitudes, V-filter fluxes to V-magnitudes, etc). If SNR was the only source of scatter then the opposite should occur. Star color is an independent variable for this analysis so in theory the residuals could be the same for unfiltered and filtered images. I believe the greater scatter for the CV and CR residuals is due to the fact that an unfiltered flat was used with unfiltered images, and the redder or bluer the star the worse the flat field correction. Since the all-sky solution procedure is designed to minimize RMS scatter the final coefficients are a compromise for all star colors in the Landolt set. Typically, I achieve RMS scatter of 0.025 magnitude for the B, V, Rc and Ic data, but only 0.035 magnitude for CV and CR. From this I estimate that the level of systematic effects that can be expected for transit monitoring should be <20 mmag when using a filter and <30 mmag when observing unfiltered. These levels would only be encountered if the target and reference stars were far apart and their pixel locations varied by large amounts during the observing session. When the flat field pattern varies significantly from filter to filter I would expect greater systematic errors from a drift of the star field over the pixel field during an observing session.

CHAPTER 8 – FLAT FIELDS

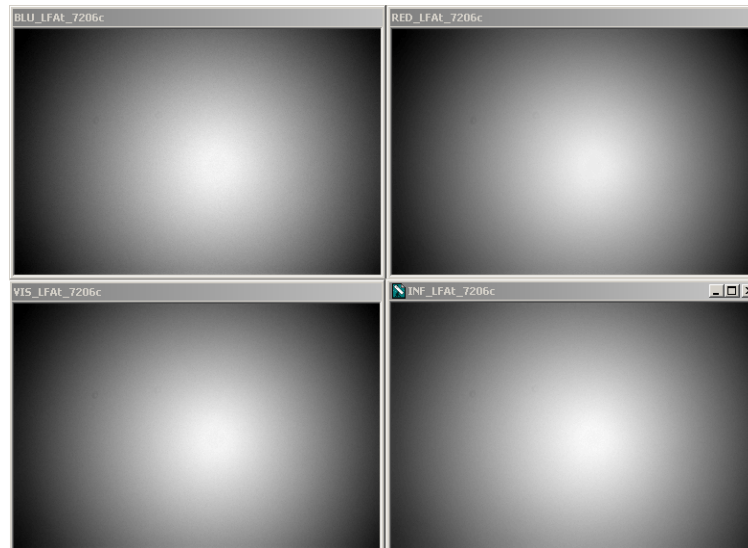


Figure 8.03 Flats for B, V, Rc and Ic filters for a configuration with a focal reducer lens placed far from the CCD chip. The edge responses are ~63% of the center.

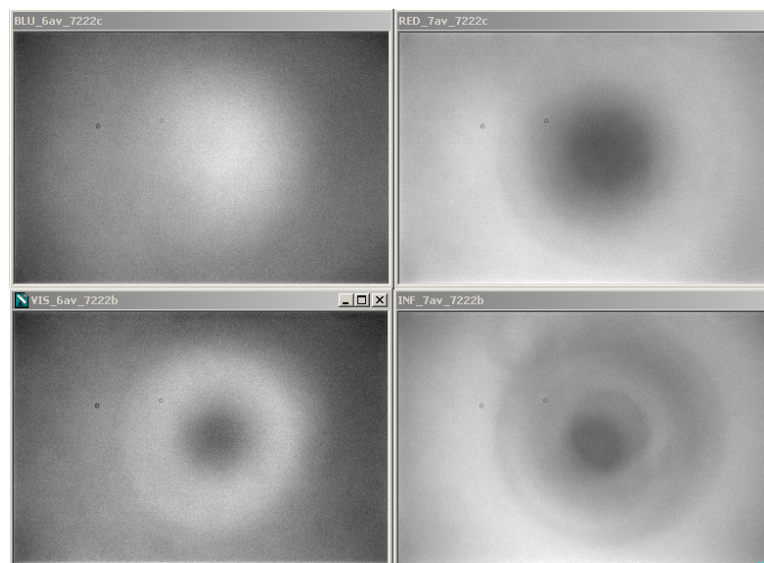


Figure 8.04 Flats using the same filters but with a configuration with the same focal reducer close to the CCD chip. The response range, smallest response to maximum, are 88, 90, 89 and 89% for the B, V, Rc and Ic filters.

These figures show how flat fields can change with filter band. Figure 8.03 was made with a focal reducer lens far from the CCD (in front of an AO-7 image stabilizer). Figure 8.04 was made with the focal reducer lens between the AO-7 image stabilizer and the CFW/CCD assembly. What a difference location makes! Also, what a difference filter band makes! For the second set of flats it is easy to imagine that stars of different colors will require flats that are intermediate between the measured

CHAPTER 8 – FLAT FIELDS

blue sky flats, and the reddest stars will have requirements that depart the most from the measured ones.

Appendix A contains methods for evaluating the quality of your master flat field. The procedures described in that appendix are time-consuming, and they are meant for consideration by only advanced users.

The entire situation of how to make good quality flat fields and how to use them properly is so confusing to me that I propose the following simple solution. Keep the star field fixed with respect to the pixel field during the entire observing session! If this can be accomplished then the expected small movements of the star field can be counted on to produce only small changes in flat field error for each star, regardless of its color.

This solution requires that polar axis alignment be accurate to approximately 2 'arc, which is achievable using the “declination drift” method. The solution also requires the use of some form of autoguiding to keep the star field fixed with respect to the main chip's pixels. By doing these things all the fundamental flaws in flat field correcting will be reduced to second-order effects.

Returning to our original question relating to the June 18, 2010 observations of XO-1, we want to know when flat field observing should begin if we use a CBB filter, unbinned. We can use the clear filter trace in Fig. 8.02 (because CBB and C have approximately the same “throughput” of photons), which shows that we should start exposing the flat field images about 5 minutes before sunset. Since sunset on this date is 7:25 PM (local time). So we need to be open, and have the CCD somewhat cooled, by 7:20 PM in order to start CBB flat fields. Let's plan on opening the observatory at 7:15 PM.

This completes planning for the evening's observations, and now we have time for that dinner break at Delio's Italian Restaurant, where they have my favorite beer on tap (Guinness) and the best pizzas in town.

Chapter 9

Dark Frames

Creating a master dark frame is straightforward compared with creating a master flat frame. Whereas a master **flat** frame can only be used with light frames taken with the same filter, dark frames can be used with light frames taken using any filter – for obvious reasons. Whereas CCD temperature doesn't matter for flat frame calibrations, the same cannot be said for dark frames. Temperature differences have effects that grow with temperature difference. It's true that image processing programs allow you to specify "Auto Scale" and "Auto Optimize," which are supposed to compensate for differences in both exposure times and CCD temperatures. These options may work for "pretty pictures," but I don't trust them for precision exoplanet transit observing.

It is common practice to set the CCD cooling to as cold as can be stabilized with a thermoelectric cooler duty cycle of ~95% just prior to the time target observations are to begin. When I finish taking flat frames there's usually a half hour before target observations can begin, so during that time my cooler is working at full duty cycle to get the CCD as cold as possible. After acquiring the target, and synchronizing the mount's pointing, I back-off on the cooler setting to about a degree C warmer than what had been achieved at that time, and this produces an approximate 95% duty cycle.

Before starting observations of the target I'll perform a set of focus images at about the same area in the sky as the target. The FWHM at the best focus setting will be used for determining exposure time (explained in the next chapter). During the time it takes to determine focus the CCD cooling has stabilized. If there's time I'll take dark frames before starting to observe the target. The best quality dark frames, however, will be made at the end of the target observations.

A total of at least 10 dark frames should be taken with the same exposure time and CCD temperature. These images must be **median** combined, not averaged. Median combining will remove the effect of cosmic ray defects that are usually present in most of the dark frames, especially if their exposure times are as long as 60 seconds. Dark current "thermal" noise averages down approximately as the square-root of the number of images that are median combined. Whereas averaging causes a "square-root of N" reduction in noise, median combining is about 15% less effective. Thus, when 10 images are median combined the master dark produced this way will have a noise level that is ~0.36 times the thermal noise level of the individual images. When this master dark is subtracted from a single light frame during calibration the calibrated image will have a slightly greater thermal noise level than the uncalibrated image. The increase will be only 6%: $\text{SQR}(1.00^2 + 0.36^2) = 1.06$.

Bias frames aren't needed if the dark frames are taken with the same exposure time as the light images. If more than one exposure time is used during the night then bias frame calibration should be used.

Some observers claim that they can use the same master dark frame for several observing sessions. This is not a good practice, because every CCD camera ages, and if a pixel changes between observing sessions you'll want to use dark frames taken with the current pixel's performance.

Chapter 10

Exposure Times and Defocusing

The factors influencing the choice of exposure time can be thought of as belonging to one of two categories: saturation and information rate.

Avoiding Non-Linearity and Saturation

Images are not useful for photometry if any of the stars to be used in the analysis are saturated, which will occur when the maximum count is at the greatest value that can be registered, such as 65,535 (for a CCD with a 16-bit A/D converter); this is called “A/D converter saturation.” Images are also not useful when a star to be used has a maximum count value that exceeds a linearity limit; this is called “linearity saturation.” Not many amateurs measure where their CCD begins to become non-linear, so they are guided by the “conventional wisdom” that anything greater than mid-range is unsafe. According to this guideline the maximum counts shouldn’t exceed ~35,000.

If you measure your CCD’s linearity limit you may be pleasantly surprised. When I measured mine (a Santa Barbara Instruments Group ST-8XE) I discovered that it was linear over a much greater range than represented by “conventional wisdom.” It was linear all the way to 59,000 counts! This measurement can be done using several methods, described in Appendix E. Knowing this has allowed me to use longer exposure times, and longer exposures are desirable for at least three reasons: 1) scintillation and Poisson noise (cf. Chapter 20) are reduced slightly because a greater fraction of an observing session is spent collecting photons (instead of downloading images), 2) read noise is reduced since exposure times can be longer and there are fewer readings per observing session, and 3) a smaller fraction of an observing session is “wasted” with image downloads (i.e., more time is spent collecting photons). I highly recommend that you measure their CCD’s linearity to see if you too can benefit in the same way. For the remainder of this chapter I’ll assume that this measurement has not been made, and you will want to be cautious by using exposure times assuring that all stars to be used have maximum counts, $C_{max} < 35,000$.

You might think that when observations are started it’s OK to just set an exposure that keeps the brightest star from producing a count greater than ~35,000. That’s OK when the star field is already setting, when you can count on images becoming less sharp for the remainder of the observing session. But for rising star fields images are likely to become sharper as they approach transit, and since the same number of total counts from each star will be concentrated on a smaller number of pixels C_{max} will increase. Furthermore, atmospheric extinction is lower at transit, and for this reason alone star flux, and hence C_{max} , should increase as transit is approached.

I recommend taking test exposures for determining exposure time as soon as the target star field has been acquired and focus has been established. Based on previous observing sessions you’ll know whether the sharpness of these images is typical for your site. In making this assessment air mass has to be taken into account. That’s worth an aside.

CHAPTER 10 – EXPOSURE TIMES & DEFOCUS

Image sharpness is described by the “full-width at half-maximum” (FWHM) of the “point spread function” (PSF) of an unsaturated star near the middle of the image. For example, at my site I can expect FWHM ~ 2.5 ”arc for short exposures (< 5 seconds) near zenith. For longer exposures, such as 60 seconds, FWHM is typically ~ 3.0 ”arc. I have determined that at my site short-exposure FWHM varies with air mass (AirMass) in accordance with the following empirical equation:

$$\text{FWHM [”arc]} = 2.5 \times \text{AirMass}^{1/3}$$

This is a useful equation for estimating how sharp an image will be later in an observing session. Suppose the test images at the start of a session show FWHM = 4.0 ”arc when the air mass is 3 (elevation ~ 20 degrees). If “atmospheric seeing” conditions don’t change for the duration of the observing session, and if the region of interest will pass overhead, we should expect that near zenith FWHM ~ 2.8 ”arc.

We can make use of the fact that a star’s Cmax increase as $1/\text{FWHM}^2$ - which is true under the assumption that flux remains constant. For example, when FWHM changes from 4.0 to 2.8 ”arc we can expect Cmax to increase by the factor 2.1. An equivalent way to calculate Cmax is to note that Cmax is proportional to $1/\text{AirMass}^{2/3}$. In our example, AirMass goes from 3 to 1, so Cmax will increase by a factor $(3/1)^{2/3} \sim 2.1$. This means that we want our test images to show the brightest star’s Cmax = 16,700 (35,000 / 2.1). A more useful version of the previous equation is therefore:

$$\text{Cmax at AirMass}_i = \text{Cmax at AirMass}_0 \times (\text{AirMass}_i / \text{AirMass}_0)^{-2/3}$$

This equation assumes star flux doesn’t change with air mass. Therefore we must account for changing flux with air mass caused by atmospheric extinction. The biggest effect will be for the B-band filter. Using our example of the test images being made at AirMass = 3, what can we expect for Cmax when AirMass = 1? For my observing site, at 4670 feet above sea level, the B-band zenith extinction is typically 0.25 [magnitude / AirMass]. Changing AirMass from 3 to 1 can therefore be expected to change a star’s measured brightness by 0.50 magnitude. This corresponds to a flux ratio of 1.6 (i.e., $2.512^{0.5}$). We therefore must reduce our desired Cmax for test images to 10,400 counts (16,700 / 1.6). At lower altitude observing sites the correction would be greater. See Fig. 6.07 for a graph that can be used to estimate zenith extinction for other observing site altitudes for each filter band.

Imagine the frustration of choosing an exposure time that produces Cmax $\sim 35,000$ counts at the beginning of a long observing session, and discovering the next day when the images are being reduced that the brightest stars, and maybe the target star, were saturated in images near transit! This must be a common problem because on a few occasions when I helped an observer figure out what went wrong to produce bad light curves it turned out that the target was saturated near transit. This is a case where a small effort at the beginning of observations can lead to big payoffs for the entire observing session.

Information Rate

When all stars of interest in the FOV are faint the previous considerations may not be important. In this case different criteria should be used to choose exposure time. Starting with a trivial example, if

CHAPTER 10 – EXPOSURE TIMES & DEFOCUS

transit length is expected to be 3 hours it would be foolish to take exposures as long as an hour, even though at least one of them would be completely within the transit phase. At the other extreme we don't want exposures to be significantly shorter than the time required for downloading each image because that would be very inefficient.

Let's approach this by adopting 60 seconds as a default exposure time, and then ask "what are the merits of either increasing or decreasing exposure time?"

A typical transit will last 3 hours and the ingress and egress portions of this will be ~20 minutes. Referring to the figure on the cover, ingress is from contact 1 to contact 2, and egress is from 3 to 4. For such a transit it is desirable to obtain information about the shape of ingress and egress in order to constrain model fitting (the size of the exoplanet in relation to the star, and also the star center miss distance). Therefore, exposure times should be less than about 4 minutes on account of this consideration. Another reason to have ingress and egress shapes well-established is to be able to assign an accurate mid-transit time. A transit timing archive can be used to establish the presence of "timing anomalies," and these can be used to infer the existence of another exoplanet in the same star system, or possibly an exomoon. I think 4 minutes is the longest exposure time that should be considered for any exoplanet transit observing situation.

What about shorter exposure times? We now must consider a concept called "information rate." Information rate can be described as inversely proportional to the observing time required to achieve a specified SNR for a specific star using a specified filter. Long image download times reduce information rate. My CCD requires 8 seconds to download (full resolution, or unbinned, or 1x1). If I used an exposure time of 8 seconds half of an observing session would be spent downloading images. Another way of saying this is that such an observing schedule has a 50% duty cycle. Consider the absurd example of exposing for 2 seconds when downloading requires 8 seconds. This corresponds to a duty cycle of 20%, which means 80% of an observing session would be spent simply downloading images. The higher the duty cycle, the greater the information rate. The longest possible exposures will produce the greatest possible information rate.

So why not increase the exposure time from our starting value of 60 seconds, and make it 120 seconds (assuming saturation issues are not a problem at this longer exposure time)? To answer this we must consider "risk." Suppose a satellite, or airplane, passes through the FOV and ruins an exposure? The more exposures you have in an observing session, the smaller is the percentage loss when one image is ruined. There are a myriad of things that can ruin an image. For me, winds vibrate the Meade fork-mounted telescope in the sliding roof observatory, and when winds exceed about 5 mph the stars begin to take on oval shapes. This not only lowers the signal-to-noise ratio (SNR) but it introduces the possibility of systematic errors. Cosmic ray defects are present in most exposures, especially the long ones, and if they appear on top of a star's image there's no way for simple aperture photometry to correct for it. If such a cosmic ray defect is within the signal aperture of the target star, or any of the reference stars, the affected image will produce a brightness for the exoplanet that has to be rejected as an outlier. The fewer images that have to be rejected because they appear to be outliers, the better. This is an argument for short exposures.

Consider the information rate for 60-second exposures versus 120-second exposures when download time is 8 seconds: the two duty cycles (proportional to information rate) are 88% and 94%. That's a gain of only 7% for the longer exposure time, but a doubling of "risk" related to ruined images.

CHAPTER 10 – EXPOSURE TIMES & DEFOCUS

Scintillation noise is a possible consideration when choosing exposure time. Scintillation noise is a fractional fluctuation of all stars in a FOV, uncorrelated with each other, caused by wave front interference effects produced by small-scale temperature inhomogeneities at the tropopause (11 - 16 km overhead). Scintillation fluctuations of a star's intensity decrease with exposure time as $1/g^{1/2}$ (where g is exposure time). Thus, 4-minute exposures will exhibit half the scintillation of 1-minute exposures. Also, the average of four 1-minute exposures will exhibit half the scintillation of a single 1-minute exposure. The only improvement in reducing scintillation by using longer exposures comes from the fact that a 4-minute exposure can be obtained more quickly than four 1-minute exposures (due to the difference in number of image downloads). This fact is apparently not appreciated by even some professional astronomers (two that I know about). This warrants repeating (slightly reworded):

The average of four 1-minute exposures will exhibit the same level of scintillation as a single 4-minute exposure.

Using the previous example, in which a 4-minute exposure has a 7% advantage in duty cycle compared to 1-minute exposures, we can calculate that a sequence of 4-minute exposures will have a 3.4% lower scintillation per unit of observing time than the sequence consisting of 1-minute exposures, due simply to the slight improvement in duty cycle ($\sqrt{1.07} = 1.034$).

The same argument can be applied to Poisson noise (described in Chapter 20). The fractional uncertainty of a flux measurement due to Poisson noise is **proportional** to $1/\text{flux}^{1/2}$ and since flux is proportional to exposure time the same $1/g^{1/2}$ relationship exists between Poisson noise and exposure time. This leads to the same rule stated above for scintillation:

The average of four 1-minute exposures will exhibit the same level of Poisson noise as a single 4-minute exposure.

I hope these concepts are clear because they are the basis for a lot of observing strategy formulation. It has always puzzled me that “information rate” concepts are lacking from all the text books aimed at amateur astronomers, so I feel the need to compensate for this lack by emphasizing it here.

When to Defocus

When a star is so bright that keeping it from saturation requires ridiculously short exposures (that produce poor duty cycle values), three options can be considered: 1) use a standard filter (such as V-band), 2) place a mask over the telescope that reduces your telescope's effective aperture, or 3) defocus.

Consider the first transiting exoplanet discovered, HD 209458. It's also the brightest BTE, with V-mag = 7.65. With my 11-inch Celestron, and a CBB filter, exposure times have to be kept shorter than 2.4 seconds. With an 8-second download time I'd be spending a wasteful 77% of an observing session simply downloading images. Changing to a V-band filter would allow 15-second exposures, and a 35% of time downloading. Using a z'-band filter would permit exposure times of 29 seconds, and a 22% wasted time downloading. The z'-band option is therefore an acceptable option; it has the added advantage of very low atmospheric extinction and sharper ingress/egress shapes. With an aperture of 11 inches and a z'-band filter it should never be necessary to employ options 2 and 3 in the previous paragraph.

CHAPTER 10 – EXPOSURE TIMES & DEFOCUS

A 14-inch aperture delivers 62% more photons to the CCD than a 11-inch aperture. An observer with a 14-inch telescope and no z'-band filter would be forced to use exposure times of 9 seconds when using a V-band filter, and about half the time would be spent downloading. Option 2 could be employed, masking the aperture to 11 inches, for example. Two unwanted things would happen if this were done: SNR would be reduced (by 38%) and scintillation noise would increase (by 17%). This is a situation when Option 3 should be employed.

Option 3 is to intentionally defocus, and remain defocused (the same amount) throughout the entire observing session. With this option SNR is not lost and scintillation is not increased, and there are actually slight improvements to both SNR and scintillation because longer exposure times are permitted and duty cycle is therefore increased (increasing information rate). There's a third payoff for defocusing: more pixels are involved in delivering photo-electrons to the count, so any imperfectly calibrated defect in a specific pixel will have less effect on the total flux measured. Technically, every pixel contributes a finite calibration error due to bias frame subtraction (if it is used), dark frame subtraction and flat field division. The resultant error from some pixels will be positive and for others the errors will be negative. When many pixels contribute to a total count there will be an averaging down of the various individual pixel errors; if each pixel error is uncorrelated with its neighbors then this component of error will average down as $1/\sqrt{N}$, where N is the number of pixels contributing significantly to the total count.

How much defocusing is required to achieve these benefits? Not much! The goal is to reduce C_{max} , the highest count in the point-spread-function (PSF). A sharply focused PSF has a Gaussian shape (on top of a low level pedestal that is much broader, but fainter, than the main Gaussian component). Counts as high as C_{max} are typically isolated to just one pixel when image scale and seeing are such that $FWHM = 2.5$ to 3 pixels; the high counts will be limited to just a few pixels when FWHM is more than ~ 3 pixels. A small amount of defocusing changes the shape by moving photons from the peak location to nearby ones, and quickly the PSF takes on a flat-topped shape. Additional defocusing for a Schmidt-Cassegrain telescope produces a PSF that looks like a donut, with the donut hole corresponding to light that's blocked by the secondary mirror attached to the corrector plate. It's not necessary to defocus this much, but in practice this is what's done. Consider the following images from a defocus experiment I conducted.

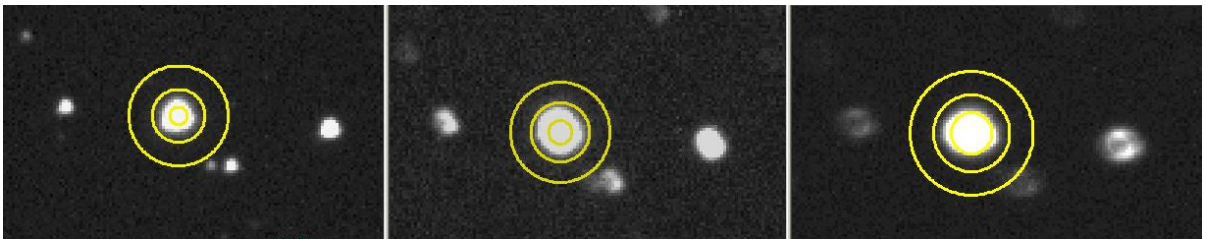


Figure 10.01. Sharp image, slightly defocused image and greatly defocused image. The inner photometry aperture has been adjusted to include 98% of the total flux. The stars have FWHM of 2.7, 4.3 and 6.5 pixels. $C_{max} = 31, 10$ and 6.9 kct.

In this sequence of images C_{max} ranges from 31,000 counts to 6,900 counts. Notice that the slightly defocused middle image had a dramatic 3-fold C_{max} reduction, with only a small increase in PSF radius (2.7 to 4.3 pixels), whereas the highly defocused image exhibits a less dramatic reduction in C_{max} . Clearly, the big payoff can be gained by only small amount of defocus.

CHAPTER 10 – EXPOSURE TIMES & DEFOCUS

If only a small defocus amount is employed then it is important to maintain this amount of defocus throughout the entire observing session. Otherwise, a part of the observing session might have sharply focused images that could be unusable due to Cmax saturation. All focusers should have a “focus temperature compensation” feature, and once the temperature coefficient is established this is the way to maintain a specific amount of defocus for long observing sessions (when temperature is likely to change). If your telescope has a low thermal expansion tube, then life is easier because you won’t need to invoke automated focus adjustments to track temperature changes.

If you’re going to observe defocused very often it might be worth investigating which defocus direction is better, in or out. For my telescope I evaluated RMS performance versus focus setting and determined that the best RMS performance was to defocus in the “out” direction 20 focuser counts. Of course every telescope system will be different.

I have a more extensive description of my defocusing investigation at the following two web sites:
http://brucegary.net/AXA/Defocus/defocusing_genl.htm
http://brucegary.net/AXA/Defocus/defocusing_hd80606.html

Professional astronomers are often burdened with too many photons, especially for exoplanet transit observations, and they employ defocusing to overcome the problem of saturation and the desire to avoid excessively short exposure times. A literature search of this topic might be instructive when the professionals create web pages or write articles addressing the topic.

Actually, the best response to the challenges of observing a too bright star could be a combination of options 1 and 3. In other words, use a narrower filter and defocus the required amount. In doing this you’ll lose SNR but you won’t increase scintillation (discussed in greater detail in Chapter 20).

Chapter 11

Focus Drift

I once neglected to "lock the mirror" after establishing a good focus, and went to sleep while observing a transit candidate. I'm glad this happened; the focus drifted and caused an effect that was too obvious to ignore, and this led me to investigate causes. The problem showed itself as an apparent "brightening" of the target (relative to several reference stars) near the end of the observing session.

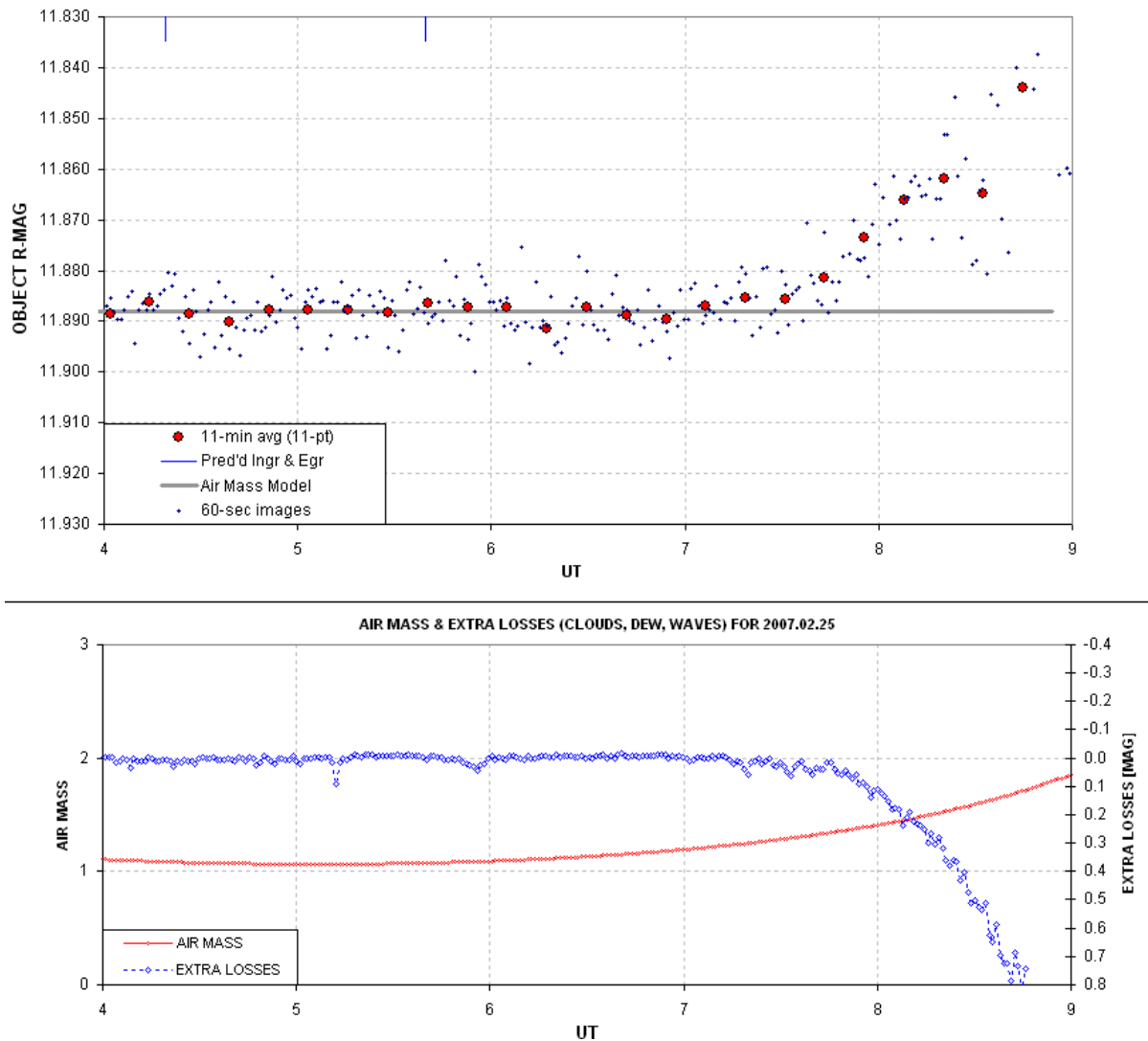


Figure 11.01. Light curve showing effect of focus drift starting at ~7.2 UT. The lower blue trace shows that the "sum of fluxes for all reference stars" decreased starting at the same time.

CHAPTER 11 – FOCUS DRIFT

I recall upon awakening, and looking at the image on the monitor, that the focus was bad and I immediately suspected that this was caused by focus drift, but I didn't know what effect it would have on the light curve (LC). After processing the images and seeing the LC, I knew right away that focus drift had affected it. Here's a plot of FWHM (and “aspect ratio”).

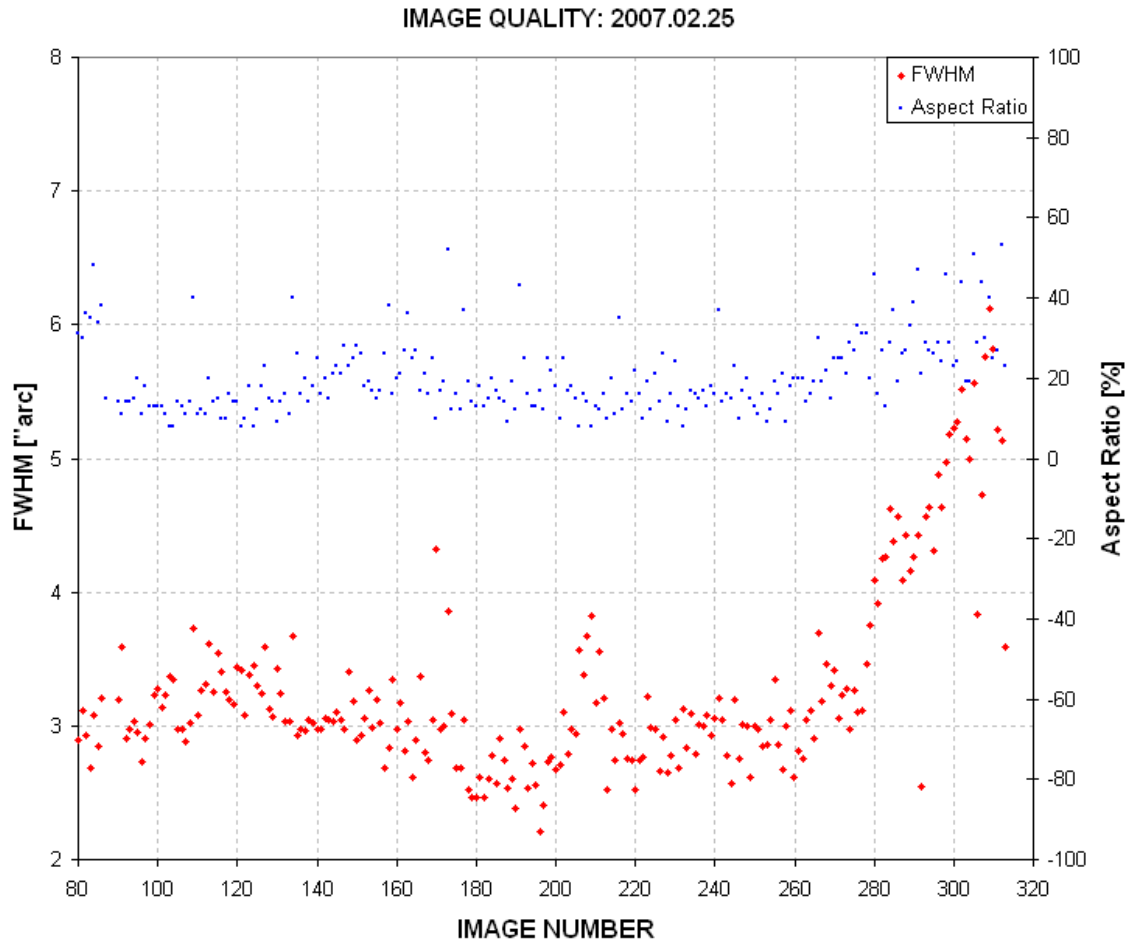


Figure 11.02. Plot of FWHM ["/>arc] and "aspect ratio %" (ratio of largest PSF dimension to smallest, expressed as a percentage) for the images used to produce the light curve. Image numbers near 260 correspond to 7.0 UT. (Produced using the automatic analysis program CCDInspector, by Paul Kanevsky.)

There's clearly a good correlation between focus degrading and the apparent brightening of the target star (~7.0 UT). But how can an unfocused image affect the ratio of star fluxes? To determine this, consider how MaxIm DL (and probably other programs as well) establish magnitude differences from a set of images. I'll use two images from the above set to illustrate this.

An image in good focus was chosen from ~7.0 UT and another from ~8.5 UT. They were treated as a 2-image set using the MaxIm DL photometry tool. The next figure shows the sharp focus image after a few stars were chosen for differential ensemble photometry.

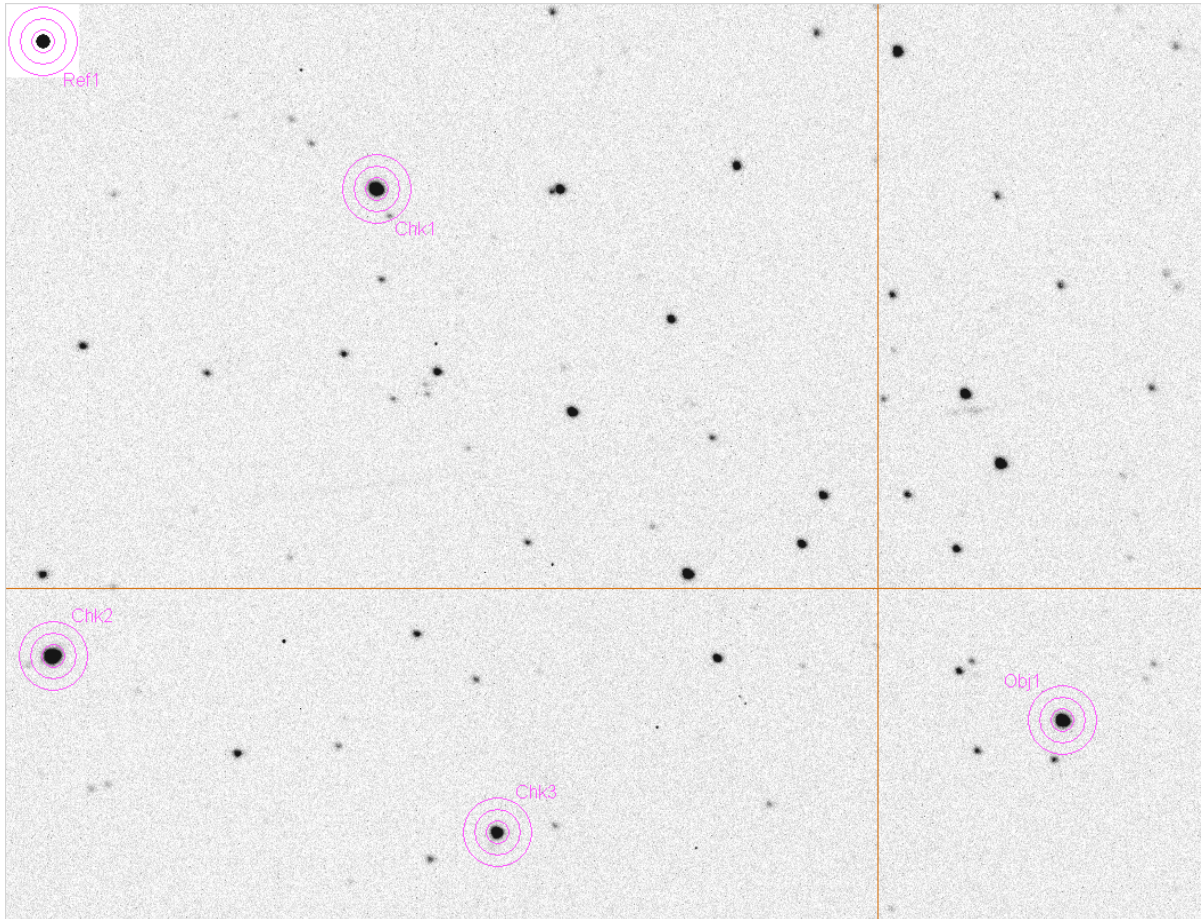


Figure 11.03. *Location of photometry apertures after using this image to select an object (the “target” or exoplanet candidate), check stars and a reference star (upper-left corner, my artificial star). (These notations are slightly misleading, as explained in the text.)*

The measured star fluxes are recorded to a CSV-file (comma-separated-variable in ASCII format) which can be imported to a spreadsheet, where the user can select from among the “check stars” to serve as reference. The artificial star is not used for reference; instead it serves to determine “extra losses” that might be produced by clouds, dew on the corrector plate, or image quality degradations due to poor tracking, wind shaking the telescope or poor focus (causing the PSFs to spill outside the photometry aperture). These details are not relevant to this chapter’s message, and they’ll be treated at length in Chapters 13 and 18.

Note that in this image essentially all of each star’s flux is contained within the signal aperture. The next figure is a screen capture of the photometry circle locations on the defocused image.

CHAPTER 11 – FOCUS DRIFT

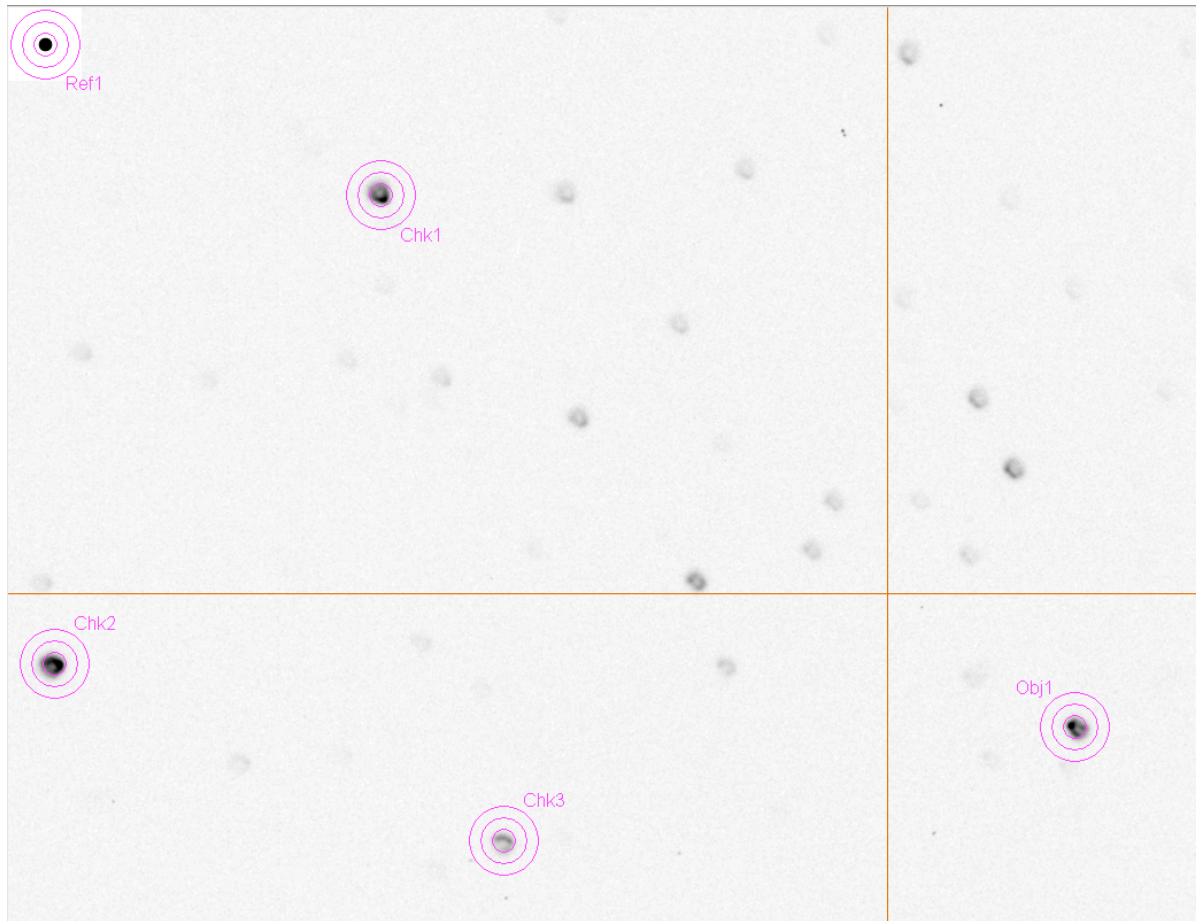


Figure 11.04. Same photometry apertures (at the same x,y locations as in the previous image) for the defocused image.

In the defocused image some stars have PSFs that are spread out in the infamous “comet shape” coma pattern, with the comet tails directed away from the optical center (indicated by the cross hair). The length of the coma tail is greater the farther the star is from the center. Thus, stars near the edges have a smaller fraction of their total flux within the aperture than stars near the center. The ratio of fluxes, and hence magnitude differences, will therefore be affected. The object's measured brightness can have either sign, depending on whether the target star (the exoplanet candidate, labeled “Obj1” in the figure) is closer to the center, or farther from it, compared with the reference stars (labeled “Chk” in the figure). For this image we can expect the reference stars to suffer greater losses than the target, leading to an apparent “brightening” of the target. The magnitude of this effect will be greater for smaller photometry apertures. Larger apertures would reduce this effect. However, the best solution is to never have to use poorly focused images.

Referring back to Fig. 11.01, and noting the blue trace labeled “Extra Losses [mag]”, an increase in losses is usually produced by cirrus clouds. However, in this case it was produced by a spreading out of the PSF beyond the signal aperture circle as focus degraded.

CHAPTER 11 – FOCUS DRIFT

The lesson of this chapter is “keep all images in good focus” (unless you’re intentionally observing defocused because the target star is too bright, as described in the previous chapter). If that doesn’t work, for whatever reason, then when processing the images use a large photometry aperture to assure that most of the flux is measured for all stars (“most” means ~99%). If you’re not sure that the aperture size was sufficiently large, then if you use an artificial star for setting the differential magnitudes check to see if the magnitude for any of the stars, or the magnitude corresponding to total flux for all the non-target stars, drops when the target appears to change values. Any correlation between target brightness and fading of reference stars should be viewed as a “red flag” for the presence of focus drift problems.

Observing Log Entries

I like to record in the observing log FWHM measurements of a chosen star at regular intervals, such as every half hour. This helps in identifying the need for a focus adjustment; it also will show the presence of atmospheric seeing trends. For one of my telescopes focus setting depends on elevation as well as temperature, so I also record these values.

Whenever I record a FWHM in the observing log I also record the magnitude that MaxIm DL displays when the photometry circles are over the star that I’ve chosen for that purpose. It doesn’t matter that the magnitude scale is uncalibrated (*i.e.*, having an offset error) because the only thing I’m monitoring is constancy of the chosen star’s brightness. This is a good way to detect the presence of cirrus clouds. It also can alert for the presence of dew accumulation on the corrector plate. You can’t do anything about cirrus clouds, but dew accumulation will require use of a hair dryer, dew heater strip or dew shield. By choosing a bright (unsaturated) star for this purpose the magnitudes should be constant at a level of <0.01 mag (assuming $SNR > 100$). Changes from one image to the next that exceed this usually indicate the presence of clouds. Slow changes will of course occur due to changing air mass, but these changes are small and easily identified as air mass related. For example, R-band observing will increase the star’s magnitude by ~ 0.13 magnitude per air mass, and if the observing log includes elevation notations it is easy to verify that trends are compatible with an atmospheric extinction explanation. I also like to record outside air temperature, dew point, wind max (during the past 5 minutes) and wind direction. Whenever focus is adjusted I note this as well.

Precaution when Focusing the Mirror

Focusing is accomplished in one of two ways: moving the primary mirror or moving the CCD camera assembly. The latter is preferable. However, I once used a backend optical configuration that required removing the “microfocuser” from my Meade LX200GPS telescope (in order to clear the base for reaching the north celestial pole as part of the pointing calibration). This forced me to adjust focus using the primary mirror. I’ll never do that again! In the First Edition of this book I devoted 2 pages to the problems this caused, but for this edition may I simply warn you to never conduct long observing sessions when mirror focus adjustments are required. If it means not using an AO-7 image stabilizer, then this is a good trade-off.

Chapter 12

Autoguiding

Some CCD cameras have two chips, a large main one for imaging and a small one beside it for autoguiding. CCDs with just one chip can be autoguided if a separate CCD camera is attached to a piggy-backed guide telescope. If you have neither of these ways to autoguide, may I suggest that you consider a hardware upgrade.

My CCD camera is a Santa Barbara Instruments Group (SBIG) ST-8XE. The X and E at the end just signify that I've upgraded a ST-8 to have a larger autoguider chip (SBIG's TC237) and USB communication.

There are a couple ways to automatically autoguide for an entire observing session. One is to use the autoguider chip to nudge the telescope drive motors. This can be done whether the autoguider chip is in the same CCD camera as the main chip or on a separate CCD camera attached to a piggy-back guide telescope. The main drawback for this method is that the telescope drive motors have hysteresis (poor backlash performance), especially the declination drive, and this produces uneven autoguiding. This method at least keeps the star field approximately fixed with respect to the pixel field (assuming a good polar alignment), but it permits star field location "wanderings" in both directions (RA and Dec) that are potentially sources of systematic errors (due to calibrations using an imperfect master flat field).

Image Stabilizer

The second method for autoguiding is to use a tip/tilt mirror image stabilizer. I have an SBIG AO-7 tip/tilt image stabilizer. SBIG now sells a more compact version (AO-8), which I would love to have since it shortens the optical backend path to the CCD. For large CCD format cameras SBIG sells an AO-L image stabilizer. As far as I know SBIG is the only company selling an image stabilizer that's priced for amateurs. The AO-7 allows me to use the autoguider image to adjust a tip/tilt mirror at the rate of up to ~10 Hz, depending on the brightness of the star I have in the autoguider's FOV. When the required mirror movement exceeds a user-specified threshold (such as 40% of the range of mirror motion) the telescope is nudged (i.e., using the RA and Dec motors) in the appropriate direction for a user-specified preset time (such as 0.1 second). I use MaxIm DL for both telescope control and CCD control, and I assume other control programs have the same capability.

In the planning chapter I described choosing a sky coordinate location for the main chip that assures the autoguider's FOV includes a star bright enough for autoguiding. Using a 14-inch telescope a star with V-mag ~ 11 is acceptable for 5 Hz autoguiding when using an R-band filter. When using a CBB filter the same autoguider performance can be achieved for stars as faint as 12th magnitude. If a B-band filter is to be used, autoguiding is almost always impossible. This illustrates the point made in Chapters 5 and 7 that autoguider requirements should be a consideration in choosing a filter for a specific observing session.

CHAPTER 12 – AUTOGUIDING

With an SBIG tip/tilt image stabilizer it is usually possible to produce long-exposure images that are as sharp as those in the average short-exposure, unstabilized images. Tracking is possible for the entire night provided cirrus clouds don't cause the autoguide star to fade significantly.

Image Rotation and Autoguiding

As pointed out earlier, whereas a successful autoguided observing session that lasts many hours will keep the autoguide star fixed to a pixel location on the autoguide chip, if the telescope mount's polar axis is imperfectly aligned the main chip's projected location on the sky will rotate about the autoguide star during the observing session. This will be seen in the main chip images as a star field rotation about an imaginary location corresponding to the autoguide star. Each star will move through an arc whose length will be greater for stars farthest from the autoguide star. The main chip's FOV will change during the observing session, and any reference stars near the FOV edge are at risk of being "lost." Such stars are also at risk of experiencing varying amounts of flat field correction error since image edges are where flat fields have the poorest quality. An important goal of exoplanet transit observing is to keep the star field viewed by the main chip fixed with respect to the main chip's pixels. Therefore, autoguiding will be most successful if the mount's polar axis is aligned accurately.

Observer Involvement with Monitoring

Amateurs have different philosophies about how much attention must be given to an observing session. Some prefer to start the entire process with a script that controls the various control programs. I prefer a greater presence in the control room throughout the observing session. After the flats have been made, and an observing sequence has been started, it may be theoretically possible to go to bed with an alarm set for the end of the session. I like to spot check such things as auto-guiding, focus setting, seeing, extra losses due to thin cirrus clouds, CCD cooler setting, and record items in an observing log at regular intervals. After all, if a passing cirrus cloud causes the autoguide star to lose track, the following observations will be useless until the observer reacquires the autoguide star. Autoguiding needs are the main reason I stay involved with observing for the entirety of an observing session. As you may have gathered from my "observatory tour" (chapter 2) my observing control room is comfortable. This is primarily in response to the requirements of autoguiding, which requires that I check-in on the telescope's tracking and record things on the observing log at frequent intervals.

Warning to Those not Autoguiding

When autoguiding is not used the star field will drift across the pixel field and cause systematic errors that vary during the observing session; all star flux ratios throughout the image will vary. These systematics won't be completely removed by the flat field calibration because no flat field is perfect. It's amazing how often this drifting can produce a light curve that resembles an ingress or egress feature. This is only a problem for short observing sessions of a predicted ingress or egress; it rarely affects a long observing session involving a full transit. I've intercepted several data files submitted to the AXA that exhibited an uncanny resemblance to a partial transit and with some e-mail exchanges these were identified as false transit features and the data files were not archived.

Chapter 13

Photometry Aperture Size

Before describing how images can be processed to produce light curves it is necessary to have an understanding of some basic concepts related to photometry aperture size.

The following descriptions will be based on my use of MaxIm DL, or MDL as I will refer to the program. I've never used other image analysis programs that are supposed to be comparable, but I'll assume that they're capable of performing similar operations. It will be up to the user of another program, such as AIP4WIN, CCDSoft, FotoDif or Mira, to figure out the equivalent procedure. I don't want this paragraph to seem like an advertisement for MDL, but I do want to say that I've never encountered anything related to image manipulation needed for photometry that wasn't performed easily with MDL.

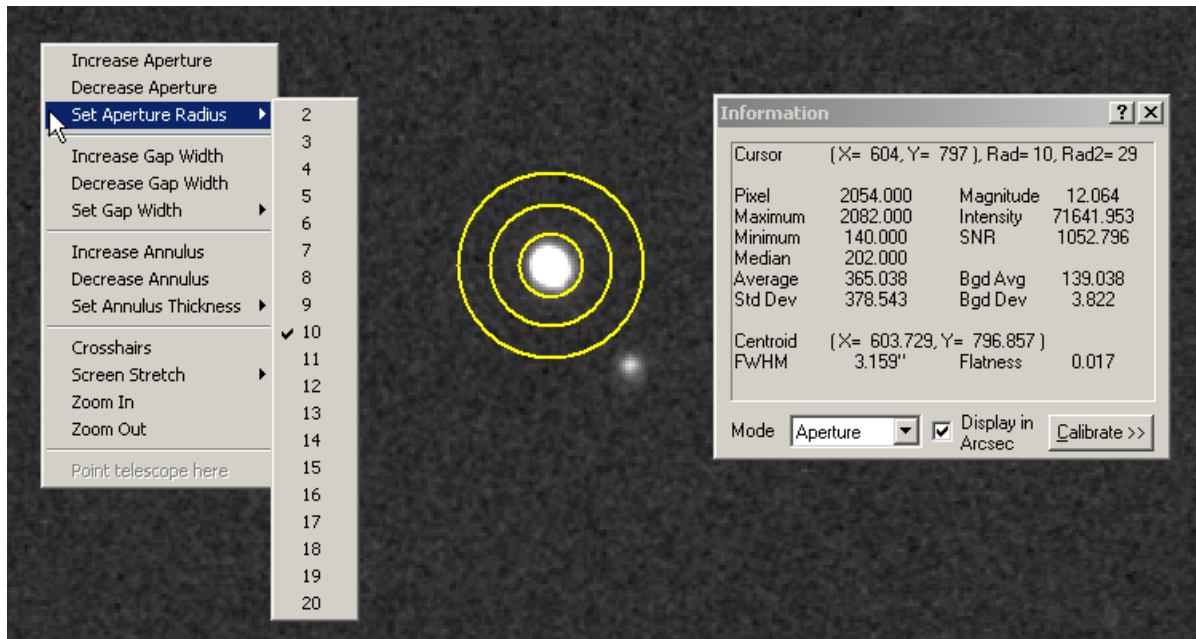


Figure 13.01. Three aperture circles with user-set radii of 10, 9 and 10 pixels. The Information window gives the cursor location, the radius of the signal circle (10 pixels) as well as the radius of the sky background annulus outer circle 29 pixels). The Information window shows many other things, such as magnitude, star flux (labeled "Intensity"), SNR and FWHM.

MDL uses a set of three circles for performing aperture photometry measurements. Figure 13.01 shows photometry aperture circles centered on a star. Notice that in this image the central circle, which I shall refer to as the "signal aperture," appears to enclose the entire pixel area where the star's light was registered. Note also that the outer sky background annulus (the area between the outer two circles) is free of other stars. When these two conditions are met the star flux reading displayed in the

CHAPTER 13 – PHOTOMETRY APERTURE SIZE

Information window (labeled “Intensity”) will be valid. If the signal aperture is too small the flux reading will be too small, and if the signal aperture is too large the flux may be correct but it will have a larger component of noise due to the many pixels involved. With a too large signal aperture the pixels near the outer edge will contain no information about star flux, but they will contribute noise to the flux reading. This can be easily seen by changing the signal aperture size and noting the way SNR changes, as shown in the next figure.

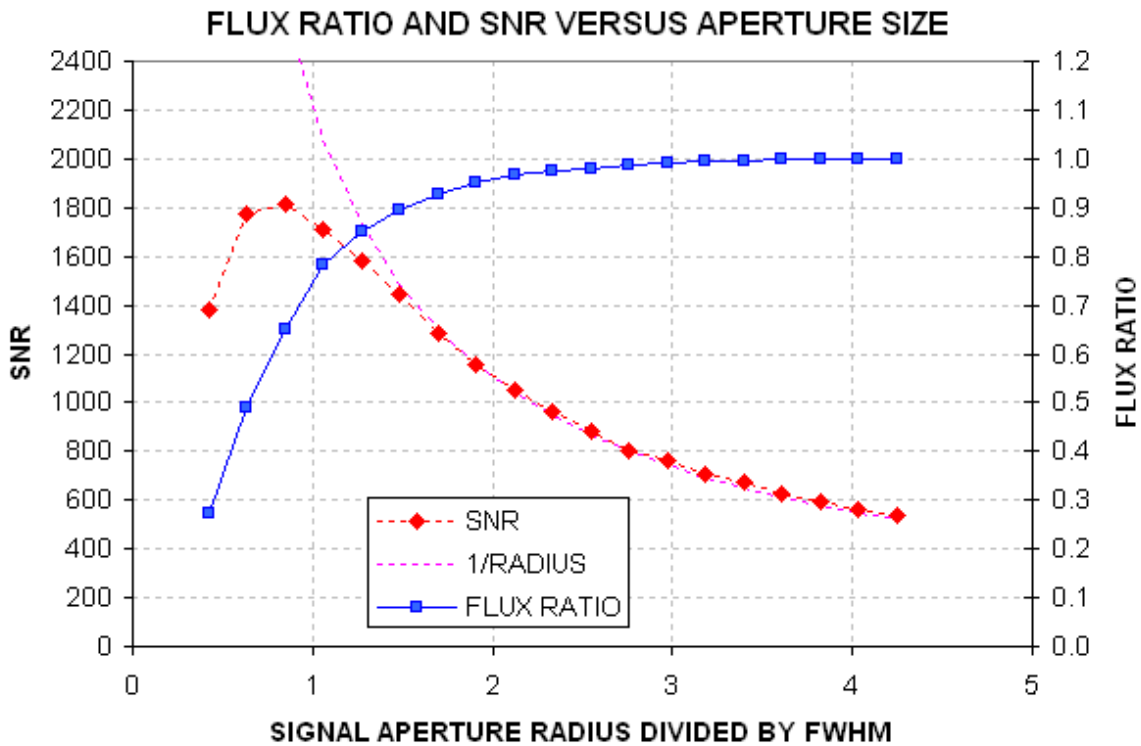


Figure 13.02. SNR and flux ratio (“aperture capture fraction”) versus signal aperture radius (normalized to FWHM) for the star in the previous figure. The purple dotted trace is “1 / radius.”

This figure shows a maximum SNR when the aperture radius is about $\frac{3}{4}$ of the FWHM. This agrees with theoretical calculations for a Gaussian shaped PSF. There are good reasons for not choosing a signal aperture radius where SNR is maximum when the goal is to produce an accurate exoplanet light curve. Notice that when the maximum SNR size is chosen the photometry aperture circle captures only ~ 65% of the total flux from the star. This is easily understood by considering that as the radius is increased more pixels are used to establish the star’s flux, but these new pixels are adding parts of the star’s PSF that are less bright than the central portion. Although the new pixels are adding to the total flux, they are also adding to the noise level of the total flux. This happens because each pixel’s count value is compared with the average count value within the sky background annulus, and a difference is added to the total flux. But each pixel is “noisy” (due to thermal jostling of electrons in the CCD elements and electronics, read noise and sky brightness contributions to the counts from each pixel). For example, in this image the RMS noise for each pixel is 3.5 counts. The noise level of the total flux increases with the square-root of the number of pixels added, and since

CHAPTER 13 – PHOTOMETRY APERTURE SIZE

the number of pixels increases as the square of the radius the noise on total flux readings should be proportional to the signal aperture radius. Beyond a radius of $\sim 1.4 \times \text{FWHM}$, where total flux has essentially reached an asymptote, the SNR does indeed decrease as $1/\text{radius}$.

For some observing projects small signal apertures are appropriate, such as detecting and tracking faint asteroids. For the asteroid situation SNR could be 2 to 3 and precision isn't important. For my rotation light curve observing of faint asteroids I use an aperture set to the above indicated $1.4 \times \text{FWHM}$ value, and whenever I've made comparisons this choice produces the best results. But consider some of the problems that might occur with bright stars where brightness precision is paramount. In Chapter 11, describing focus drift, it was shown that when PSF changes during an observing session "aperture capture fraction" may differ across the image.

In this situation the user faces competing goals: the desire for small stochastic noise levels versus small systematic errors. If we adopt an aperture radius of twice FWHM the aperture capture fraction rises to 96% but SNR is reduced to $\sim 60\%$ of its peak value. Even this may be too risky. Consider the implications of one part of an image having a PSF for which this aperture captures 95% of the total flux versus 96% at the center. This 1% difference corresponds to 10 mmag, and if our goal is to eliminate systematic errors above the 2 mmag level, for example, then we cannot tolerate 1% changes in the aperture capture fraction for the target star, or any of the reference stars, during the entirety of the observing session. By choosing a radius that is 3 times FWHM, $\sim 99\%$ of the total flux is captured. I feel comfortable with this choice, but there's no clear way of arguing for a best aperture size since each observing session is different and one might be absolutely OK using a small aperture while another would be riddled with intolerable systematic errors.

My subjective solution to this problem of not knowing how small a signal aperture is acceptable is to process the images using three aperture sizes: radius = 2.5, 3.0 and $3.5 \times \text{FWHM}$. As Chapter 15 describes, MDL can easily produce ASCII files of flux measurements with different aperture sizes, so this is one option to consider – especially in those cases where image sharpness varies greatly from image to image or from image center to the edges.

There's more to choosing photometry apertures than the concern about aperture capture fraction. The same image in Fig. 13.01 has a bright star (not shown in this figure) that would be useful to use as a reference star, but a fainter star is located 9" arc (12 pixels) away. The next figure's left panel shows these stars with a photometry pattern for which the signal aperture radius is $3.0 \times \text{FWHM}$. This aperture choice is unacceptable because some of the nearby star's flux is within the signal aperture. The right panel shows that the nearby star can be excluded from the signal aperture by reducing the aperture radius from 12 pixels to 10 pixels, corresponding to $2.4 \times \text{FWHM}$. Before choosing a signal aperture radius it is important to check all bright stars to see if a radius adjustment like this one should be made.

CHAPTER 13 – PHOTOMETRY APERTURE SIZE

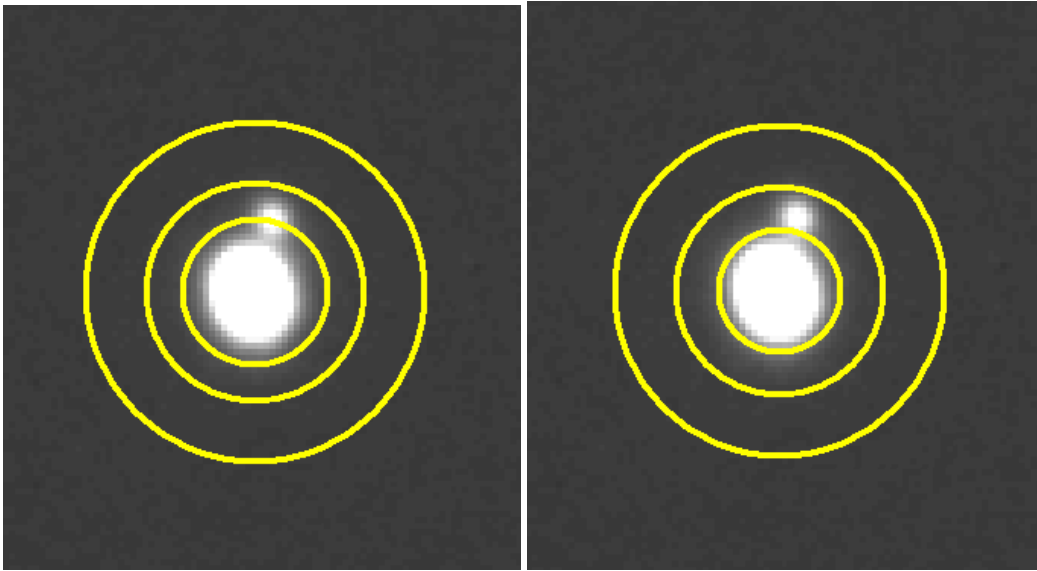


Figure 13.03. Left panel: *Candidate reference star showing photometry aperture circles with the signal aperture radius = $3.0 \times FWHM$.* Right panel: *Same star with signal aperture radius = $2.4 \times FWHM$.*

What about stars in the sky background annulus, as shown in the next figure?

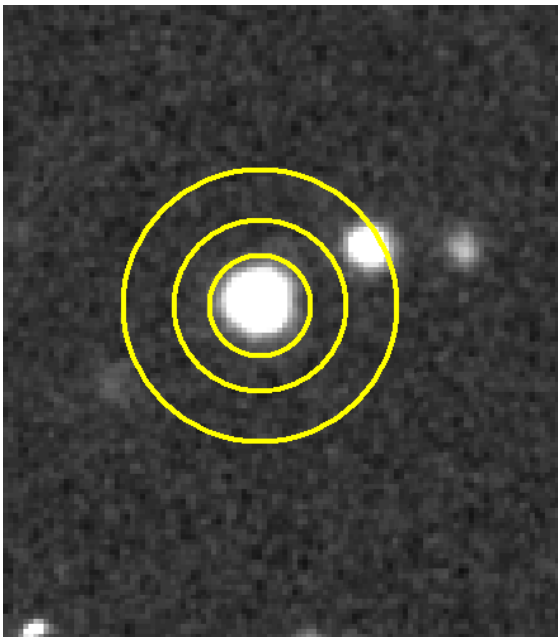


Figure 13.04. *Example of a star with a nearby star that's within the sky background annulus.*

Actually, this is not a problem because MDL's photometry tool uses a sophisticated algorithm for eliminating outlier counts in this annulus. AIP4WIN does the same using a different algorithm. (Note:

CHAPTER 13 – PHOTOMETRY APERTURE SIZE

The current version of MDL’s “on the fly” photometry doesn’t use the sophisticated algorithm for rejecting sky background counts from such stars, so be careful when using the MDL Information Window’s “Intensity” readings.)

In conclusion, the most important aperture size to choose carefully is the signal aperture radius. Whenever there’s concern about what aperture size to choose it is very easy (in MDL) to process the images with several choices. The files produced with different aperture sizes can be imported to different spreadsheets and systematic behaviors of each star can be performed to determine which aperture size to accept.

This chapter’s message is to start with a default signal aperture radius of about $3.0 \times \text{FWHM}$, and adjust in response to the presence of interfering stars. Consider using $2.5 \times \text{FWHM}$ and $3.5 \times \text{FWHM}$. Only the “brave” or “foolhardy” will use $2 \times \text{FWHM}$ for precision photometry.

Chapter 14

Photometry Pitfalls

This chapter is meant to prepare you for the next three chapters, which are a daunting description of my way of overcoming pitfalls of the standard ways of producing light curves that may be acceptable for variable stars but inadequate for exoplanet transits.

Most variable star light curves (LCs) require precisions of 0.05 to 0.01 magnitude, whereas exoplanet LCs should be about 10 times better, i.e., 2 to 5 mmag precision per minute.

Perfection can indeed be the enemy of good enough, because achieving perfection takes so much more effort. It should not be surprising that producing exoplanet LCs should require more than twice the effort of a typical variable star LC. Sometimes I'll spend more than half a day with just one LC.

The amount of effort needed for producing good exoplanet LCs will depend on the shortcomings of your telescope system. The closer to "professional" your system, the less effort required. If your telescope tube is made with materials that don't expand and contract with changing ambient temperature, then one category of concern is removed. If your observing site is high, and remote from city lights, other categories of concern are reduced. If your aperture is large and collimation is good, SNR and blending issues are less important.

The next three chapters are presented for observers with "moderate" apertures (8 to 14 inches), at poor to moderate sites (sea level to 5000 feet), with telescope tubes that require focusing adjustments as temperature changes and with equatorial mounts that may have polar alignment errors of ~ 0.1 degree or greater. These shortcomings probably apply to most exoplanet observers.

Let's review some of the LC shortcomings that may be acceptable for variable star observing but which are not acceptable for exoplanet observing. Some of these have been mentioned in the preceding chapters, but others have not.

An imperfect polar alignment will cause image rotation, which causes the star field to drift with respect to the pixel field during a long observing session. This causes temporal drifts, and possibly variations, whenever the flat field is imperfect, and no flat field is perfect. The systematic errors produced by this are on the order of 10 mmag. This is an acceptable level for all AAVSO projects (that I'm aware of), but it is unacceptable for exoplanet LCs.

The size of star images will vary with air mass, as approximately the $1/3$ power of air mass. When aperture photometry is employed with the same aperture size for all images, the photometry aperture capture fraction will vary in a systematic way with air mass, and this leads to an incorrect derivation of atmospheric extinction. There's a way of overcoming this (use larger apertures is one), but the price paid is lower SNR and more blending. This is a potential systematic error to keep in mind and I will describe ways of dealing with it later.

CHAPTER 14 – PHOTOMETRY PITFALLS

Ensemble differential photometry of star fields that have not been studied thoroughly for the purpose of identifying variables present an increased risk that one of the stars used for reference is variable. If one of these stars is indeed variable there could be drifts, or sinusoidal variations, in the exoplanet LC. Since most exoplanet star fields have not been investigated with a thoroughness that would identify low amplitude variables, which is a worthy task underway by AAVSO Director Arne Henden, the amateur observer must keep this issue in mind when choosing reference stars. To achieve the highest precision in an exoplanet LC there are strong incentives to employ many reference stars (to reduce both scintillation and stochastic noise levels). The exoplanet observer should therefore be motivated to identify stars that are not constant enough to be used for reference. The importance of this precaution will be appreciated after the capability for doing it has been accomplished. I am continually surprised by how many stars are variable at the mmag level. In the past three years I have discovered two Delta Scuti type pulsating variable stars, plus several stars with longer period variations, because I was checking many nearby stars for constancy before accepting them for use as reference. An amateur who contributes to the Amateur Exoplanet Archive (Patrick Wiggins) notified me about suspicious behavior of a star he was trying to use as a reference star (only 2.4 ‘arc away from HD 149026), and it turned out to be a dwarf eclipsing binary – which he is credited with for discovering! All of the stars that turned out to be variable were candidates for use as reference stars, and they underscore the need for not trusting in the constancy of stars chosen at random when selecting stars for reference. For AAVSO projects this problem is minimized by using one of the “sequence stars” as the “comp” star (reference), and these stars are supposed to have been measured enough times to rule out their variability (at maybe the 40 mmag level). EB events constitute such a small fraction of the EB period that even the AAVSO sequence stars can’t be guaranteed constant (to the level required for exoplanet work), but using a “check star” would reveal when this situation exists. Even when the bright transiting exoplanets (BTEs) do not have a “sequence” of calibrated stars their constancy at the mmag level will be unknown. Chapters 15 and 18 describe image analysis and spreadsheet processing methods that permit the use of a large number of reference stars within the exoplanet image’s FOV.

Star color matters when choosing reference stars. For example, if the exoplanet candidate star is red and all nearby stars are blue, be prepared for an air mass correlated curvature of the LC baseline level. To minimize these effects extra work will be required to select suitable stars using their J and K magnitudes for deriving star color. Other methods for accomplishing the rejection of “off color” reference stars are described in Chapter 18.

Other subtle systematic effects are present at the mmag level but this review should suffice to convince the reader to be prepared for extra work if you want to produce good quality LCs. Most of the extra work will involve spreadsheets. I hope you like using spreadsheets, because anyone who hates them won’t do a good job using them.

Two years ago I created the Amateur Exoplanet Archive, and this led many amateurs to ask me for advice on this new thing called “exoplanet light curves.” It eventually became apparent to me that most of the questions arose from observers who had learned “good observing practices” for AAVSO projects, and they were having trouble unlearning some of those practices and replacing them with new ones essential for exoplanet observing. For example, there was puzzlement over not having a sequence of calibrated “comp” stars near each exoplanet star. I had to explain that an exoplanet transit light curve does not use a calibrated magnitude since all the things to be learned from the LC (e.g., mid-transit time, transit depth, transit shape, etc) are unrelated to magnitude zero shifts that are used

CHAPTER 14 – PHOTOMETRY PITFALLS

to put an object on a standard magnitude scale. Another puzzling issue was the fact that exoplanet work didn't require CCD Transformation Equation adjustments. It must have been surprising for the observer steeped in AAVSO traditions to enter any old magnitude that came to mind for the "comp" star magnitude, or zeros for all ensemble reference star magnitudes. There are so many differences between AAVSO variable star observing and exoplanet transit observing that I have devoted an entire chapter to this subject, called "Exoplanet Stars are not Variable Stars" (Chapter 21). That chapter will make more sense after reading the next few chapters, which make clear why certain things have to be done, and others don't have to be, to achieve millimag precision exoplanet transit light curves.

The next three chapters should be viewed as a guide to the concepts that matter. My specific implementation of the precautions that should be taken is just one implementation out of many that must exist. Every month I improve my image processing techniques and my spreadsheets. A year from now I would probably be embarrassed by the shortcomings of what is presented in the next three chapters. I therefore recommend that you read these chapters for "concepts" instead of specific implementations.

As patent attorneys like to write into every first paragraph: "The following description is merely one embodiment of the invention and it is meant to include all other embodiments."

Chapter 15

Image Processing

Image processing can be done with several programs. A survey of exoplanet observers who contribute to the Amateur Exoplanet Archive (AXA) reveals the following usage statistics:

MaxIm DL	8
FotoDif	5
Iris	5
AIP4WIN	4
Mira	1

As is probably obvious by now, I champion MaxIm DL (MDL)! I've tried to use the other programs, but maybe because I'm familiar with MDL they just seemed too cumbersome and limited in capability. I apologize to anyone who has reason to disagree with this assessment, but the important considerations should be "Can everything be done that needs to be done?" and "Do I feel comfortable using this program?"

This chapter describes image processing procedures that will be needed for creating photometrically-measured data files that can be submitted to an exoplanet archive, such as the AXA or the ETD (Czech Republic's Exoplanet Transit Database). This chapter will include additional descriptions for creating an "Artificial Star" photometry data file that is meant for importation to a special spreadsheet where the user can select a sub-set of stars for use as reference, which then permits the creation of a file for submission to the AXA or ETD. As the next chapter explains there are three paths to a data file that can be submitted to an archive, and each of these three paths also allows the user to plot a light curve and adjust a simple transit model to achieve a fit to the data. I'll just list them here, and ask the reader to wait for a fuller description in the next three chapters:

Comp/Chk, using 1 comp (reference) star and one check star

Ensemble, using several reference stars (and no check stars)

Artificial Star, using the artificial star for reference and many stars as "chk" (which will serve as candidates for reference in a spreadsheet)

All paths to a data submission file and light curve plot require that images be manipulated in ways similar to what is described in this chapter. Please view the specific instructions in this chapter as merely one way to achieve the desired result. My examples will be for the MDL user, so if you use another image processing program just glean concepts from the following explanations.

Imagine that we have 600 raw images from a night's observations. This could be from a 6.5-hour observing session consisting of 40-second exposures. Given that my RAM is limited to 2 GB there are limits to how many images I can load without having to use virtual RAM (which really slows things down). By setting MDL to disable the "undo" feature it is possible to work with twice as many images in working memory. My CCD has pixel dimensions of 1530 x 1020, and a 1x1 (unbinned) image uses 1.1 Mb of memory (compressed). I can safely load 200 raw images into working memory

CHAPTER 15 – IMAGE PROCESSING

without involving virtual RAM. This is 1/3 of the 600 images to be processed, so what I'll describe in the next few paragraphs will be done three times. Each user will have a different limit for the maximum number that can be loaded into working memory, so if you want to use MDL and the following processing procedure you will simply have to determine how to replace my use of "200 images" with whatever applies to your computer's capabilities.

The first step is to calibrate the 200 images using the master dark and master flat frames. For the rest of this chapter I'll present a detailed version of how to do something using MDL in small, italicized font. The next paragraph describes in more detail how I prefer to calibrate the images in working memory using MDL.

Specify the master flat and master dark files in MDL's "Set Calibration" window. Select "None" for "Dark Frame Scaling" (assuming the dark frame is at the same temperature and has the same exposure as the light frames to be calibrated). Check the Calibrate Dark and Calibrate Flat boxes. Don't check "bias" unless either the exposure time or CCD temperature were different for the master dark and target frames. Exit the calibration set-up and calibrate all 200 raw images (~10 seconds).

Review a few images to see if the calibration "worked." Sometimes the master dark doesn't do a proper job and "hot pixels" are scattered at the same locations of all images. If this is the case it's recommended to "remove" the hot pixels. Actually, the "removal" process consists of identifying them and replacing their count value with the average of their neighbors. It is important to not be too aggressive in setting the threshold for hot pixel removal. I have found that 30% is usually safe, meaning that a pixel is identified as "hot" when its value exceeds 30% of the average of its neighbors. For poorly focused (or for defocused) images, where the PSF for all stars have a FWHM of many pixels, it can be safe to employ a more aggressive threshold, such as 20%. However, checks should be made on a sample (sharp) image to be sure that the star flux is not altered by the hot pixel threshold. When the threshold is too aggressive the maximum counts will be reduced. Establishing a safe hot pixel threshold is better performed before loading the 200 images so that the "Undo" feature can be enabled. A few sharp images are loaded, calibrated, and a trial hot pixel correction is performed. Because the Undo feature is enabled it is a simple matter to switch back and forth between images (before and after hot pixel correction) to see if any stars have different maximum counts in the before and after versions.

Why worry about hot pixels? After all, when they are present in the sky background annulus they are not used by the photometry tool. But if they are present anywhere within the photometry signal aperture, however, they will lead to a brighter than true star flux. The broader the PSF the more important it is to remove hot pixels before using the photometry tool.

After you're satisfied that hot pixels are rare (by either noting that they don't exist after calibration, or by removing them), the third step is to "star align" all 200 images. This will consist of x and y offset adjustments, as well as image rotations if necessary. (Hot pixel removal cannot be performed after star alignment since slight pixel movements of an image cause what were hot pixels to be smeared to a lower % contrast with its neighbor pixels).

Invoke MDL's Align command and select Add All images. The Align Images window appears; select "Auto – star matching" and click "OK" to align all images. The result (after ~1.5 minutes) will be a set of images in working memory that have been shifted in x and y, and rotated if necessary, to achieve alignment of the star

CHAPTER 15 – IMAGE PROCESSING

field, using the first image in the list as a template. This set of images might be worth saving to a directory, but that's optional (to do this with MDL, select File/BatchSave&Convert, etc).

Consider what we have in working memory now: 200 calibrated images, with all stars at the same pixel locations.

It will be useful later to have a printed image for making notations of which star is the target and which stars are to be used for reference. Select a few sharp images and median combine them; invert the image and save it. Switch to a program for printing the image (I use Total Commander to view files, with ACDSee specified for viewing; with the ACDSee view of the image printing is accomplished with a Ctl-P command). Having a printed inverted image (that's mostly white) is especially useful for the third of the following three image analysis paths, because it will entail using as many as 29 reference stars and when each of the 200-image groups are processed it's essential that the same reference stars are used, in the same order.

The remaining image processing step consists of measuring star magnitudes. Because the three paths lead to the recording of three different CSV-file products (corresponding to Comp/Chk, Ensemble and Artificial Star), there are 3-path divergence in this chapter's instructions. Until you read the following two chapters, that describe the strengths and weaknesses of these three methods for producing transit light curves, you won't know which of these paths you will want to use. I recommend that you at least read the first two path descriptions.

Comp/Chk

Before invoking the image processing program's "photometry tool" it is important to consider which aperture size is likely to be optimum. Chapter 13 deals with this in more detail than here. If you are unsure about the best signal aperture radius, create files for each of several plausible signal aperture sizes. The "rule of thumb" for which aperture sizes will be best is to multiply FWHM [pixels] by 3, then straddle this value. For example, if FWHM ~ 4 pixels, the most likely best signal aperture radius will be 12 pixels; so straddling this will mean using aperture radii of 10, 12 and 14 pixels (producing 3 sets of CSV-files).

Invoke the "photometry tool" of your imaging processing program and select the exoplanet star as your target (also called "object"), select a comp star (also called "reference") and select a check star. When the comp ("reference") star is selected you will have to enter a magnitude for it. It's OK to enter a correct magnitude for this star, corresponding to the filter in use, but it is totally unnecessary! I always ignore this request, which MDL interprets as an entry of "zero", and the only consequence is that the target star will have a large magnitude offset that's the same for every image. This, of course, is irrelevant to the goal of determining mid-transit time, or transit depth, or transit shape – which are the only things amateur light curves will be used for (99.9% of the time). The photometry tool will go through all images and measure the flux of each star and convert them to magnitudes based on the measured flux and user-entered magnitude for the reference star. The user will be asked to specify a filename for recording magnitudes for the three stars in each of the (200) images in memory.

After the first set of 200 images has been recorded (three times, once for each photometry aperture size), proceed to repeat the above until all images have been processed and recorded.

CHAPTER 15 – IMAGE PROCESSING

Ensemble

The procedure for this is almost identical to the Comp/Chk procedure. The only differences are that many reference stars can be chosen and no check stars are required. As each reference star is selected the photometry tool will ask for a magnitude, and again it is OK to enter correct magnitudes, but it is totally unnecessary! I neglect to enter magnitudes for each reference star, which MDL interprets as a zero entry each time. When a CSV-file is recorded you will notice that the average for all reference stars is zero, which is OK – as explained above.

After the first set of 200 images has been recorded (three times, once for each photometry aperture size), proceed to repeat the above until all images have been processed and recorded.

Artificial Star

There's an extra step for the Artificial Star analysis path that has to be performed before invoking the photometry tool. This step is to add an artificial star in the upper-left corner of all images. This is done using a free plug-in written by Ajai Sehgal. You can get a 32x32 pixel version from the MDL web site. A 64x64 version was written at my request, and you may download the plug-in from the following web site: http://brucegary.net/book_EOA/xls.htm. I prefer to use the 64x64 version since it allows the use of large photometry apertures. The artificial star will be Gaussian shaped with the brightest pixel equal to 65,535 and a FWHM = 3.77 pixels. The flux for this artificial star is always 1,334,130 counts.

With MDL, the artificial star is added to all images by opening the Plug-In menu and clicking “Add 64x64 reference star.”

As an aside, consider again what we have in working memory now: 200 images, all stars are at the same pixel locations, including an artificial star with a fixed flux at the same location in the upper-left corner of each image. If we compare the flux of a star with that of the artificial star, and convert that to a magnitude difference, we have a way of keeping track of the star's flux in all images. Compared to the previous two paths (for Comp/Chk and Ensemble) this has the advantage of retaining more information than a simple magnitude difference (e.g., “differential photometry”). With differential photometry the user specifies a reference star (or an ensemble of several stars for reference), and all object and check stars have their fluxes compared to the reference star (or the average of the reference stars when doing ensemble). The flux ratios are converted to magnitude differences, and a file is created that contains these magnitude differences. For some users the appeal of this set of magnitude differences is that changes in extinction, such as changes in cirrus cloud losses, are removed (to first order). Or, to put it another way, information about atmospheric extinction and losses due to cirrus clouds is “lost” when recording a differential photometry file. Sometimes this loss of information won't matter, which is often the case for ordinary variable star observing (where 0.01 magnitude errors are acceptable), but when it does matter (i.e., for the exoplanet observer trying to achieve 0.002 magnitude precision) the user will be rewarded by better quality light curves that employ the Artificial Star method. This will be illustrated in the next two chapters. I'll mention just one example here: Suppose the comp star (or one of the ensemble reference stars) is variable? You'd never know this by viewing the target star's light curve. If you suspected this was a problem you would have to reprocess the entire image set using a different comp star (or different set of reference stars). One value of using the artificial star for reference is that when the magnitude differences file is imported

CHAPTER 15 – IMAGE PROCESSING

to a spreadsheet the user will have full control over which stars to choose for use as reference. The user can view LC plots for all stars that were measured and evaluate their constancy, and be guided by this analysis in choosing which stars to use as a final ensemble reference set. Further, because the artificial star has a fixed flux, all magnitudes referenced to it contain star flux information. (Don't let anyone tell you that MDL can't record star fluxes.) This requires extra work for the user, but with the extra effort comes a significant increase in "analysis power" – as Chapter 18 will illustrate.

After choosing photometry aperture size, as described above, you will invoke the image analysis program's "photometry tool" in order to create files containing star magnitudes for the 200 images.

Using MDL, invoke the photometry tool (Analyze/Photometry). All images in working memory are selected by default in the "Image List" and the highlighted image in this list is displayed in the work area. Check the boxes labeled "Act on all images" and "Snap to centroid." Open the drop down menu "Mouse click tags as:" and select "New Object." Navigate around the highlighted image and find the exoplanet star; left-click it. The aperture circles appear and are snap-centered on the star; the "Obj1" label is displayed (it can be dragged to an "out of the way" location nearby if the label overwrites stars to be measured). You may not notice it, but all images have the same photometry circles centered on the same star (you can check this by highlighting an image in the "Image List" to see that image highlighted in the work area). Next open the drop down menu "Mouse click tags as:" and select "New Reference Star." Navigate to the artificial star in the highlighted image and left-click its approximate location; the set of photometry circles appear snap-centered over the artificial star with the label "Ref1". All images automatically have their reference star identified with the same aperture circles and "Ref1" label. Next, open the drop down menu "Mouse click tags as:" and select "New Check Star". Navigate the highlighted image to the first star chosen earlier to be the first in the series of "check stars" – to be considered for use as reference stars during the spreadsheet phase of analysis. Left-click this star, and proceed to do the same for the rest of the check star list. Finally, click the "View Plot..." button. The "Photometry" graph appears. It can be resized to exaggerate the magnitude scale if you want to see if any of the stars are variable or noisy. This encompasses a large magnitude range, so small variations won't be visible, but it's worth a cursory look. The real purpose for displaying this graph is that it has a "Save Data..." button; click it and navigate the directory structure to where you want to record the magnitude differences CSV-file. Enter a file name, such as "1-r" (where r is the signal aperture radius), and click "Save". If other signal aperture sizes are of interest, right-click on an image and a drop-down menu will appear that allows you to change the radius. The photometry for all images is immediately recalculated; click the graph's "Save" button and save the CSV-file with another descriptive name, such as 1-r, where the value for r is different. When finished creating CSV-files for all the signal apertures of interest, click "Close" and you're back to MDL's main work area. All files in working memory may be deleted (alt-F, E).

Perform the above analysis with the other two groups of 200 raw images. Use different CSV-filenames, of course, such as "2-r" and "3-r" – where the "r" stands for the signal aperture radius. If more than one signal aperture is used the CSV-file names could look like the following: 1-10, 2-10, 3-10 for the 10-pixel radius photometry, and 1-12, 2-12, 3-12 for the 12-pixel radius photometry, etc.

This completes the image processing phase of analysis. The next three chapters describe what to do next using spreadsheets to produce transit light curves.

Chapter 16

Three Photometry Methods Previewed

The task of converting a set of images to a light curve consists of two parts: 1) using an image processing program to process images and photometrically measure magnitudes for several stars on all the images, and 2) using a spreadsheet or an auto-fit program to convert these star magnitudes to a light curve and overlay a model fit to the transit feature. The previous chapter dealt with the first of these tasks, and this chapter presents an **overview** of three methods for performing the second task.

Three Ways to Produce a Light Curve

Assume that a set of images from an exoplanet observing session has been calibrated (bias, dark, flat) and measured by one of the three methods described in the previous chapter. There are three corresponding data file types created by the image processor's photometry tool, so there are three methods for producing a light curve from these data files.

- 1) Comp/Check
- 2) Ensemble
- 3) Artificial Star (AS)

AAVSO observers who use a CCD will be familiar with the first two. Both are “differential photometry” methods. The third method is more powerful, but it requires learning new tricks. This chapter reviews the three methods briefly; the following two chapters contain more details about them. I recommend that you begin by practicing using Method #2 (don't bother with #1, since it offers no advantages and suffers from serious disadvantages). You will then have an easier time understanding the method I recommend, #3.

Comp/Check Method

This procedure specifies one star as the target (called “Obj1”), another as reference (called “comp” by visual observers), and a third star as “check” (to verify that the “comp” star is stable, which assumes that the “check” star is also stable). MaxIm DL (MDL) photometry produces a CSV-file (comma-separated-variables) which for the Comp/Check method will have four columns: JD, MagObj, MagComp and MagChk. For purposes of illustration the WASP-10 event used to produce the light curve on the cover of this book has also been processed according to this method. Reference and check stars were chosen for being nearby and of similar brightness. The reference star was assigned a magnitude of zero (since it doesn't matter). Header lines were inserted in front of the MDL CSV-file to produce a data file in the format accepted by the Amateur Exoplanet Archive (AXA), shown as Fig. 16.01. The AXA's “auto-fit” program was used to generate a model fit, shown as Fig. 16.04. This Comp/Check LC looks OK, and for this example there are no obvious shortcomings (thanks to ideal observing conditions and a lucky choice of “comp” star).

CHAPTER 16 – THREE PHOTOMETRY METHODS

```
StartDate      : 20081114
Object         : wasp10
Observer       : Gary, Bruce (GBL)
E-mail        : 123@brucegary.net
Country/State : Arizona
Latitude      : +31.452
ELongitude    : -110.237
Aperture      : 14-inch
Filter        : C
Exposure      : 60 sec
ClockCorrn    : 0 sec
Loss column   : N
Comment       : Clr. CompChk method.
Comment       : "T (JD)", "obj1", "Ref1", "chk1"
```

```
2454784.5529629630,0.269,-0.000,-0.094
2454784.5537962965,0.270,0.000,-0.084
2454784.5546412035,0.264,0.000,-0.093
2454784.5554745370,0.266,0.000,-0.092
2454784.5563078704,0.269,0.000,-0.092
2454784.5571412039,0.266,0.000,-0.089
2454784.5579745369,0.268,0.000,-0.095
```

Figure 16.01. Data file in AXA format using Comp/Check method.

Ensemble Method

The “Ensemble” method is the same as the previous one with the difference that many stars are chosen for reference (instead of just one star) and none are chosen for check. When MDL asks for reference star magnitudes you may simply enter zero for all of them (again, because it doesn’t matter). For this illustration I chose only 4 reference stars (although a couple dozen would be better). Figure 16.02 shows a data file in AXA format for this method. Note that for both data files illustrated here the user must insert header lines ahead of the CSV-file created by MDL.

```
StartDate      : 20081114
Object         : wasp10
Observer       : Gary, Bruce (GBL)
E-mail        : 123@brucegary.net
Country/State : Arizona
Latitude      : +31.452
ELongitude    : -110.237
Aperture      : 14-inch
Filter        : C
Exposure      : 60 sec
ClockCorrn    : 0 sec
Loss column   : N
Comment       : Clr. Ensemble method.
Comment       : "T (JD)", "obj1", "Ref1", "Ref2", "Ref3", "Ref4"
```

```
2454784.5529629630,0.588,0.319,0.225,-0.541,0.247
2454784.5537962965,0.584,0.314,0.230,-0.540,0.246
2454784.5546412035,0.582,0.319,0.225,-0.541,0.247
2454784.5554745370,0.585,0.319,0.227,-0.543,0.250
2454784.5563078704,0.585,0.316,0.224,-0.542,0.254
2454784.5571412039,0.580,0.314,0.225,-0.540,0.251
2454784.5579745369,0.589,0.320,0.225,-0.540,0.245
2454784.5588078704,0.584,0.317,0.226,-0.542,0.251
```

Figure 16.02. Data file in AXA format using Ensemble method.

CHAPTER 16 – THREE PHOTOMETRY METHODS

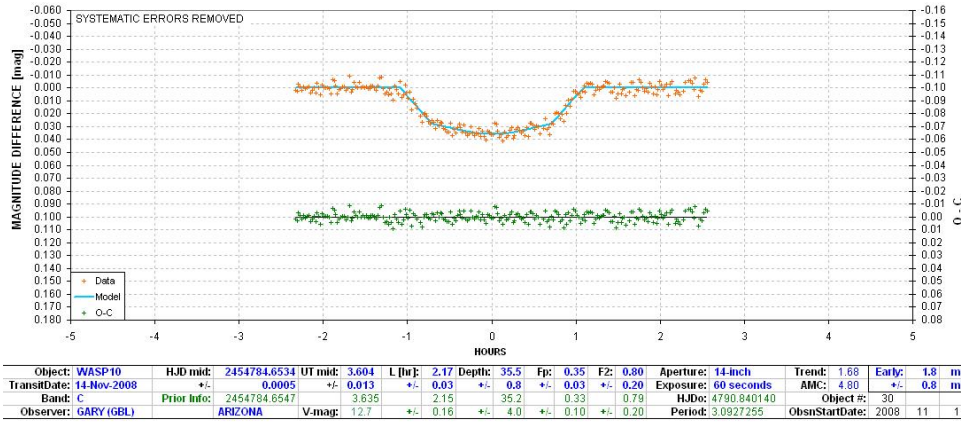


Figure 16.04. Light curve produced by the AXA auto-fit program from the Comp/Chk data file.

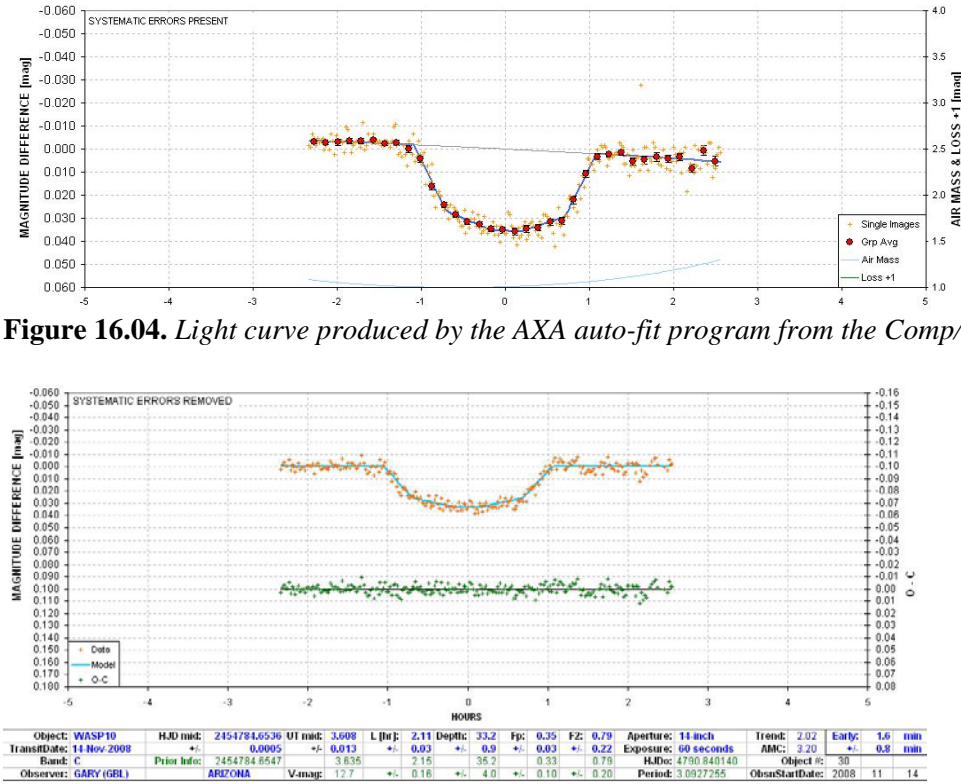


Figure 16.05. Light curve produced by the AXA auto-fit program from the Ensemble data file.

CHAPTER 16 – THREE PHOTOMETRY METHODS

The AXA auto-fit program was used to process the ensemble file (cf. Fig. 16.02), with a light curve result shown in Fig. 16.05. Both the Comp/Chk and Ensemble light curves look OK, and in fact by visual inspection they appear comparable to the Artificial Star LC. These two simple methods are usually acceptable when a set of properly exposed and calibrated images are processed and all reference stars are well-behaved. Differences become significant when a nearby star used for reference has a greatly different color than the target star, or when it is itself a variable (usually a Delta Scuti type). Differences also will exist when scintillation during the observing session is greater than normal. These are subtle effects that will be dealt with in the next two chapters.

Artificial Star Photometry

The third method probably should not be called “differential photometry” because the CSV file records magnitude differences from an artificial star; the recorded magnitudes are not differences from another star (or group of stars), which is as defining trait for differential photometry. Because the artificial star has a fixed flux (of 1,334,115 counts), this method is recording magnitude-equivalents of star fluxes. Figure 16.06 is a partial screen capture of the beginning portion of an Artificial Star CSV-file (with informational header lines inserted by the observer). An artificial star CSV-file cannot be submitted to the AXA for processing; rather, it is meant for importing to a special spreadsheet where the user can experiment with assigning various subsets of “chk” stars for use as reference.

```
StartDate      : 20081114
Object         : wasp10
Observer       : Gary, Bruce (GBL)
E-mail        : 123@brucegary.net
Country/State : Arizona
Latitude      : +31.452
ELongitude    : -110.237
Aperture      : 14-inch
Filter        : C
Exposure      : 60 sec
Clockcorr     : 0 sec
Loss column   : N
Comment       : C\l.r. ArtificialStar method.
Comment       : "T (JD)", "obj1", "Ref1", "chk1", "chk2", "chk3", "chk4", "chk5", "chk6", "chk7", "chk8", "C\l
```



```
2454784.5529629630,1.985,0.000,1.716,1.622,0.856,1.645,2.273,1.548,1.016,2.349,2.925,2.560,2.066
2454784.5537962965,1.944,0.000,1.674,1.590,0.820,1.606,2.236,1.505,0.975,2.300,2.869,2.519,2.029
2454784.5546412035,1.974,0.000,1.711,1.617,0.851,1.638,2.267,1.544,1.009,2.339,2.903,2.546,2.057
2454784.5554745370,1.964,0.000,1.698,1.606,0.836,1.629,2.269,1.533,0.997,2.328,2.895,2.541,2.041
2454784.5563078704,1.917,0.000,1.649,1.557,0.790,1.586,2.221,1.486,0.945,2.281,2.852,2.485,1.994
2454784.5571412039,1.918,0.000,1.653,1.563,0.798,1.589,2.226,1.495,0.950,2.287,2.854,2.502,2.000
2454784.5579745369,1.925,0.000,1.656,1.561,0.796,1.581,2.215,1.489,0.954,2.289,2.856,2.503,2.003
2454784.5588078704,1.927,0.000,1.660,1.569,0.801,1.593,2.226,1.494,0.957,2.292,2.862,2.513,2.005
```

Figure 16.06. Data file using Artificial Star Photometry method.

Note that this format includes just one “Ref” entry, and it’s zero for every image (because that’s what I allowed MDL to use for the reference star). Since each of the magnitude entries in this file is easily convertible to flux the file can be used to determine atmospheric extinction. Although the entries are not differential star magnitudes, differential magnitudes can be easily computed for any subset of “chk” stars selected for use as reference by the user (in a special spreadsheet). Everything that the previous two methods can do, this method can do also. It’s the power of being able to do many additional things that makes this method attractive – provided you like working with spreadsheets!

CHAPTER 16 – THREE PHOTOMETRY METHODS

For some observers this last statement will be enough to dampen enthusiasm for the third method. If you don't like working with spreadsheets, then you should probably restrict your use to Method #2, which is fast, easy and usually produces acceptable results. Most of the 650 submissions to the AXA were made using Methods #1 and #2. The Comp/Chk method has absolutely no advantages over Ensemble (#2), and it has potentially serious disadvantages, so I don't recommend using it.

A fuller explanation of the strengths and weaknesses of the three methods will be given in the next two chapters.

Chapter 17

Spreadsheet Processing – Comp/Check & Ensemble Methods

This chapter is a more detailed explanation of the Comp/Chk and Ensemble methods for processing files created by the image processing program's photometry tool. Recall these three analysis methods:

- 1) "Comp/Check" photometry (single reference star, single check star),
- 2) "Ensemble" photometry (many reference stars, no check stars), and
- 3) "Artificial Star" photometry (many "chk" stars measured for use as reference by spreadsheet user).

Most amateurs use either Method #1 or #2. Even if you're planning on using Method #3 a close reading of this chapter is advised because similar procedures are involved and their descriptions won't be repeated in the Artificial Star chapter (next).

Although I advise never using Method #1, the "Comp/Check" method, since many amateurs use it I will describe it. The ASCII file (in CSV-format) consists of 4 columns: 1) JD, 2) magnitude of the target star (based on the magnitude assigned to the "comp" star), 3) the "comp" star's magnitude (same for all images) and 4) magnitude of the check star (based on the magnitude assigned to the "comp" star). After adding header lines the data file will look something like this:

```
StartDate      : 20081114
Object         : wasp10
observer       : Gary, Bruce (GBL)
E-mail        : 123@brucegary.net
Country/State : Arizona
Latitude       : +31.452
ELongitude    : -110.237
Aperture       : 14-inch
Filter         : C
Exposure       : 60 sec
ClockCorrn    : 0 sec
Loss column    : N
Comment       : Clr. CompChk method.
Comment       : "T (JD)","obj1","Ref1","chk1"
```

```
2454784.5529629630,0.269,-0.000,-0.094
2454784.5537962965,0.270,0.000,-0.084
2454784.5546412035,0.264,0.000,-0.093
2454784.5554745370,0.266,0.000,-0.092
2454784.5563078704,0.269,0.000,-0.092
2454784.5571412039,0.266,0.000,-0.089
2454784.5579745369,0.268,0.000,-0.095
```

Figure 17.01. Example of "Comp/Check" data file after the user adds informational header lines.

The "Ensemble" method is similar except that several stars are used for reference. No check stars are needed since the other references stars can serve that purpose. When the AAVSO recommends the ensemble method it is assumed that several calibrated "sequence" stars are present in the FOV containing the target star. For exoplanet work this requirement doesn't exist, and all stars within the

CHAPTER 17 – SPREADSHEET FOR COMP & ENSEMBLE

FOV, calibrated or not, can be used and can be assigned any magnitude the observer wishes to assign. I always use zero for all reference stars (it doesn't matter what magnitudes are assigned 99.9% of the time, as explained in the "Filter Choice" chapter). The next figure shows what an ensemble CSV data file might look like:

```
StartDate      : 20081114
Object         : wasp10
observer       : Gary, Bruce (GBL)
E-mail         : 123@brucegary.net
Country/State : Arizona
Latitude       : +31.452
ELongitude    : -110.237
Aperture       : 14-inch
Filter         : C
Exposure       : 60 sec
ClockCorrn    : 0 sec
Loss column    : N
Comment        : Clr. ArtificialStar method.
Comment        : "T (JD)", "obj1", "Ref1", "chk1", "chk2", "chk3", "chk4"

2454784.5529629630, 0.588, 0.319, 0.225, -0.541, 0.247
2454784.5537962965, 0.584, 0.314, 0.230, -0.540, 0.246
2454784.5546412035, 0.582, 0.319, 0.225, -0.541, 0.247
2454784.5554745370, 0.585, 0.319, 0.227, -0.543, 0.250
```

Figure 17.02. Example of “ensemble” data file after the user adds informational header lines.

In the above data file the average of the four reference stars is zero because I assigning zero magnitude to all reference stars. Note that files in the above two formats can be submitted to the Amateur Exoplanet Archive (AXA), or the Exoplanet Transit Database (ETD), where the data will be archived and displayed with an overlay of a transit light curve model based on an auto-fitting program. Both web sites also include results of the auto-fit program: mid-transit time, transit depth, transit length, etc.

Data submitted to the AXA before 2010.01.01 will also be included in the Caltech NStED archive (NASA/IPAC/NExSci Star and Exoplanet Database). The NStED archive is where professional astronomers search for data by other professionals on their favorite star or exoplanet, and with the inclusion of AXA-submitted data from amateurs it is a convenient place for professionals to search for amateur data as well. As this Second Edition was being prepared a decision was made by Caltech to not proceed with plans to upgrade their NStED archive program to accept amateur data submissions directly in the future due to staff and budget limitations. I therefore recommend that all data submissions be made to the Czech Republic's ETD.

Observers may also create a light curve plot with a model fit overlay using a spreadsheet. The data file can be plotted as a light curve starting with any blank spreadsheet, which I recommend trying; but fitting a model to the data and comparing mid-transit time and other transit properties to what is expected on the basis of what is already known about the exoplanet requires a special spreadsheet that has been prepared for this purpose. The author has created such a “template” spreadsheet, using Microsoft's Excel. The spreadsheet is called LCcep.xls, and a zipped version can be downloaded from the following web site: http://brucegary.net/book_EOA/xls.htm

CHAPTER 17 – SPREADSHEET FOR COMP & ENSEMBLE

Using LCep.xls is simple. The first “page” (I use “page” interchangeably with “worksheet”) has a list of the known exoplanets, and a vertical “slide bar” for selecting which one to use. Here’s a screen capture of what part of this page looks like:

Object	RA	RA RA	DE	DE DE	B	Y	R	I	L	SE	D	SE	Band	Fp	SE	F2	SE	HJDo
Object Name	RA	RA RA	DE	DE DE	Mag	Mag	Mag	Mag	hr	hr	mmag	mmag						add 2450000
WASP-10	23 15 58.3		31 27 46	99.99	12.7	99.99	99.99		2.13	0.12	37	2.5	?	0.32	0.07	0.73	0.15	4357.85803
WASP-17	15 59 51		28 3 42	99.99	11.6	99.99	99.99		4.27	0.2	20.3	5		0.26	0.15	0.82	0.15	4559.18102
WASP-16	9 20 24.7		33 52 57	99.99	10.42	99.99	99.99		3.84	0.07	8.4	0.3		0.26	0.15	0.82	0.15	4491.6161
HAT-P-13	9 20 24.7		33 52 57	99.99	10.42	99.99	99.99		3.84	0.07	8.4	0.3		0.26	0.15	0.82	0.15	4491.6161
WASP-13	9 20 24.7		33 52 57	99.99	10.42	99.99	99.99		3.84	0.07	8.4	0.3		0.26	0.15	0.82	0.15	4491.6161
HAT-P-12	13 57 33.5		43 29 37	99.99	12.84	99.99	99.99		2.30	0.05	28.1	3.0		0.32	0.15	0.78	0.15	4419.19556
WASP-15	13 55 42.7		32 9 35	11.3	10.9	11.0	99.99		3.5	0.15	11.5	1.5		0.26	0.15	0.82	0.15	4584.69823
HD80606	9 22 37.6		50 36 13	99.99	8.5	7.9	99.99		11.3	3	10	1.5		0.62	0.2	0.75	0.25	4876.295
WASP-6	23 12 37.7		22 40 26	99.99	11.9	99.99	99.99		2.61	0.1	26.4	1.5		0.26	0.15	0.82	0.15	4596.43267
HAT-P-11	19 50 50.2		48 4 51	10.64	9.59	99.99	99.99		2.30	0.03	4.2	0.3	z	0.11	0.03	0.80	0.15	4605.89132
WASP-12	6 30 32.8		29 40 20	12.11	11.69	99.99	11.03		2.93	0.02	16.5	0.6	z,C	0.23	0.12	0.81	0.18	4508.9760
CoRoT-4	6 48 47.3		0 40 22	99.99	13.7	13.45	99.99		4.42	0.10	14.0	0.4	C	0.20	0.10	0.78	0.15	4141.36416
CoRoT-3	19 28 13.3		0 7 19	14.2	13.29	99.99	99.99		3.77	0.04	5.2	0.4	C	0.23	0.10	0.88	0.15	4283.1383
CoRoT-1	6 48 19		0 6 8	14.2	13.6	99.99	99.99		2.46	0.01	24.8	0.4	C	0.35	0.08	0.84	0.12	4159.4532
HAT-P-8	22 52 10		35 26 48	99.99	10.26	99.99	99.99		3.6	0.25	7.0	1.5	z	0.25	0.20	0.75	0.25	4437.67582
WASP-11/HAT-P-10	3 9 28.6		30 40 25	99.99	11.89	99.99	99.99		2.59	0.15	22.4	1.5		0.23	0.10	0.81	0.15	4729.90631
HAT-P-9	7 20 40.4		37 8 26	12.80	12.30	99.99	99.99		3.22	0.08	15	1	R,z	0.13	0.08	0.83	0.12	4417.9077
WASP-10	23 15 58.3		31 27 46	99.99	12.7	99.99	99.99		2.13	0.12	37.0	2.5	?	0.32	0.07	0.73	0.15	4357.85803
WASP-14	14 33 6.3		21 53 41	10.21	9.75	99.99	99.99		2.77	0.07	10.9	0.7	YR	0.25	0.15	0.88	0.15	4465.81963

Figure 17.03. First page of LCep.xls, meant for use with both the “Comp/Chk” and “Ensemble” data files. This is where an exoplanet is selected for use in other pages.

Notice that in this figure WASP-10 has been selected by the vertical slide bar and an information line for this object is shown at row 8. Other pages make use of this information.

The second page (Fig. 17.04) is where the CSV-format data file is imported. An example of importing a “Comp/Chk” file is shown. (More detailed instructions are given on each spreadsheet page than will be given here.) The header lines aren’t required for anything in the spreadsheet, but it saves time to have all the relevant header information as part of the data file. Normally, only the first two columns of data are needed (columns B and C). If for some reason JD is not in the full format (7 characters before the decimal), the JD and object magnitude columns (B and C) should be reproduced somewhere to the right of the imported data region with the correct format. Also, if “ClockCorm” is non-zero a new column should be created to the right that includes the correction.

The “Chk1” column isn’t normally used, but it can be handy to work with if something unusual is found in the exoplanet’s light curve. The JD/magnitude data section (columns B and C) are to be copied and pasted in the next page.

CHAPTER 17 – SPREADSHEET FOR COMP & ENSEMBLE

	A	B	C	D	E	F	G	H	I	J	K	L	M	N	O	P
1		This page is where you import your CSV-data file that was created by the image processing program's j														
2		This page assumes you have a CSV-format text file (created by Maxim DL, for example) that has columns J														
3		Before importing your data file you should delete the data that's already here (if you're starting to learn how to														
4		If you're importing your data file to this page (and after you've deleted the data that's already here), place your														
5		It's optional to have header lines. For this example I show header lines that are used for submitting to the AX/														
6																
7		StartDate	:	20081114												
8		Object	:	wasp10												
9		Observer	:	Gary, Bruce (GBL)												
10		E-mail	:	123@brucegary.net												
11		Country/State:		Arizona												
12		Latitude	:	+31.452												
13		ELongitude	:	-110.237												
14		Aperture	:	14-inch												
15		Filter	:	C												
16		Exposure	:	60 sec												
17		ClockCorrn	:	0 sec												
18		Comment	:	This data file was prepared by AXA from an observer-submitted data file.												
19		Comment	:	Clr. Comp/Chk method.												
20		Loss column	:	N												
21		Comment:		JD, Obj, Ref1, Ref2, Ref3, Ref4												
22																
23		T (JD)		Obj1	Ref1	Chk1										
24		2454784.5530		0.269	0.000	-0.094										
25		2454784.5538		0.270	0.000	-0.084										
26		2454784.5546		0.264	0.000	-0.093										
27		2454784.5555		0.266	0.000	-0.092										

Figure 17.04. Screen capture of part of the 2nd page (of LCep.xls). The data file (with header) is imported to cell B7. The data shown is from a “Comp/Chk” data file; an “Ensemble” data file would show more columns of reference stars (and no “Chk” star).

	A	B	C	D	E	F	G	H	I	J	K	L	M	N	O	P
2		Enter you observing site coordinates in cells D13 and D14.														
3		Enter your filter name in cell D15, and enter an approximate magnitude for the BTE (using your filter														
4		It's optional to enter your exposure time in cell D16.														
5		Now, here's the important part: delete what's here, then copy the first two columns of data in the prev														
6		In previous page place cursor over upper-left most data (cell B26 in this example),														
7		While holding Shift key, navigate one column to right, then all the way down to the last row of data. This highlights														
8		Copy this data to the Excel clipboard (Ctrl-C).														
9		Move back to this page and paste the contents of what's on the clipboard to data area (e.g., place cursor over ce														
10																
11	WASP-10	23	15	58.3	+	31	27	46	99.99	12.70	99.99	99.99	2.13	0.12	37.00	2.50
12		Observer		HAO					B	V	R	I	L		D	
13		II. Latitude		31.45												
14		E. Longitude		-110.24					RA/DE	23	15	58.3	31	27	46	
15		Filter		C	12.70	Mag										
16		Exposure time		60	62	Remember to TRIM bottom of imported data if you didn't delete data before cc										
17		Last row # with data		255												
18		For HD102195	Obj1	AS	Ref1	Ref2	Ref3	Ref4	Ref5	Chk2						
19				1	2	3	4	5	6	7	8	9	10	11	12	1
20	Im#	T (JD)	Obj1	Ref1	Chk1											
21	1	2454784.5530	0.269													
22	2	2454784.5538	0.270													
23	3	2454784.5546	0.264													
24	4	2454784.5555	0.266													
25	5	2454784.5563	0.269													
26	6	2454784.5571	0.266													
27	7	2454784.5580	0.268													
28	8	2454784.5588	0.267													
29	9	2454784.5596	0.266													
30	10	2454784.5605	0.271													
31	11	2454784.5613	0.269													
32	12	2454784.5622	0.267													
33	13	2454784.5630	0.271													
34	14	2454784.5638	0.264													

Figure 17.05. Third page of spreadsheet LCep.xls (described in text).

CHAPTER 17 – SPREADSHEET FOR COMP & ENSEMBLE

The third page of this spreadsheet is screen captured for Fig. 17.05. Before copying data from the previous page any data on this page leftover from a previous use should be deleted (everything below B21:C21). Observing site information is entered in cells D13:D14, as well as filter, exposure time and approximate magnitude of the exoplanet star. To the right of what is shown in this figure are calculations leading to air mass. Appendix C contains a description of the algorithm that is used to calculate air mass. (An easier way to have this capability is to download a sample spreadsheet from http://brucegary.net/book_EOA/xls.htm.) Nothing else has to be done by the user on this page.

Figure 17.06 is a screen capture of part of the 4th page. It may seem silly that the principal thing the user has to do on this page is to enter a number suggested by a nearby cell. The explanation has to do with the “evolution” of spreadsheets from versions that do one thing to versions that do other things. I made the fewest “mutations” to arrive at this spreadsheet from the one that handles artificial stars. Actually, a more important user task for this page is “trimming.” By trimming is meant deleting rows that are “below” the last row of valid data (displayed as row 255 in cell E12), or copying rows from the penultimate one present to fill out what’s needed. When I use the term “trim” on other web pages this is what I mean.

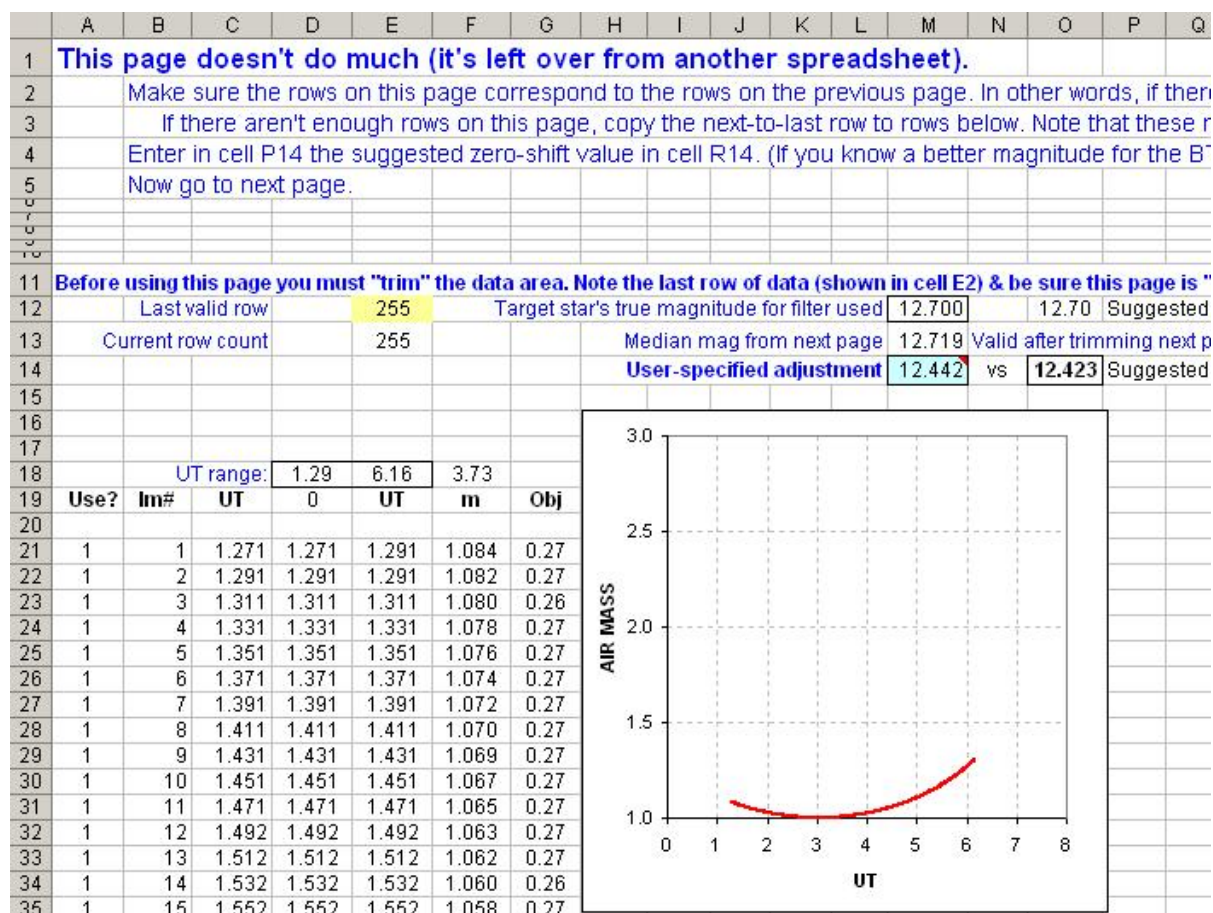


Figure 17.06. Fourth page of *LCep.xls*, where the user must “trim” the rows below valid data.

CHAPTER 17 – SPREADSHEET FOR COMP & ENSEMBLE

1	This page is where outlier data is rejected & accepted data is averaged.																			
2	Before using this page you must "trim" it. Be sure that all rows (columns A to AF) are "populated" in a way																			
4	Noisy data can be rejected by specifying a rejectYou are returning to this page from the LC page. The plo																			
5	Other features of this page will be described latAdjust data rejection criterion (cell AR16) to achieve ~ 99																			
6	Upon returning to this page (as instructed on next page), resume following instructions found on this page																			
11	UT range:		1.291	6.2														0.996		
12	Last row # with data:		255															3.87	RMS [mmag]	
13	Current row count		255															3.87	RMS 1 min [mmag]	
14																			Select RMS criterion (AC6) the	
15	Min	Max		Max	12.76				Nr of values	245	Meridian								99.6	% OK
16	12.72	12.7	Median	Avg	12.72				Accepted [%]	100.0	Flip								14.0	mmag
17				Min	12.69				Corr'd										9.8	Suggest
18				Min	12.69				For copying to ymddhhnn.TXT			Use column AC for histogram								
19	Use	Im#	UT	Use column?	Obj	JD4	dMag	UT	9.2	Median	Diff	Both	MC						OK	3
20									0.0282	of 8										
21	1	1	1.291	1.084	12.711	4784.55296	12.711	1.291	12.711	12.711	12.710	12.710	2	2	12.71					
22	1	2	1.291	1.082	12.712	4784.55380	12.712	1.291	12.712	12.712	12.708	12.708	4	4	12.71	0.00				
23	1	3	1.311	1.080	12.706	4784.55464	12.706	1.311	12.706	12.706	12.711	12.711	-5	-5	12.71					
24	1	4	1.331	1.078	12.708	4784.55547	12.708	1.331	12.708	12.708	12.710	12.710	-2	-2	12.71					
25	1	5	1.351	1.076	12.711	4784.55631	12.711	1.351	12.711	12.711	12.709	12.709	2	2	12.71	0.00				
26	1	6	1.371	1.074	12.708	4784.55714	12.708	1.371	12.708	12.708	12.710	12.710	-2	-2	12.71					
27	1	7	1.391	1.072	12.710	4784.55797	12.710	1.391	12.710	12.710	12.709	12.709	2	2	12.71					
28	1	8	1.411	1.070	12.709	4784.55881	12.709	1.411	12.709	12.709	12.710	12.710	-1	-1	12.71	0.00				

Figure 17.07a. Fifth page of *LCep.xls*, explained in the text.

The fifth page needs to be “trimmed,” like the previous page (add or delete rows as necessary so that only the rows of this observing session are “populated”). This page is where you can specify an “outlier rejection criterion.” All data that is noisier than the value in cell P16 (14 mmag in this example) is to be rejected from plotting and model fitting. The “noise” value for a datum is calculated in column P to be the difference between that row’s magnitude for the target minus the average of the nearest 8 neighbors. Column R shows all accepted data. Cell P15 shows the percentage of data that is accepted for the user-specified criterion in the cell below it. I recommend experimenting with criterion values until an acceptance of ~ 98% to 99% is achieved.

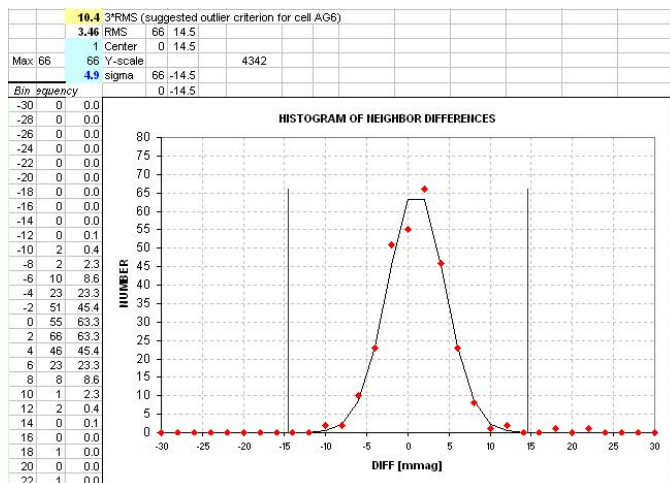


Figure 17.07b. Histogram of neighbor differences with a Gaussian fit.

CHAPTER 17 – SPREADSHEET FOR COMP & ENSEMBLE

Figure 17.07b shows a histogram of the magnitude differences (column P in Fig. 17.07a). The user may, as an option, calculate this histogram. The user may change cell values to see how a Gaussian model fits the histogram, and the width of this model is used to suggest a rejection criterion (Fig. 17.07a's cell R16).

The next spreadsheet page is where the accepted data are plotted as a light curve (Fig. 17.08).

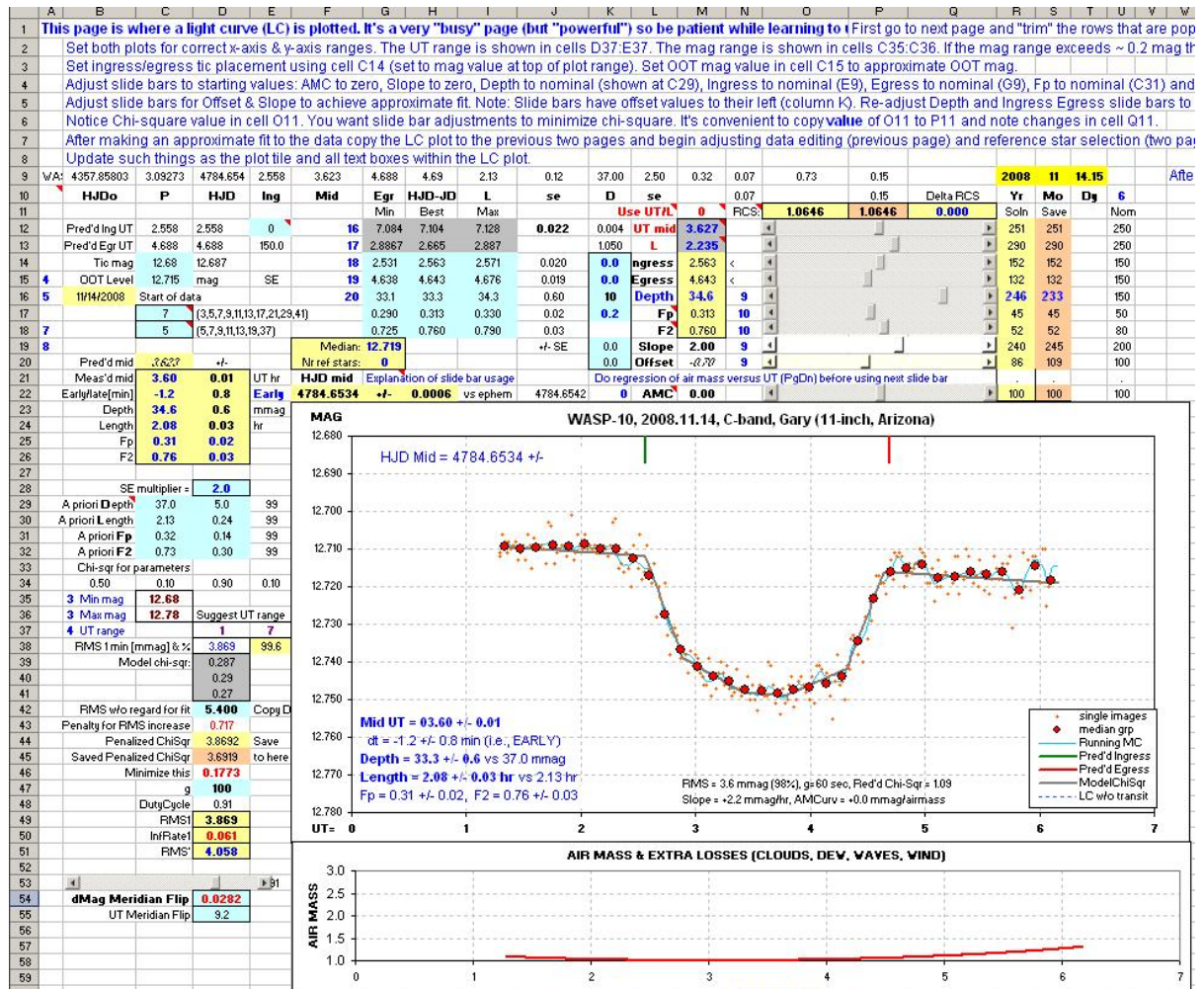


Figure 17.08. Overview of spreadsheet page 6, where the light curve data is displayed and the user gets to adjust light curve model parameters to achieve a good model fit.

Various data averaging options can be chosen by entering a group size in cell C17. Choices for running average (blue trace) can also be made (cell C18). Both of these can be done whether or not a model fit is performed.

Model fitting is a laborious process. I use the term "model" reluctantly because my model is primitive compared with the models used by professionals. The following diagram illustrates what I'm calling a "model."

CHAPTER 17 – SPREADSHEET FOR COMP & ENSEMBLE

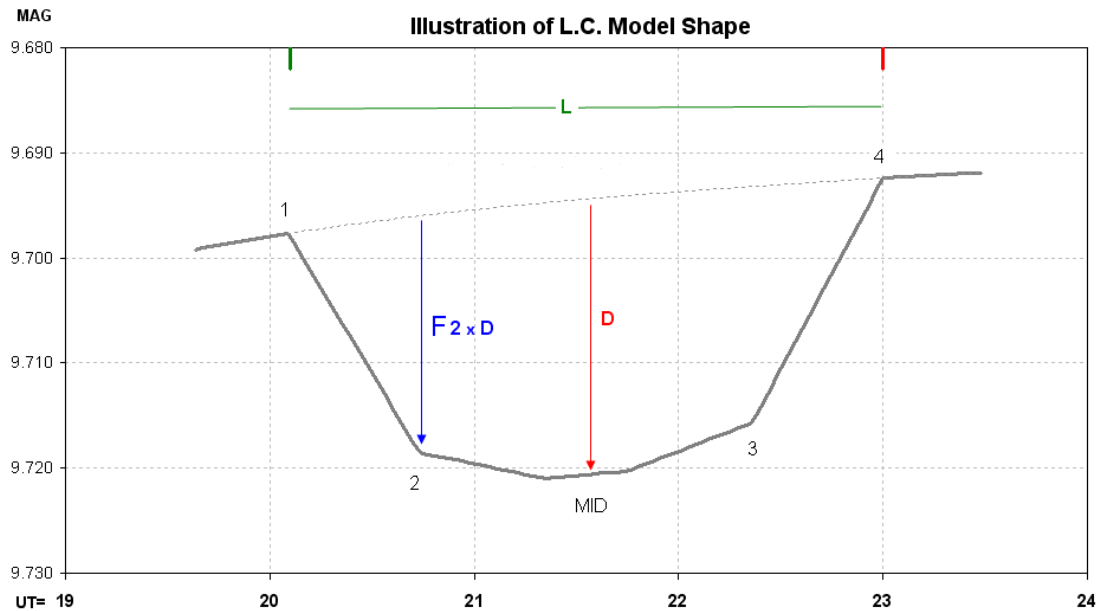


Figure 17.09. Line segment model specified by 7 parameters (described in the text).

This "model" includes 7 parameters (plus an offset), listed here:

- 1) ingress time, t_1
- 2) egress time, t_4 (Length, $L = t_4 - t_1$)
- 3) depth at mid-transit, D [mmag]
- 4) fraction of transit that's partial, $F_p = [(t_2 - t_1) + (t_4 - t_3)] / (t_4 - t_1)$
- 5) relative depth at contact 2, F_2 (depth at contact 2 divided by depth at mid-transit),
- 6) temporal trend [mmag/hour], and
- 7) air mass curvature [mmag/airmass].

Mid-transit is "flattened" for a time interval given by $(t_3 - t_2)/4$. Including an "air mass curvature" term requires that *air mass versus time* be represented by an equation including terms for powers of $(t - t_0)$. I use a 4th power expansion with " t_0 " set to the mid-point of the observations.

The intervals t_1 to t_2 and t_3 to t_4 correspond to "partial transit." The parameter " F_p " is the fraction of the total transit time that's partial. When a transit is "central" (impact parameter $b = 0$) F_p can be used to estimate the size of the transiting exoplanet (or brown dwarf star) compared with the size of the star being obscured (after estimating something about limb darkening). The parameter " F_2 " is used to specify the amount of this limb darkening effect.

The interval t_2 to t_3 should be "bowl-shaped" due to stellar "limb darkening."

Professional observations with larger telescope apertures produce much higher precision light curves, requiring a more sophisticated model than this line-segment version. Very few amateur light curves warrant that extra detail.

CHAPTER 17 – SPREADSHEET FOR COMP & ENSEMBLE

Before we can fit a model to the measurements we must “trim” the next page (following the LC page). This page is called “ChiSqr” because it compares data with the user-specified model and divides differences by a measurement SE (derived from a smoothed RMS noise versus UT). These calculations are needed to derive chi-squared for the model being evaluated. Here’s a plot of RMS during the observing session and a model that is being evaluated.

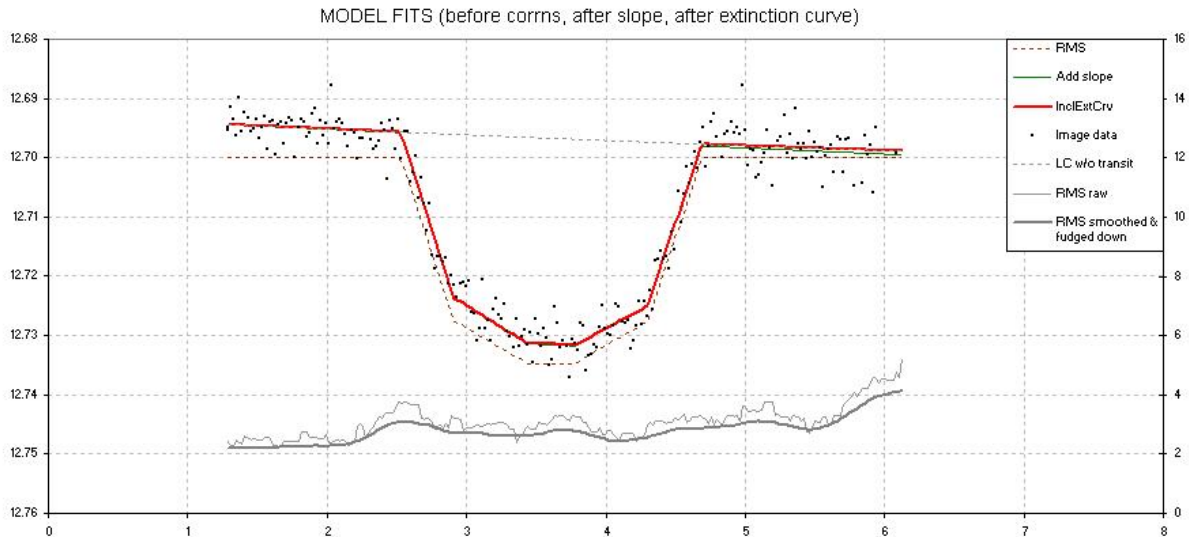


Figure 17.10. Lower trace is $RMS(t)$. The red model trace and the smooth version of RMS are used to calculate chi-square, described in the text.

A chi-squared solution resembles a “least squares” solution, and when the noise level is assumed to be the same for all data points they are equivalent and produce the same solution. Since an observing session can exhibit large variations in noise, especially if one end of the observations is at high air mass, the chi-squared approach is better suited to fitting exoplanet observations. For the case illustrated in this figure RMS varies from ~ 2.0 mmag at the beginning to ~ 4.0 mmag at the end, due mainly to increasing cloudiness. For this transit the chi-square solution justifiably “tolerates” greater departures of a model from the data at the end of the observing session.

Adjusting the 7 parameters for the line-segment model that overlies the data takes a lot of work. The user can put as much, or as little, effort into refining the model. In fact, the user may choose to ignore model fitting and simply display the data. Plenty of instructions are present on the web page, and there is no need for repeating them here.

The “Comp/Chk” and “Ensemble” photometry methods use the same spreadsheet but they differ significantly in their light curve quality. Here’s a list of the advantages of the Ensemble method:

- 1) Scintillation and other noise levels are $\sim 30\%$ lower,
- 2) Systematic errors will usually be smaller,
- 3) Nearby stars used for reference may be discovered as either variable or EB.

Since Ensemble is just as easy as Comp/Chk why would anybody choose Comp/Chk. The only reason it’s done, I assume, is that this is the method first-learned by AAVSO members, and these observers

CHAPTER 17 – SPREADSHEET FOR COMP & ENSEMBLE

never bothered to improve. If there's a valid reason for using Comp/Chk please e-mail it to me, because I am continually baffled by its staying power.

This concludes a description of the spreadsheet template LCep.xls. For anyone inexperienced in using spreadsheets this chapter's description may seem daunting. However, for anyone who has worked with spreadsheets it will be seen as easy to use. I will try to maintain the downloadable version of LCep.xls as more exoplanets are discovered, and as "bugs" or suggestions for improvement are implemented.

The next chapter describes the task of using a spreadsheet designed for accepting Artificial Star data files.

Chapter 18

Spreadsheet Processing – Artificial Star Photometry

The previous chapter described a specific spreadsheet designed for displaying a light curve for use with Comp/Chk and Ensemble data files of star magnitudes, the two most common methods used by amateurs for creating exoplanet light curves. This chapter is devoted to an alternative method, called “Artificial Star” (AS) photometry. It involves more spreadsheet work, but it offers several important advantages over the other two methods. The principal advantage is that a best sub-set choice of reference stars from among a large number of candidates can be determined by the user, leading to smaller noise levels and smaller systematic effects. Why are there these benefits? The answer will become clear in this chapter.

In my opinion it is just as easy to create an AS data file as Comp/Chk or Ensemble file using an image processor’s photometry tool. Adding the artificial star to a set of 200 images, for example, adds an extra couple seconds to the analysis process, and it can be started by a mere couple of keystrokes. One reason the AS method is not widely used is that most amateurs have never heard of it. A better reason for it to not be widely used is that additional effort is required to produce both a light curve and a data file that can be submitted to the AXA or ETD archives. Whereas Comp/Chk and Ensemble CSV data files can be submitted after just adding header lines, the AS data file **has** to be processed in a spreadsheet before it can be submitted.

The spreadsheet that I’ve created for the AS files is called LCas.xls. It can be downloaded from the following web site:

http://brucegary.net/book_EOA/xls.htm

This is the same web site where the spreadsheet for Comp/Chk and Ensemble can be found, LCep.xls. I will try to maintain it as new exoplanets are discovered.

The first page of this spreadsheet is for selecting the BTE of interest, and it functions the same way as shown in Fig. 17.03. The second page is also the same (see Fig. 17.04). Page 3 is also the same as for LCep.xls (see Fig. 17.05). Differences begin with page 4. The page is wide, and Fig. 18.01 shows the top-left section. As with all pages detailed instructions appear at the top of each page. This area of the page displays an extinction plot and a plot showing air mass and “extra losses.” Since this observing session was during cloudy weather the extinction plot is too noisy to be useful, so a site-typical zenith extinction value was entered in cell G15 (0.16 mag/airmass). The right side of this page will be described later.

Figure 18.02 shows part of Page 5, which is similar to the Ensemble page 5. For this example, however, there are 22 “chk” stars available for use as reference. It will be the user’s task to figure out which subset of these 22 stars provide the lowest noise level and best fit to a transit model. The procedure for accomplishing this will be given later in this chapter. For now, note that in this figure there is a sort of light curve plot of all 22 candidate reference stars, and this can be used to detect any obvious misbehavior that would eliminate a star from consideration for use as reference. The star 5th from the bottom is for WASP-10, which already is showing a transit feature.

CHAPTER 18 – SPREADSHEET FOR ARTIFICIAL STAR

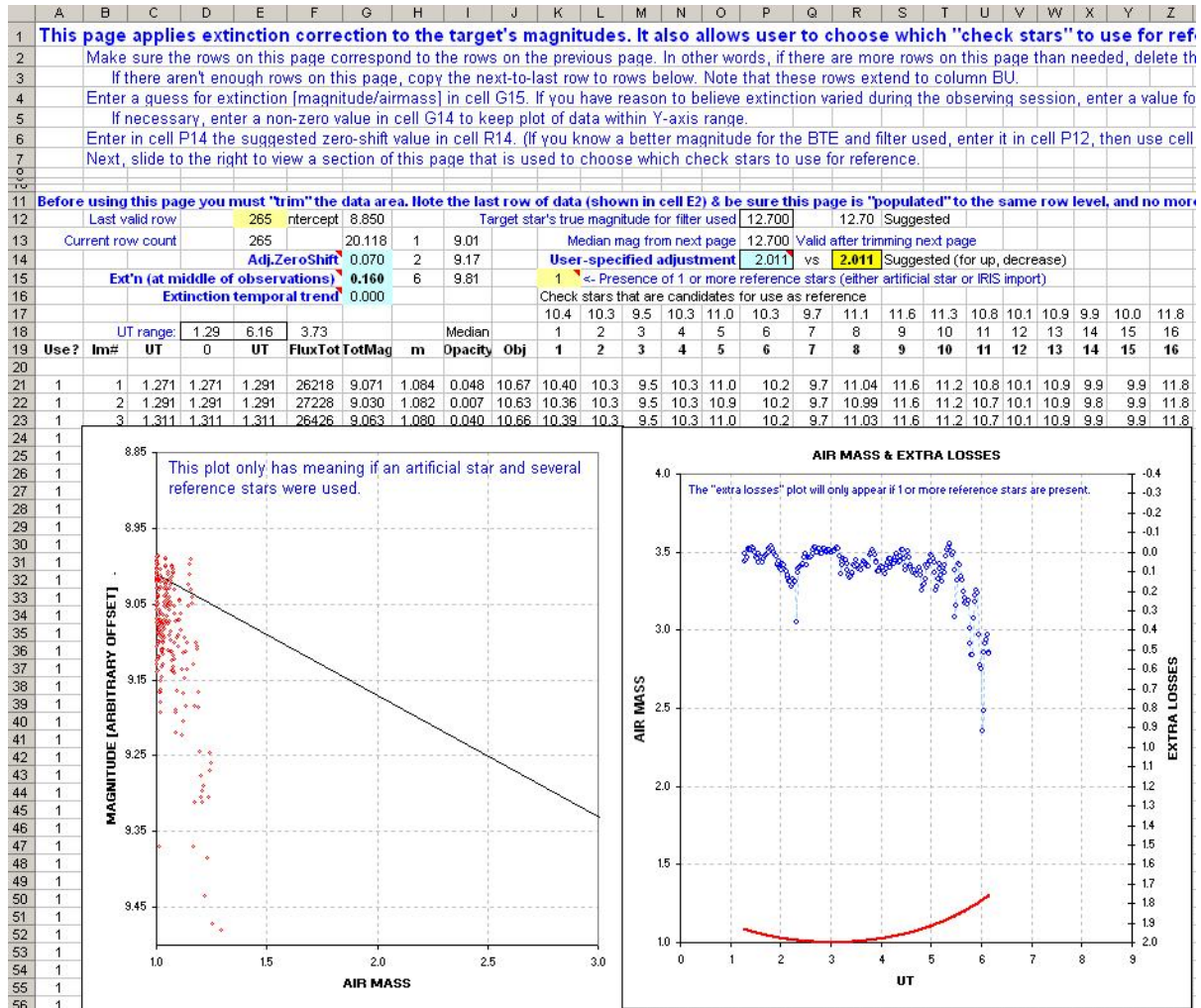


Figure 18.01. LCas.xls for, page 4, left side. See text for description.

Column E in Fig. 18.02 is an extinction-corrected magnitude for the target star, using whatever selection of “chk” stars for reference is present on the previous page (illustrated and described later). This accounts for the light curve plot in this figure showing no correlation with air mass.

A few bad data points can be seen in the plot, and it is the job of the right side of this page to identify bad data and reject them from subsequent consideration (in the final WASP-10 light curve plot and model fitting). The way this data rejection is decided is very similar to what was described for the Ensemble spreadsheet, LCep.xls, except that there are two criteria for rejecting data: 1) extra losses exceeding a threshold, and 2) an outlier threshold. In Fig. 18.03 it can be seen that the “extra losses” rejection criterion for this page has been set to 0.5 magnitude (cell AN16), and this led to an acceptance of 95.9% of data.

CHAPTER 18 – SPREADSHEET FOR ARTIFICIAL STAR

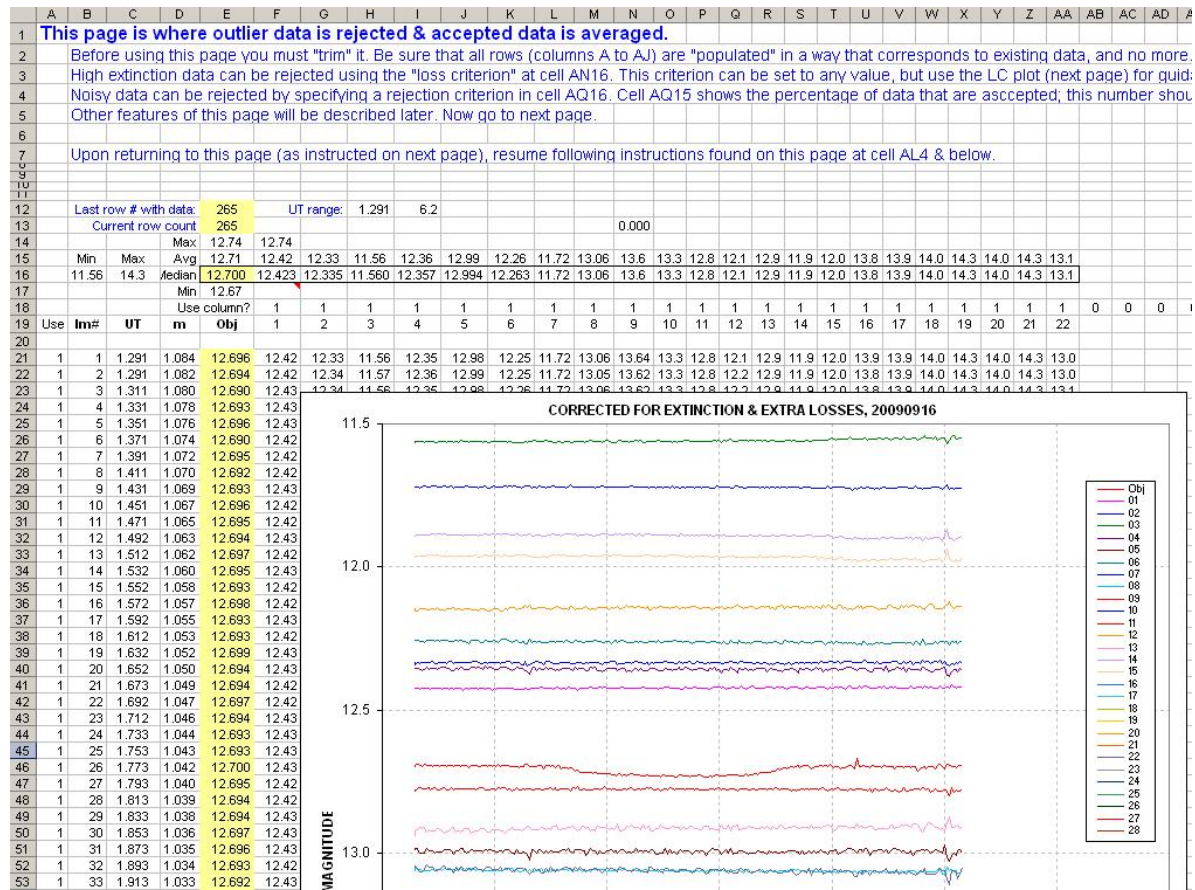


Figure 18.02. Page 5 of LCas.xls, showing the 22 candidate reference stars in plot form.

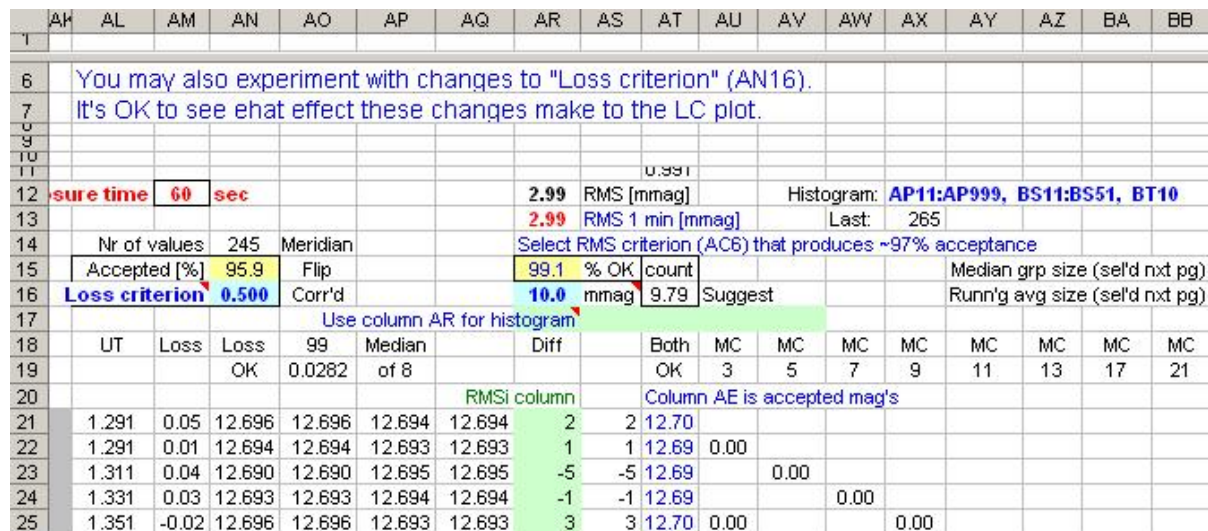


Figure 18.03. Page 5, middle section, where user specifies noise acceptance criterion (cell AR16) for neighbor noise level in column AR. Extra Loss acceptance criterion is shown in cell AN16.

CHAPTER 18 – SPREADSHEET FOR ARTIFICIAL STAR

Column AR shows object magnitudes compared with the median of the nearest 8 neighbors. This is where “outlier” data in an image (row) will stand out. For example a cosmic ray within the photometer circle won’t be rejected by the image processing photometry tool, and it will appear as an anomalously bright reading. Rejecting such data is accomplished by specifying a “noise” rejection criterion (cell AR16). If the “noise” for an image (row) exceeds this threshold (set to 10 mmag in this example) the data in that row is “rejected.”

The user has the option of updating a histogram plot (c.f., Fig. 17.07b), which can be “fit” by a Gaussian shape. The Gaussian width is used to “suggest” a RMS rejection criterion, shown as cell AT16. This criterion is 2.33 times width, which corresponds to a rejection of 2% of valid Gaussian data. This small loss of valid data is thought to be worth the likely rejection of outlier data.

The next spreadsheet page includes a light curve plot based on “accepted” measurements.

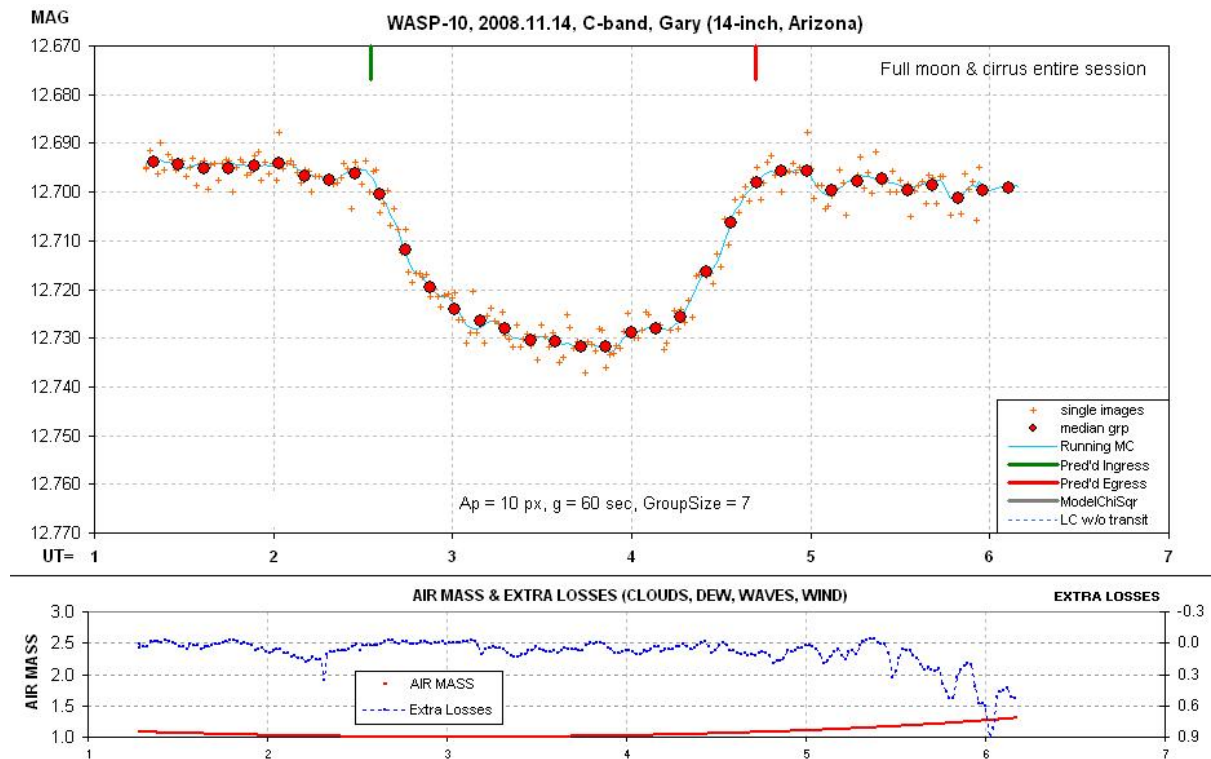


Figure 18.04. Light curve (without a model fit). The lower panel shows air mass and “extra losses.”

The large red symbols are averages of groups of 7 measurements (small orange crosses), where each measurement corresponds to a 60-second exposure image. The “extra losses” plot shows the presence of cirrus clouds that were present the entire observing session.

The user may view the top figure and declare that the data is good enough to submit to an archive, which may be true, but the data won’t be “optimum.”

CHAPTER 18 – SPREADSHEET FOR ARTIFICIAL STAR

Recall that for this case there are 22 “chk” stars available for use as reference, and at this point in the analysis all stars are being used. Some of them may be noisy, or variable, or otherwise unsuitable for use as reference. The way to identify which sub-set of candidates for reference produces an optimum quality LC we have to do a few things that, sorry, may “test your patience.”

Figure 18.05. Reference usage switches (Page 4).

Two pages back, at Page 4, where there are plots for extinction and air mass and extra losses, there’s a large work area to the right for selecting reference stars (c.f. Fig. 18.05). A column is devoted to each candidate for use as a reference star. Each candidate has an on/off switch located at rows 12 to 13. Each time the switch is clicked (in either the up or down direction) a number in row 17 changes by one. If the number is odd the column is turned “on” – and “off” for even numbers. Notice cell AR14. It’s RMS noise for the entire observing session (copied from Page 5). Step one for selecting reference stars is to step through the switches, one at a time, and note whether RMS can be decreased by switching a reference star “off.” If a large improvement is achieved by switching off a reference candidate, then another run through the switches is recommended. This leads to a sub-set of reference star candidates that produce the least noisy data set. It’s our starting point for fitting a model.

Now return to Page 6, where the LC is displayed, and enter approximate values for the transit model (as explained in the previous chapter, before starting model-fitting the page called “ChiSqr” has to be trimmed). The transit model consists of five parameters related to the transit itself plus two parameters related to observing session systematics. The user must adjust all of them: ingress UT, egress UT, depth at mid-transit, fraction of time spent during ingress (or egress) in relation to the time from ingress to mid-transit, ratio of depth at completion of ingress (or start of egress) to the mid-transit depth, systematic trend error and systematic air mass curvature. The systematic trend term is most likely produced by image rotation (imperfect polar alignment) that causes stars to move across pixel space during the entire observing session. If the master flat frame was perfect there shouldn’t be such a term, but no flat field is perfect. The air mass term is a coefficient times “air mass minus one.” This term is required when stars are used for reference that are not exactly the same color as the object (as explained in the next chapter). The trend and air mass terms are adjusted using the “out of transit” (OOT) portions of the light curve. A detailed description of the transit model is given in Appendix I.

CHAPTER 18 – SPREADSHEET FOR ARTIFICIAL STAR

Figure 18.06 shows some of the cells and slide bars that will be used to produce an approximate model fit. Cells C35 and 36 are suggestions for setting the plot’s Y-axis range (done by right-clicking on the plot, etc). Cells D37 and E37 are suggestions for the X-axis range. C14 should correspond to the “brightest” value for the Y-axis range, which causes the ingress and egress ticks to display at the top of the plot. C15 is the OOT magnitude for the model. The OOT magnitude can be offset in small amounts by using the slide bar at O20:Q20. A slope for the model can be adjusted in small increments using slide bar O19:Q19. The model’s depth can be set by using the slide bar O16:Q16. Similar adjustments can be made for ingress time and egress time. Large changes to the slide bar values can be made by changing the offset cells K14:K20.

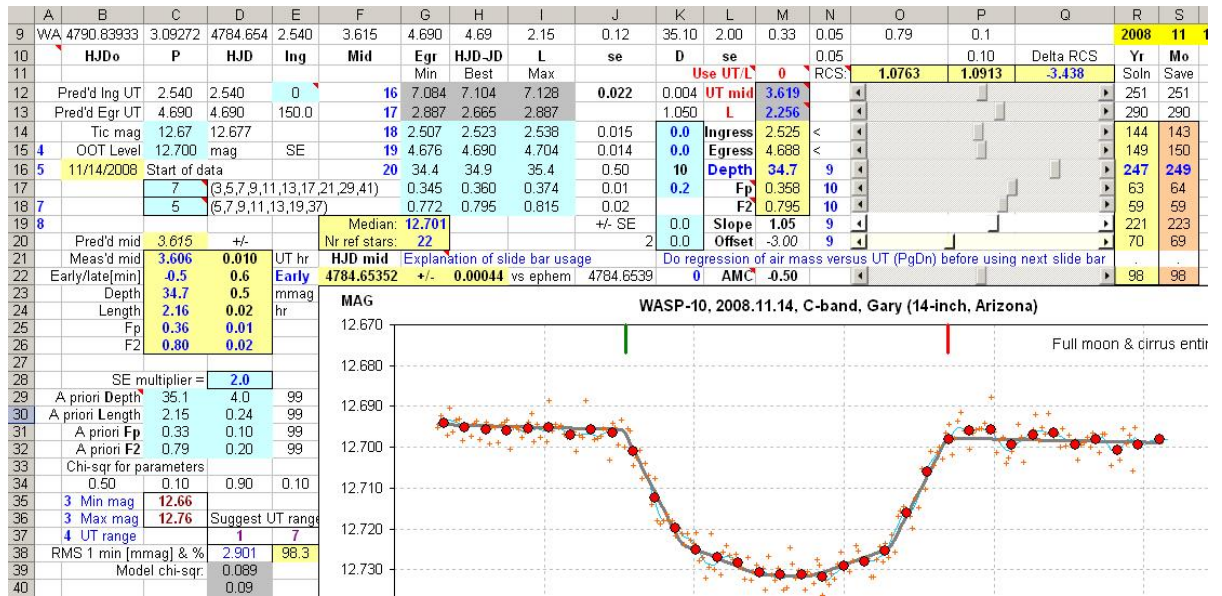


Figure 18.06. Work area for setting model parameters to achieve a fit.

Notice section C29:D32. This is *a priori* information about the transit taken from the first page. It can be used as a guide in setting the slide bars for an approximate fit. Cell D28 is a “multiplier” that increased the SE for a priori depth, length, etc. A larger number (nominally 2) leads to more conservative chi-square solutions (more constrained by data than *a priori* information).

When a fairly good visual fit has been achieved notice the value of cell O11. This is “reduced chi-square,” defined as chi-square divided by the “number of observations plus model degrees of freedom.” Another way to describe reduced chi-square is that it is the average of all the values for “ratio of data to model difference, normalized by the SE for the data, squared.” A value of ~ 1.0 is to be expected when a good model fit has been achieved (and data SE is properly represented). Every adjustment of a model parameter will produce a change to reduced chi-square (cell O11). By copying the value of cell O11 to P11 the difference cell, Q11, can be monitored as parameter adjustments are made in search of changes that produce a negative change in that cell.

When a moderately good model fit has been achieved there may be systematic variations above and below the model trace. This could be produced, for example, by one of the reference stars being a short period variable. More likely, though, such variations could be produced by a reference star

CHAPTER 18 – SPREADSHEET FOR ARTIFICIAL STAR

being close to the FOV edge and slight movements of the star field with respect to the pixel field cause any imperfections in the flat field to change the star’s apparent brightness. Our job is to find out if any stars are misbehaving in this way. To do this we must first note a cell that displays the RMS of data off the model fit, shown in Fig. 18.07 as cell D43. This is something we want to minimize with the reference star on/off switches. Copy the value of D43 to D44, then go to Page 4.

At Page 4, start going through the reference on/off switches while noting whether cell AR13 (cf. Fig. 18.05) goes negative. A negative change means that the reference star that was switched off (or on) led to an improvement in the data fit to the model. This is good, and when a large negative change occurs we must repeat the exploration of all other switches to see if that’s the “minimum” that we’re searching for.

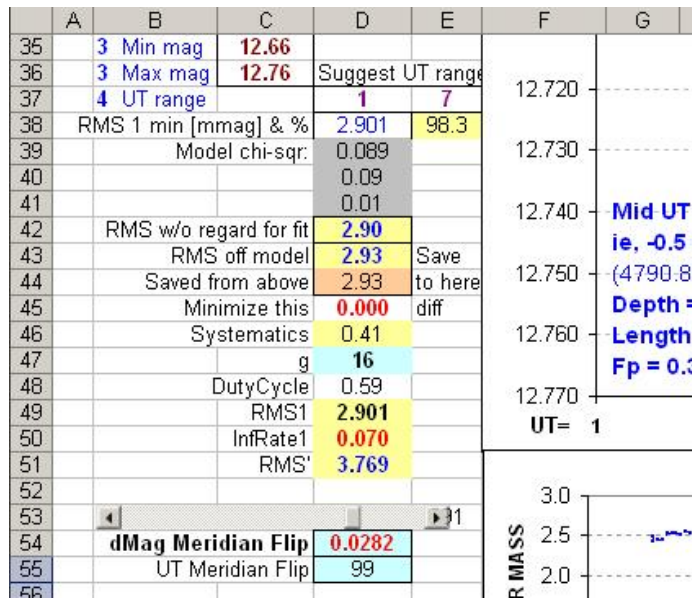


Figure 18.07. Part of the light curve page (#6) showing “RMS off model” cell D43. Also shown is a place for adjusting an offset for meridian flip observations.

Here’s the minimum that I found for this data set.

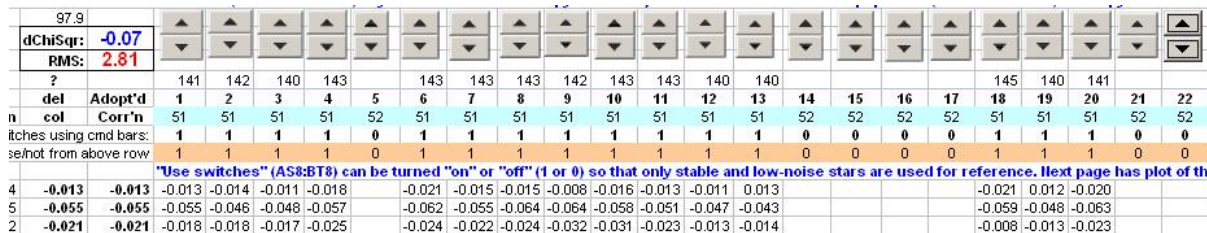


Figure 18.08. Switch settings that produce a minimum for “delta Chi-Square” and hence the best subset of reference stars for this observing session.

CHAPTER 18 – SPREADSHEET FOR ARTIFICIAL STAR

Since it's possible that this group of reference stars requires a significant model fitting change it is a good practice to iterate. By iterate I mean return to the model fitting page to refine the model, then repeat the reference star sub-set selection. Yes, that's a lot of work, but it would be more work to write a program to do it automatically.

So far I know of only one group of professional observers who do what I have described. Presumably they've written a program to automate the process.

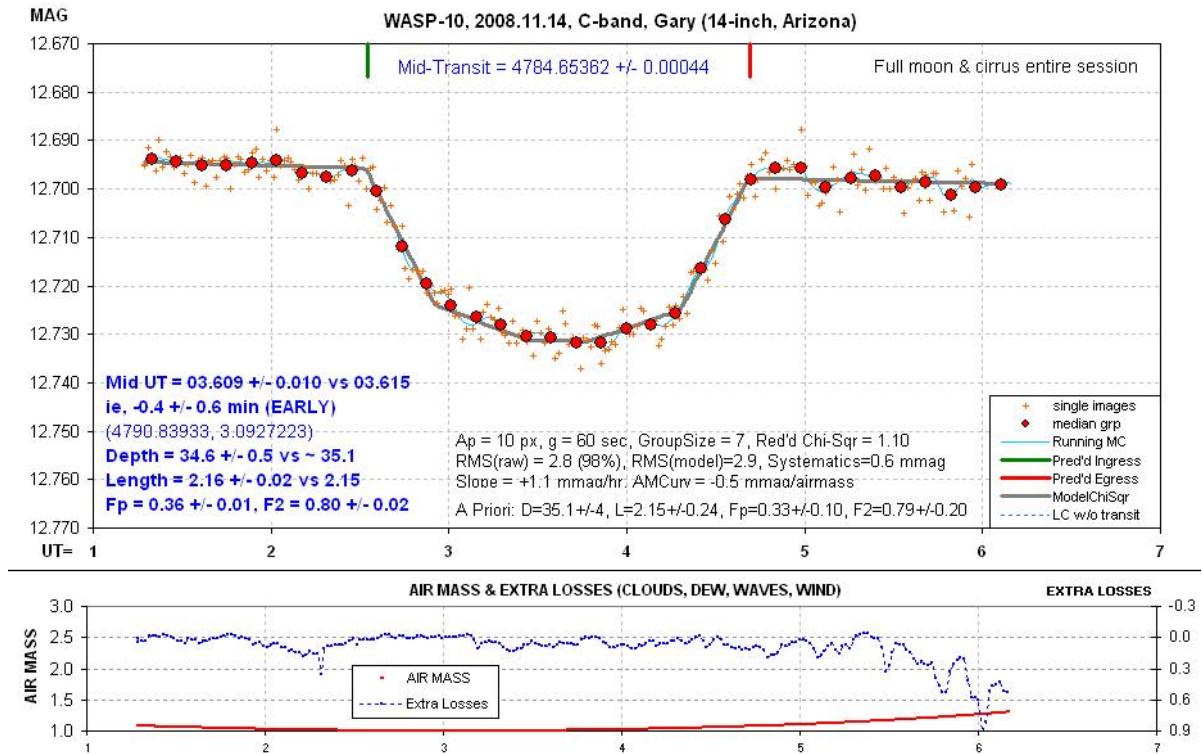


Figure 18.09. Final light curve solution for the “artificial star” method.

Figure 18.09 is the final light curve. In this figure the small red dots are from individual 60-second images that passed the acceptance criteria for both “extra losses” and outlier rejection. The large red circular symbols are 7-point, non-overlapping averages of the accepted data. At the top of the panel are two vertical lines indicating the predicted times for ingress and egress.

I think it's important to always be mindful of the distinction between stochastic uncertainties and systematic ones. If a model provides a sufficiently accurate representation of actual transit light curve shapes the RMS of measurements with respect to a best fitting model can be used to estimate the size of systematic uncertainties. This is done by merely orthogonally subtracting the short-term RMS stochastic noise level from the model referenced RMS; this should be the component of systematic errors. This is calculated on Page 6, and the results are summarized in the text box: “RMS(raw) = 2.8 (98%), RMS(model) = 2.9, Systematics = 0.6 mmag.”

The RMS(raw) is the observing session's short-term RMS (calculated on the previous page), and presumably it is all stochastic. RMS(model) is the RMS of measurements with respect to the best

CHAPTER 18 – SPREADSHEET FOR ARTIFICIAL STAR

fitting model. Systematics, 0.6 mmag, is the orthogonal difference, $\text{SQRT}(2.9^2 - 2.8^2)$. This level of systematics is low, which suggests two things: 1) the level of un-modeled systematics is small (0.6 mmag), 2) the straight-line segmented model is an adequate representation of the transit light curve shape. The same message is present in the fact that reduced chi-square is close to one (1.10).

The text box in the lower-left corner (Fig. 18.09) has mid-transit UT, depth, length, etc with SE estimates. The SE values come from adjusting one parameter at a time from its best value until reduced chi-square increases by at least 2.0. If all parameters were orthogonal (had distinct effects not mimicked in any way by other parameters) the increase criterion should be 1.0, not 2.0. A proper way for establishing SE is to experiment with different parameter value offsets from the optimum and for each offset solve for all the other parameters, and when the offset increases reduced chi-square by one that's the SE (of one sign). I've done this a few times, and have shown that the non-orthogonality of the line-segment transit model is such that the same answer can usually be obtained by the simpler method of adjusting just one parameter (without optimizing the others at each adjustment) until the adjustment produces a reduced chi-square increase of ~ 2 .

When the user is satisfied with a model fit solution it is possible to create a data file suitable for submission to the AXA or ETD archives. This is done by copying columns on Page 5 to a text file, as shown in the next figure.

	AH	AI	AJ	AK	AL	AM	AN	AO
11								
12			Exposure time	60	sec			
13								
14					Nr of values	245	Meridian	
15					Accepted [%]	95.9	Flip	
16					Loss criterion	0.500	Corr'd	
17	For copying to ymddhmmn.TXT						Use	
18	For processing by AXA.				UT	Loss	Loss	99
19	JD4	dMag	Loss			OK	0.0282	
20								
21	4784.55296	12.695	0.048		1.291	0.05	12.695	12.695
22	4784.55380	12.695	0.007		1.291	0.01	12.695	12.695
23	4784.55464	12.691	0.040		1.311	0.04	12.691	12.691
24	4784.55547	12.694	0.029		1.331	0.03	12.694	12.694
25	4784.55631	12.696	-0.019		1.351	-0.02	12.696	12.696

Figure 18.10. On Page 5 columns AH to AJ contain information in the required format for submission to archives AXA or ETD.

By copying the values of data in these columns to a text file, and adding header lines, the text file has not only the JD time tag and magnitude for the target star (the exoplanet), it also has a third column of “extra losses.” The AXA auto-fit program produces a data file that can be imported to a special plotting spreadsheet that includes a plot of extra losses, as illustrated by the next figure.

The AXA auto-fit program makes use of almost all of the fitting concepts described in this chapter for LCas.xls. The AXA auto-fit light curve display top panel has two systematics removed: trend and air mass curvature. The same type of plot can be done within LCas.xls (Page 9, shown as Fig. 18.12). The auto-fit program also processes data files of the Comp/Chk and Ensemble types. The comment line “Loss column : Y” indicates that the data file’s third column is “extra losses” (produced by the

CHAPTER 18 – SPREADSHEET FOR ARTIFICIAL STAR

“artificial star” method) whereas “Loss column : N” indicates that any columns after the first two are to be ignored because the data file was produced by either the Comp/Chk or Ensemble” method.

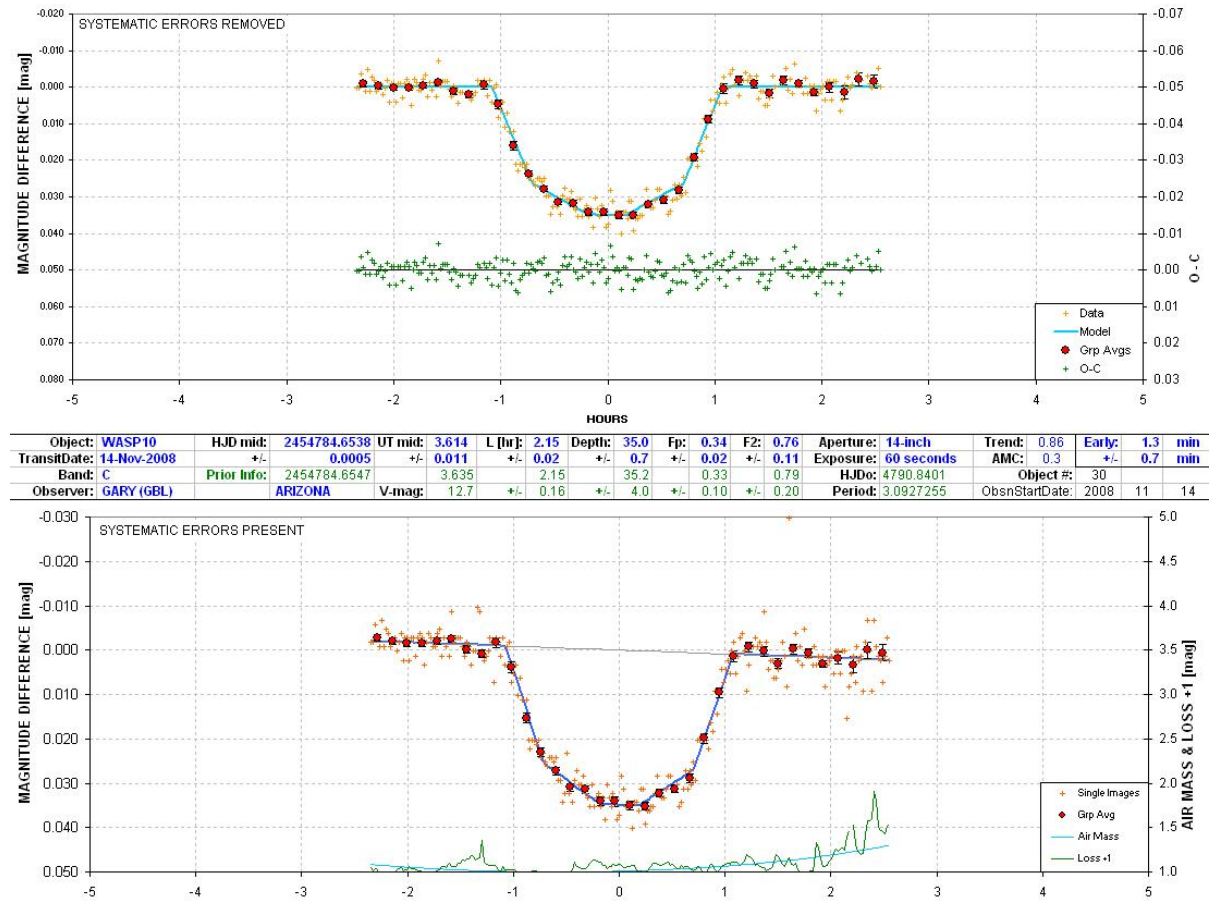


Figure 18.11. Light curve plots of a data file created by the AXA auto-fit program that processed a data file created from a copy of columns in the spreadsheet LCas.xls. The green trace at the bottom of the lower panel is “extra losses.” The upper panel has trend and air mass curvature removed.

To summarize, LCas.xls can be used by observers using the Artificial Star method for the purpose of creating a data file for submission to an international archive, such as AXA or ETD. As a bonus, LCas.xls can be used to produce informative light curve plots (like Fig.’s 18.04, 09 and 12) for the observer’s records or a personal web page.

Appendix I describes the simple, straight-line segmented model in detail. It also explains how LCep.xls and LCas.xls make use of *a priori* information about each exoplanet’s archive average of transit length, depth and shape.

CHAPTER 18 – SPREADSHEET FOR ARTIFICIAL STAR

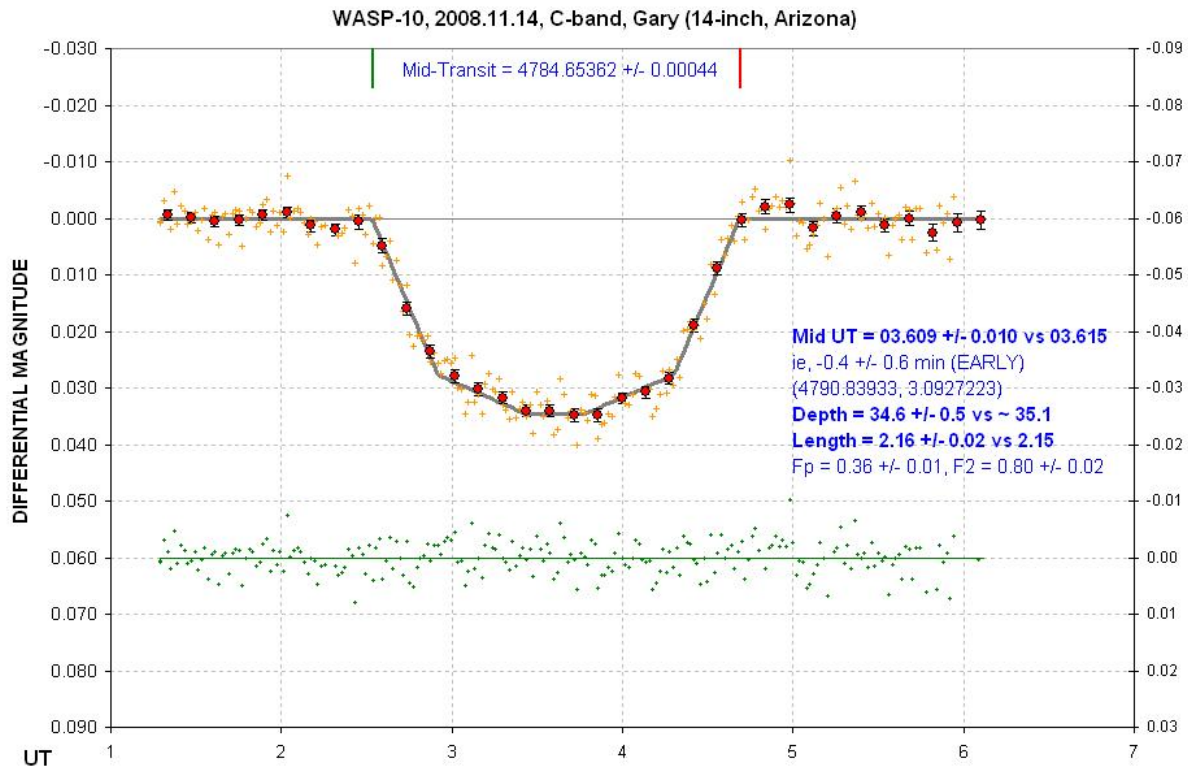


Figure 18.12. *LCas.xls* light curve plot with systematics “trend” and “air mass curvature” removed.

The spreadsheets *LCep.xls* and *LCas.xls* represent merely one algorithm for converting an exoplanet transit data file to a light curve plot with transit parameter solutions. I encourage observers to create their own spreadsheets and programs for this purpose.

The next chapter treats the important matter of light curve baseline curvature produced by the use of reference stars having a different color than the transited star.

Chapter 19

Star Colors

For LC analyses of **variable stars**, where the goal is to measure changes with precisions of ~ 10 to 50 mmag, it is common practice to use as many reference stars as possible in an ensemble mode. For eclipsing binaries, which have deep transits, this is also an acceptable practice. But when the transit depth is less than ~ 25 mmag, as most exoplanet transit will be, it matters which stars are used for reference. The problem arises when the target and reference stars have different colors. This is because a red star exhibits a smaller atmospheric extinction compared to a blue star, regardless of the filter used (unless the bandpass is much narrower than any of the standard BVRcIc set, etc).

One of my purposes in presenting the Chapter 6 “Atmosphere Tutorial” was to prepare you to appreciate the importance of slopes of extinction **within** a filter bandpass. How can the extinction slope within a given filter band possibly affect differential photometry measurements? We now need to review some stellar blackbody spectrum theory.

Blackbody Spectra and Filter Bandpasses

Hot stars shine mostly in the blue, whereas cool stars shine mostly in the red, as the following graph shows.

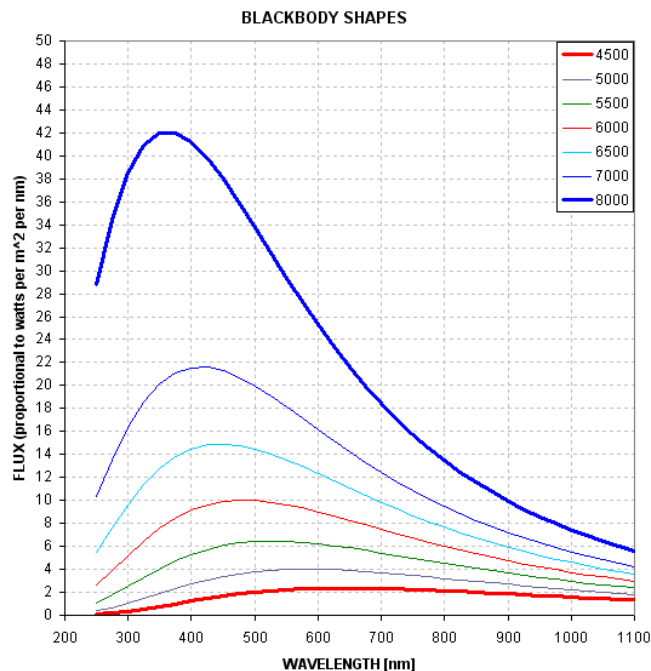


Figure 19.01. Blackbody spectral shape versus temperature (4500 K to 8000 K). $T = 4500$ K corresponds to spectral class K3 and 8000 K corresponds to A2.

CHAPTER 19 – STAR COLORS

Notice that not only do hot stars radiate more photons at every wavelength region, but the difference is greatest at short wavelengths.

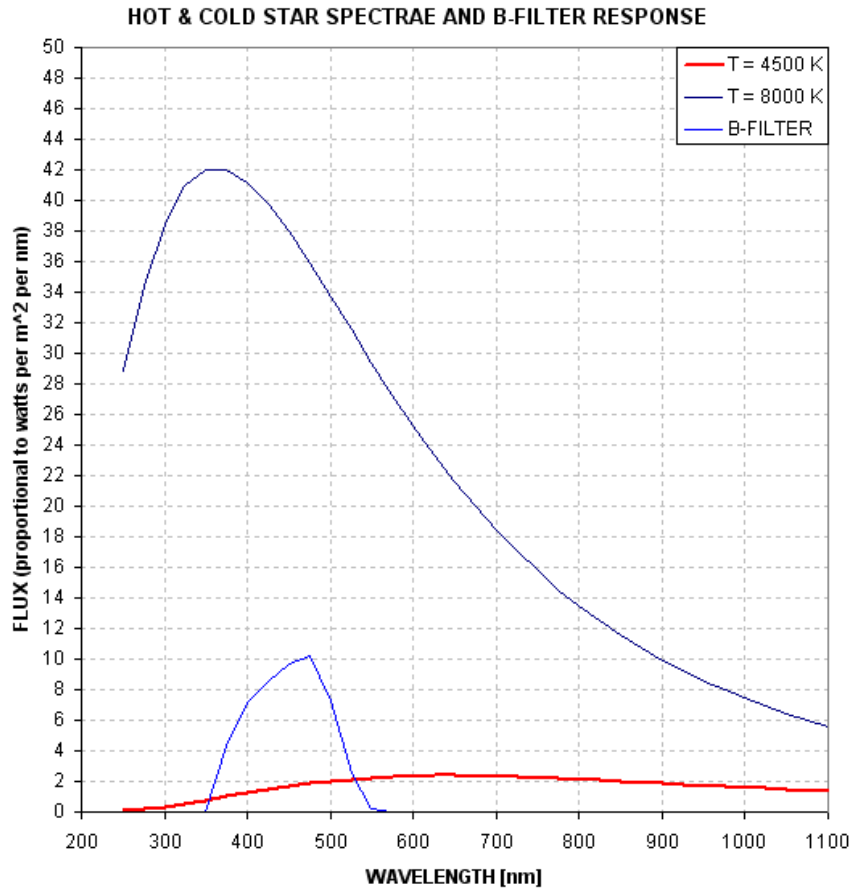


Figure 19.02. *B-filter response and spectral shapes of hot and cold stars.*

Notice in Fig. 19.02 that within the B-band response a cool star radiates less and less going to shorter wavelengths, whereas it is the reverse for the hot star. The effective wavelength for a cool star is 467 nm whereas for a hot star it is 445 nm. The more interesting parameter for light curve systematics is the equivalent zenith extinction coefficient for the two stars. For the cool one it's 0.228 mag/airmass whereas for the hot star it's 0.244 mag/airmass (I use the term "airmass", "AirMass" and "air mass" interchangeably). In other words, a cool star's brightness will vary less with airmass than a hot star, the difference being ~ 0.016 mag/airmass.

Effect on Light Curves of Reference Star Color

Consider an observing session with a B-band filter that undergoes a range of airmass values from 1.0 to 3.0. Consider further that within the FOV are two stars that are bright, but not saturated; one is a cool star and the other is hot. The magnitude difference between the two stars will change during the course of the observing session by an impressive 32 mmag! This is shown in the next figure.

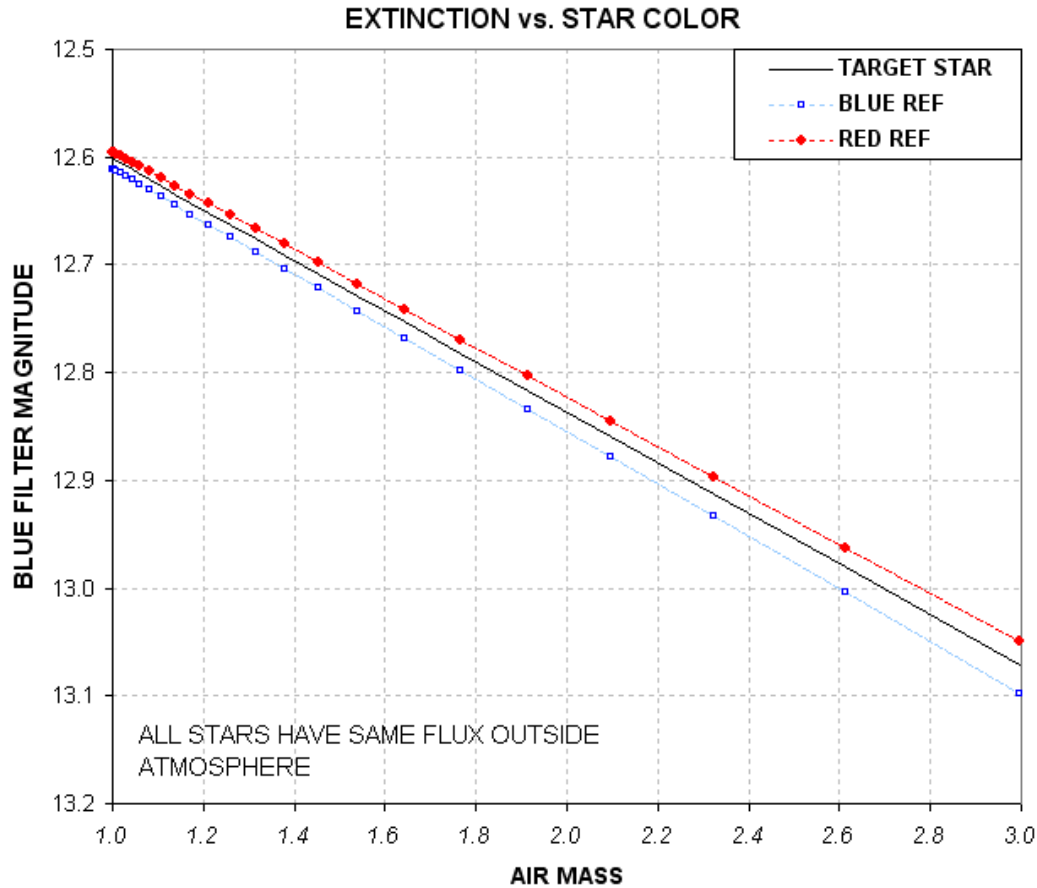


Figure 19.03. Extinction plot for red and blue stars (based on model).

If the target star is cool then the cool reference star should be used. If instead the hot star is used for reference there will be a 32 mmag distortion of the LC that is correlated with airmass. The shape of the LC will be a downward bulge in the middle (at the lowest airmass), as shown in the next figure.

We've just shown that when using a B-band filter hot and cool stars can distort LC shapes by the amount ~ 16 mmag per airmass in opposite directions, producing opposite LC curvatures. What about the other filters? For R-band the two zenith extinctions are 0.120 and 0.123 mag/airmass (for cool and hot stars). The difference is only 3 mmag/airmass, which is much less than for B-band. Nevertheless, a LC bulge of 3 mmag/airmass is important for depths as shallow as 10 to 20 mmag.

Unfiltered observations are more dangerous than filtered ones when choosing reference stars on the basis of color. A cool star has an effective zenith extinction coefficient of 0.132 mag/airmass, unfiltered, versus 0.191 mag/airmass for a hot star. That's a whopping 59 mmag/airmass! Clearly, attention to star color is more important when observing unfiltered. A much less serious warning applies to observations with a blue-blocking filter (described in greater detail later).

All of the above-cited zenith extinction coefficient dependencies on star color are for a site at 4660 feet. Lower altitude sites will experience greater effects.

CHAPTER 19 – STAR COLORS

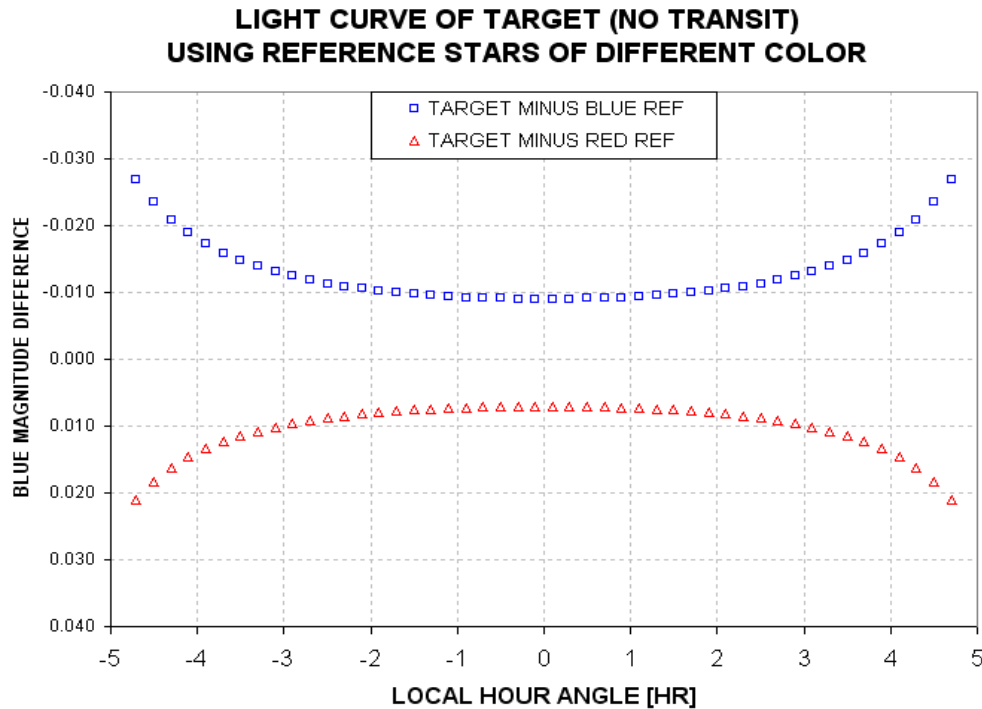


Figure 19.04. Light curve shapes of normal-color star when blue and red reference stars are used and observations are made with a B-band filter.

Is there any evidence for this effect in real data? Yes. Consider Fig. 19.05, showing the effect of reference star color on measured LCs.

The middle panel uses a reference star having the same color as the target star. The top panel shows what happens when a red reference star is used. It is bowed upward in the middle. Air mass was minimum at 5.5 UT, which accounts for a greater downward distortion of the LC at the end (when airmass = 1.3, compared when airmass = 1.2 at the beginning). The bottom panel, using slightly bluer stars for reference, has an opposite curvature. The curvature is less pronounced in this panel compared to the middle one due to a smaller color difference.

Notice also in this figure that reference star color not only affects transit shape, it also affects transit depth. Assuming the middle panel is “correct” we can say that the red star (top panel) produced a 10% increase in apparent depth, whereas the blue star (bottom panel) produced a 8% decrease.

One additional effect to note when using a different color reference star is “timing” – by which I mean the time of mid-transit as defined by the average of the times for ingress and egress. For this example the red reference star produced a -2.4-minute error while the blue reference star produced a +2.1-minute error.

CHAPTER 19 – STAR COLORS

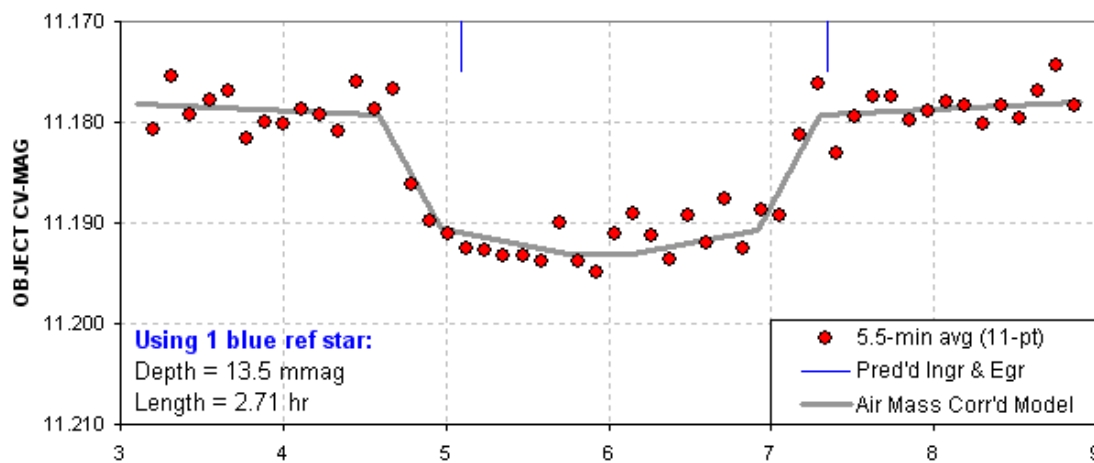
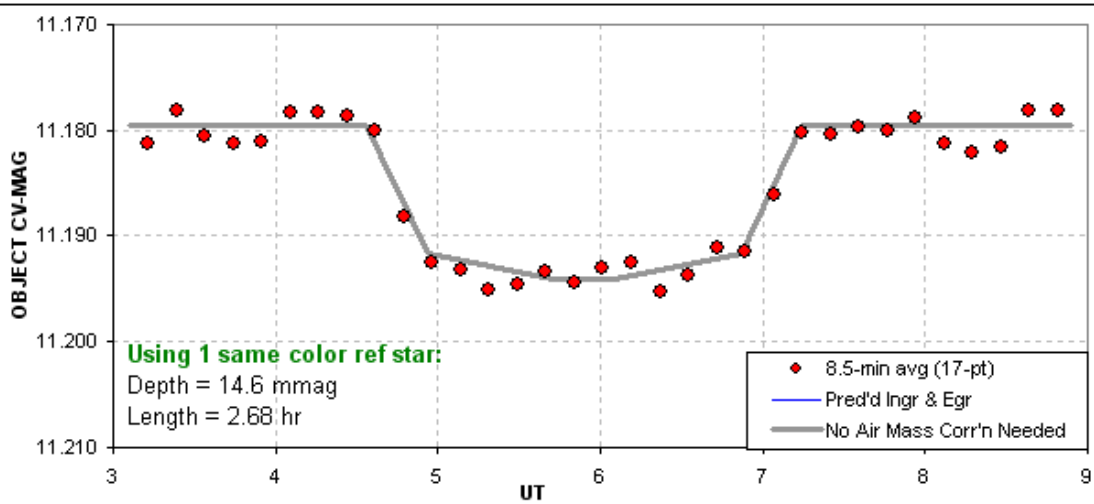
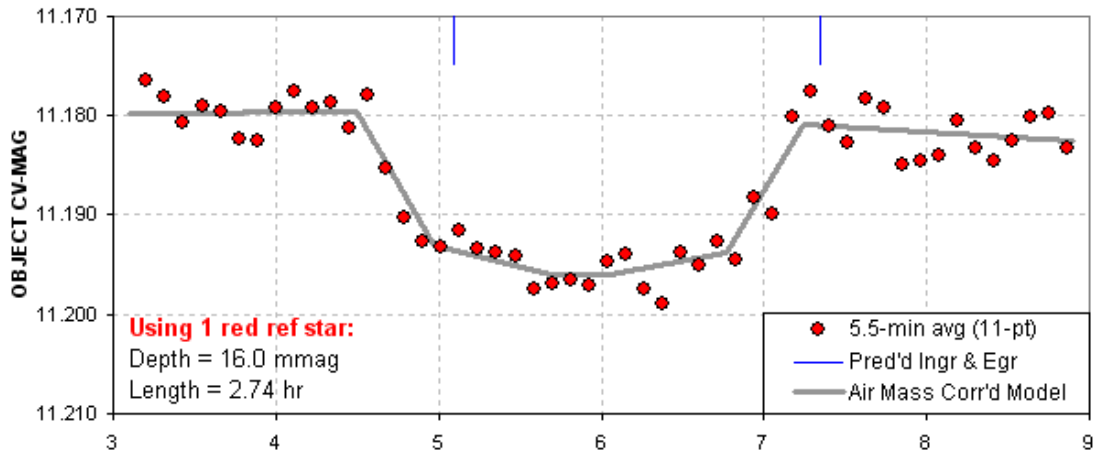


Figure 19.05. Effect of reference star color on LC shape, depth, length and timing.

CHAPTER 19 – STAR COLORS

For shallow transits it is therefore preferable to use a reference star with a color similar to the target star. If this can't be done then an air mass model may have to be used to interpret the LC. The longer the out-of-transit (OOT) baseline the easier it is to derive a proper fitting model. With experience, and familiarity with the color of stars near the target, it is possible to process the OOT baselines to reduce curvature effects. But when there is uncertainty in star colors it is prudent to plan on a long observing session. Even when a reasonable “fit” is achieved using different color reference stars be prepared for errors in transit depth and timing.

“Clear with Blue-Blocking” (CBB) Filter

Some observing situations are best approached using a “clear with blue-blocking filter,” CBB. This filter was discussed at length in Chapter 7 (“Filter Choice”). As the next graph shows it blocks everything blueward of V-band.

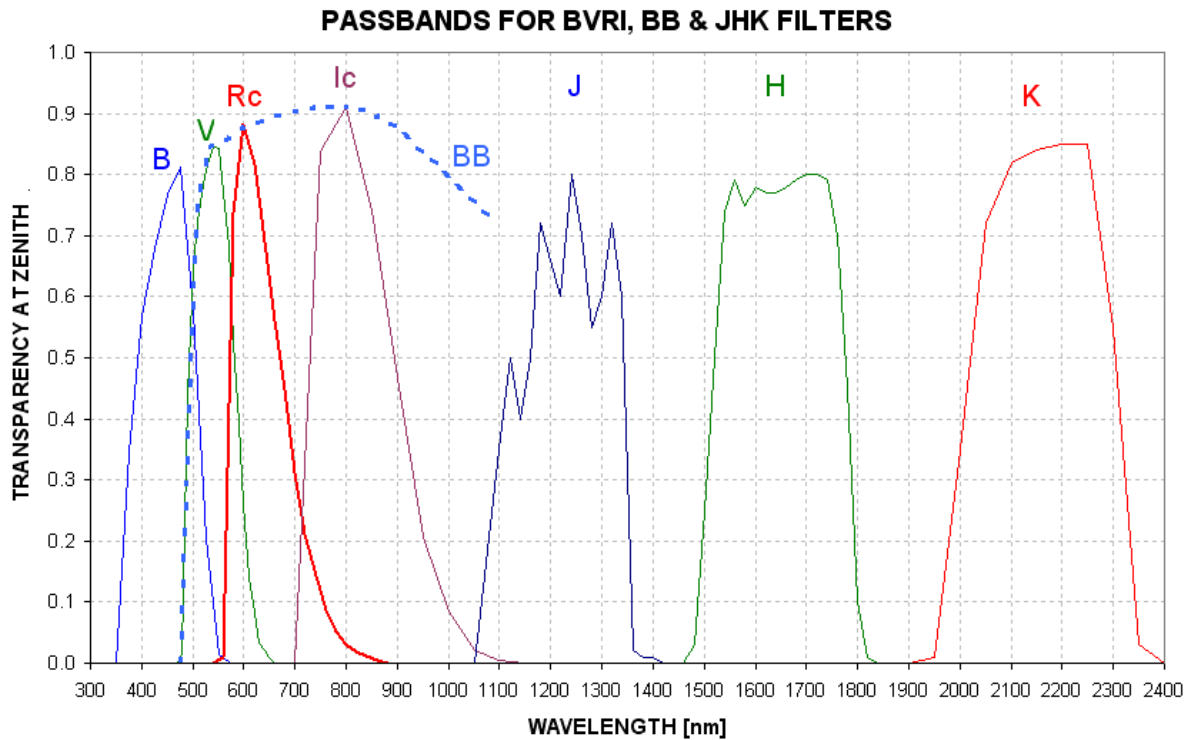


Figure 19.06. Filter response functions times atmospheric transparency for standard B, V, Rc, Ic filters, as well as the 2MASS J, H and K filters. Also shown is the “clear with blue-blocking” (CBB) filter response. Actual response functions will depend on the CCD response.

The CBB-filter is attractive for two reasons: 1) it reduces a significant amount of sky background light whenever the moon is above the horizon, and 2) it reduces extinction effects by a large amount without a significant SNR penalty. Concerning the first point, the night sky brightness spectrum will be similar to the site's extinction spectrum during moon-lit nights. (On moonless nights there's no reduction of sky background level from use of a CBB-filter.) For these reasons at least one wide-field survey camera project used a CBB-filter (Ohio State University's KELT Project, based at the Winer Observatory, AZ).

CHAPTER 19 – STAR COLORS

When a typical CCD response function is used (my ST-8XE), and adopting my site altitude, the CBB-filter's "white star" effective wavelength is calculated to be 700 nm. This is intermediate between the Rc-band and Ic-band filters.

Using a CBB-filter, stars that are blue and red have calculated extinctions of 0.124 and 0.116 mag/airmass. If a set of images that contain red and blue stars within the FOV were measured and plotted versus air mass they would exhibit these two slopes, i.e., they would separate at the rate of 8 mmag/airmass.

The following list summarizes the calculated extinction slope differences for various filters between stars that are blue (spectral type A2, 8000 K) and red (K3, 4500 K).

B-band	16 mmag/airmass
V-band	~6 mmag/airmass
R-band	3 mmag/airmass
I-band	~1 mmag/airmass
Unfiltered	59 mmag/airmass
CBB-band	8 mmag/airmass

The CBB-filter offers a dramatic 7-fold reduction of extinction effects compared with a clear filter! Keep in mind that the red and blue stars used for these calculations are near the extremes of blueness and redness, so the values in the above list are close to the maximum that will be encountered.

The CBB-filter's loss of SNR, compared to using a clear filter, will depend on star color. For a blue star the CBB-filter delivers 89% of the counts delivered by a clear filter (at zenith). For a red star it is 94%. The corresponding increases in observing time to achieve the same SNR are 41% and 13%. However, SNR also depends on sky background level, and the CBB and clear filters respond differently to changes in sky background. During full moon the sky background is highest, being ~3 magnitudes brighter than on a moonless dark night (away from city lights). Also during full moon Rayleigh scattering of moonlight produces a blue-colored sky background. I haven't studied this yet but I suspect that whenever the moon is in the sky the CBB-filter's lower sky background level is more important than the few percent loss of signal, leading to an improved SNR instead of a degraded one. In any case, a slight loss of SNR is worth extra observing time in order to achieve dramatic reductions of systematic errors in light curve "air mass curvature" that would have to be dealt with for unfiltered observations.

Getting Star Colors

The 2MASS (2-Micron All-Sky Survey) star catalog contains ½ billion entries. It is about 99% complete to magnitudes corresponding to V-mag ~17.5. TheSky/Six includes J, H and K magnitudes for almost every star in their maps. The latest version of MPO Canopus (with PhotoRed built-in) makes use of J and K magnitudes to calculate B, V, Rc and Ic magnitudes. J-K star colors are correlated with the more traditional star colors, B-V and V-R, as shown by Caldwell *et al* (1993), Warner and Harris (2007) and others. The strong correlation breaks down outside the J-K range -0.1 to 1.0, but within this wavelength region it is possible to predict V-R star colors with an accuracy of 0.021 magnitude (Warner and Harris, 2007). This is adequate for selecting same color reference stars.

CHAPTER 19 – STAR COLORS

Occasionally J and K magnitudes are missing from the star map programs in common use by amateurs (these programs are also referred to by the unfortunate name “planetarium programs”). When you need J-K for only a few such stars the following web site is useful: <http://irsa.ipac.caltech.edu/>

Converting between J-K and B-V can be done using the following equivalence (based on a scatter plot published by Warner and Harris, 2007):

$$B-V = +0.07 + 1.489 (J-K) \quad \text{or} \quad J-K = -0.15 + 0.672 (B-V)$$

In choosing same-color reference stars be careful to not use any with $J-K > 1.0$, where J-K to B-V and V-R correlations can be double-valued. Staying within this color range corresponds to $-0.1 < B-V < 1.5$. For stars meeting this criterion the median B-V is +0.64, based on a histogram of 1259 Landolt star B-V values.

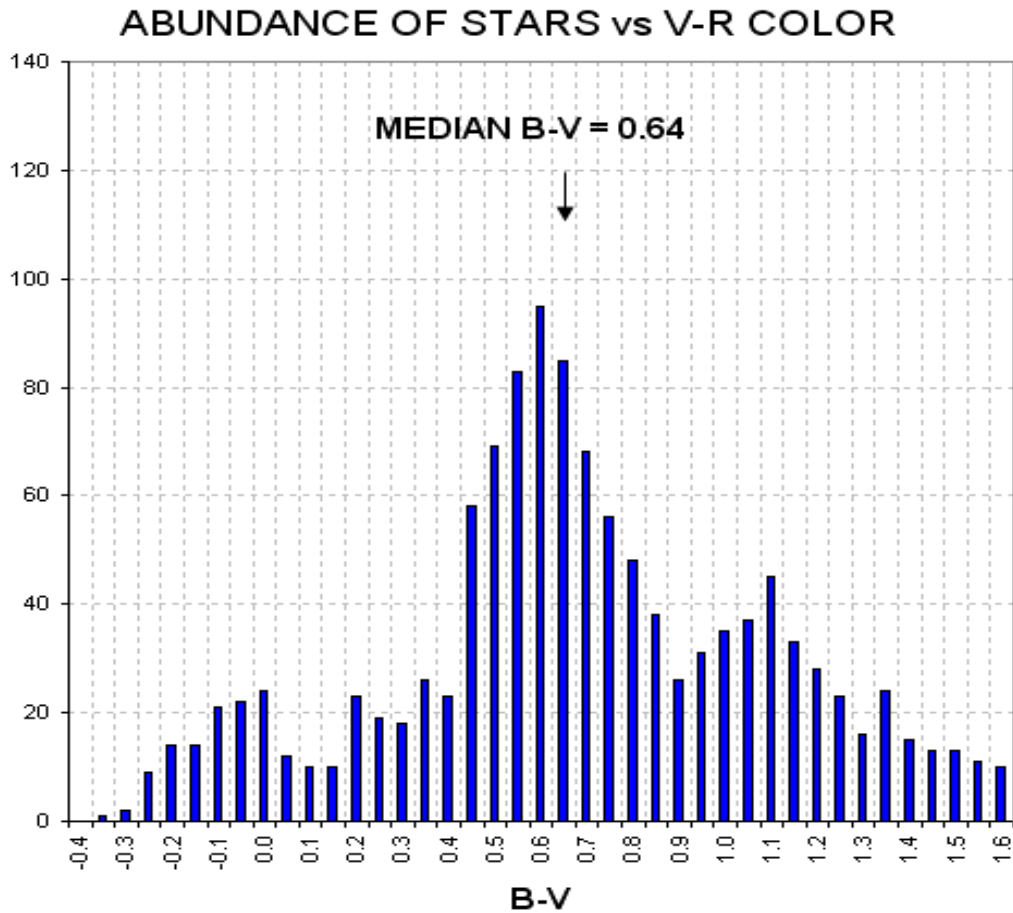


Figure 19.07. Histogram of B-V for 1259 Landolt stars (note: the figure title should read B-V).

This histogram shows that the bluest 25% of stars have $B-V < +0.47$. Using the Warner and Harris equation this corresponds to $J-K < +0.26$. The reddest 25% of stars with acceptable colors have $B-V > +1.01$, which corresponds to $J-K > +0.64$. If there were 12 candidate reference stars in a FOV, for

CHAPTER 19 – STAR COLORS

example, it is likely there would be 3 with $J-K < +0.26$ and another 3 with $J-K > +0.64$. If the target star is typical, with $J-K \sim 0.39$, there should be ~ 6 stars with a $J-K$ color difference less than ~ 0.2 . Therefore:

A reasonable goal for “same color” stars is a J-K difference $< \sim 0.2$ magnitude.

It's possible to associate $J-K$ with star surface temperature. The typical $J-K$ of $+0.4$ corresponds to $T_{\text{star}} = 5800$ K. The bluest 25% of stars have $T_{\text{star}} > \sim 7700$ K, and the reddest 25% have $T_{\text{star}} < \sim 4000$ K. These are close to the temperature extremes that were used to calculate zenith extinction sensitivities to star color. Therefore, the list of extinction slope differences for red and blue stars, for various filters (in the previous section of this chapter), should be representative of situations faced by exoplanet transit observers. In other words,...

Star color matters!

Chapter 20

Stochastic Error Budget

This chapter will illustrate how stochastic noise contributes to the “scatter” of points in a light curve. I will treat the following error sources: Poisson noise, aperture pixel noise, scintillation noise and seeing noise. All of these components can be treated as stochastic noise. Poisson and scintillation noise are usually the most important components.

“Stochastic” uncertainty is produced by a category of fluctuation related to random events. For example, it is believed that the clicking of a Geiger counter is random because the ejection of a nuclear particle is unrelated to events in the larger world; such events are instead prompted by laws that are not yet understood governing events within the nucleus. To observers in the outer world the particle ejections of radioactive nuclei occur at random times.

Photons from the heavens arrive at a CCD and release an electron (called a “photoelectron”) at times that can also be treated as random, even though there’s a steady flow of photons that is “constant” for long time averages. As a practical matter, the noise generated by thermal agitation within the CCD and nearby circuitry is also a random process. Scintillation is generated at the tropopause and causes destructive and constructive interference of wave fronts at the CCD, causing the rate of photon flux at the detector to fluctuate about an average value in what appears to be a random manner. All of these processes exhibit an underlying randomness, and their impact on measurements is referred to as “stochastic noise.” The “Poisson process” is a mathematical treatment of the probabilities of the occurrence of discrete random events that produce stochastic noise.

The previous chapters dealt with “systematic uncertainties” and tried to identify which ones were most important. This chapter deals with sources of stochastic uncertainty in an effort to identify which ones are most important. Both sources of uncertainty are important aspects of any measurement, and I’m a proponent of the following:

“A measurement is not a measurement until it has been assigned stochastic and systematic uncertainties.”

This may be an extreme position, but it highlights the importance of understanding both categories of uncertainty that are associated with EVERY measurement, in every field of science. This chapter therefore strives to give balance to the book by describing the other half of uncertainties in photometry. The components of stochastic noise will be treated using the XO-3 star field as an example, with specific reference to my 2007.04.15 observations of it.

Case Study Example

Whenever an exoplanet’s light curve is to be produced from a set of images there will usually be several stars suitable for use as reference stars (e.g., “ensemble” photometry). Consider the example of XO-3, whose star field is presented in the figure on the next page.

CHAPTER 20 – STOCHASTIC ERROR BUDGET

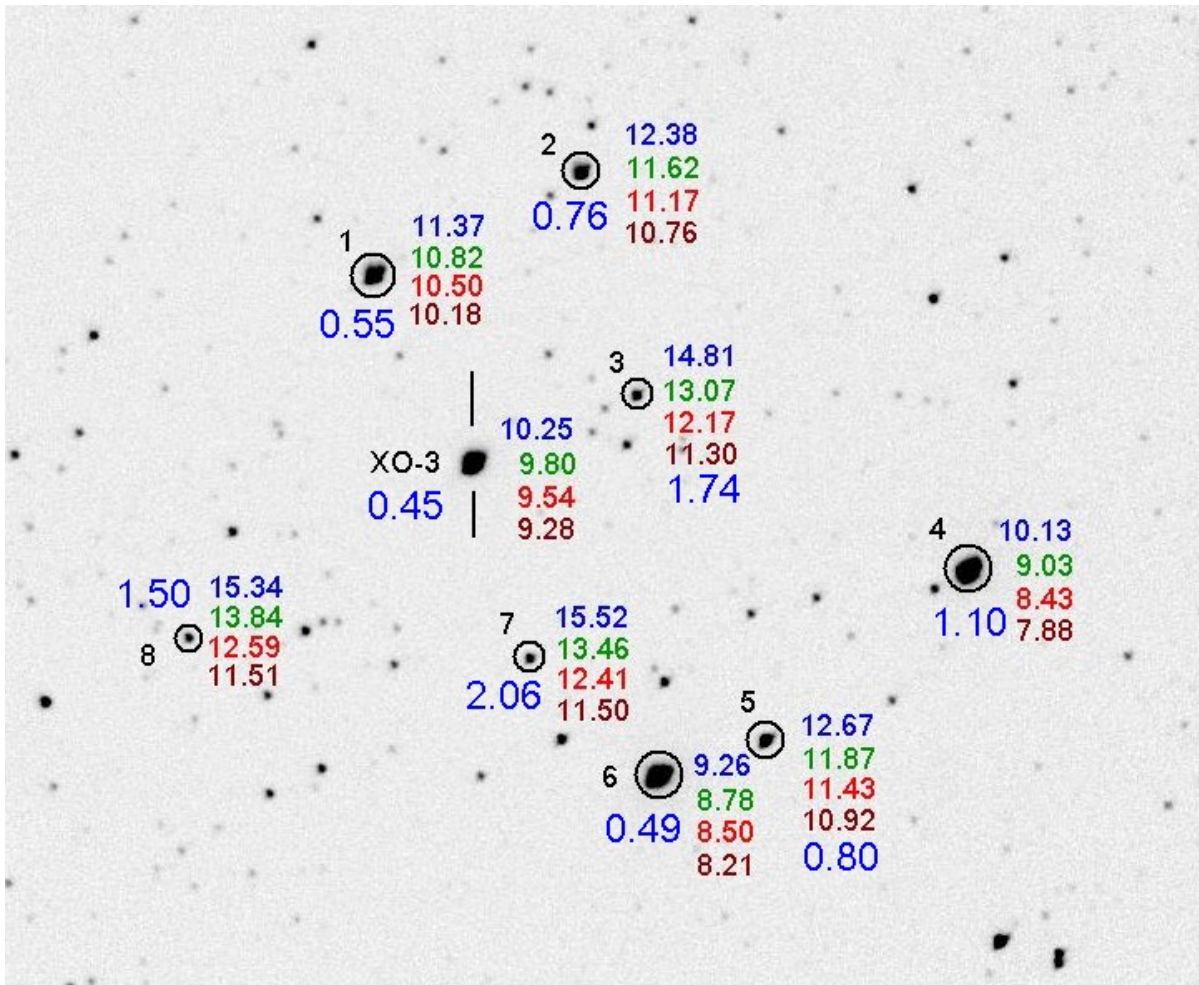


Figure 20.01. XO-3 star field, showing BVRcIc magnitudes of several stars. The B-V star colors are shown in large blue numbers. Observations were made 2007.04.15.

Note that XO-3 has a B-V color of 0.45, whereas all other stars are redder (larger values of B-V). Only two stars have close to the same color, stars #1 and #6. In the following example these two stars will be used for reference.

In the case study example used in this chapter I will use the term “flux” to mean the total number of counts in an image produced by a star. This may be common usage for the term but the technical definition for flux is really energy incident upon a unit area, per unit time, for photons within a specified wavelength range. Since this book is for “observing” instead of “modeling” I will continue to use “flux” with the first meaning.

On the date 2007.04.15 this star field was observed with an I-band filter, with exposure times of 60 seconds, unbinned (i.e., 1x1) and CCD cooler set to -24 °C (with my 14-inch telescope). FWHM was typically 6 pixels, so I chose a signal aperture photometry radius of 15 pixels ($2.5 \times \text{FWHM}$, a safe choice). With this aperture the measured fluxes for XO-3, Star #1 and Star #6 were 346000, 161000

CHAPTER 20 – STOCHASTIC ERROR BUDGET

and 963000 counts. The maximum counts for these stars varied with FWHM, of course, but typically they were ~9200, 4300 and 22000 counts (SNR ~3000, 1100 and 8000), so none of the stars were saturated. The next four sections of this chapter illustrate calculations of the four sources of stochastic uncertainty using this set of observations as an example.

1) Aperture Pixel Noise

Consider noise contributions from the process of "reading" the CCD ("CCD read noise"), plus noise produced by thermal agitation of the crystal's atoms ("CCD dark current noise"), and finally from noise produced by a sky that is not totally dark ("sky background noise"). These are sources of noise in each CCD reading (the last two are Poisson themselves since they are based on discrete stochastic events, but we'll treat them here in the traditional manner). These three noise sources are small when the star in the photometry aperture is bright and the CCD is very cold (to reduce dark current noise). For that situation it can be stated that the star's measured flux (total counts within the aperture minus an expected background level) will **not** be affected by measurement hardware, but instead will be due to a fundamental limit of stochastic sampling theory, described in the following section (Poisson noise). If, however, the CCD is not very cold (which is going to be the case for amateurs without LN2 cooling), and when the sky is bright (too often the case for amateur observing sites), these components of noise cannot be ignored.

I'll use the term "aperture pixel noise" to refer to the sum of these three sources of noise (sky background level, CCD dark current noise and CCD readout noise). It's convenient to lump these three noise sources together because that's what can be easily measured. Using MaxIm DL (MDL), when the photometry aperture is moved to a location where there are no stars the information window displays the RMS scatter (per pixel) for both the signal aperture and sky background annulus (which should be the same if no stars are present in either). For the 2007.04.15 observations this RMS was typically 4.3 counts. This is what I'm referring to as "aperture pixel noise." Let's represent this noise as N_i . For this example, $N_i = 4.3$ counts.

The fact that each pixel's reading has a finite uncertainty, N_i , has two effects: 1) the average level for the sky annulus background is not perfectly established, and 2) the flux within the aperture (the sum of differences between the signal aperture pixel readings and the average background level) is also uncertain. Among the \mathbf{b} pixels within the sky background annulus the average count is C_b and the standard deviation of these counts is $N_i = 4.3$ counts. We will assume that every pixel in the image has an uncertainty of N_i . The average value for the sky background level has an uncertainty given by:

$$\text{SE on average background level, } N_b = N_i / \sqrt{\mathbf{b}-1},$$

where \mathbf{b} = number of pixels in sky background annulus.

Star flux is defined to be the sum of counts **above** a background level. One way to view this calculation is to subtract the background level from each signal aperture pixel count, and then perform a summation. An equivalent view is to sum the signal aperture counts, then subtract the sum of an equal number of background levels. The second way of viewing the calculation lends itself to a simple way of calculating SE on the calculated flux, since we're simply subtracting one value from another and each value has its own uncertainty. The first value, the sum of signal aperture counts, will be uncertain by the amount:

CHAPTER 20 – STOCHASTIC ERROR BUDGET

SE on sum of counts within signal aperture, $N_{ss} = N_i \times \text{sqrt}(s)$,

where s is the number of pixels within the signal aperture. The second number, the sum of counts that would be expected for these s pixels if no star were present within the signal aperture, will have an uncertainty:

SE on expected counts within signal aperture if no star present, $N_{bs} = N_b \times \text{sqrt}(s)$
 $= N_i \times \text{sqrt}(s) / \text{sqrt}(b-1)$

The uncertainty on calculated star flux (neglecting Poisson noise) will be the orthogonal sum of these two uncertainties: $N_s^2 = N_{ss}^2 + N_{bs}^2$. We derive that $N_s^2 = s \times N_i^2 \times (1 + 1/b)$, and since $(1 + 1/b) \sim 1$, we can state that:

SE on star flux counts (due to dark, read and background), $N_s = \text{sqrt}(s) \times N_i$.

Converting this counts noise to mmag,

SE of star (dark, read and background) [mmag] = $1086 \times \text{sqrt}(s) \times N_i / \text{Star Flux [counts]}$

Since the 2007.04.15 images exhibit $N_i \sim 4.3$ counts, and since $s = \pi (15)^2 = 707$ pixels, we calculate $N_s = 114$ counts. This SE will be the same for all stars in the image, so here's a table of how this translates to mmag for each star:

XO-3, flux = 346000 counts, SE' = 0.36 mmag (aperture pixel noise)	
Star#1, flux = 161000 counts, SE' = 0.77 mmag	“
Star#6, flux = 963000 counts, SE' = 0.13 mmag.	“

where SE' means that these are only the “aperture pixel noise” components of uncertainty (that neglect Poisson noise, treated in the next section). Since the magnitude of an exoplanet star used for producing a light curve is based on the fluxes of all stars (target and reference), the uncertainties for the reference stars will affect the calculated magnitude for the target, XO-3 in this case. When using ensemble photometry, we must orthogonally add the target's SE' to the SE' for the average of the reference stars to obtain SE' for the target's ensemble magnitude solution. For the present case, SE' for the average of the reference stars = $\frac{1}{2} \times \text{sqrt}(0.77^2 + 0.13^2) = 0.39$ mmag. The general equation for calculating “SE' for the average of reference stars” (homework for the reader) is:

Ensemble SE for reference stars = $\{\text{sqrt}(SE'_1{}^2 + SE'_2{}^2 + SE'_3{}^2 + \dots + SE'_n{}^2)\} / n$

where SE'_n is SE' for reference star n . Our goal is to calculate “ensemble SE for target” and this is done by orthogonally adding SE'target and the above “ensemble SE for reference stars.” The orthogonal sum of 0.36 and 0.39 is 0.53, which is XO-3's “ensemble SE due to aperture pixel noise”. If you prefer, the two steps can be combined:

Ensemble SE for target = $\text{sqrt}\{SE'_{\text{target}}{}^2 + (SE'_1{}^2 + SE'_2{}^2 + SE'_3{}^2 + \dots + SE'_n{}^2)/n^2\}$

where SE'_n is SE' for reference star n . The greater “ n ” the smaller “ensemble SE for target” (assuming reference stars SE' have similar values), which makes intuitive sense. No matter how many

CHAPTER 20 – STOCHASTIC ERROR BUDGET

reference stars are used, and no matter how small the reference star term of the above equation, the “ensemble SE for target” can never be less than SE_{target}, which also makes intuitive sense.

How good a value can we expect for “SE due to aperture pixel noise” for a properly configured telescope used for optimally designed observing session using amateur hardware? Sophisticated observers optimize their telescope configuration so that image scale is about 1/3 FWHM under good seeing conditions. For example, if good seeing produces FWHM ~ 2.5 “arc, the focal reducer location is adjusted so that image scale ~ 0.8 “arc/pixel. Good observing practices also call for setting exposure time so that maximum counts is close to, but never exceeds, saturation; this means that under good seeing conditions the target star produces maximum counts of ~35,000. If $C_{max} = 35,000$ and FWHM = 3 pixels, flux ~ 450,000 counts. If the photometry aperture radius is set to $2.7 \times \text{FWHM} = 8$ pixels, then the number of pixels within the signal aperture is 804. If aperture pixel noise is similar to my system, $N_i = 4.3$ counts, then “SE of star (dark, read and background)” = $1086 \times \sqrt{804} \times 4.3 / 450000 = 0.29$ mmag. If 4 similar stars are used as reference, their average will have SE ~ 0.15 mmag. After ensemble photometry the SE for the target, due to “aperture pixel noise,” will be ~0.33 mmag. This is only slightly better than what was calculated for the specific case of XO-3 on 2007.04.15 (0.53 mmag). As we will see, shortly, “aperture pixel noise” is almost always an unimportant component in the stochastic error budget.

2) Poisson Noise

A Poisson distribution describes what can be expected when a finite number of “random” events produce a measured “count” (an integer) during a pre-set time interval. This is the situation for readings of each CCD pixel at the end of an exposure. Consider the process of a photon dislodging an electron from a silicon crystal in the CCD (related to the “photoelectric effect”). This one event yields one electron for detection after the exposure is complete. When a pixel is “read” by electronic circuitry this one electron will contribute to that pixel’s ADU (analog digital unit) count by an amount that depends on the CCD gain. For my SBIG ST-8E CCD, the gain is 2.3 electrons per count (where each “count” is also called an ADU). Therefore, the number of photoelectrons needed to produce a count of C is $n = 2.3 \times C$ (for my CCD). This is true whether I define C to be the count from just one pixel or the sum of counts produced by a star that may be registered by several pixels (commonly referred to as “intensity” or “flux”). You can measure your CCD’s “gain” (actually, the reciprocal of what gain should mean) and it may differ significantly from the value given in the User’s Manual. For example, my CCD has a gain of ~2.7 instead of the manual’s 2.3 electrons per ADU.

Stochastic events have the property that the SE uncertainty of the total number of events is the square-root of the number of such events (provided the number of events is large). Thus, when we measure n stochastic events occurring within a specified integration interval, we must state that we have really just measured a value $n \pm \sqrt{n}$ events. Since the measurement C is based on $2.3 \times C$ events (for this particular CCD) we must state that we have measured: $2.3 \times C \pm \sqrt{2.3 \times C}$ “events.” Dividing both sides by 2.3 yields the statement that we measure $C \pm \sqrt{C/2.3}$. This fundamental uncertainty is referred to as Poisson noise. To summarize, Poisson noise from a bright star is:

$$\text{Poisson noise, } N_p = \sqrt{C / \text{gain}}$$

For my SBIG ST-8E CCD, $N_p = \sqrt{C / 2.3}$.

CHAPTER 20 – STOCHASTIC ERROR BUDGET

We can express noise as a fraction, so starting with the statement that we measure $C \pm \text{sqrt}(C/2.3)$, the ratio of uncertainty when the thing we measure is:

$$\text{Poisson Noise SE [dimensionless fraction]} = 1 / \text{sqrt}(2.3 \times C)$$

It is useful to express uncertainties in terms of milli-magnitude (mmag), using the following equation that applies to fractional SE is small:

$$\text{SE [mmag]} = 1086 \times \text{SE [counts]} / \text{Star's Flux [counts]}$$

When Poisson noise is small:

$$\text{Poisson Noise SE [mmag]} = 1086 / \text{sqrt}(2.3 \times C)$$

Using the above example, the ensemble photometry adjustment will have an uncertainty given by $\frac{1}{2} \times (1.78^2 + 0.73^2)^{0.5} = 0.96$ mmag. This is the same mathematical situation as in the previous section, where it was alleged that:

$$\text{Ensemble Photometry Reference Stars Poisson SE} = 1/n \times (\text{SE}_1^2 + \text{SE}_2^2 + \text{SE}_3^2 + \dots + \text{SE}_n^2)^{1/2}$$

where “n” is the number of reference stars and SE_n are the Poisson uncertainties for each reference star (expressed in mmag units). Clearly, as “n” increases, the effect of uncertainties (due to Poisson noise) diminishes, approaching the limit zero for an infinite number of reference stars.

Using the above equation we calculate N_p values for the three stars to be 388, 265 and 647 counts. Measurements of each star will have Poisson uncertainties of 1.22, 1.78 and 0.73 mmag (using $1086 / \text{sqrt}(2.3 \times \text{Flux})$). For each image the three flux readings will be converted to magnitudes and the XO-3 magnitude will be adjusted by whatever amount is needed to bring the average magnitude of the two reference stars into agreement with what is expected for them from an atmospheric model for extinction.

XO-3's Poisson noise uncertainty of 1.22 mmag must be orthogonally added to the Poisson uncertainty produced by the reference stars. Hence, after performing an ensemble photometry adjustment using these two reference stars XO-3 can be expected to exhibit a total Poisson noise uncertainty of $(1.22^2 + 0.96^2)^{1/2} = 1.55$ mmag. This is the Poisson component of RMS scatter for each image that can be expected in a final light curve. Note that Poisson noise for this example is larger than “aperture pixel noise,” calculated in the previous section to be 0.53 mmag.

3) Scintillation Noise

At tropopause altitudes clear air turbulence is common, and the temperature inhomogeneities produced by turbulence cause slight bending of the wave fronts of starlight. At ground level these bent waves produce a component of constructive and destructive interference that vary with location. If a snapshot could be taken of the star's apparent brightness at locations on the ground we would see a pattern with structures as small as an inch or less. A large telescope aperture would include many of the “bright spots” and “faint areas” so the total flux from the star would be close to the spatial-

CHAPTER 20 – STOCHASTIC ERROR BUDGET

average value; for a small aperture telescope the total flux would not be as close to the spatial-average. The instantaneous pattern of brightness at ground level will drift in the direction of the wind at the tropopause. From the standpoint of a telescope fixed to the ground there will be a variation of total flux with time produced by the horizontal movement of this “frozen” spatial pattern. The variation of total intercepted flux by a telescope’s aperture is called “scintillation.” The smaller the telescope aperture, the greater the scintillation.

The naked eye’s aperture is so small that an additional component of scintillation is produced by temperature and humidity inhomogeneities near ground level (where “atmospheric seeing” degradation is produced). These visual changes in brightness are called “twinkling” and because the tropopause component is common to both there is a correlation between the amount of twinkling and scintillation. Incidentally, since atmospheric seeing is degraded mostly by turbulence near the ground, visually perceived twinkling and scintillation are correlated whereas twinkling and seeing are less correlated. Everyone knows that stars “twinkle” different amounts on different nights. Twinkling also is greater near the horizon. Faint stars twinkle as much as bright stars. Planets don't twinkle. What’s going on?

These common facts are helpful in understanding what to expect for attempts to monitor the brightness of a star that is undergoing an exoplanet transit. For example, the fact that planets don't twinkle means that a reference star's scintillation (closely related to twinkling) will be **uncorrelated** with the target star's scintillation (since the angular separation of reference and target stars is greater than the angular size of a planet, and planets don’t twinkle). This is unfortunate, for it means that a differential photometry analysis that uses one reference star will increase the target star's brightness variations due to scintillation by ~41% (*i.e.*, the fluctuations are root-2 times the value that would occur without using a reference star). Using many reference stars reduces the effect of uncorrelated reference star scintillation back to where it is dominated by just the target star's scintillation. It also can be stated that there's no need to choose reference stars that are near the target star to reduce scintillation, since essentially all correlation is lost beyond angular distances of ~10 "arc (a typical planet angular diameter).

A classic study of scintillation was published by Dravins *et al* (1998) as part of a series of articles on the subject. They studied scintillation’s dependence upon telescope aperture, air mass, observing site altitude and exposure time. Their equation relating all these parameters is:

$$\sigma \approx 0.09 \times D^{-2/3} \times \sec(Z)^{1.75} \times \exp(-h/h_0)/(2g)^{1/2}$$

where σ = fractional intensity RMS fluctuation (scintillation), D = telescope diameter [cm], $\sec(Z)$ = air mass, h = observatory site altitude above sea level [m], atmospheric scale height $h_0 = 8000$ [m], and g = exposure time [sec].

The next figure plots scintillation noise for a range of exposure times and air mass values for a 14-inch telescope at sea level.

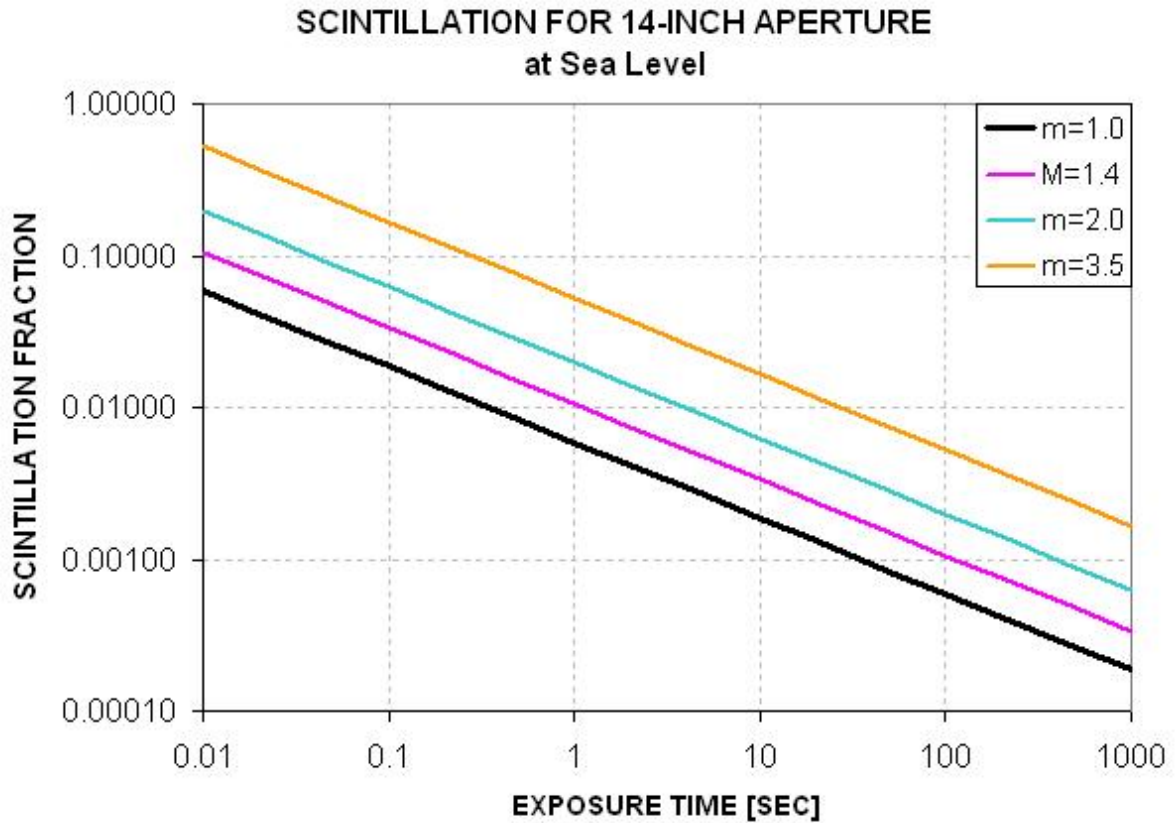


Figure 20.02. Scintillation versus exposure time and air mass for a 14-inch telescope at a sea level observing site. For 8-inch telescope, multiply by 1.45; for 24-inch, multiply by 0.70. For an altitude of 5000 feet, multiply by 0.83. Scintillation can vary by factor of two in matter of hours so this plot is only a guide to what can be encountered.

For me, $h = 1420$ meters and $D = 35.6$ cm, so I calculate an expected typical scintillation noise to be:

$$\text{Scintillation noise [mmag]} = 5.35 \times \text{AirMass}^{1.75} / \text{sqrt}(g)$$

where $g =$ exposure time [seconds]. For air mass = 1.9 and $T = 60$ seconds, scintillation = 2.12 mmag. Keep in mind that the magnitude of scintillation may vary greatly from night-to-night, as well as on time scales of a few minutes. This is the level of noise due to scintillation that can be expected for the XO-3 observations serving as a case study for this chapter. Scintillation noise, therefore, exceeds both Poisson noise (1.55 mmag) and aperture pixel noise (0.36 mmag).

4) Seeing Noise

The last category of noise that I treat is called “seeing noise” because it is only present when atmospheric seeing (e.g., FWHM) varies significantly during an observing session.

Once, when I made about 1000 short exposures of the moon for the purpose of creating an animation showing terminator movement, I noticed two unexpected things: 1) sharpness varied across each

CHAPTER 20 – STOCHASTIC ERROR BUDGET

image, and 2) position distortions were present. The first item means that no single image was sharp at all parts of the image. One image might be sharp in the upper-left hand area (FWHM $\sim 1.5''$ arc) and fuzzy elsewhere ($3.5''$ arc), while the next image might be sharp in the middle only. My impression is that the sharpness auto-correlation function usually went to zero $\sim 5''$ arc away, and the areas where one image was sharp were poorly correlated with the next image's sharp areas. The second item means that position distortions within an image were present, which made it impossible to combine two images with just one offset for bringing all regions of the FOV into alignment. A time-lapse movie of these images resembles looking into a swimming pool and seeing different parts of the pool bottom move in ways that were uncorrelated. These two phenomena were seen for about two hours, so it wasn't just an early evening atmospheric effect. I used a V-band filter, an exposure time of 0.1 second and images were spaced ~ 8 seconds apart. (Some of these moon images can be seen at <http://brucegary.net/Moon/Moon7524.htm> and an animation of seeing can be found at <http://brucegary.net/ASD/x.htm>, Fig. 4.)

Since these were short exposures the spatial seeing differences were entirely atmospheric, unlike long exposures that can be influenced by imperfect tracking. Even with perfect tracking we can predict that the longer the exposure the smaller the spatial differences in sharpness. To understand this, imagine a 3-dimensional field of atmospheric temperature with inhomogeneities that are "frozen" with respect to the air. Now imagine that the air is moving and carrying the temperature structure across the telescope's line-of-sight. At one instant the line-of-sight to one part of the FOV may be relatively free of temperature structure, and exhibit sharpness, while the opposite is true for another line-of-sight. But as the air moves past the telescope the regions of sharpness in the FOV will vary. If a typical time for variation is 1 second, for example, then after 16 seconds the contrast in sharpness will be of order $1/4^{\text{th}}$ as large compared with the contrast for individual short exposures. In theory, there will always be some variation of FWHM sharpness across an image, regardless of exposure time.

Consider using an aperture that captures a fraction, slightly less than one, of the complete PSF for a star. Refer to Fig. 13.02 for a plot of photometry signal aperture "capture fraction" versus size of the aperture in relation to FWHM. For a typical choice of aperture radius ~ 2.5 times FWHM, 99% of a star's total flux is captured by the photometry aperture. If FWHM varies across the image within the range 3.0 to $3.3''$ arc, for example, the capture fraction could vary between 0.987 and 0.980, or 7.6 mmag. Smaller apertures would produce even larger differences.

Since patterns of seeing across an image will be uncorrelated from one image to the next the errors in relating an exoplanet's flux to the fluxes of reference stars (produced by seeing variations) will be different from image to image. The effect of this upon a light curve is to merely increase RMS scatter. In other words, there won't be any systematic effects that would change the shape of the light curve. This is my reason for including variable seeing in this chapter as "noise."

I don't know of any study analogous to that by Dravin's et al (1998) that can be used to predict the magnitude of noise introduced to a light curve by seeing variations. For the moment let's simply treat it as an unknown small effect, and if empirically-determined RMS scatter requires invoking something unknown we can consider seeing variations to be a candidate for explanation.

CHAPTER 20 – STOCHASTIC ERROR BUDGET

Comparing Observed with Predicted RMS Scatter

For the 2007.04.15 observations of XO-3 using my 14-inch telescope I measured an RMS scatter of 2.63 mmag for a one-hour period. How does this compare with the expected total RMS calculated in the previous sections? Here's the list:

0.53 mmag	Aperture pixel noise
1.55 mmag	Poisson noise
~ 2.12 mmag	Scintillation noise
?..? mmag	Unidentified sources of noise (“seeing” noise, etc.)
~ 2.68 mmag	Total noise predicted
2.63 mmag	Measured noise

The agreement is pretty good, especially considering that the largest component (scintillation) is so variable. The amplitude of scintillation can change by a factor two during the course of hours, and night to night variations can differ by similar amounts (depending on the location of jet stream winds, which generate clear air turbulence).

It's possible to evaluate the presence of “seeing noise” by reprocessing images using a large photometry aperture. For example, when the 2007.04.15 images are processed using an aperture radius of 20 pixels instead of 15, the measured RMS scatter increases to 2.76 mmag. Some increase can be expected from a larger “aperture pixel noise” (the predicted total noise changes from 2.65 to 2.67 mmag), but the fact that the measured noise increased more than the predicted amount, instead of decreasing, suggests that “seeing noise” was not important for this observing session.

I use a special spreadsheet to help guide the choice of reference stars. It allows me to see the predicted effect of adopting various sets of reference stars and aperture sizes. For example, notice in Fig. 20.01 that Star #4 is much brighter than the other stars that I adopted for use as reference. If it replaced Star #1 the RMS scatter is predicted to be reduced to 2.50 mmag. This is a small payoff considering the extreme redness of Star #4, which can be verified in the photometry analysis spreadsheet by actually trying out the use of Star #4 instead of Star #1 for reference.

It should be noted here that the case of 2007.04.15, based on use of an I-band filter, is not meant to show a representative RMS scatter for light curves. Lower scatter can be achieved by observing with an R-band filter (1.7 times as much flux), or a “clear with blue-blocking” CBB-band filter (4 times the flux). Also, the XO-3 star field does not have a good choice for same color stars, and this affects the level of RMS scatter that can be achieved. XO-1 and XO-2, for example, provide better reference star candidates. It is almost possible to achieve the “gold standard” of ~1 mmag RMS scatter per 1-minute image using a 14-inch telescope provided a good set of reference stars is nearby, a CBB-band filter is used, and scintillation conditions are low.

Larger telescope apertures should be able to achieve better “mmag precision” in spite of the fact that exposure times would have to be shortened to avoid saturation. It should be each observer's responsibility to use the concepts described here to calculate an observing strategy that produces light curves with a minimum RMS scatter as well as a minimum of systematic errors based on the observer's specific telescope and observatory situation.

CHAPTER 20 – STOCHASTIC ERROR BUDGET

Summary

Here's a summary of useful equations for estimating a target star's SE for each image when several reference stars are used:

1) Aperture Pixel Noise for a Star [mmag] = $1086 \times \sqrt{s} \times N_i / C$,

where s = number of pixels in signal aperture, N_i = pixel noise as reported by MDL for area free of stars and C is the star's flux. When a single reference star is used ("comp/chk" photometry) the SE for target and reference star must be orthogonally added to obtain the desired target star's SE after "comp/chk" photometry. When more stars are used for reference ("ensemble" photometry) the SE for the average of reference stars can be calculated using this equation:

$$\text{Ensemble SE for ref stars} = \{\sqrt{SE'_1{}^2 + SE'_2{}^2 + SE'_3{}^2 + \dots + SE'_n{}^2}\} / n$$

where SE'_n is SE' for reference star n . This SE is to be orthogonally added to the target star's SE to obtain the desired target star's SE after "ensemble" photometry.

2) Poisson Noise for a Star [mmag] = $1086 / \sqrt{\text{CCDgain} \times C}$

where "CCDgain" \sim 2.5 electrons per count (for ST-8XE) and C = total counts for the star.

Poisson Noise for the average of several reference stars after ensemble photometry = $1/n \times (SE_1{}^2 + SE_2{}^2 + SE_3{}^2 + \dots + SE_n{}^2)^{1/2}$, where "n" is the number of reference stars, each having SE_n .

SE for target after ensemble photometry is orthogonal sum of Poisson SE for the target and Poisson SE for the average of the reference stars.

3) Scintillation Noise = $\sigma \approx 0.09 \times D^{-2/3} \times \sec(Z)^{1.75} \times \exp(-h/h_0)/(2g)^{1/2}$

where σ = fractional intensity RMS fluctuation (scintillation), D = telescope diameter [cm], $\sec(Z)$ = air mass, h = observatory site altitude above sea level [m], atmospheric scale height $h_0 = 8000$ [m], and g = exposure time [sec].

4) Seeing noise can be estimated by comparing measured noise levels with different photometry apertures. To do this right you'd have to repeat steps 1) and 2), above. I don't recommend it.

I use a spreadsheet for these calculations, which can be tedious. I invite each observer to do the same.

Chapter 21

Exoplanet Stars are Not Variable Stars

During the two years that I managed the Amateur Exoplanet Archive I occasionally noticed that a new observer was using procedures for observing and image analysis that are meant for use with variable stars and which therefore are not optimized for the task of exoplanet observing. Whereas experience with AAVSO tasks is helpful to someone starting to observe exoplanets, the two tasks are different enough that many of the procedures for AAVSO tasks should not be adhered to while learning to observe exoplanets. This chapter is meant to highlight the differences, and provide ideas for adjusting strategies in observing, image measurement and spreadsheet analysis that are closer to optimum for producing good quality exoplanet light curves.

Overview of Differences

The goal of AAVSO is to produce accurate plots of brightness variation from many observers in order to study changes that occur on many time-scales. The goal of exoplanet observations is to produce a precise light curve during a 4 to 8 hour interval that includes an exoplanet transit.

In the above description notice the use of the words “accurate” and “precise” to describe the two tasks. Photometric accuracy involves calibration to a standard magnitude scale; precision does not! The purpose for accuracy is to permit the combining of observation segments from many observers to produce one long stretch of data. The purpose for precision is to produce a light curve from one observer that has high signal-to-noise while maintaining calibration errors that are constant, though unknown, for the duration of the observing session. The AAVSO observer strives for accuracy while the exoplanet transit observer strives for precision, and the differences between these two goals have many consequences for observing strategy, image measurement and spreadsheet data analysis. In this chapter we will “count the ways” the two goals differ.

1. “Where are the Comparison Star Sequences?”

Occasionally someone will ask me where to find “comparison stars” for the exoplanet star fields. After all, as any good AAVSO observer knows, you can’t contribute to an observing program involving many observers if your reported magnitudes aren’t based on nearby stars that are well-calibrated.

For AAVSO variable stars it is necessary to use a reference star whose magnitude has been established by a professional astronomer. Two or more such reference stars can be used, called “ensemble differential photometry.” When this is done the variable star’s magnitude is reported (by the image processing program) to be the average of what each of the reference stars calls for. The set of calibration stars are chosen so that their brightness span is within the range that the variable star undergoes during the many years it is to be monitored. This isn’t necessary for CCD observers, but it is for visual observers. The stars that are calibrated for this purpose are called a “sequence” for the

CHAPTER 21 – EXOPLANETS NOT VARIABLE STARS

variable in question. Since establishing accurate magnitudes for the "sequence" requires all-sky photometry, and since this is too difficult for amateurs, a variable star cannot be adequately observed by more than one observer until a professional astronomer has established a "sequence" of calibrated stars near the variable, and has also confirmed that none are variable themselves.

Most variable star observing consists of using a standard filter (from the BVRcIc set) to measure a target star's brightness in relation to the nearby "comp" stars. For CCD observers each target star field can be observed with two filters, such as V and Rc, for an observing segment lasting a few minutes; afterwards another target star is observed in the same way, and so on for the rest of the observing session. The hard part comes the next morning when the images are measured and instrumental magnitude readings are processed to derive each target star's brightness on a standard magnitude scale. A decision has to be made whether to employ CCD Transformation Equations to correct for telescope system dependencies on star color, or whether to report magnitudes without transformation equation corrections. I think it's the case that most observers don't perform the transformations, for reasons that will be clear with the following example:

$$(V_s - R_s) = (V_c - R_c) + T_{vr} * [(v_s - r_s) - (v_c - r_c)]$$

$$V_s = v_s + (V_c - v_c) + T_v * [(V_s - R_s) - (V_c - R_c)], \text{ using the solution for } (V_s - R_s) \text{ in the above line}$$

$$R_s = V_s - (V_s - R_s), \text{ using } V_s \text{ from the line above, and } (V_s - R_s) \text{ from the first line}$$

Where:

V_c = known V-band magnitude of comparison star,
 R_c = known R-band magnitude of comparison star,

v_s = instrumental (i.e., measured and uncorrected) V-band magnitude of star of interest,
 v_c = instrumental V-band magnitude of known comparison star,

r_s = instrumental R-band magnitude of star of interest,
 r_c = instrumental R-band magnitude of comparison star,

using the following coefficient definitions (unique to an observing system and usually unchanging):

T_v = slope of (V-v) plotted versus (V-R)
 T_{vr} = reciprocal of slope of (v-r) plotted versus (V-R)

This daunting set of CCD Transformation Equations is just for observations with just two filters (V and Rc). When three or more filters are used more equations are involved. If you're a "glutton for punishment" I invite you to spend a few hours reviewing my web page where these equations are derived from first principles: http://reductionism.net.seanic.net/CCD_TE/cte.html.

Other ways of achieving the same result are possible, and my favorite is based on the "basic photometry equation," illustrated here:

$$Mag = Z - 2.5 \times \text{LOG}_{10} (Flux / g) - K' \times \text{AirMass} + S \times \text{StarColor}$$

where **Z** is a zero-shift constant, specific to each telescope system and filter (constant for many months),
Flux is the star's flux (sum of counts associated with the star). It's called "Intensity" in MaxIm DL,
g is exposure time ("g" is an engineering term meaning "gate time"),
K' is zenith extinction (units of magnitude),
S is "star color sensitivity." S is specific to each telescope system (should remain the same for many months),
StarColor can be defined using any two filter bands. B-V is in common use.

CHAPTER 21 – EXOPLANETS NOT VARIABLE STARS

The purpose for using either the CCD Transformation Equations or the basic photometry equation is to adjust measured (instrumental) magnitudes of the target star so that they can be reported on a standard magnitude scale, which in turn is needed so that these observations can be combined with similarly transformed observations from other observers for the purpose of producing a “light curve” with a length of days, weeks, months, years or even decades.

None of these transformations are needed for exoplanet observing! Indeed, reported magnitudes for an exoplanet transit can be wrong by a magnitude, or 10 magnitudes, or a hundred magnitudes (I’m just making a point here) without compromising the information that is desired: mid-transit time, transit length, transit depth and transit shape.

For exoplanet observing it is not necessary to know the magnitude for any stars that are to be used for reference! The only requirement for using a nearby star for reference is that it not vary during the several hours of the observing session. (Well, sometimes there's an additional "requirement" - actually a "preference" - to not use any reference stars that have a color vastly different from the target star.) Any observer who is accustomed to using a commercial program for processing images for AAVSO tasks is likely to be puzzled about this, and will wonder what to do when it's time to select a "comp" star (an archaic term left over from the days when most monitoring of variables was done visually). My advice to such an observer is to choose any nearby star you want for use as a "comp" star, provided it's not saturated at any time during the observing session, and assign it any old magnitude that catches your fancy. For "thrills" give it a magnitude of 100; it just won't matter in the final analysis. If you want to use a second "comp" star for reference, you may also assign it any magnitude you want; try -100. Mathematically it just won't matter. Remember, for an exoplanet star we don't care what magnitude offset error is present for the entire set of measurements; we only care how the star varies in brightness during the observing session.

Therefore, when a new observer of exoplanet transits asks me “where are the comparison stars?” I smile, knowing that the person is probably an accomplished AAVSO observer, and I begin explaining why there aren't any for exoplanet stars, and even if they existed they'd be useless!

Whereas an AAVSO observer strives to achieve an accuracy of ~ 0.03 magnitude for a specific filter band, for a night's several-minute observations of a given variable star, the exoplanet observer has absolutely no *accuracy* goals in mind. The exoplanet observer strives for *precision*, not *accuracy*! His task is for a precision of 0.002 magnitude, and accuracy be damned! (If you don't understand the difference between accuracy and precision, it is described at the end of this chapter.)

So the first lesson for experienced AAVSO observers to learn is that every (uncalibrated) star is a suitable candidate for use as a reference star. Instead of using 3 or 4 calibrated stars for reference, as is common for AAVSO work, use 20 or 30 uncalibrated stars!

2) Scintillation

Scintillation is a variation on very short time scales (millisecond to seconds) of a star's brightness, and it is related to "twinkling." Scintillation was described in the previous chapter. The scintillation at one location will differ slightly from that at another location, such as a few inches away, and this means that large telescope apertures will average down the amplitude of scintillation. The eye, with an aperture of $\sim 1/3$ inch, sees a larger scintillation amplitude than is measured using a telescope (and the eye is subject to a component of scintillation produced by temperature and humidity inhomogeneities at low altitudes). For example, a 10-inch aperture telescope observing at 30 degrees elevation for a

CHAPTER 21 – EXOPLANETS NOT VARIABLE STARS

10-second exposure will typically exhibit scintillation variations of ~ 0.008 magnitude. For an AAVSO task, where the goal may be an accuracy ~ 0.03 magnitude, scintillation is unimportant. But for an exoplanet observer, with a goal of ~ 0.002 magnitude precision, a 0.008 magnitude component of variation is important. If one nearby star is used as reference, the magnitude difference between the two stars will exhibit a root-2 greater scintillation than for either star alone (because scintillation variations are uncorrelated for separations greater than about $10''$). Using just one reference star in our example would produce a scintillation component of ~ 0.012 magnitude per 10-second exposure. By using many reference stars the target star's scintillation can be brought back to the 0.008 magnitude level. The penalty for not using many reference stars is equivalent to using exposure times that are half of what in fact were used, so this is equivalent to reducing the "information" from an observing session by a factor two! Exoplanet observers therefore want to use many reference stars.

3) SNR: Exposure Time and Focus

SNR, or signal-to-noise ratio, is very important for exoplanet observers, and it is relatively unimportant for AAVSO variable star observers. Variations in an exoplanet's light curve due to SNR are given (approximately) by $1/\text{SNR}$; so when each image exhibits $\text{SNR} = 500$ the level of fluctuations per exposure will be 2 mmag. It is therefore important for exoplanet observing to choose an exposure time that produces counts whose maximum value is just below saturation for the entire observing session. For a typical CCD the saturation level may be $\sim 40,000$ counts. If a nearby star is to be used for reference it also must be kept below this level. During the observing session focus changes will change the size of star images on the CCD; the so-called point-spread-function will undergo changes in FWHM as focus changes. This, in turn, will change the maximum counts for a star (C_x) during an observing session. C_x will be proportional to $1/\text{FWHM}^2$, so as the star field approaches its highest elevation, where seeing is best (FWHM is smallest), C_x is likely to be at greatest risk of saturating. Some observers will intentionally de-focus when seeing improves so much that saturation might occur. This is OK for bright stars ($< 11^{\text{th}}$ mag for a 14-inch), but for faint stars the loss of SNR due to a broader FWHM is undesirable. Careful attention has to be paid to choosing an exposure time at the beginning of an observing session that does not produce saturation when seeing is best. These considerations do not apply to variable star observing when a measurement sequence might last only a few minutes.

4) SNR: Image Scale

High precision can be lost if the fraction of photons falling close to CCD pixel edges is high. This means that you don't want FWHM to be small in terms of pixels. The rule-of-thumb is that FWHM should exceed ~ 2.5 pixels in order to maintain high precision (~ 2 mmag). This has implications for image scale (also referred to as "plate scale" by old-timers), defined as "seconds of arc per pixel." If your seeing is typically $\text{FWHM} \sim 3''$, for example, image scale should be no greater than $\sim 1.2''/\text{px}$. If it's larger, don't count on high precision. If it's smaller, don't count on the best SNR. The reason smaller image scales have lower SNR is related to the noisiness of CCD pixels, treated next. Only exoplanet observers worry about these things.

5) SNR: CCD Cooling and Photometry Aperture Sizes

Each pixel reading will exhibit a "noisiness" that is the sum of three components: dark current (thermal agitation of molecules and movement of electrons in the electronics), sky background brightness (e.g., moonlight) and read-out noise. When a bright star contributes to the counts at a pixel

CHAPTER 21 – EXOPLANETS NOT VARIABLE STARS

location there's an additional component of noise that becomes important: Poisson noise, an uncertainty that is proportional to the square-root of the total counts. To minimize dark current it's important to cool the CCD. The professionals use liquid nitrogen (~80 K), but we amateurs must be content with the smaller amount of cooling produced by a thermoelectric cooler (TEC). To minimize sky background noise it is important to use as small a signal aperture size as possible while using a large sky background annulus. Choosing the best aperture sizes (signal radius, gap width and background annulus width) is a big subject (treated in Chapter 13). However, I will state that noisiness problems are reduced by maintaining good focus because this provides flexibility in choosing small photometry signal apertures for the purpose of maximizing SNR. The effect of read-out noise is reduced by using long exposures, with as few readouts per observing session as possible. Clearly, lots of issues have to be considered in choosing an optimum observing strategy and an optimum image measuring strategy for exoplanet observing. Few of these issues concern the AAVSO variable star observer since their goal of ~ 0.03 magnitude accuracy is much larger than the exoplanet observer's goal of 0.002 magnitude precision.

6) Auto-Guiding and Polar Axis Alignment

For AAVSO variable star observing it's not important to autoguide or have a perfect polar axis alignment, but for exoplanet observing this is important.

Let's first consider the demands of exoplanet observing. If the star field can be kept fixed to the pixel field during a long observing session there should be no temporal trends or variations in an exoplanet's light curve due to an imperfect flat field. Indeed, it would not be necessary to even apply a flat field calibration if the star field could be kept perfectly positioned. Autoguiding may keep the autoguider star at the same location on the autoguider chip, but unless the polar axis alignment is perfect image rotation will cause the star field to move across the pixel field. This motion will be greatest at declinations near a celestial pole, and will be greatest on that part of the main chip that is physically farthest from the autoguider chip. It is difficult to achieve flat fields that are more accurate than ~0.025 magnitude across most of the FOV, and for small pixel movements the imperfect flat field calibration may produce variations in flux, compared to other locations, that amount to a few mmag. By plotting magnitude/magnitude scatter diagrams of star pairs during an observing session it is possible to evaluate how large these variations are.

When variations of a few mmag are unimportant, as with AAVSO type observing of variable stars, it won't matter that the image rotates, and it won't matter where the stars are positioned on the CCD. This is because flat field calibration can be achieved at the 0.05 magnitude accuracy level with little effort. Furthermore, if several reference stars are used their flat field errors will "average out" somewhat. Therefore, polar axis alignment is not something variable star observers have to worry about.

7) Aperture Photometry

Setting the photometry apertures properly for exoplanet images is an important part of achieving stability during an observing session. There are three aperture values to be chosen: signal aperture radius, gap annulus width and sky background annulus width. The most important of these is the first one, which I'll refer to as R. The value of R in relation to FWHM determines the fraction of flux captured by the signal aperture in relation to the total flux from the star that's registered by the CCD. The "missing flux" can be expressed as a "flux correction" that should be applied if all photons are to

CHAPTER 21 – EXOPLANETS NOT VARIABLE STARS

be accounted for. The following graph is a plot of "required correction" versus the ratio R/FWHM for a typical image.

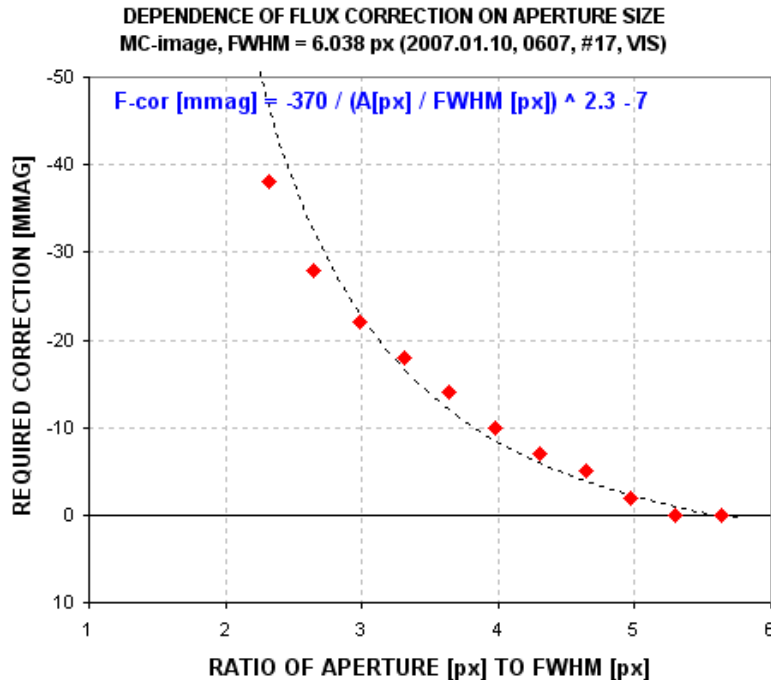


Figure 21.01. Typical relationship between aperture size and missing flux (flux that's not captured by the signal aperture).

If R is small the "flux capture fraction" is small, which requires a large "correction." For example, in the above graph if $R = 3 \times \text{FWHM}$ the measured flux should be increased by ~ 22 mmag. As seeing varies while R remains fixed this correction will vary. For a telescope with imperfect optics (that includes all telescopes), the size of the point-spread-function, PSF, will vary across the image. The details of this variation will change with focus setting. Therefore, a too small R will produce flux capture fractions that differ across the image, that change during an observing session. If R is set too large SNR suffers. A large R also increases the likelihood that the signal aperture will contain defects, such as cosmic ray hits or hot and cold pixels due to an imperfect dark frame calibration, or possibly a faint background star. A large R also increases the chances that a nearby star will swell in size during bad seeing episodes and contribute some of its flux to the target star's signal aperture. I've seen this last effect cause trends of several mmag. One solution is to employ a "dynamic aperture" such that the image measuring program takes a measure of FWHM for each image and then sets R to whatever multiple of FWHM the user specifies (such as $R = 2.7 \times \text{FWHM}$). Unfortunately, MaxIm DL does not provide this feature yet, and I can't afford to pay them to develop it. (I sometimes perform a "poor man's dynamic aperture" by repeating the readings using a range of R values then later combining them to match FWHM versus time.)

For AAVSO observations it won't matter if they're affected by a few mmag of systematic errors. Therefore, if the variable star goal is an accuracy of 0.03 magnitude, for example, aperture choices are not very important. Simply adopting $R = 3 \times \text{FWHM}$, assuming that all stars suffer the same

CHAPTER 21 – EXOPLANETS NOT VARIABLE STARS

"missing flux fraction" (corresponding to ~ 20 mmag), would be acceptable. For exoplanet observers this would not be acceptable!

Precision Versus Accuracy

Precision is the consistency of measurements, regardless of any calibration error shared by all of them. Accuracy consists of two components: precision and calibration uncertainties. Since these two components are uncorrelated (the sign and size of one is unrelated to the sign and size of the other), the two components are added orthogonally. This means the accuracy uncertainty, $SE_a = \text{SQRT}(SE_p^2 + SE_c^2)$, where SE_p is precision (also called stochastic uncertainty) and SE_c is calibration uncertainty. SE_c is almost always subjectively estimated.

For AAVSO photometry a worthy goal is an accuracy of ~ 0.03 magnitude (although 0.02 and slightly lower are possible from ground-based observations if careful procedures are followed). For exoplanet observing, on the other hand, it is acceptable that a set of observations have an accuracy SE of 0.1 magnitude, or 1 magnitude or even 10 magnitudes! It's totally irrelevant how accurate an exoplanet light curve is. Only precision matters. For AAVSO variable star observing accuracy is everything, and accuracy $SE > 0.1$ magnitude is almost never acceptable. In order to achieve an accuracy of 0.05 magnitude, for example, it is adequate for precision to be $< \sim 0.02$ magnitude (SNR ~ 50). This level of imprecision is useless for ALL exoplanet work. No wonder the two tasks require different strategies for observing and image analysis.

For the many reasons listed above variable star observing and exoplanet observing require different observing strategies, different image measuring strategies and different spreadsheet data processing strategies. Experience in one realm does not necessarily mean that competence in the other is assured. New tricks, and new ways of thinking, must be learned by anyone switching from one observing task to the other.

Chapter 22

Archiving Amateur Data and Searching for Anomalies

Archiving Amateur Data

In 2006 *Sky & Telescope* published an article about the XO Project's professional/amateur collaboration that was leading to exoplanet discoveries. Since my picture was in the article I began to receive e-mails from amateurs with their light curves and a question of whether their data could be useful. Some of the light curves sent to me were pretty good, even better than most of those produced by the XO extended team of amateurs. The most impressive of these was from Portuguese amateur Joao Gregorio, in 2006. Most of the amateur exoplanet transit light curves that were sent to me were also found on their personal web pages devoted to more than just exoplanet observations. Because exoplanet transit light curves were distributed on dozens of individual observer web pages there was little chance that professionals looking for such data would find all of them. It was apparent to me that they should be collected and archived on a "one-stop shopping" web site. In addition to creating a convenient place for professionals to search for what amateur data might exist for a favorite exoplanet, such an archive would assure that potentially valuable data was not lost to posterity. Thus was born the idea of creating what later became the Amateur Exoplanet Archive, AXA.

The idea for AXA had to "incubate" for an entire year before I acted. Continued good light curves sent to me by Joao Gregorio, and others, finally moved me to action. The AXA home page was created 2007.08.07, with links to pages devoted to each exoplanet where a small collection of light curves could be found. I invited amateurs to send their data files to me so that I could fit a transit model to the data and post the light curve in a standard format at the appropriate AXA web page.

As more amateurs began submitting data I could see that the AXA might grow too large for an individual to maintain if data files are processed and posted on a web page manually. I tried to interest the AAVSO to take over the AXA, but their budget couldn't accommodate the cost of the programming task for automating the processing and posting process. I tried to interest many agencies (NASA, NSF, Ames, JPL, etc) but there was no interest in the project. Finally, Caltech agreed to incorporate the AXA database in their NStED archive, and to add software on the IPAC computer to accept amateur data file submissions that would be processed and added to NStED using an auto-fit program that I had started to write. My role in this collaboration was to complete the auto-fit program so that Caltech could translate it to C programming language so it could run on the IPAC computer, which would then assume responsibility for accepting and processing amateur data. This plan was appealing because professional astronomers were beginning to submit their exoplanet transit data to the NStED for exchange with other professionals, and to the extent that amateur data might also be useful there was merit in having access to it on the same computer and in the same data format.

Alas, the best plans sometimes fail to reach completion, and because of budget and staff limitations at Caltech my auto-fit program will not be installed on the IPAC computer, and plans for NStED to accept and process amateur data have been abandoned.

CHAPTER 22 – ANOMALIES

I've given this background to explain why the AXA will expire on 2009.12.31. After more than two years of accepting and archiving amateur data files to preserve them for posterity the AXA will cease to accept new data files, and the plan for Caltech to assume this task will not proceed.

Fortunately, the Czech Republic's Astronomical Society has created an archive for amateur data submissions, called the Exoplanet Transit Database (ETD). It includes a table of submitted data, with data file download capability, and it includes plots of most of the transit properties that were present on the AXA. All of the data that has been submitted to the AXA has been duplicated on ETD. I therefore encourage amateurs to begin using ETD instead of AXA for data archiving and light curve display. The URL for ETD is: <http://var2.astro.cz/ETD/>

Every amateur who submits transit light curve data to an archive is contributing an increment of information that can be used to advance the understanding of exoplanets and distant solar systems. Professional astronomers and amateurs may study data in the archive in pursuit of discoveries such as those listed below.

Timing Anomalies and Discovering New Exoplanets

A transiting hot Jupiter exoplanet in a circular orbit with no other planets in the system will produce transits at uniformly spaced intervals. If the hot Jupiter is in an elliptical orbit the transits will shift steadily in time due to precession of the orbit's periastron (location of closest approach to the star). In that case the transits may also change shape, or entirely disappear (though unlikely in a lifetime), and these changes might be detectable on time scales of a few years.

A more interesting possibility is for the hot Jupiter to exhibit anomalies that change over the course of a few months due to another planet in an orbit close to that of the hot Jupiter (Algol *et al*, 2005; Holman and Murray, 2005, Steffen, 2006). The greatest effects will be produced when the orbit periods are resonant. For example, if an Earth-like planet is in a 2:1 period resonance with the hot Jupiter, it can cause the hot Jupiter to shift its orbital position in ways that cause transits to alternate between coming early or late with a periodicity on the order of a year. The amplitude of these "timing anomalies" can be as high as 3 minutes (Steffen, 2006).

This is perhaps the most exciting aspect of amateur participation in exoplanet transit observing. Ground-based professional telescopes are too expensive, on a per minute basis, for such long term monitoring. Space-based telescopes devoted to such a project could do a good job with this, but so far the ones in orbit, or in planning, are designed for specific tasks that render them unsuitable, or unable, to conduct the required follow-up observations of all transiting exoplanets. For example, the Kepler Mission telescope will stare at the same star field (Lyra/Cyngus) for 4 to 6 years. It will therefore not be used to search for Earth-sized planets in most of the known transiting exoplanet systems. Only HAT-P-7 is within the FOV of Kepler, and it has already detected a 0.13 mmag secondary transit, or occultation of the hot Jupiter HAT-P-7b by the star HAT-P-7a. Kepler can't observe the other 45 bright transiting exoplanets, so this is a job for ground-based monitoring, or future space-based telescopes. I hope amateurs will contribute to detections of transit timing variability studies.

Any transit observation submitted to an archive for possible use in the study of mid-transit timings should be made with careful attention to accurate image time-tags. This means the computer that records images should use a program that automatically synchronizes the computer's clock with a

CHAPTER 22 – ANOMALIES

time standard. I use AtomTimePro, which I've set for updates every 3 hours. The user should also pay attention to the “meaning” of image time tags. For example, MaxIm DL records start times in the FITS header, but when it performs photometry the CSV-file has a JD value corresponding to the mid-exposure time.

Amateur timings are likely to exhibit uncertainties of 1 or 2 minutes for each transit's mid-transit time. This is based on my analysis of XO-1 amateur timing measurements. Averaging of many timing measurements will reduce this uncertainty, but lots of averaging is required to reach the desired level of much less than 30 seconds.

The next graph is a plot of 79 XO-1 transit timings by mostly amateurs during the period 2004 to 2009. There appears to be a sinusoidal variation in the timing of mid-transits. The peak-to-peak amplitude of the variation is 1.96 K, and the periodicity is 350 days. Most observations are clustered near “opposition” at yearly intervals, so a one-year periodicity is difficult to confirm. If this periodic variation in mid-transit timings is confirmed it would constitute evidence that another exoplanet is in orbit with XO-1b with a resonant period, such as 2:1 or 3:2. The mass of such a hypothetical planet could be as small as few Earth masses.

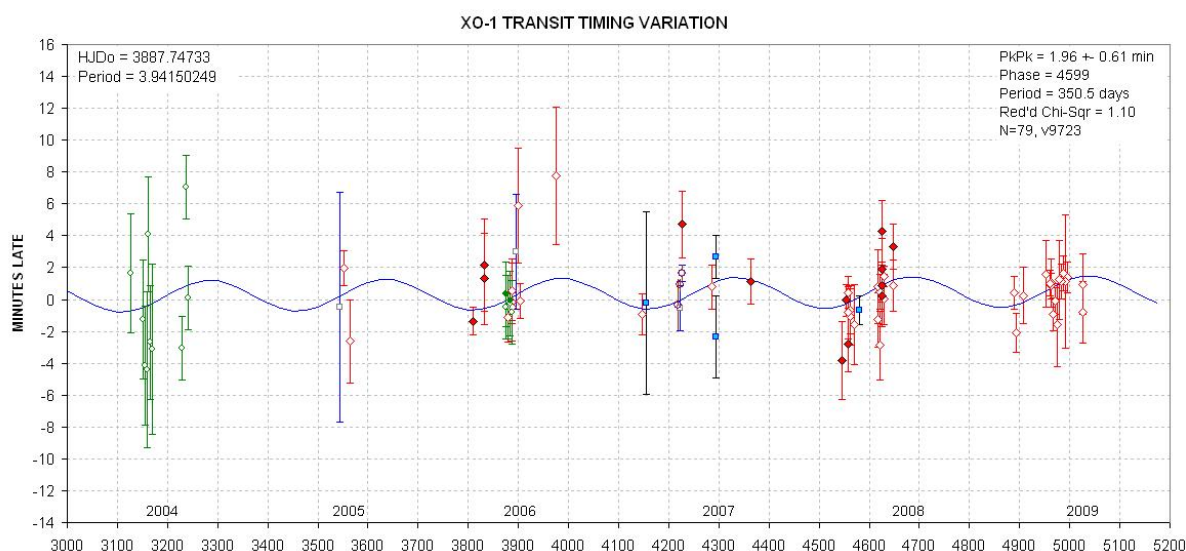


Figure 17.01. *Transit timings for XO-1.*

Subsequent observations may reveal that apparent sinusoidal variation in transit timing is not real, or possibly a subtle artifact of seasonal systematics that produce artifacts with a one-year period. The case of XO-1 in this figure should therefore be viewed as just an example of what amateurs are capable of doing in a search for timing anomalies. As more amateurs join the ranks of exoplanet transit observers there will be a greater density of data in the archive of timings to work with for this and the other exoplanets.

Light Curve Shape Anomalies

Jupiter and Saturn both have rings and moons, so it is reasonable to wonder if hot Jupiter exoplanets also have them. Specifically, can amateurs detect their presence from high quality light curves?

CHAPTER 22 – ANOMALIES

Shortly after TrES-1 was announced (in 2004) a group of amateurs observed transits of this exoplanet and shared their light curves. I saw evidence of a brightening right before ingress and possibly right after egress in several of these light curves. Joe Garlitz, an amateur in Oregon, also noticed this unusual feature. Someone called my attention to studies by Barnes and Fortney (2003) who had investigated the possibility of detecting the presence of rings around giant exoplanets by searching for light curve brightening just outside transit that would be produced by forward scattering of star light. Ron Bissinger performed a detailed analysis of light curve observations (mostly amateur) and concluded that the brightening features were statistically significant but required confirmation (Bissinger, 2005). The Hubble Space Telescope later failed to confirm these brightenings. Nevertheless, each new transiting exoplanet discovery represents another possibility for detecting exoplanet rings.

Another light curve anomaly to look for is an extra loss of brightness just before ingress, or just after egress, caused by a large moon of the exoplanet responsible for the main transit event. Searches have so far failed to detect the expected feature of an exoplanet moon, but the value of such a discovery means that every new exoplanet discovered should be studied with this feature in mind.

Rings and Moons

Rings and moons will produce brightening and fading anomalies that are much smaller than the main transit event's mid-transit depth. The Hubble Space Telescope is ideal for this task. However, HST will eventually degrade and become unusable, and this may happen before the James Webb Space Telescope begins operation (in 2014?). Amateurs wishing to beat the big space-based telescopes in detecting rings or moons should consider performing a median combine of many ingress and egress observations. Rings are likely to be present for both ingress and egress, so folding of egress to match the shape of ingress is permissible. If moons of an exoplanet are in a resonant orbit their distortion of the light curve would probably repeat for each transit, in which case folding many light curves and median combining would be one strategy for searching for the moon's signature.

If, however, the moon is in a much shorter orbit around the exoplanet than the exoplanet's orbit around the star, a totally different strategy can be employed. Folding of mid-transit times about a large number of hypothetical timing distortion intervals, shorter than the exoplanet's orbital period, might reveal a statistically significant pattern corresponding to the moon's orbital period. This can only be done when a large number of accurate mid-transit timings are available.

Starspots

Small amplitude anomalies within a transit will exist if the surface brightness of the star being transited is uneven. "Starspots" (analogous to sunspots) must be common, and if the starspot is comparable in size to the exoplanet, then a central crossing of the starspot should produce a large increase in brightness, to almost the out-of-transit (OOT) brightness level. Amateur light curves tend to exhibit variations, both during the transit and during the OOT parts, and these must be produced by observing systematics. A likely way for these unwanted variations to be produced is for the star field to drift through the CCD pixel field, combined with an imperfect flat field. Any apparent starspot feature will not have credibility unless at least another observer sees the same feature. Observer teams may some day coordinate observations of the same transit for this purpose.

CHAPTER 22 – ANOMALIES

OOT Observing

Don't forget that it is always worth observing a transiting exoplanet between transits in a search for anomalous fades caused by another exoplanet in the same star system. The length of such a fade event could be shorter than the main transit length (if the new planet is in an inner orbit) or longer (if in an outer orbit). On a beautiful observing night when no bright transiting exoplanets are predicted to undergo transit, consider observing an exoplanet in a favorable sky location just on the chance that you might be lucky and discover a smaller second exoplanet.

Other subtle anomalies of exoplanet light curves may become important as theoreticians and observationalists continue the study of this new field. Every observer should therefore be prepared to accept as “real” an observational anomaly that is not readily explained. Part of the excitement of exoplanet observing is that this is a young field that may produce future surprises not yet imagined.

Since amateurs have a unique opportunity to contribute to timing studies of known exoplanets, and thereby contribute to the discovery of Earth-mass exoplanets, there is a growing need for more advanced exoplanet observers as more exoplanets are discovered. It will be important for these amateurs to coordinate their observations, and to contribute them to a standard format archive.

I claim that attention should be paid to what constitutes an “optimum observatory” for exoplanet observing. This is a topic for the next chapter.

Chapter 23

Optimum Observatory

Dreaming! Every amateur dreams about upgrades to their backyard observatory.

Whenever someone asks for a recommendation of what telescope to buy, I have to first ask “What do you want to do with it?” For “pretty pictures” of a specific category of objects the answer would be one kind of telescope and camera (about which I would be clueless, since I’m no good at that). But for exoplanet transit light curves, I could give a pretty specific answer. That’s what this chapter is about.

Some of the following paragraphs (presented in smaller font) are taken from a “white paper” I submitted to the NASA/NSF “Exoplanet Task Force” (ExoPTF) in March, 2007. My white paper argued for government sponsorship of a network of amateur observatories for coordinated monitoring of known transiting exoplanets for the purpose of discovering Earth-sized exoplanets. Part of the case I presented was that the optimum observatory for this task is only slightly more expensive than existing amateur budgets, yet sufficiently more expensive for those few amateurs who are capable of participating in such a search that financial help is needed. (If you interpret this to be a shameless, self-serving attempt to upgrade my observatory by responding to a future “request for proposal” by NASA, you would be correct!)

Here is the argument I presented to the ExoPTF in which I derived that the optimum observatory would consist of a 20 to 30-inch aperture telescope as part of an observatory costing ~\$75,000. (I now realize that the aperture range should be 20 to 40 inches).

Precision photometry (i.e., 1-minute precision of ~2 mmag) has many requirements: 1) the plate scale should assure that a star’s full-width at half-maximum (FWHM) be at least 3 pixels. For CCD cameras using chips having 9 micron pixels, and for sites with FWHM ~ 2.5 “arc, this means the plate scale should be ~0.7 “arc/pixel. If the plate scale is smaller too many pixels are within the photometry aperture circle, leading to SNR degradation. 2) An aperture should be large enough that Poisson noise and scintillation noise are small. 3) The focal length should be short enough that the FOV is likely to contain same-color stars for use as reference; this requirement translates to FOV larger than ~12 x 18 ‘arc. 4) The telescope should be in a mount that does not require meridian flips. 5) Image quality must be the same for the entire FOV; in other words, focal reducers cannot be used. 6) There should be minimal degradation of image sharpness due to winds vibrating the telescope; this translates to either the use of an open tube or a closed tube inside a dome.

The optimum effective focal length (EFL) is ~100 inches when 9 micron pixel dimensions are used and FWHM seeing of ~2.5 “arc is to be accommodated. A 30-inch telescope would have to have an f-ratio of 3.3 to achieve this EFL without using a focal reducer lens. When f-ratio becomes small, maintaining optical collimation becomes more difficult. This is one reason larger apertures are undesirable. A 40-inch aperture with f-ratio = 5 will have EFL = 200 inches, a plate scale of 0.35 “arc/pixel and a FOV =17 x 11 ‘arc when a large format CCD is used (35 mm longest dimension). The plate scale is acceptable since the noise penalty of having to use 4 times as many pixels in the signal aperture for a 2.5 “arc FWHM star will be compensated by the larger aperture collecting area. Any larger aperture, however, will reduce the FOV, which will begin to limit the number of stars

CHAPTER 23 – OPTIMUM OBSERVATORY

available for use as reference. Thus, a 40-inch aperture is an approximate upper limit for the range of apertures that are optimum for exoplanet light curve measurements. (XO-2 is a special case, because an identical star is located 31 “arc away.)

To illustrate some considerations in selecting an “exoplanet optimum” telescope system, consider the following specific components. The 20-inch Meade RCX 400 has a tube made with low-thermal expansion material, which would reduce the need for focus adjustments. The optical design is a modified version of Ritchey-Chrétien, and produces sharp images for a large FOV. It has an f-ratio of 8, so the EFL is 160 inches, yielding a plate scale of 0.46 “arc/pixel. The FOV with a large format CCD chip would be 20x30 ‘arc. The German equatorial mount that it normally comes with is unacceptable for exoplanet observing. The Optical Tube Assembly (OTA) alone would cost ~\$20k and a quality fork mount purchased separately would cost ~\$25k. Integrating the OTA to the fork mount might cost another \$5k. Since the RCX telescope is a closed-tube OTA a dome would be needed to protect it from wind vibrations. This will add another ~\$15k for an automated dome. A large format CCD would cost ~\$10k. SBIG’s AO-L tip/tilt image stabilizer costs \$2k. Buried cables for controlling the telescope, CCD and dome, plus a computer system with control software would cost ~\$3k. The total cost for this system is ~\$80k.

Other options are possible. A ScopeCraft 24-inch, f/3.1, open tube telescope with a roller-driven horseshoe mount would cost ~\$45k. A dome would not be needed for such a telescope, but a sliding roof observatory would be, costing ~\$10k. The same CCD camera and other items would be needed, so the total cost would be about the same, or ~\$70k.

Most hot Jupiter exoplanet transits last ~3 hours. Because of the need for verifying that reference star color is not affecting the transit shape, depth and mid-transit timing (in a manner that is correlated with air mass), it is important to start observations at least 1.5 hours before ingress and continue until at least 1.5 hours after egress. Thus, 6-hour observing sessions are common, and 8-hour sessions are even better. Observations for more than one observing site are sometimes needed, provided the sites span a sufficient longitude. When observations from two or more observatories are to be combined to produce one light curve, it is helpful that they be identical systems. Systematic effects can be minimized when using the same image scale (same blending of interfering stars), same FOV (allowing for use of the same reference stars) and the same image quality (use of the same photometry apertures).

From there in the white paper I went on to argue that a network of these optimum observatories should be constructed at sites spanning a wide longitude range to assure that each transit would be observed in its entirety. It is clear that such an amateur project would be cheaper than any space-based telescope mission, or any network of professional ground-based observatories.

I envision a network of 6 identical telescopes deployed in the backyards of amateur exoplanet observers who have a demonstrated history of quality observing and dedication to the task. A range of longitudes would be needed to provide coverage of entire transits. The observatories should consist of pairs, with a pair at each of three longitudes. Pair members should be at sufficient distance from each other to reduce the chances that bad weather at one location is correlated with bad weather at the other location. A more important reason for situating identical observatories in same longitude pairs is to provide redundant observations that could support each other when a real LC anomalous feature occurs. This is similar to the principle aspired to by SETI projects in which two telescopes observe the same candidate stars in coordination; if an unusual signal is detected by one telescope the other

CHAPTER 23 – OPTIMUM OBSERVATORY

one, located sufficiently far away to not be affected by the same local interferences, can provide corroboration (not yet implemented).

A network of advanced amateur observatories optimized for exoplanet transit observing should have the guidance of a professional astronomer. He will know other professionals to contact when unexpected observed behaviors are encountered. Once the initial construction costs have been borne the part-time professional would probably constitute the major cost for continued operation of the exoplanet observing network.

In the First Edition of this book I wrote: *At the present time there is no “universal archive” for exoplanet timings or light curve measurements. Each group of observers maintains their own archive, but these groups do not share because of an understandable desire to announce discoveries and continue to be funded by their sponsoring agency. However, a greater good will eventually be served by creating a global archive, fashioned along the lines of the AAVSO (American Association of Variable Star Observers). Even non-members of the AAVSO can submit observations to their immense archive of star brightness observations, and submit queries for what’s in the archive for a specific star for a specific date interval.* Since writing that I created the Amateur Exoplanet Archive (AXA), and the Czech Republic’s Astronomical Society created the Exoplanet Transit Database (ETD). The AXA will cease operation 2009.12.31, so the ETD will become the default archive for amateur observations. The ETD is a suitable solution for the archiving needs of any future 6-element network of identical exoplanet observatories.

I believe this is a good time for either government or institutional funding to create such a professional/amateur partnership. It is alleged that persuading the funding of a large project is easier than a small one, even when both have merit proportional to the funding request. I have slowly become a believer in this. I’ve secured funding for quarter-million dollar projects before retirement, yet I can’t persuade NASA to fund a network of six \$80k telescopes, or even the prototype for the network. I invite someone younger than myself, with an abundance of energy and optimism, to pick-up the “torch” and try to advance this worthy project.

The second decade of the 21st Century promises to be one of the most exciting periods in the history of astronomy, especially for exoplanet research. Let’s give amateurs a worthy and cost-effective role for this exciting journey.

Chapter 24

The Joy of Exoplanet Observing

I would like to end this little book by trying to convey “the joy of exoplanet observing.” Sometimes I ask myself why I keep doing it. On many occasions during the past 7 years that I’ve been observing exoplanet transits I’ve put a lock on my sliding roof observatory with the best of intentions to achieve “balance in my life.” But on just as many occasions, on some clear and calm night, when no one could see me, I’d go out and unlock the observatory and quietly get the telescope to work on one of those irresistible, far off planetary solar systems. The next morning I would look forward to seeing that tiny fade that proved a planet was there. How astounding this is! With my simple telescope and CCD camera I could see that a far-off planet was producing something I could see in a plot! The transit feature shouldn’t have surprised me, for everyone knew when the transit would occur and how deep it would be. But seeing it from my little telescope simply made it more real!

When the opportunity for actually contributing to the “discovery” of an exoplanet came along, with an invitation by Peter McCullough to join his XO Project’s “extended team” of amateurs, my acceptance was immediate. My thoughts turned to college, when I worked for a radio astronomer at the University of Michigan’s Astronomy Department, and I was given the assignment to create star maps from the vantage of nearby stars to see how well an alien might transmit their location. There were dreams of starting a SETI project at the university’s radio observatory. These experiences started me dreaming about life in the universe, and asking the question that was being quietly asked by astronomers in hallways: “Are we alone?”

Maybe 3 years later, while working as a radio astronomer, I obtained observing time on the Howard Tatum Radio Telescope at the National Radio Astronomy Observatory in Greenbank, West Virginia. I arrived a day before my scheduled observing time, and was given a tour of the facility by Frank Drake, who pointed out some ordinary-looking electronics in a rack that he said was being used for something called Project Ozma. I don’t think I had heard of this project before seeing where it was conducted, but this connection to a facility I was privileged to use recalled dreams of being part of a SETI project.

Then a few years later, while working at JPL and heading a small radio astronomy group, I held “goals meetings” to chart a path that took advantage of the large spacecraft tracking antennas at the Deep Space Network, such as at Goldstone Tracking Station in Southern California. I included a SETI project as a long-term goal, with hopes that some day we could be funded to build a suitable receiver to connect to the 64-meter antenna to search for those intelligent aliens, broadcasting their presence at the first harmonic of the famous 1420 GHz hydrogen line. My career took a turn to the atmospheric sciences, but the the radio astronomy group started a SETI project – which was later shut down because a U.S. Senator mocked NASA for engaging in such a foolish waste of taxpayer money.

A radio astronomer associate that I worked with at JPL, Tom McDonough, later became a coordinator of The Planetary Society’s SETI projects. I eagerly questioned him about what was being done, and how the various SETI projects were faring. In retrospect I must have envied anyone working on

CHAPTER 24 - JOY OF EXOPLANET OBSERVING

SETI, and since I had come tangentially close to SETI so many times, it was almost heartbreaking to not be a part of this exciting endeavor.

So when Peter McCullough invited me to help discover planets orbiting other stars, how could I refuse!

I have probably observed more exoplanet transits, and exoplanet candidate transits (including the “no shows”), than anyone. There are times when I exclaim “what a waste of time” – yet I keep returning. Partly, I suppose, it’s the feeling of getting a system of hardware and software humming along, doing what I want, which gives me permission to turn on a classical music station and pour a drink. I like spot checking to see how automatic systems are performing, and thinking about how procedures might be improved, or how observing strategies might be optimized. I’d check the clock, and exclaim “ingress should be occurring now” or “we’re at mid-transit,” and I’d think of what was occurring by imagining the sketch on the cover of this book. As the observing session ended I would look forward to processing the images the next morning to see if these things were true. On a few occasions I’d wonder “Could there be intelligent creatures in that solar system? Right there, on my CCD?”

Observer Joao Gregorio, the amateur in Portugal who inspired me to start the AXA, would pack a borrowed telescope in his trunk, prepare his favorite “observing soup” and head for the countryside where he would stay up most of the night to catch a transit. His observing hardships were probably among the greatest of those contributing to the AXA, yet I’m sure he enjoyed it.

Each person must respond to different aspects of exoplanet observing that makes it a joyous experience. I’d like to end by reproducing an e-mail that one of my faithful colleagues wrote to someone who asked why she was devoted to exoplanet observing. Her e-mail was forwarded to me with her permission, and later she gave her permission for me to include it in this book. It captures as much as possible the indescribable appeal of exoplanet observing, and I think she consented to my use of it because we both know the magic of this wonderful hobby and we both feel like sharing it with those who have yet to discover it.

Hi Jim,

I wish what I am going to write was profound and motivating to others, but the simple truth is that what motivated me to begin exoplanet hunting in the first place was, I heard a talk given by a guy from NASA Ames that said amateurs could find planets around other stars outside of our solar system. I remember poking my husband in the ribs and saying, "That's the coolest thing I've ever heard of, I want to do that". I got one of those looks that implied "whatever" that you get from a spouse that has just heard something that he/she probably thinks is just a passing moment. I knew nothing about photometry or even how to run a telescope for that matter, but I was pretty sure I could learn and that was all that I needed to know. I left that meeting, the end of May, with a 14" telescope in the back of my motor home. I built an observatory that summer and had it finished in early August. I worked for an entire year trying to catch the elusive transit that was implied could be done. Just about the time I thought it wasn't really going to happen for me, I observed the egress of HD 209458b. In hind sight, knowing what I've learned, it wasn't a very good observation. During that year I practiced on cataclysmic variables for the Center of Backyard Astrophysics, a group that my husband Jerry is very active in. He worked with me every night possible and taught me how to run the telescope, how to use reduction software, and how to know if I had good or bad data. I practiced and practiced until I could do it without him standing by for every move. It was tedious and annoying, and disappointing at every turn.

CHAPTER 24 - JOY OF EXOPLANET OBSERVING

May of 2006, I went to SAS (Society for Astronomical Science) with Jerry. He's on the Board of Trustees for the meeting. I sat in on the proceedings, most of which was way over my head, but was diligent, nonetheless. The great part about this portion of my story is that I met a fellow CBAer, Tonny Vanmunster who had just announced his part in the co-discovery of XO-1b. I obnoxiously glued myself to his side for much of the rest of the meeting and listened to everything he had to say. At the end of the SAS meeting he was talking about XO-1 and was talking about the variability at egress that they had yet to figure out. I asked if I could get the coordinates to try and capture it myself. He agreed and asked that I try and image in V and R. I left SAS so excited and I couldn't believe my luck. When I got home, the weather was lousy, but we caught a break and I was able to observe XO-1b, I would guess early June. I turned the data into Tonny to look at, he liked what he saw, asked if he could send it to a colleague, Bruce Gary, who in turn decided that it was pretty good for a "beginner", who then asked if my data could be sent to Peter. About six weeks later, Peter invited me to join the XO Project. I've been working for the Project ever since.

I mentioned to Bruce just today that I never tire of the anticipation waiting for the light curve to appear. This morning didn't disappoint from last night's run and what Bruce and I have talked about is that "stupid smile" that you get when you see what is potentially a planet out there waiting for Peter and the rest to confirm. It's a terrific feeling and not one that I'm sure I can describe.

So with all of the above written, I don't know what motivates me other than the original "that is the coolest thing I've ever heard of, I want to do that" and to actually have the opportunity to participate in a project like the XO Project with Peter and the rest of the team. I don't have the scientific background that most in the amateur photometry world have, but I do learn quickly. I have learned more than I can tell you in the last three + years and will probably never catch up to my fellow amateurs. What I have going for me is a husband who also does photometry, a great friend and mentor, Bruce Gary, and a professional team lead by Peter, that recognizes that someone like me, willing to do the work, can actually gather really good, useful data. THAT, is probably what motivates me. I can do it and it's been useful for a professional organization and I've been able to participate in the co-discovery of 4 of the 5 XO planets. It's an awesome feeling and I'm very proud of the work we've done.

Thanks for asking.

Cindy

As this e-mail conveys, Cindy Foote posed the question that is the title for the first chapter of this book, "Can I Do That?" and she unhesitatingly answered it with uncommon devotion.

Many things are possible with the proper motivation. May I leave you with the thought that it is your turn, dear reader, to decide how to answer the same call?

APPENDIX A – Evaluating Flat Field Quality

Chapter 8 described a way to create a master flat field. This appendix describes ways to evaluate the quality of a flat field. Recall the two sets of flat fields shown in Chapter 8 made with different optical configurations, repeated here.

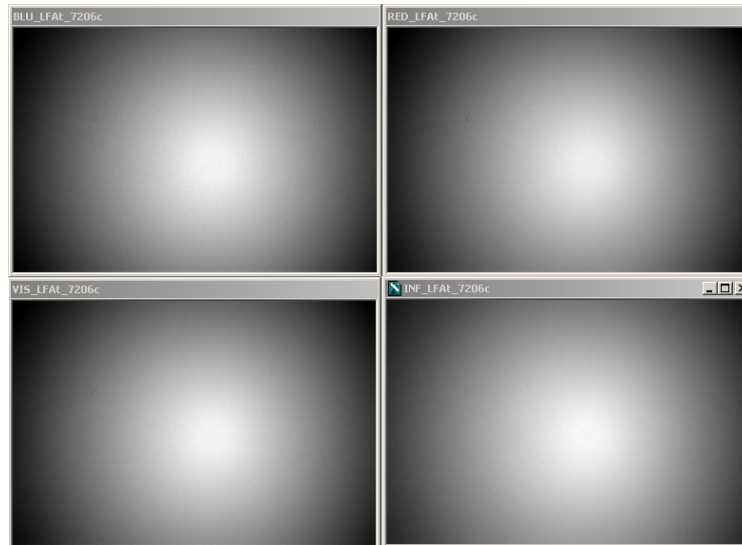


Figure A.01 Flats for B, V, R_c and I_c filters for a configuration with a focal reducer lens placed far from the CCD chip. The edge responses are ~63% of the center.

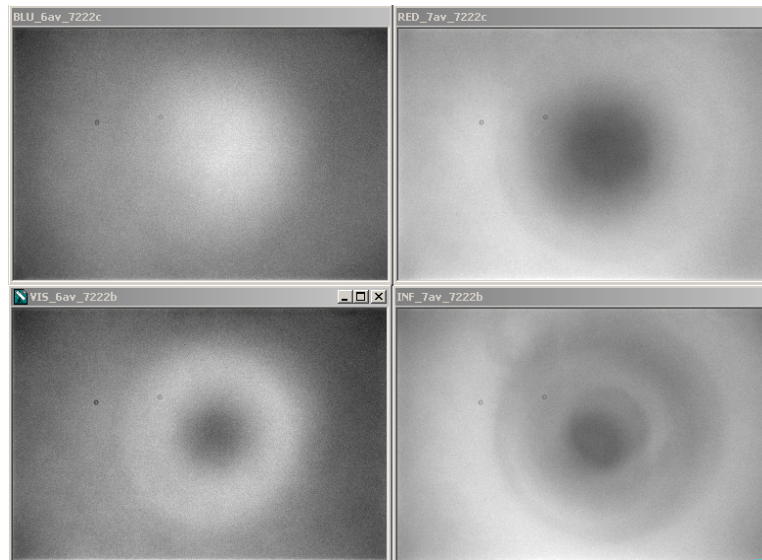


Figure A.02 Flats using the same filters but with a configuration using the same focal reducer close to the CCD chip. The response ranges, smallest response to maximum, are 88, 90, 89 and 89% for the B, V, R_c and I_c filters.

APPENDIX A – EVALUATING FLAT FIELDS

The first set of flats is relatively featureless aside from the overall pattern of a fall off toward the edges, which resembles classical vignetting. The second set shows more structure, including two dust donuts. Before we condemn the second set of flats as a bad configuration for transit systematics recall that what matters is the change of “flat field **error**” versus pixel location. There’s no straight-forward way of knowing “flat field error” versus FOV location for a given filter and a specified star color. In fact, each star must have an appropriate flat field for its color. For observations with a V-band filter what will a red star’s optimum flat field look like? It probably will be a blend of the V-band and R-band flat fields. Notice how different the V-band and R-band flat fields are in Fig. A.02. A blue star, on the other hand, may need to be corrected using a blend of the B-band and V-band flat fields.

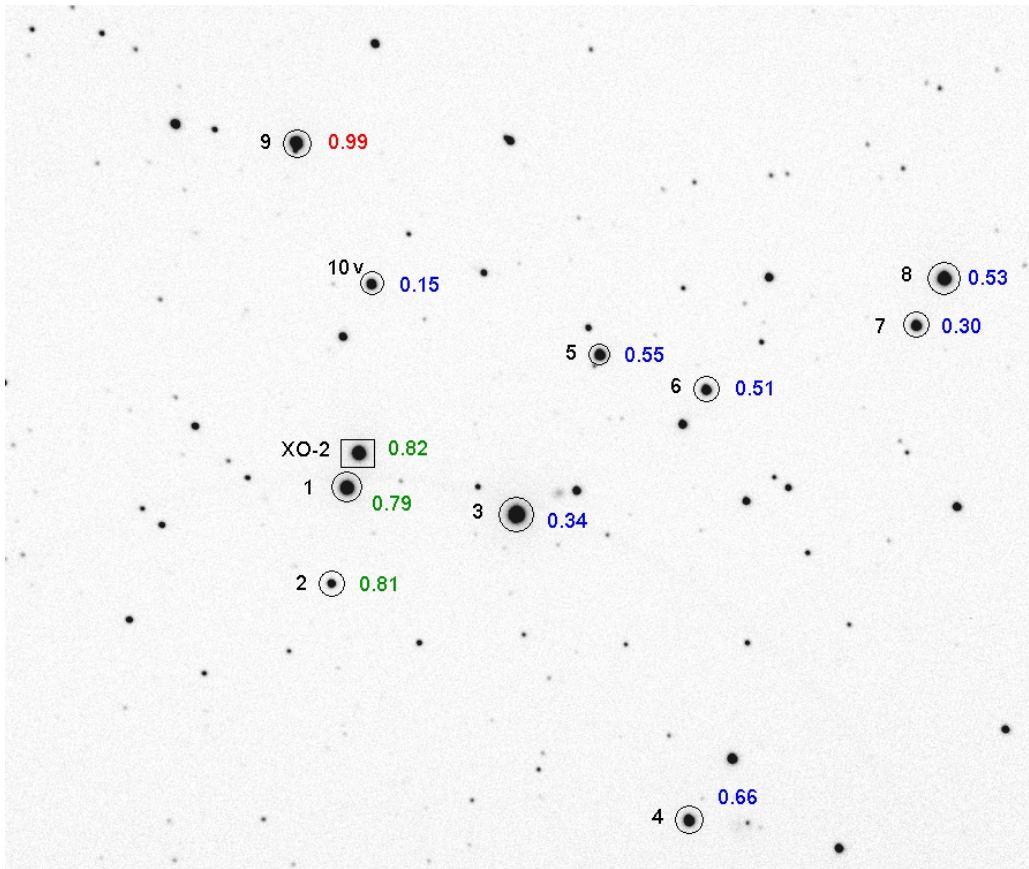


Figure A.03. Star field with B-V color labels. This is a 14.7x12.6 'arc crop of the full FOV (24x16'arc). North up, east left.

I will describe three ways to evaluate the presence of defects in a master flat field. One technique checks for patterns in magnitude-magnitude plots for two stars in a large set of images. Another method involves observing Landolt star fields and processing them using an all-sky analysis procedure. The third method involves taking a long series of images of a pair of equally bright stars within the FOV without autoguiding and comparing their ratio versus time as they traverse various parts of the CCD pixel field. It resembles the first method except that it makes use of intentional movements of the star field with respect to the CCD pixel field.

APPENDIX A – EVALUATING FLAT FIELDS

Mag-Mag Scatter Plots

There's a clever "reality check" to see if a drifting star field is producing systematic brightness changes due to flat field errors (thanks, Peter McCullough, for showing me this). I'll illustrate it with an unfiltered 6-hour observation session of the previous figure's star field.

The stars in this image were observed to rotate clockwise about the autoguider location in the sky, which was 16.5 'arc to the south of the main chip's FOV center. Stars in the center moved ~6 pixels during the 6-hour observing session, and those near the upper edge moved ~9 pixels. If the flat field did a perfect job of correcting all star fluxes to what they would be if they were near the center of the image then this motion would be unimportant. A star near the edge requires a larger flat field correction than a star near the center, and any imperfections in the flat field are likely to affect edge stars more. To see if stars have been correctly flat field corrected we can take advantage of the fact that when a star field drifts any incorrect flat field corrections are likely to differ for stars at different locations.

Consider Stars #5 and #6 (in Fig. A.03). Their measured magnitudes during the entire observing session are plotted in the next figure. Notice how "well-behaved" they are, in the sense that they did not change brightness with respect to each other. This result is unsurprising since the two stars are close together and have similar colors. It shows what can be expected if flat field errors at the two star FOV locations are not present.

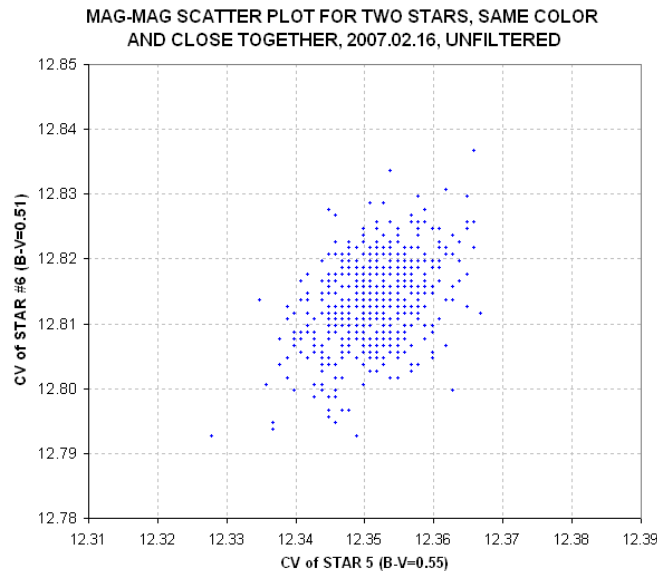


Figure A.04 Mag-mag scatter plot for two stars with same color and close together for the 6-hour clear filter observing session of 2007.02.16.

Figure A.05 shows what happens in a mag-mag scatter plot when one of the stars is near the edge (Star #8) and the other is near the center (Star #5). Keep in mind that for these observations the telescope was configured so that the flat fields had a pattern very similar to those pictured in Fig. A.01, where there's a smooth fall-off of response from 100% near the center to ~63% near the

APPENDIX A – EVALUATING FLAT FIELDS

corners. In other words, the flat field response function is steep near the edges, where Star #8 is located.

In this scatter plot Star #8 (near the FOV edge) exhibits excessive scatter whereas Star #5 (near the FOV center) is well-behaved. Star #8 moved ~8 pixels during the observing session and the flat field correction during this movement ranged from 9.4% to 10.0%. This suggests that the flat field correction was imperfect, and produced an extra component of “magnitude variation” that was not present for stars near the center of the image.

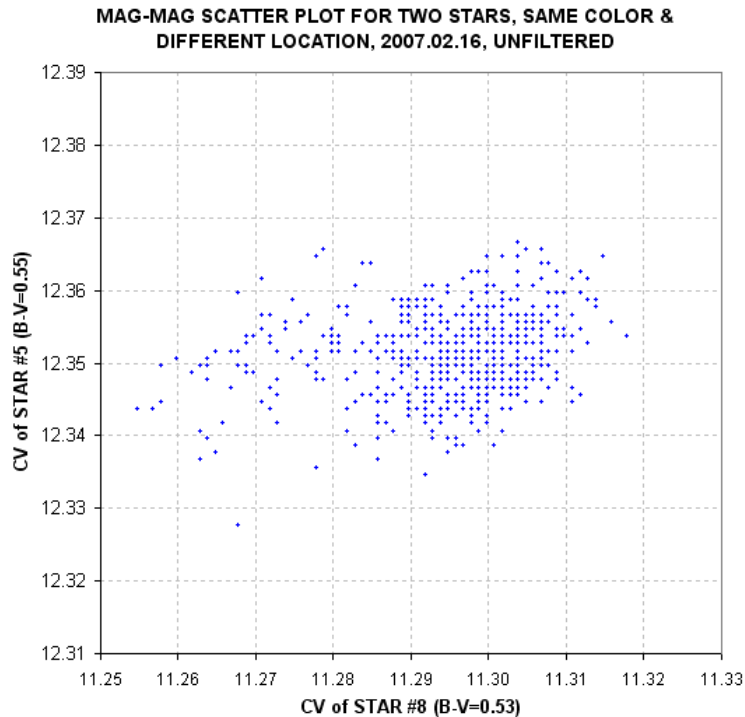


Figure A.05 Mag-mag scatter plot for two stars with same color but far apart (5 'arc) for the same 6-hour unfiltered observing session of 2007.02.16.

The purpose of the mag-mag scatter diagrams is to detect whether flat field error effects are present. For the case illustrated by the previous two figures there appears to be a problem with stars close to the FOV edge. When this happens stars near the edge should not serve as reference stars since the mag-mag scatter plot does not tell us how to adjust the flat field. This is one reason the target and candidate reference stars should be placed near the FOV center when starting an observing session.

All-sky Photometry Method for Flat Field Evaluation

There are 1259 “Landolt stars” that have been calibrated with extreme accuracy (Landolt, 1992). Most of them are in groups of 20 to 50 stars located along the celestial equator at RA intervals of ~1 hour. Most Landolt stars have been observed on several occasions and have been accepted for inclusion when they are found to be constant, but long-term variables are occasionally encountered (I’ve found two). Each group of Landolt stars is spread over an area that is usually larger than a

APPENDIX A – EVALUATING FLAT FIELDS

typical FOV. Using my FOV of $11 \times 17'$ arc, for example, it is possible to include 6 to 10 Landolt stars in one image that are bright enough for an amateur to achieve a high SNR (e.g., >500).

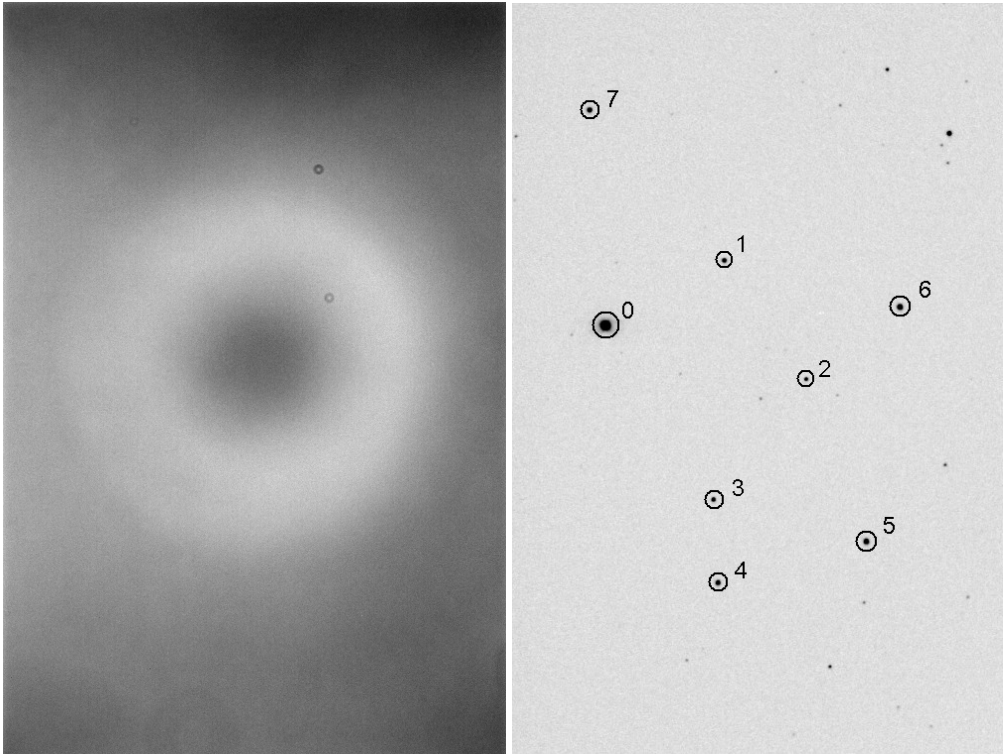


Figure A.06 (left): Flat field with V-band filter to be evaluated using Landolt stars.

Figure A.07 (right): Landolt star field at RA/Dec = 15:38:51, -00:19:33. FOV = $11 \times 17'$ arc used in evaluating flat field quality by comparing measured with Landolt magnitudes.

Figure A.06 is a flat field using a V-band filter. It is darkest in the upper-right corner, where a 1.095 flat field correction factor is required.

Figure A.07 is a calibrated image showing 8 Landolt stars. If this image had been calibrated using a good flat field then it should reveal this fact by showing agreement with the Landolt star magnitudes at each of the 8 FOV locations sampled. This is just one of ten sets of images, where each set has been positioned with RA/Dec offsets so as to uniformly sample as much of the CCD area as possible. If there is agreement between all 8 stars and their Landolt V-magnitudes for all 10 image sets then it would be fair to surmise that the flat field is accurate. A more accurate surmise would be that the large spatial wavelength components representing the flat field are accurate. Using this technique there is no way to probe the flat field's quality at short spatial wavelengths.

In theory a flat field could be constructed by repeatedly dithering RA and Dec until all regions of the CCD have been sampled by Landolt stars. I don't recommend doing this, for several reasons that are described below. Nevertheless, it is feasible to check the quality of a flat field by observing a Landolt star field with a few carefully selected RA and Dec offsets.

APPENDIX A – EVALUATING FLAT FIELDS

Figure A.07 includes 8 Landolt stars brighter than 13th magnitude. It was observed with 10 different RA/Dec offsets, producing 70 locations on the CCD pixel field where a measured magnitude could be compared with a Landolt magnitude (the number is less than 80 because some RA/Dec offsets placed Landolt stars outside the FOV). All observations were made with a V-band filter. Star color effects are removed by solving for a star color coefficient in an expression for V-magnitude:

$$V\text{-mag} = 19.670 - 2.5 * \text{LOG}_{10}(S / g) - K_v' \times \text{AirMass} - 0.055 \times C'$$

where S is star flux [counts], g is exposure time [seconds], K_v' is zenith extinction for the V-band filter [magnitude/air mass] and C' is a linearized version of star color C, defined as $C = 0.57 \times (B-V) - 0.30$. The linearized version is $C' = C + 1.3 \times C^2$. The constants 19.670 and -0.055 were derived from a least-squares fitting procedure using the 70 star flux measurements. All images for this session were made near transit, so air mass was constant and it didn't matter what value was used for K_v' .

If the flat field used in calibrating these images was good then it should be possible to achieve a good quality fit for all 70 Landolt star magnitude measurements. For this set of images the residuals had an RMS deviation of 0.023 magnitude. A plot of these residuals versus star magnitude is shown in Fig. A.08.

In this figure it is apparent that some stars are persistently brighter or fainter than the model fit and this could be due to the star changing brightness during the two decades between the time the Landolt measurements were made (1980s) and the present. It is not unreasonable to hypothesize that a star changed brightness by 0.024 magnitude during that time (the largest average difference found from the above fitting procedure). If star brightnesses are adjusted to produce zero averages the RMS scatter becomes 0.017 magnitude. Whichever choice is made the resulting conclusion is approximately the same: the flat field was successful at about the 0.02 magnitude level. The RMS residuals (range = 0.017 to 0.024 magnitude) correspond to ratios within the range 1.6 to 2.2 %.

Does this constitute a validation of the flat field? Not really! After all, the maximum flat field correction for the flat field under evaluation is 9.5%, and the typical RMS variation for star locations is ~1.2%. In other words, the “all-sky photometry method for evaluating a flat field” is simply too imprecise for evaluating typical flat fields. There is little prospect that better quality all-sky photometry can be counted on for improving the value of its use for evaluating flat fields. After all, an RMS scatter in the range 0.017 to 0.024 magnitude is pretty good for all-sky photometry.

This method for evaluating a flat field will only be useful for ruling out the presence of large errors. These large errors are more likely to be present when the flat field has a large amount of vignetting, or when there is reason to suspect the presence of a large stray light component in the flat field. Only when flat field errors of ~3% or larger are thought to be present, or need to be ruled out, will this method for evaluating a flat field be useful.

APPENDIX A – EVALUATING FLAT FIELDS

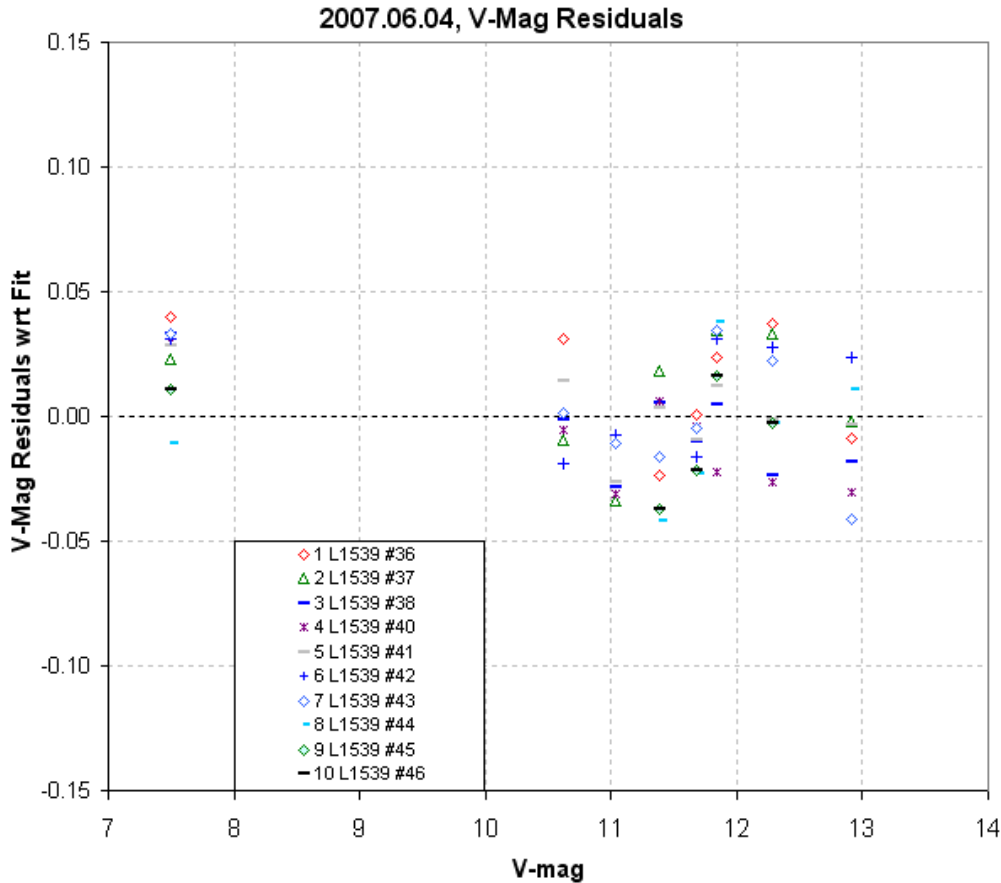


Figure A.08. *V*-magnitude residuals with respect to model fit (using the two parameter values 19.670 and -0.055) plotted versus star magnitude.

Star Ratio Changes with Star Field Offsets

The previous section shows that the goal of establishing a flat field shape using accurate magnitude information of Landolt stars is too ambitious to be considered feasible. It may be capable of identifying gross errors, such as those exceeding ~3%, but the approach cannot be used to identify errors of much lower amounts.

In this section we will pursue the less ambitious goal of answering the question:

What are typical error differences in the flat field for randomly-chosen pairs of pixel location areas?

This question is relevant to the task of producing exoplanet light curves with a minimum of systematic shape errors. After all, if it can be shown that a pair of stars maintain the same flux ratio for many pixel offset settings, then it is fair to assume that image rotation movements of a target star and its ensemble of reference stars will maintain a similar stability of flux ratios.

APPENDIX A – EVALUATING FLAT FIELDS

To perform this test we don't need Landolt star fields; we only need stars that do not vary on hourly time scales. The previous section dealt with a set of observations of a star field with a variety of position offsets, and since these images have already been processed I will use them in this section to evaluate the new, less ambitious question.

We must keep in mind that every star's flux measurement is noisy due to Poisson noise, scintillation noise and aperture pixel noise. These sources of noisiness could mask real changes in flux ratios produced by flat field errors. Let's calculate noise levels from these sources before proceeding with a calculation of observed flux ratio changes.

The images were made with 10-second exposures at air mass ~ 1.25 , so scintillation is estimated to be on the order of 2.5 mmag. Star fluxes ranged from 4100 to 590,000 counts, so Poisson noise is calculated to range from 10.7 to 0.9 mmag, respectively. Aperture pixel noise is calculated to be 0.5 mmag. Each star is therefore expected to exhibit values for fundamental SE that range from ~ 3 to 11 mmag. Since these noise sources are uncorrelated from star to star, when two stars are compared the magnitude difference should exhibit root-two greater SE, or ~ 4.2 to 16 mmag. The image sets that were processed in the previous section consisted of 10 images per set, so when average magnitude differences are used the expected SE will be root-(10-1) smaller than for single image differences. Therefore, we can expect to encounter fundamental SE uncertainties of 1.3 to 4.9 mmag when comparing the average magnitude of stars in sets of 10 images.

The measured magnitude differences between star pairs in 10 image groups (10 images per group) are SE = 17, 28, 25, 20, 28 and 24 mmag. These six SE values correspond to six star pairings. The median and average of these six SE values are both 24 mmag. Thus, the measured SE is greater than expected from the assumed Poisson noise, scintillation noise and aperture pixel noise. It is possible that scintillation noise was greater than usual for the observing session. Otherwise I would have to conclude that the flat field error map exhibited large variations, such as 17 mmag (1.6%).

The suggestion that the flat field error map has a 17 mmag RMS variation can be used to infer the magnitude of systematic light curve variations if the image rotation and movement across the pixel field was comparable to the spacing of stars used to derive the 17 mmag value. The average spacing between stars is ~ 5 'arc. Typical image movements during a light curve observing session are much less than this. We do not have information about the spatial auto-correlation distances for these flat field errors, so it is not possible to predict the magnitude of systematic light curve errors for typical movements. A proper analysis would correlate magnitude differences with star separation distance, and I have not done this.

It could be argued that the spatial structure of the flat field response distribution can be used as a guide in estimating the spatial structure of the flat field error map. Visual inspection of Fig. A.06 suggests that the error map is dominated by spatial structures having wavelengths ~ 5 'arc. Since typical movements of the star field (for my present polar alignment) are $\ll 1$ 'arc (they're on the order of 0.1 'arc), a bold prediction could be made that I should encounter systematic light curve errors < 4 mmag (and possibly as small as ~ 0.4 mmag).

The reader is invited to pursue an investigation of their own system's flat field errors using their own observations and guided by the ideas presented in this appendix. No doubt, there must be other ideas to be guided by, and the author would appreciate feedback on any results or ideas on this matter.

APPENDIX B – Selecting Target from Candidates List

This appendix is for those few amateurs who are privy to a secret list of candidates for possible exoplanet transits maintained by professionals who operate wide-field camera surveys. As I write this only the XO Project produces such a list for use by a small group of amateur observers. However, I anticipate that in the future professional teams with survey cameras will solicit amateurs to conduct follow-up observations using their secret candidate lists. When that happens, the amateurs invited to join those extended teams will want to learn how to wisely choose candidates from the list for each night's observation.

The candidate list is based on wide field camera surveys with poor spatial resolution but good sensitivity. Because of the poor spatial resolution most “candidates” are faint eclipsing binaries whose light is blended with a brighter star that is mistaken by the survey candidate analysis software for being the eclipser. This common situation is called “EB blending.” The main role for amateur observers is to determine which star is fading and by how much. As a bonus the amateur light curve can reveal the shape of the event, and if it is closer to flat-bottomed than V-shaped, as well as shallow, there will be heightened interest in additional observations.

If you're going to spend 6 or 8 hours observing a candidate it is reasonable to spend a few minutes evaluating the merits of various candidates on a list showing predicted transits for the night in question. Exoplanet candidates derived from survey camera data will contain the following information for each candidate: periodicity (P), length of transit (L), depth (D) and maybe star color J-K. Let's assume that an ephemeris of predicted transit times is available for each UT date (and possibly restricted to what's observable from the observer's site). On any given night there may be half a dozen candidates with transits that can be observed. If J-K is not given then the observer should obtain it from a star catalog (such as TheSky/Six). The following graph can be used to identify candidates that have transit lengths compatible with the hypothesis that transits produced by an exoplanet instead of an eclipsing binary that is blended with another nearby star (giving the appearance of a small depth).

Consider the following information for a survey candidate that has never been observed in a way that defines its LC accurately: $P = 3.9$ days, length of transit = 2.2 hours, $J-K = 0.41$. Using this figure locate the point for $J-K = 0.41$ and $P = 3.94$. Then read the y-axis value of 2.8 hours. This is the longest possible length for a transit (*i.e.*, it's the length for a central transit). The survey catalog's measured length of 2.2 hours is less than this maximum length, which is consistent with an exoplanet transiting far from a central crossing.

Consider another survey candidate example: $P = 2.4$ days, length = 2.6 hours, $J-K = 0.60$. Referring to the graph again we find that the longest possible transit is 2.1 hours. The survey's reported length of 2.4 hours is too long. These transit numbers are incompatible with an exoplanet transit (unless the orbit is very elliptical, which is rare for close-in orbits), and we may suspect that this is an eclipsing binary that is blended with another nearby star. An “EB blending” situation can lead to an incorrect J-K for the star undergoing transit, so it is still possible that this candidate is an exoplanet; but since there are so many more EB blending situations than exoplanet transit situations the odds favor the EB blending interpretation, and an observer should be wary of investing time in observing such a candidate.

APPENDIX B – SELECTING TARGET

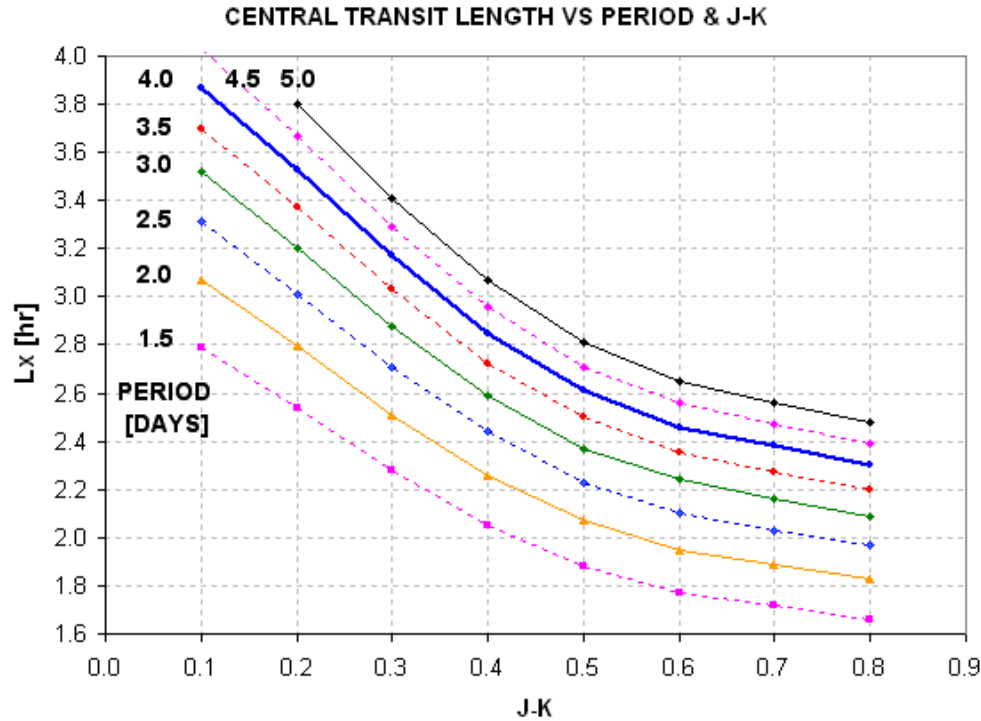


Figure B.01 Central transit length, L_x , versus J-K star color and orbital period.

Although Appendix D contains an extensive treatment of concepts for fitting LCs to exoplanet transit models, I will give a brief description here of the concepts underlying this figure. Main sequence stars, which comprise ~90% of all stars, have sizes and masses that are correlated with their colors. Since J-K colors are available for almost all stars that an amateur will encounter for this purpose I have chosen to use this color instead of B-V. Knowing a star’s J-K means that we can infer the star’s radius and mass (assuming it’s a main sequence star). Knowing the secondary’s orbital period allows us to calculate its orbital radius, using the simple relationship that orbital radius is proportional to $(P)^{2/3}$ times $(\text{total system mass})^{1/3}$. From orbital radius and period we can calculate the secondary’s orbital velocity, and combining this with the star’s radius we can derive the time it takes for a central crossing.

If we define transit length to be the “full width at 1/3 maximum” for the transit feature then we have a parameter that closely corresponds to the time it takes for the center of the secondary to traverse the transit chord across the star. Exoplanet transits from survey cameras will fold many transit events to produce a less noisy transit shape. It will have a noise level (~5 to 15 mmag) that is only slightly smaller than transit depth. In practice the transit length listed in the survey candidate catalog will be shorter than contact 1 to contact 4, and is often an approximation of “full width at 1/3 maximum.” To the extent that this is true the above figure will give reliable guidance on maximum possible transit length.

Exoplanet candidate ingress and egress times can be wrong by an hour or two. When planning an observing session for a candidate it is wise to allow extra observing time before predicted ingress or

APPENDIX B – SELECTING TARGET

after predicted egress to be sure of capturing it. Otherwise you may issue a “no show” report that can be misleading.

Exoplanet candidate observing can be useful if only a partial transit event is observed. This at least will show which star is undergoing transit, and it is usually possible to categorize the candidate as being an EB blend versus a shallow transit from measured depth of only a part of the transit event. Therefore, when planning a night’s observations it’s OK to select a candidate when only part of the predicted transit is predicted to be observed.

Many of the considerations presented in Chapter 3 for selecting an exoplanet for a night’s observations also apply to selecting an exoplanet candidate.

APPENDIX C - Algorithm for Calculating Air Mass from JD, Site Coordinates and RA/Dec

- 1) Subtract 2451545 from JD
- 2) Multiply this by 24.065709824419 and add 18.697374558.
- 3) Subtract $24 \times \text{INT}(\text{above value} / 24)$
- 4) Add EastLongitude / 15 (this is GMST)
- 5) If < 0 , add 24 (this is LST)
- 6) Multiply by 15 and subtract RA [deg] (this is LHA)
- 7) If LHA > 180 , subtract 360
- 8) Calculate cosine (LHA), *i.e.*, $\text{Cosine}(\text{LHA} / 57.2858\dots)$
- 9) Multiply by Cosine (Latitude)
- 10) Multiply by Cosine (Dec)
- 11) Add $\text{Sine}(\text{Dec}) \times \text{Sine}(\text{Latitude})$
- 12) Air mass is reciprocal of above

APPENDIX D - Planet Size Model

INTRODUCTION

This appendix is long. It has nothing to do with exoplanet transit observing tips, and that's why it's in an appendix. I present it for those readers who think it might be fun to play "modeler" and who want to interpret a well-established LC in terms of planet size. I must admit that the simple procedures leading to the final one described here has misled me a few times. However, after each failure I reviewed my assumptions and learned from them. One lesson is that if an internally consistent solution is impossible then consider the star to be "off the main sequence," where star color to size and mass conversions are questionable. Consider also the possibility that the transits are produced by a triple star system, in which the depth only appears shallow when in fact it is a deep eclipsing binary that is blended with a third star that's within the photometry aperture (and possibly a close binary with the eclipsing binary pair).

The goal of this appendix is to describe a simple model that I developed for converting a transit light curve (LC) to an estimate of the size of the secondary, which is then used to discriminate between the secondary being an exoplanet versus a small and faint star (*i.e.*, a red or brown dwarf eclipsing binary system).

A "concept description" section uses actual R-band measurements of an exoplanet to illustrate how a LC can be interpreted. The "model" employs limb darkening relationships for each filter band. The primary star's B-V color (closely associated with spectral type) is used to derive the star's mass and radius, on the assumption that it's a main sequence star (like ~90% of stars). Orbital period is used to calculate orbital velocity (assuming a circular orbit). The planet's radius and "central miss distance" ("impact parameter," related to inclination) are adjusted to match the LC depth and duration.

A proper solution for planet radius will involve a fit to the entire LC, not a solution based on agreement with the LC's depth, length and shape parameter that is employed by the simple solution in this appendix. A crude method is presented for determining if the shape is similar to what an exoplanet can produce, versus what a blend of an eclipsing binary (EB) with another nearby star would produce. My shortcuts reduce accuracy, of course, but if an approximate answer is acceptable then the procedure described here may be useful.

Section 1 is a case study that is used to illustrate the concepts employed. Far more steps are shown than would be used in practice. The goal for this section is to determine the size of the secondary (exoplanet or EB binary star).

Section 2 shows how to use information about the LC's shape to assess whether the LC is compatible with an exoplanet or an EB whose light is blended with a nearby star to produce what merely appears to be a small transit depth.

Section 3 is a summary of only those things that need to be done, after the underlying concepts are understood, to convert the basic properties of a LC and star color to a solution for secondary size and likelihood of the transit belonging to an exoplanet versus an EB.

Section 4 describes an Excel spreadsheet that can be downloaded and run to do just about everything

APPENDIX D – PLANET SIZE MODEL

described on this appendix. The user enters transit depth, transit length, period and star color (B-V) in cells corresponding to the LC's filter band and a cell displays a 3-iteration solution for R_p/R_j (if a solution exists). It also can be used to assess the likelihood of the LC shape belonging to the exoplanet domain, based on the user's input of a shape parameter, F_p .

1. CONCEPTS OF LC INTERPRETATION - A CASE STUDY

I like explaining things through the use of a specific example. The reader's job is to "generalize" from the specific. I'm going to treat real observations of a "mystery" star's transit light curve; this way we can grade the results of my crude analysis procedure using a rigorous treatment by professionals.

Let's assume the following:

GIVEN:

- B-V = $+0.66 \pm 0.05$ (which can be derived from J-K)
- orbital period, $P = 3.9415$ days,
- R-band observations
- transit depth, $D = 23.7 \pm 0.4$ mmag,
- transit length, $L = 2.97 \pm 0.03$ hours (contact 1 to 4).

The D and L values were derived from the transit light curve in Fig. D.01, measured with an amateur 14-inch telescope (pretend you don't know which star this is).

After a transiting candidate has been observed, and before radial velocity measurements have been made to assess the mass of the secondary, this is all the information we have to work with. Using this limited information there are many steps for interpreting the LC to estimate secondary size, R_p/R_j (exoplanet's spherical radius divided by Jupiter's equatorial radius).

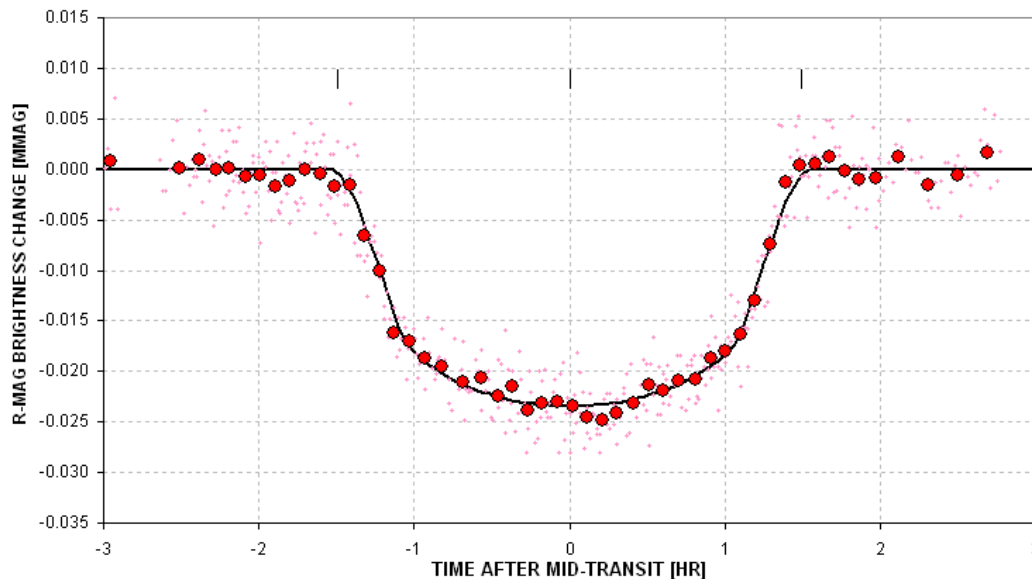


Figure D.01 *Transit light curve for a mystery star whose LC we shall try to "solve" using the procedures described in this appendix.*

APPENDIX D – PLANET SIZE MODEL

SOLUTION:

Star's radius, $R_{str} = 0.99 \times R_{sun}$ (based on equation below)

$$R_{str} = 2.23 - 2.84 \times (B-V) + 1.644 \times (B-V)^2 - 0.285 \times (B-V)^3$$

Planet radius, $R_p/R_j = 1.41$ (1st iteration)

$$R_p/R_j = 9.73 \times R_{str} \times \text{SQRT} [1 - 10^{-D/2500}],$$

which assumes a central transit and no limb darkening
(note: $R_j = \text{Jupiter radius}$, $R_{sun}/R_j = 9.73$)

At this point we have an approximate planet size. It's only a first iteration since limb darkening has been neglected. The next group of operations is a 2nd iteration.

Star's mass, $M_{str} = 0.97$ (times sun's mass)

$$M_{str} = 2.57 - 3.782 \times (B-V) + 2.356 \times (B-V)^2 - 0.461 \times (B-V)^3$$

Planet orbital radius, $a = 7.22e6$ [km]

$$a = 1.496e8 \times [M_s^{1/3} \times (P / 365.25)^{2/3}],$$

where dimensions are P [days], M_s [solar mass] & a [km]

Transit length maximum, $L_x = 3.28$ [hr] (corresponds to central transit)

$$L_x = 2 (R_{str} \times R_{sun} + R_p/R_j \times R_j) / (2 \pi a / 24 \times P)$$

where $R_{sun} = 6.955e5$ km, $R_j = 7.1492e4$ km

Impact parameter, $b = 0.42$ (ratio of closest approach to center normalized by star's radius)

$$b = \text{SQRT} [1 - (L / L_x)^2]$$

Limb darkening effect, $LDe = 1.16$ (divide D by this)

$$I(b)/I(av) = [1 - 0.98 + 0.15 + 0.98 \times c - 0.15 \times c^2] / 0.746, \text{ for B-band}$$

$$" = [1 - 0.92 + 0.19 + 0.92 \times c - 0.19 \times c^2] / 0.787, \text{ for V-band}$$

$$" = [1 - 0.85 + 0.23 + 0.85 \times c - 0.23 \times c^2] / 0.828, \text{ for R-band}$$

$$" = [1 - 0.78 + 0.27 + 0.78 \times c - 0.27 \times c^2] / 0.869, \text{ for I-band}$$

where $c = \text{SQRT} (1 - b^2)$

Corrected transit depth, $D = 20.4$ mmag (1st iteration for D)

$$D = D / LDe \text{ (D that would have been measured if the star were uniformly bright)}$$

Planet radius, $R_p/R_j = 1.31$ (2nd iteration for R_p/R_j)

(Same eqn as above but now assumes $b = 0.42$ and appropriate limb darkening)

Transit length maximum, $L_x = 3.25$ [hr] (2nd iteration for central transit length)

(Same eqn as above)

Impact parameter (miss distance), $b = 0.405$

(Same eqn as above)

Limb darkening correction, $LDe = 1.165$ (divide D by this)

APPENDIX D – PLANET SIZE MODEL

(Same eqn as above)

No more iterations are needed since the two impact parameter results (& limb darkening corrections) are the same. We have a stable solution:

$$R_p/R_j = 1.306$$

To assign a SE to this solution it is necessary to repeat the above procedure using a range of values for the measured transit depth and length. When this is done (using an Excel spreadsheet) we get $R_p/R_j = 1.306 \pm 0.063$ (with B-V uncertainty contributing the greatest component of SE). Note that the stated SE doesn't include the uncertainties associated with the equations converting B-V to stellar radius and mass, nor does it allow for the possibility that the star is "off the main sequence."

EVALUATING THE SOLUTION

How good is this result? Let's compare it with a detailed model-fitting analysis by professional astronomers. The "mystery" exoplanet is no mystery. It's **XO-1**, whose discovery was announced May 18, 2006 and published in the September issue of the *Astrophysical Journal* by McCullough *et al* (2006):

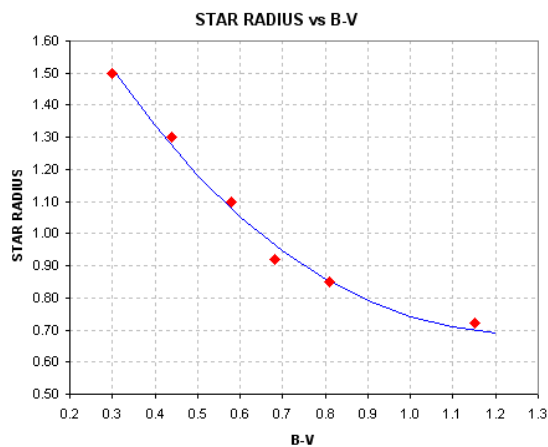
<http://xxx.lanl.gov/abs/astro-ph/0605414> (abstract), and
http://arxiv.org/PS_cache/astro-ph/pdf/0605/0605414.pdf (complete article).

This article reports that $R_p/R_j = 1.30 \pm 0.11$. This compares well with the simple model result calculated here, of $R_p/R_j = 1.31 \pm 0.07$. (The larger SE for the professional result reflects a realistic assessment of such systematic uncertainties as converting B-V to stellar radius and mass.)

The B-band light curve for XO-1 is measured to have $D = 24.8 \pm 0.5$ and $L = 2.95 \pm 0.03$. For these inputs the procedure described above gives $R_p/R_j = 1.29 \pm 0.06$.

GRAPHICAL REPRESENTATION OF EQUATIONS

The following graphs can be used instead of the equations for deriving star radius, mass and limb darkening correction (derived from *Allen's Astrophysical Quantities*, Fourth Edition, 2000):



APPENDIX D – PLANET SIZE MODEL

Figure D.02. Converting star color $B-V$ to stellar radius (assuming main sequence).

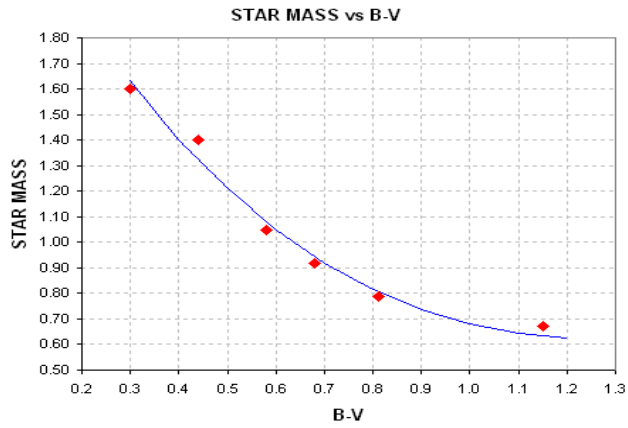
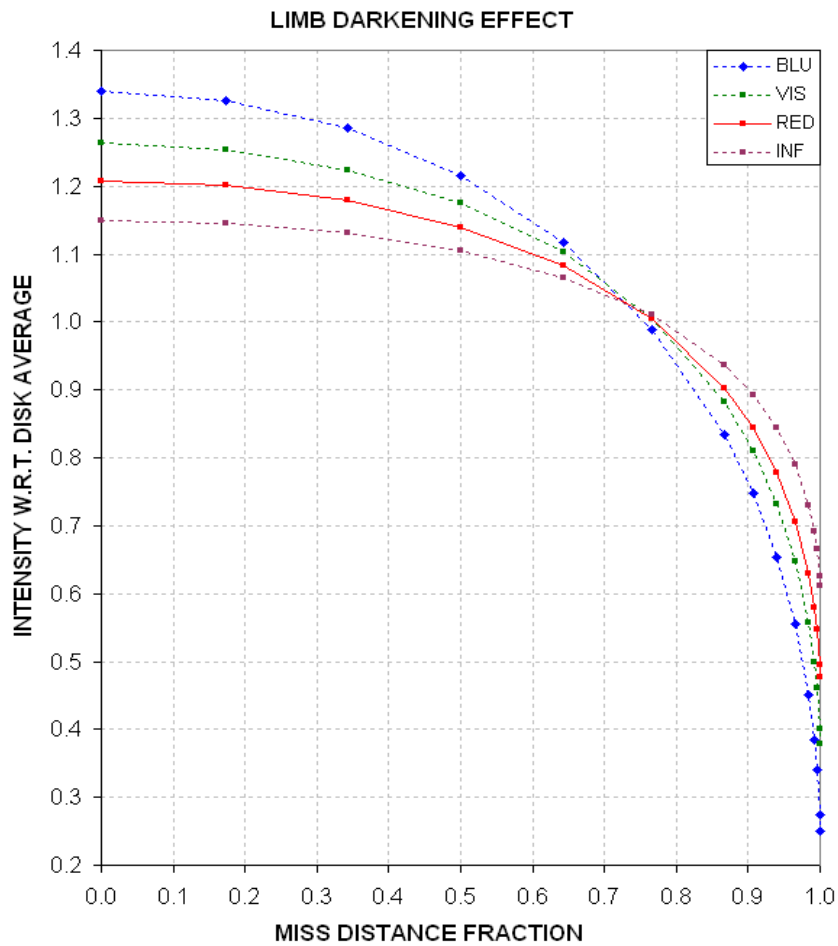


Figure D.03. Converting star color $B-V$ to stellar mass (assuming main sequence).



APPENDIX D – PLANET SIZE MODEL

Figure D.04. *Converting miss distance (impact parameter) and filter band to intensity at that location, normalized by disk-average intensity (assuming a sun-like star).*

The following two figures show how transit shape and depth behave when the impact parameter changes from near-center to near-edge. These are real measurements (graciously provided by Cindy Foote) that were categorized as EB based on the depth values. The concept is the same, whether it's an exoplanet or small EB, because in both cases a central transit should produce a greater loss of light in B-band than R-band, and for a near-edge transit the reverse is true.

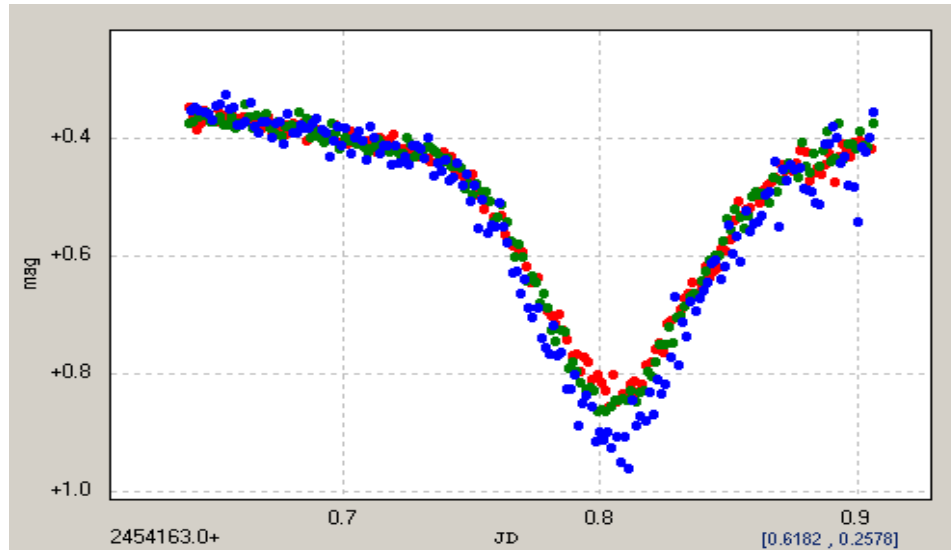
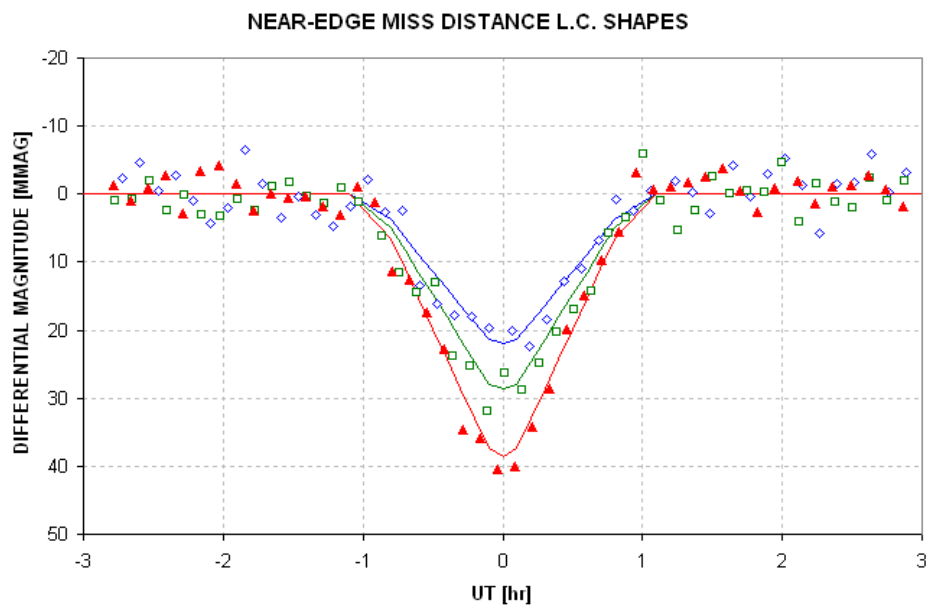


Figure D.05. *Transit depth is greatest for B-band, consistent with miss distance <0.73 (courtesy of Cindy Foote).*



APPENDIX D – PLANET SIZE MODEL

Figure D.06. *Transit depth is greatest for R-band, consistent with a miss distance >0.73 (courtesy of Cindy Foote).*

2. VERIFYING THAT LIGHT CURVE SHAPE IS NOT AN E.B. BLENDING

Wide-field survey telescopes provide an efficient means for detecting stars that are undergoing periodic fades with depths small enough to be caused by an exoplanet transit (e.g., depth < 35 mmag). A fundamental limitation of such a survey is that in order to achieve a wide field of view the telescope's resolution is poor, and this leads to many "false alarms" due to the "blending" of light from stars within the resolution-determined photometry aperture circle. If, for example, resolution corresponds to a circle with radius 1' arc and the flux from all stars within this circle corresponds to ~ 11 th magnitude, it is common for several stars to be present within the resolution circle that are fainter than 11th magnitude but with fluxes that add up to 11th magnitude. If this situation occurs, and if one of those stars is an eclipsing binary (EB) with a large transit depth, the transit depth measured by the survey telescope will be smaller, and possibly small enough to resemble one produced by an exoplanet. This is a common occurrence.

There are two blending situations that need to be considered: 1) the EB is part of a triple star system, so the blending star is too close to the EB to be resolved by ground-based telescopes, and 2) the EB and the blending star are far enough apart (usually gravitationally unrelated but close together in our line-of-sight) that their angular separation is within the resolution limits of ground-based telescopes. The second of these blending situations is probably more common than the first.

When a survey telescope produces many candidates per month it is not feasible to rule out an EB explanation for each one by measuring radial velocities during the course of a few nights with a telescope large enough to produce spectrograms that have the required accuracy. Although radial velocity measurements would allow the determination of the secondary's mass, and thus distinguish between EB and planet transits, large telescope observing time is too costly for such an approach.

A better alternative is to perform follow-up observations of the survey candidates using telescopes with apertures sufficient to identify the most common blending situation. Amateurs with telescope apertures 8- to 14-inches, for example, have more than sufficient resolution to determine which star within the survey's resolution circle is undergoing transit, thus easily identifying most cases of EB blending. These amateur telescopes also have sufficient SNR for an 11th magnitude star, for example, to allow the transit light curve to be determined with good enough quality to sometimes identify the presence of a triple star system EB. There may be more cases of triple star EBs that resemble exoplanet transits than there are actual exoplanet transits. Therefore, it is important to be able to interpret a transit light curve to distinguish between a triple star EB and an exoplanet.

This section demonstrates how amateurs can distinguish between exoplanet light curves and "EB triple star blended light curves" of similar depth, so that additional amateur observing time is not wasted on non-exoplanet candidates.

As an additional check the shape of the measured transit light curve can be compared with a model calculation. First, let's consider LC shapes for various sized secondaries (either an exoplanet or EB star) transiting across the center of the star they orbit. Figure D.07 was derived from a model that used sun-like R-band limb darkening.

APPENDIX D – PLANET SIZE MODEL

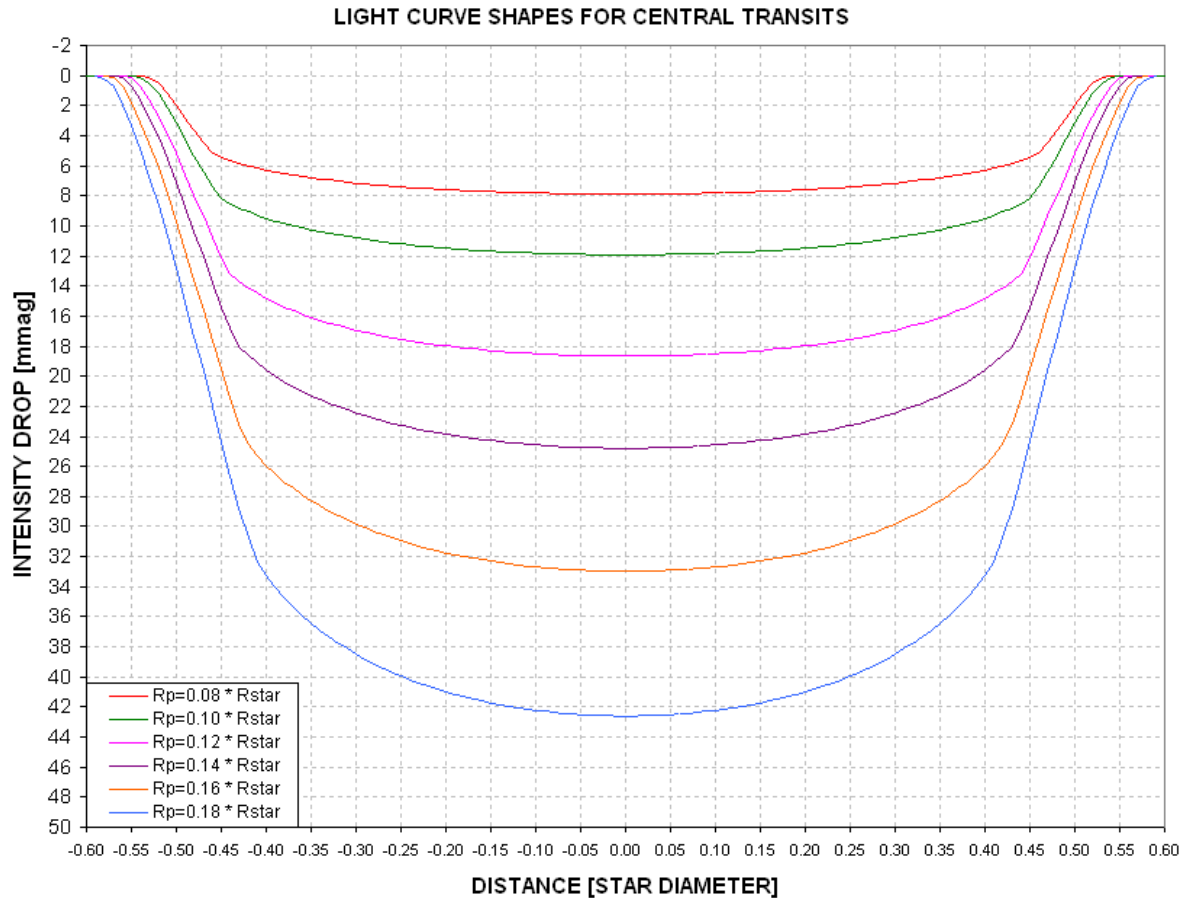


Figure D.07. Model light curves for central transits by different sized secondaries. An R-band sun-like limb darkening function was used.

First contact occurs when the intensity begins to drop, and second contact can be identified by the inflection where the slope changes from steep to shallow. A "shape" parameter, also referred to as F_p elsewhere in this book, is defined as the ratio of time the secondary is partially covering the star to the entire length of the transit (e.g., contact 1 to contact 2 divided by contact 1 to mid-transit). For example, in the above figure consider the trace for $R_p/R_{str} = 0.12$: contact 1 and 2 occur at -0.55 and -0.44, and contact 1 to mid-transit is 0.55. For this transit the shape parameter is $F_p = (0.55 - 0.44) / 0.55 = 0.20$.

Let's estimate F_p for a real transit.

In Fig. D.08 my readings of contact 1 and 2 are -1.48 and -1.05 hour. The shape parameter F_p is therefore 0.29 (0.43 / 1.48). Assigning SE uncertainties and propagating them yields: $F_p = 0.29 \pm 0.01$.

Figure D.09 shows how F_p varies with secondary size for central transits.

APPENDIX D – PLANET SIZE MODEL

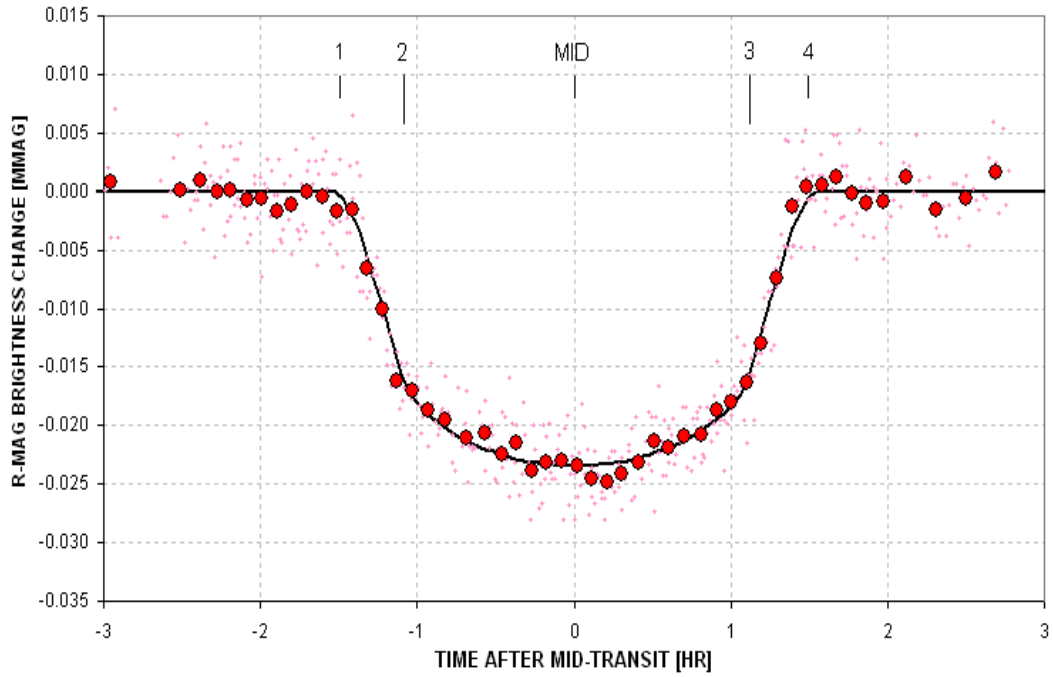


Figure D.08. Measured light curve with the contact times indicated.

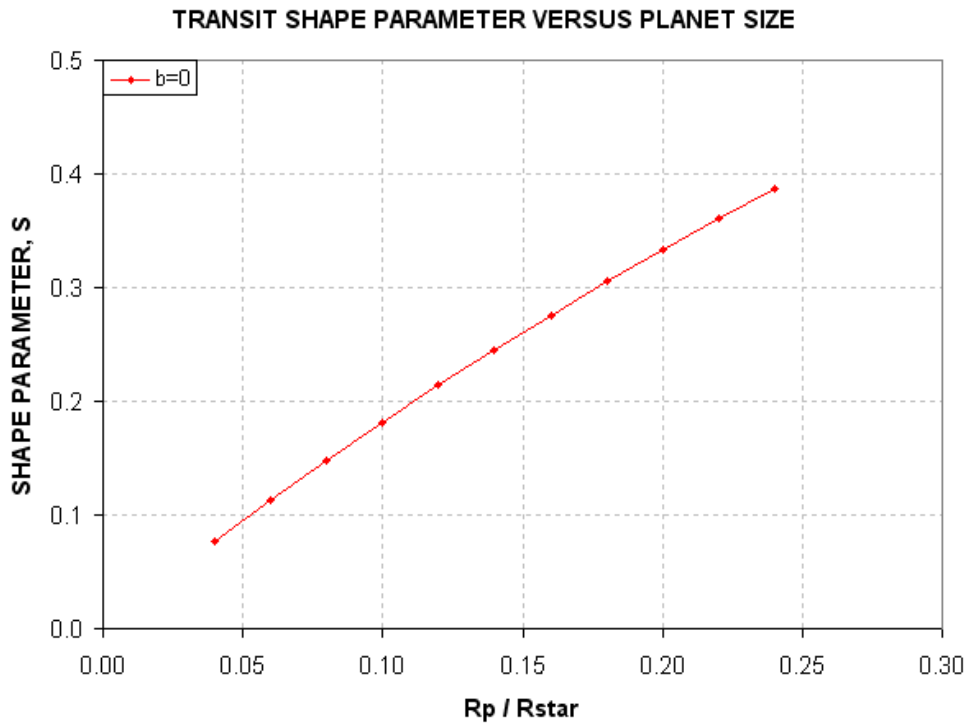


Figure D.09. Shape parameter, F_p , versus planet size for central transits.

APPENDIX D – PLANET SIZE MODEL

We next consider how the LC shapes vary with miss distance (also called “impact parameter”). We'll adopt one secondary size and vary the miss distance.

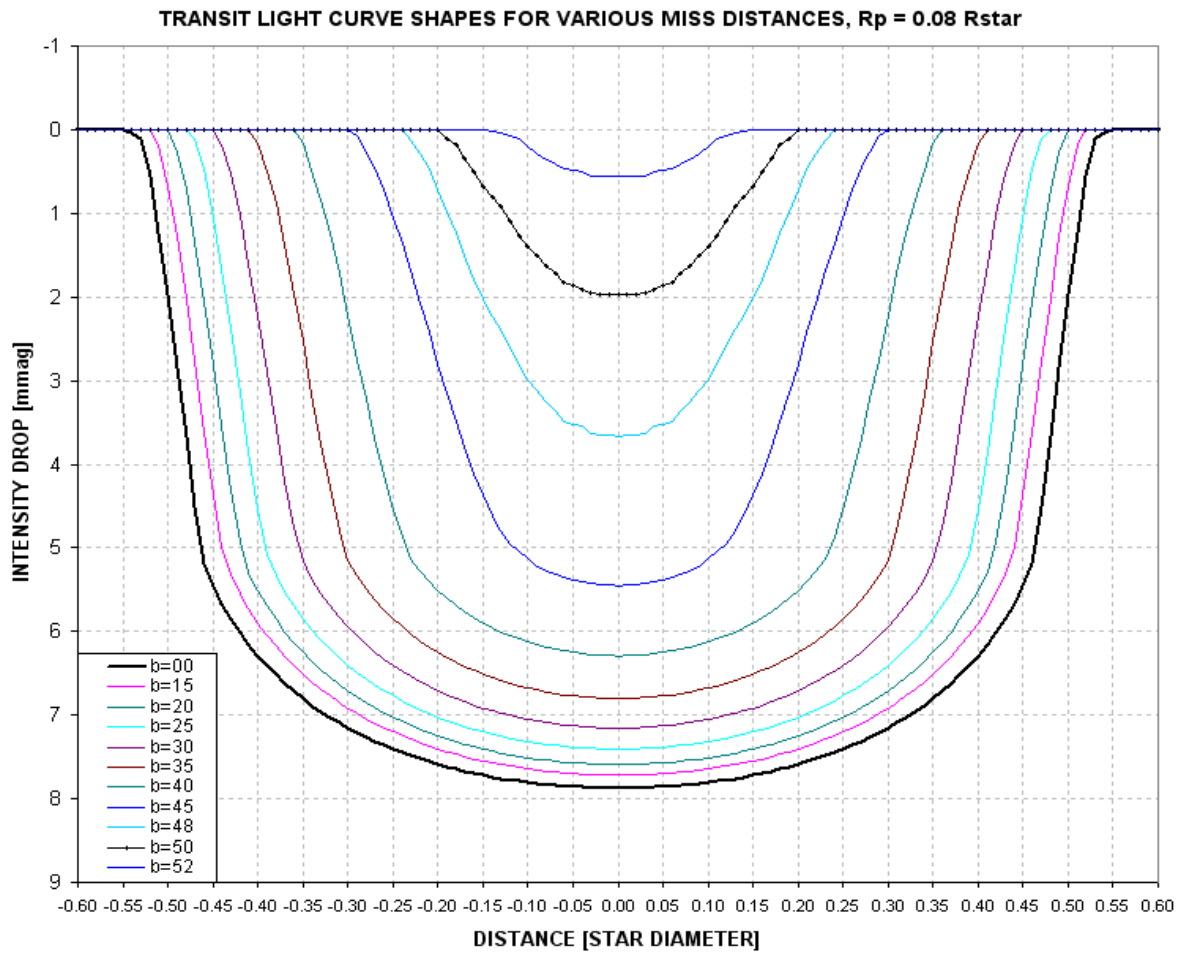


Figure D.10. Shape of LCs for various miss distances (b) and a fixed secondary size of $R_p/R_{str} = 0.08$.

The following figure summarizes the dependence of F_p on many choices for planet size and miss distance.

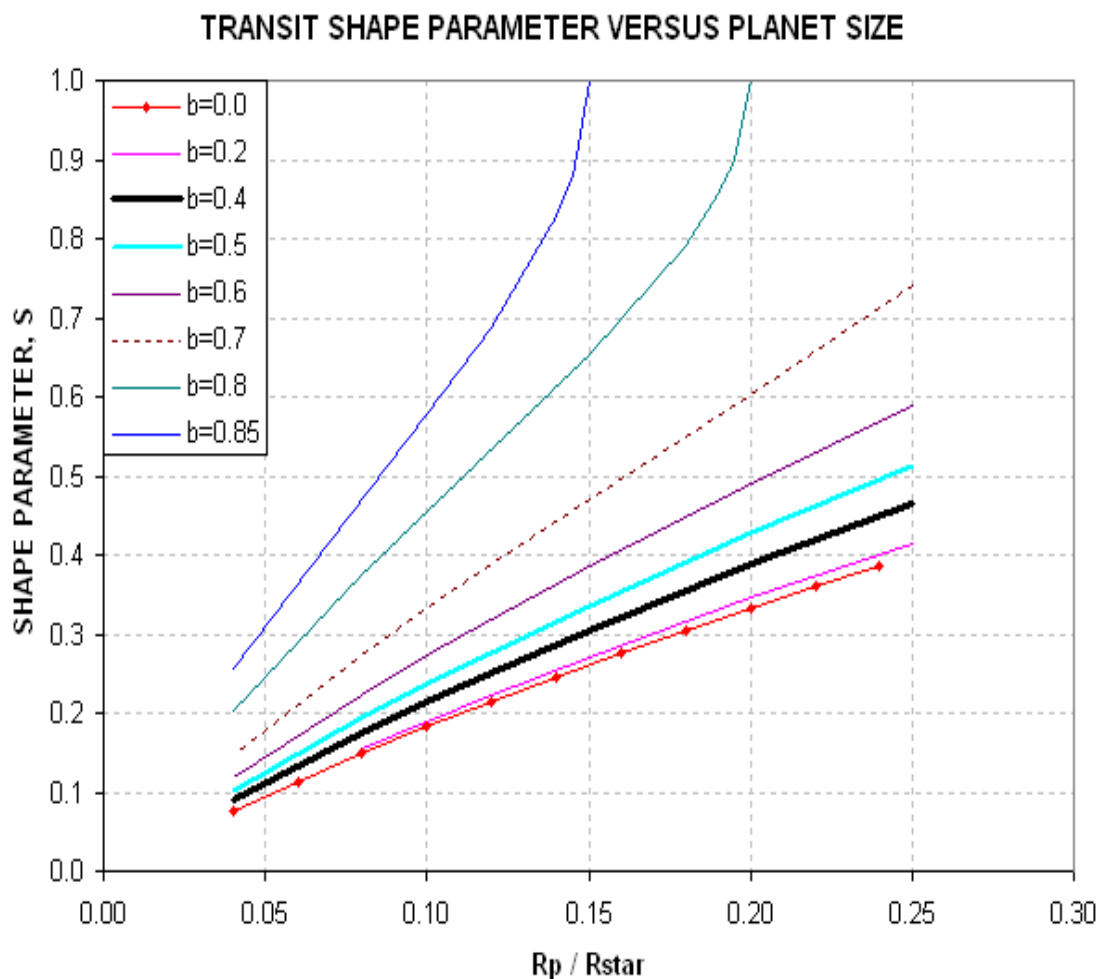


Figure D.11. Shape parameter F_p (referred to in this figure as S) for a selection of secondary sizes and center miss distances, b .

Recall that for this LC we determined that $F_p = 0.29 \pm 0.01$. The shape alone tells us that $R_p/R_{str} < 0.17$. From the previous section we derived $b = 0.40$ (the thick black trace in the above figure), so this means $R_p/R_{str} \sim 0.13$. It's not our purpose here to re-derive R_p/R_j , but let's do it to verify consistency. $R_p/R_j = 9.73 \times R_p/R_{str} \times R_{str}/R_{sun} = 9.73 \times 0.13 \times 0.99 = 1.25$. This is smaller than 1.31 derived from the transit depth, but notice that the 1.25 estimate came from the light curve shape, F_p , and extra information about miss distance. The consistency check is successful.

Our goal in this section is merely to distinguish between exoplanet light curve shapes and EB shapes. It will be instructive to consider secondaries at the threshold of being a star versus a planet. This is generally taken to be $R_p/R_j \sim 1.5$. For such "threshold secondaries" the R_p/R_{str} will depend on the size of the star, which in turn depends on its B-V (spectral type). Let's list some examples, going from blue to red stars.

APPENDIX D – PLANET SIZE MODEL

Blue star: (B-V ~ 0.30, spectral type F1V), Rstr/Rsun ~1.5, Rp/Rstr ~0.10
 Sun-like: (B-V ~ 0.65, spectral type G2V), Rstr/Rsun ~1.0, Rp/Rstr ~0.15
 Red star: (B-V ~ 1.20, spectral type K6V), Rstr/Rsun ~0.7, Rp/Rstr ~0.22

The following figure shows the dependence of "threshold secondary" Rp/Rstr versus B-V.

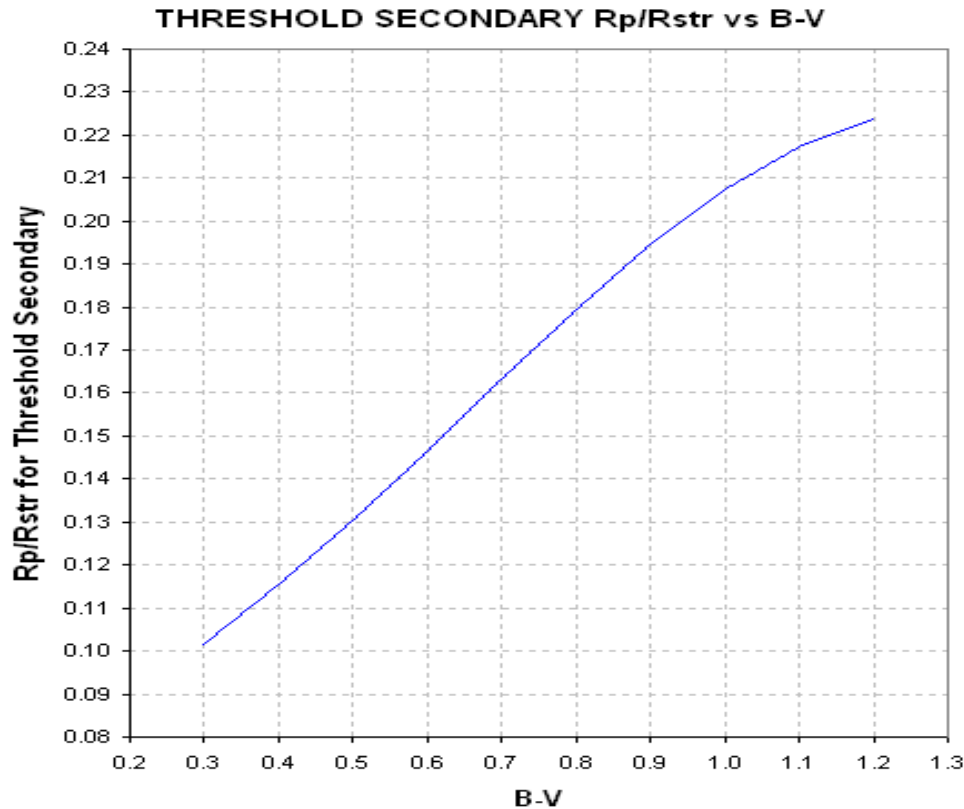


Figure D.12. Relationship of "threshold secondary" Rp/Rstr versus B-V.

In order to use the above figure to distinguish between exoplanet versus EB shapes we need to take into account the primary star's color. For example, if B-V is sun-like, we can draw a vertical line at Rp/Rstr = 0.15 and consider everything leftward to be exoplanets and everything rightward to be EBs. Similarly, for any other B-V a vertical line can be placed upon this figure to show the domains where exoplanets and EBs are to be found, as Fig.'s D.13a,b illustrate.

Since XO-1 has $B-V = 0.66 \pm 0.05$ we can use the left panel to determine that it must be an exoplanet. This determination is based on the shape parameter, **Fp**, and the miss distance that was determined from Section 1 (plus the B-V color for XO-1). Even if we hadn't performed a solution for miss distance we could say that's it was likely that the B-V and S information was in the exoplanet domain. If **Fp** were slightly smaller, say 0.27, then there would be no dispute about the light curve belonging to an exoplanet. (Well, all this is subject to my model assumptions, such as the "main sequence" one.)

APPENDIX D – PLANET SIZE MODEL

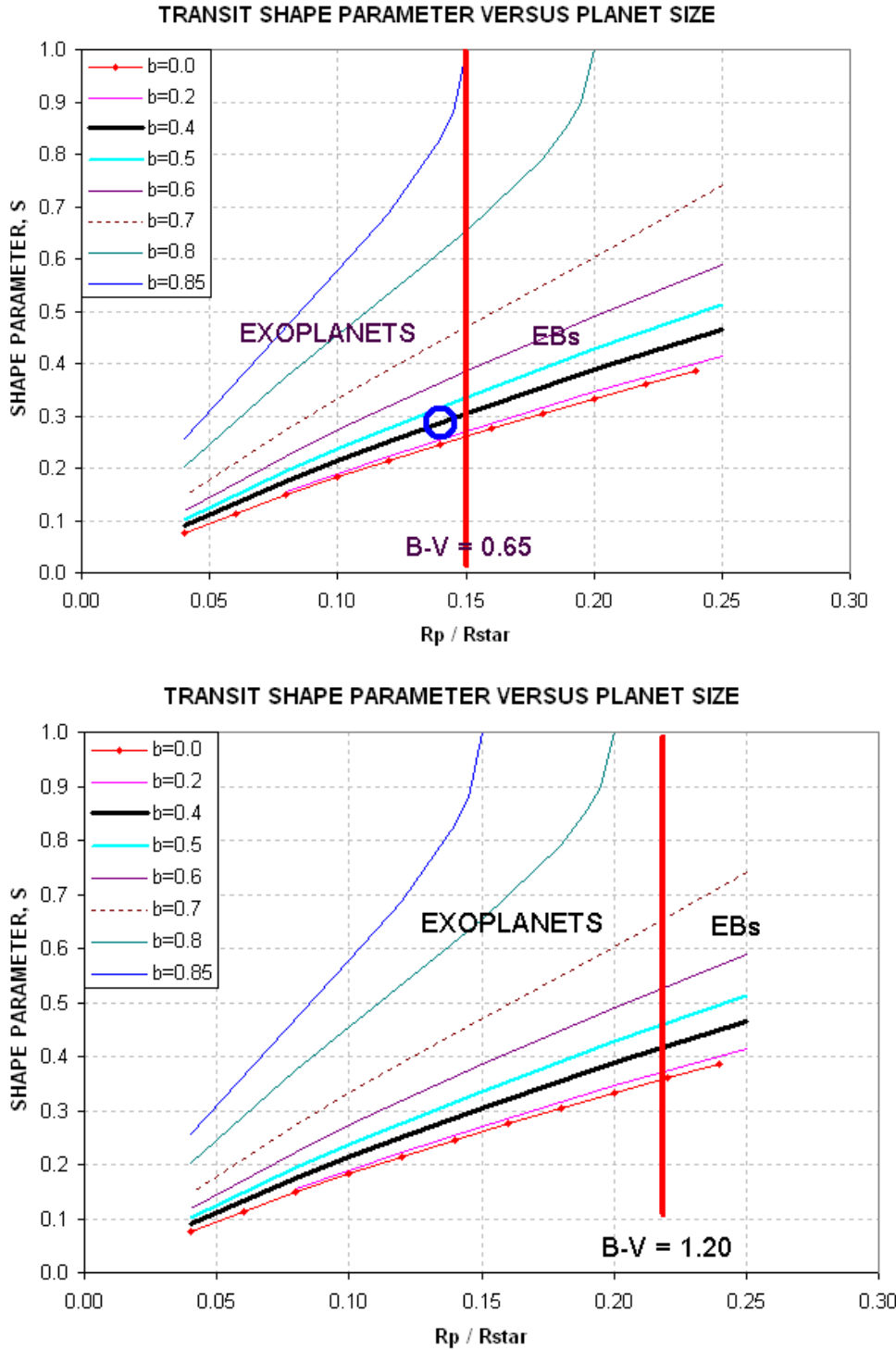


Figure D.13a,b. Domains for distinguishing exoplanets from EBs based on $B-V$, shape parameter F_p (referred to as S in the figures) and miss distance b , for two examples of $B-V$. The blue circle in the left panel is located at the measured F_p and center miss distance for XO-1.

APPENDIX D – PLANET SIZE MODEL

There's another graph that can be used for the same purpose as the previous ones, and I think it's much more useful than the graphs in the previous figure because it doesn't require knowledge about miss distance. Instead, it requires knowledge about transit depth, D , which is easily measured.

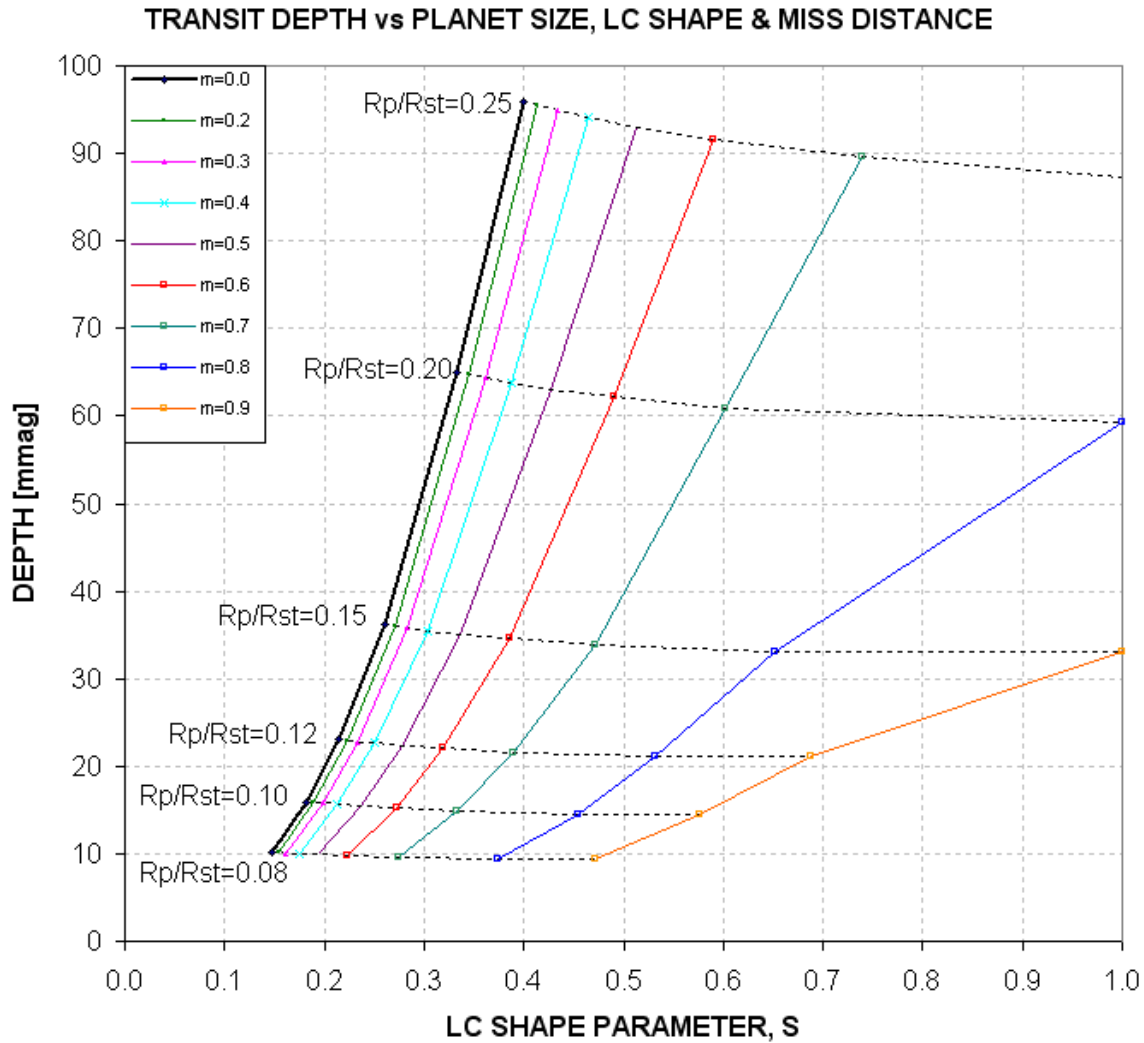


Figure D.14. Domains for exoplanets and EBs, using parameters F_p and D as input (yielding R_p/R_{str} and miss distance as answers).

This figure requires knowledge of transit depth, D , instead of miss distance. This is better since D is easily determined by casual inspection of a LC. The shape parameter F_p is also easily determined by visual inspection. Therefore, without any attempts to "solve" the LC this plot can be used to estimate R_p/R_{str} and miss distance. Then, by knowing B-V we can specify an R_p/R_{str} "threshold secondary" boundary in the figure that separates the exoplanet and the EB domains.

Consider the previous example, where XO-1 was determined to have $F_p = 0.29$ and $D \sim 24$ mmag. Given that $B-V = 0.66$ we know that a "threshold secondary" will have $R_p/R_{str} = 0.156$ (cf. Fig. D.06). Now, using the above figure, draw a trace at this R_p/R_{str} value, as in the following figure.

APPENDIX D – PLANET SIZE MODEL

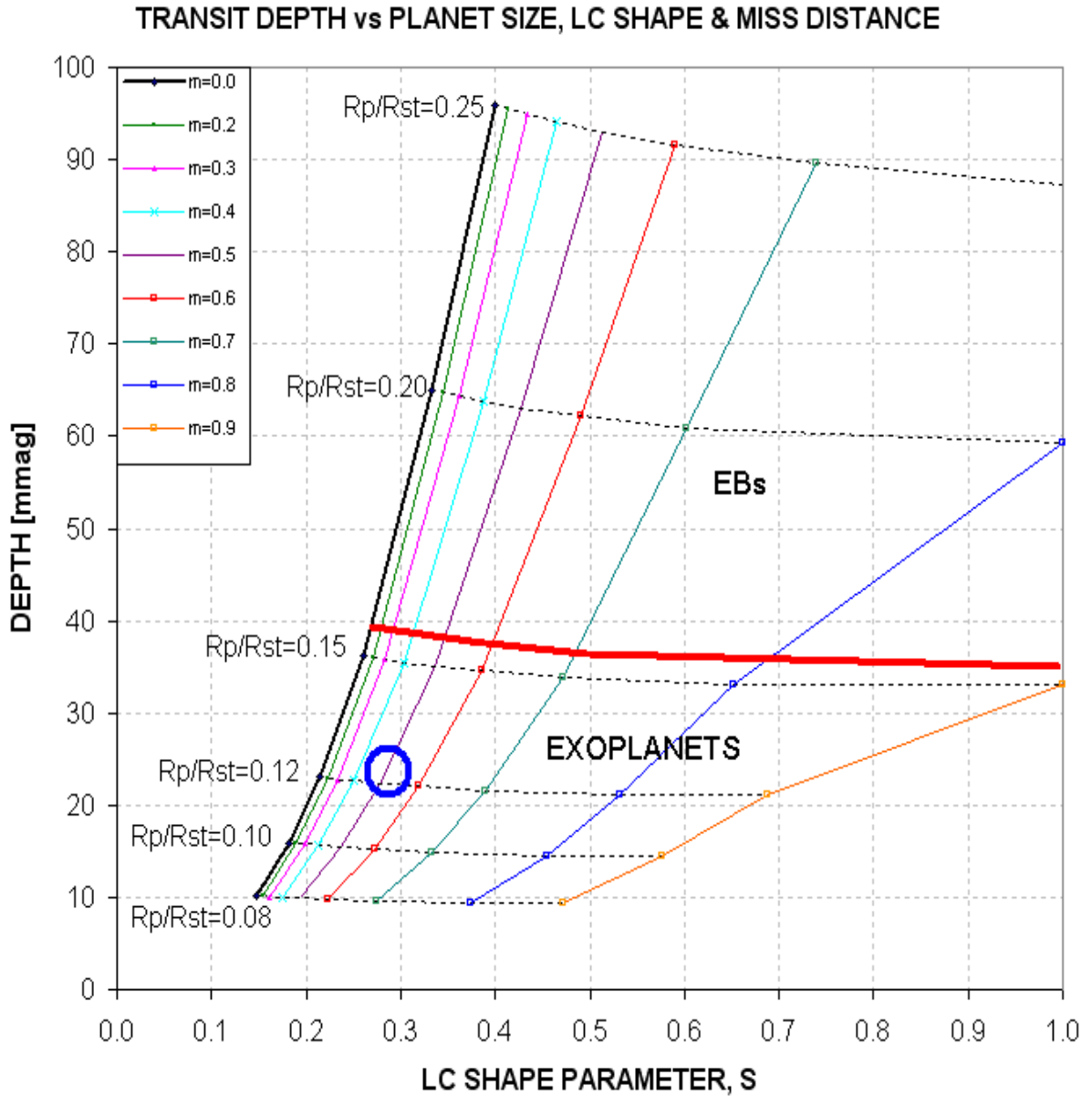


Figure D.15. Domains for exoplanets and EBs for independent variables F_p and D with a "threshold secondary" R_p/R_{str} domain separator (thick red trace) at $R_p/R_{str} = 0.16$, corresponding to $B-V = 0.66$. The blue circle corresponds to the F_p and D location for XO-1. (Note: this figure uses the symbol S for shape parameter F_p .)

From this graph it is immediately apparent that, subject to the assumptions of the model, XO-1 is an exoplanet instead of an EB. This conclusion does not require solving the LC for R_p/R_{str} , as described in Section 1. Indeed, this graph gives an approximate solution for miss distance, $b = 0.5$ (not as accurate as the solution in Section 1, but somewhat useful).

APPENDIX D – PLANET SIZE MODEL

Here's a handy plot showing "threshold secondary" boundaries for other B-V values.

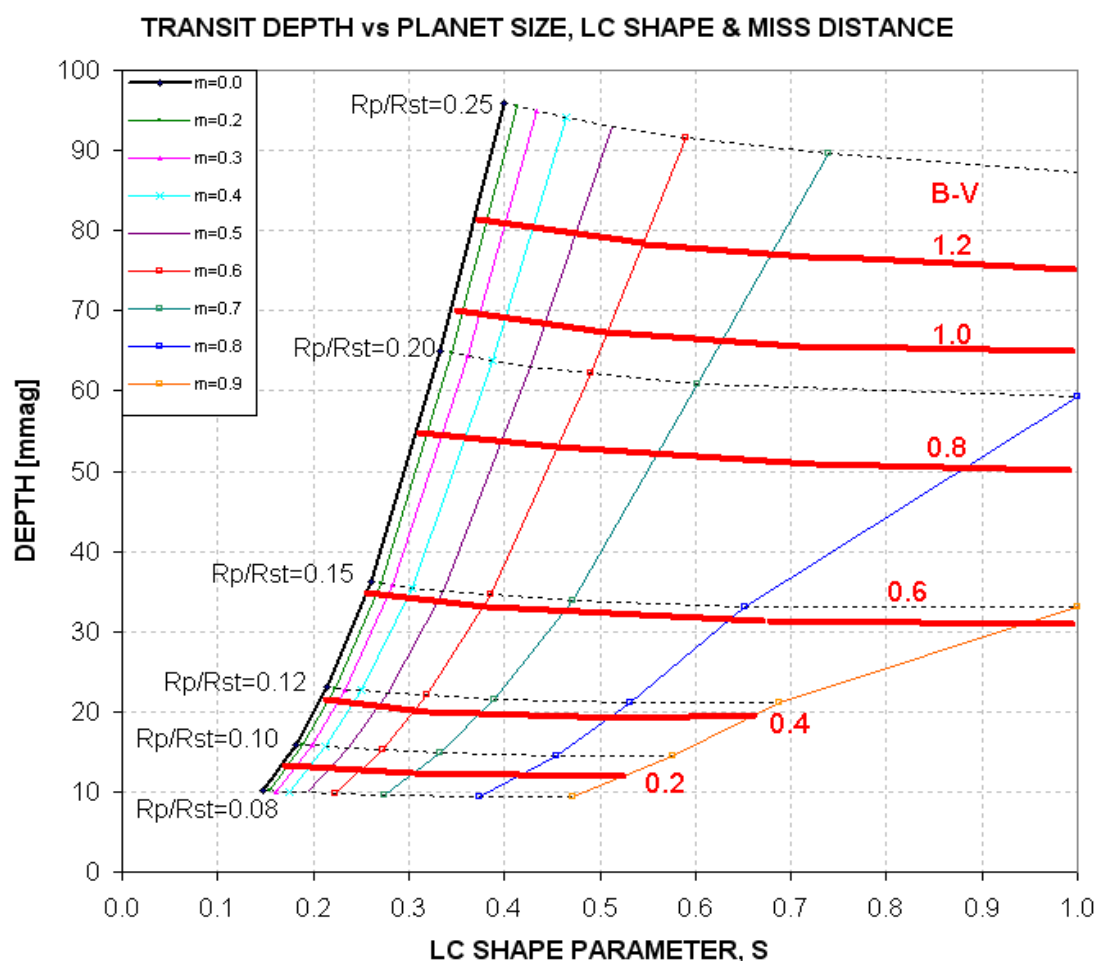


Figure D.16. The thick red traces are "secondary threshold" boundaries, labeled with the B-V color of the star, above which is the EB realm and below which is the exoplanet realm. (Note: this figure uses the symbol S for shape parameter F_p .)

This figure allows a quick assessment of a LC's association with an exoplanet versus an EB. If the LC is an EB blend, such as the triplet case described by Mandushev et al (2005), there may not be a "solution" using either the above figure or the analysis of Section 1. To assist in evaluating this it is helpful to have transit light curves for more than one filter band.

Again, this procedure is only as good a guide as the underlying assumptions, the principal one being that the star undergoing transit is on the main sequence.

3.0 SUMMARY OF TRANSIT LIGHT CURVE ANALYSIS

Much of the preceding was meant to show the underlying concepts for quickly evaluating a transit LC. It may have given an unfair impression of the complications involved. This section will skip the

APPENDIX D – PLANET SIZE MODEL

explanations for "why" and just present a sequence of what to do, like a cookbook. The figures needed by these steps are repeated after the instructions.

- 1) **Determine the candidate star's B-V (OK to derive it from J-K)**
- 2) **Use the measured LC to determine transit depth, D, and shape parameter, Fp**
- 2) **Using D and Fp to determine if the LC is likely to be an exoplanet, or EB, or neither (cf. Fig. D.17)**
- 3) **If the LC is for an EB, no more analysis is needed. If it's an exoplanet, then proceed**
- 4) **Use the Excel spreadsheet (link below) to convert B-V, D, L and filter band to Rp/Rj and miss distance,**

OR, do it manually by following the steps below...

- 4) **Determine the star's radius, Rstr, and mass, Mstr, from B-V (cf. Fig. D.18)**
- 5) **Calculate 1st iteration of Rp/Rj, using following equation:**
Secondary size, $R_p/R_j = 9.73 \times R_{str} \times \text{SQRT} [1 - 10^{-(D/2500)}]$
- 6) **Calculate secondary's orbital velocity, central transit length and miss distance using these equations:**

Planet orbital radius, $a = 1.496e8 \times [M_{str}^{1/3} \times (P / 365.25)^{2/3}]$, where P[days],
Mstr[sun's mass] & a[km]

Transit length maximum, $L_x = (R_{str} \times R_{sun} + R_p/R_j \times R_j) / (\pi a / 24 \times P)$ where
Rsun = 6.955e5 km, Rj = 7.1492e4 km

Miss distance, $b = \text{SQRT} [1 - (L / L_x)^2]$

- 7) **Using the miss distance and filter band, determine limb darkening effect, LDe (cf. Fig. D.19)**
- 8) **Convert the measured transit depth D to a value that would have been measured if there were no limb darkening, using the following eq:**

$$D' = D / LDe$$

- 9) **Repeat steps 5, 6 and 7 using D' instead of D.**
- 10) **If step 7 LDe is the same as the 1st time, then there's no need for additional iterations. The last calculated Rp/Rj is the answer. Otherwise, repeat steps 5-8 until a stable solution emerges.**

APPENDIX D – PLANET SIZE MODEL

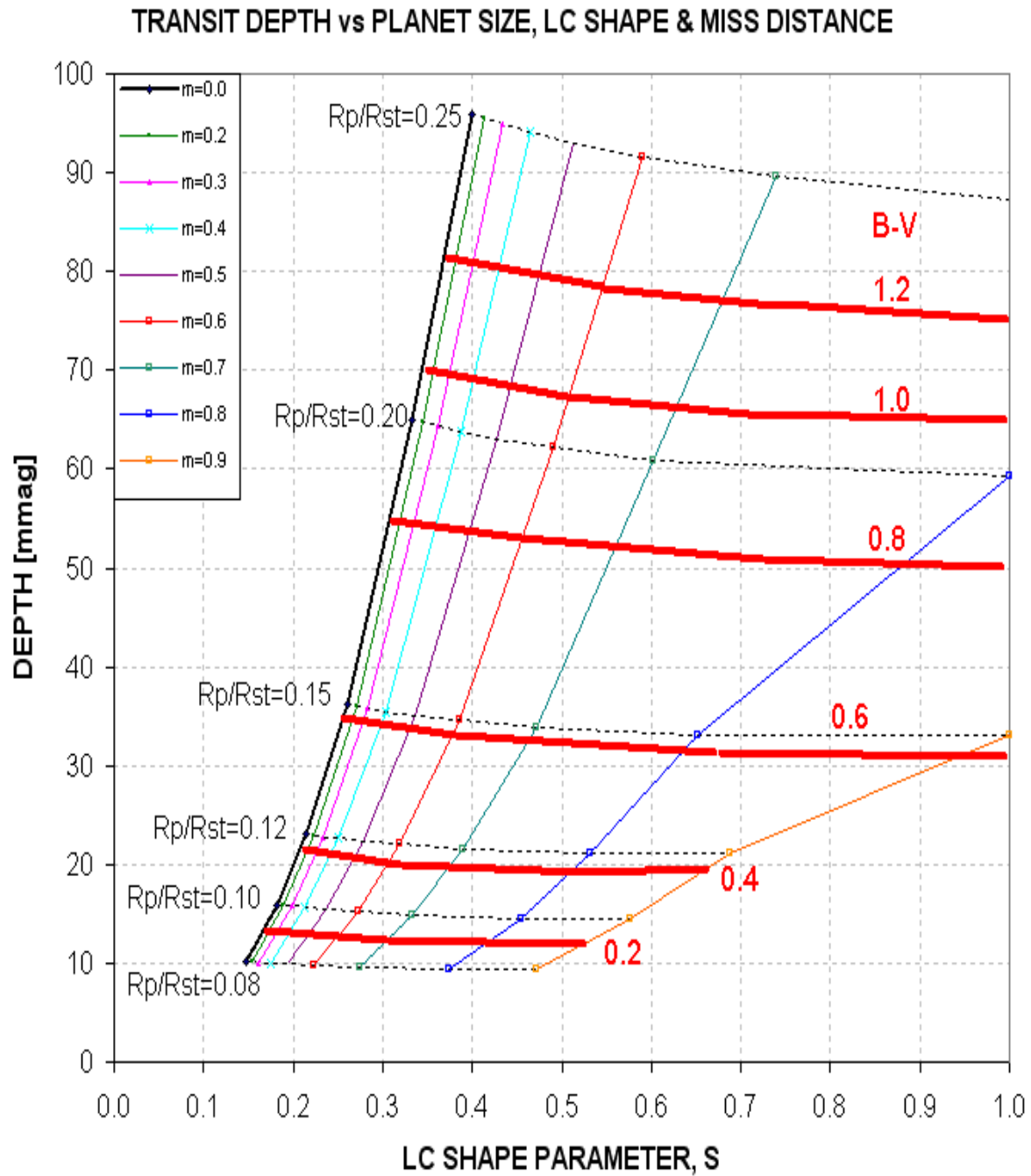


Figure D.17. If the D/F_p location for the LC is above the red line corresponding to the star's B-V, then it's probably an EB. If D/F_p is below then it's probably an exoplanet. If it is to the left of the upward sloping trace (central transit), then there's no solution, and you may be dealing with an EB blending or triple star system. (Note: this figure uses the symbol S for shape parameter F_p .)

APPENDIX D – PLANET SIZE MODEL

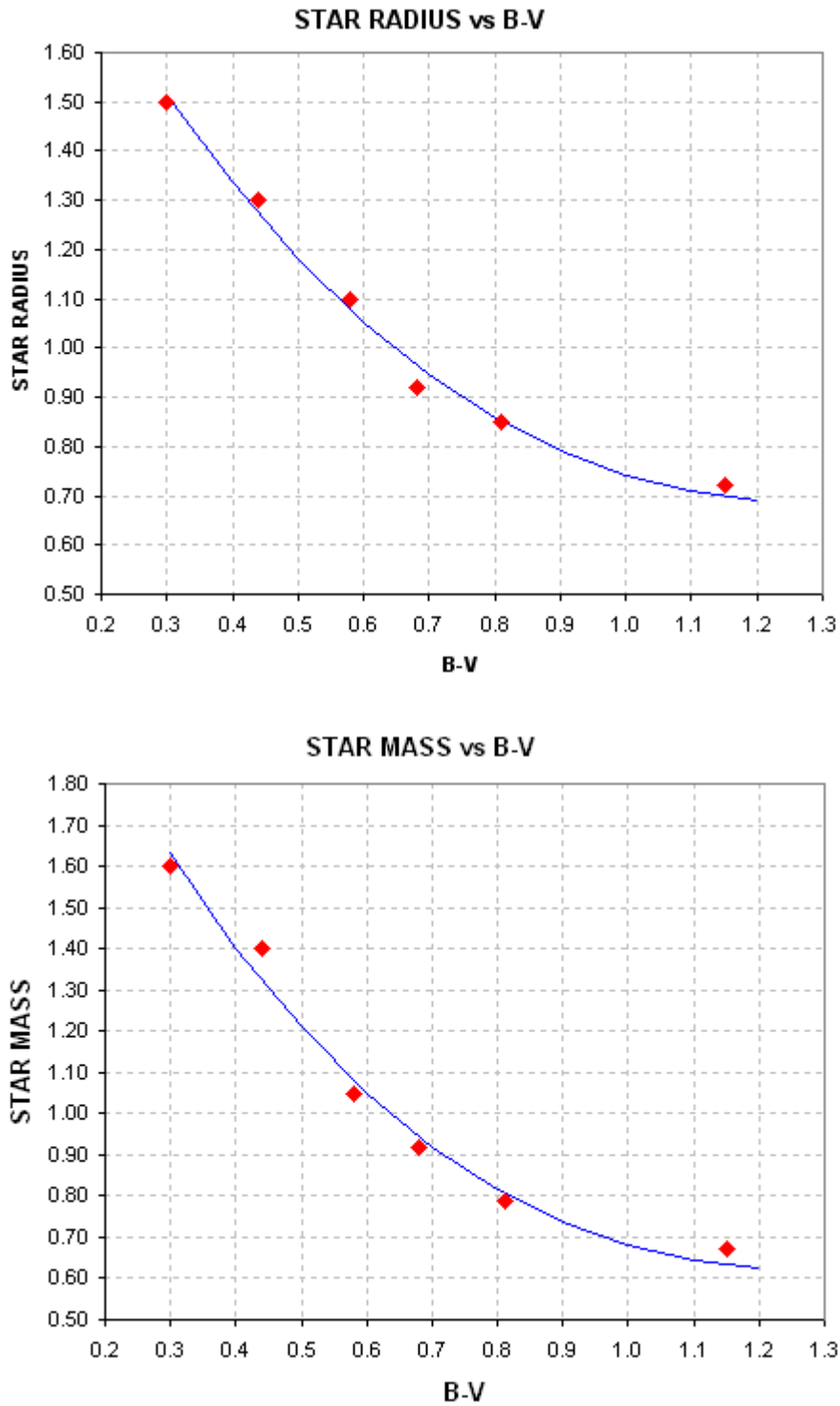


Figure D.18. *Star's radius and mass from B-V.*

APPENDIX D – PLANET SIZE MODEL

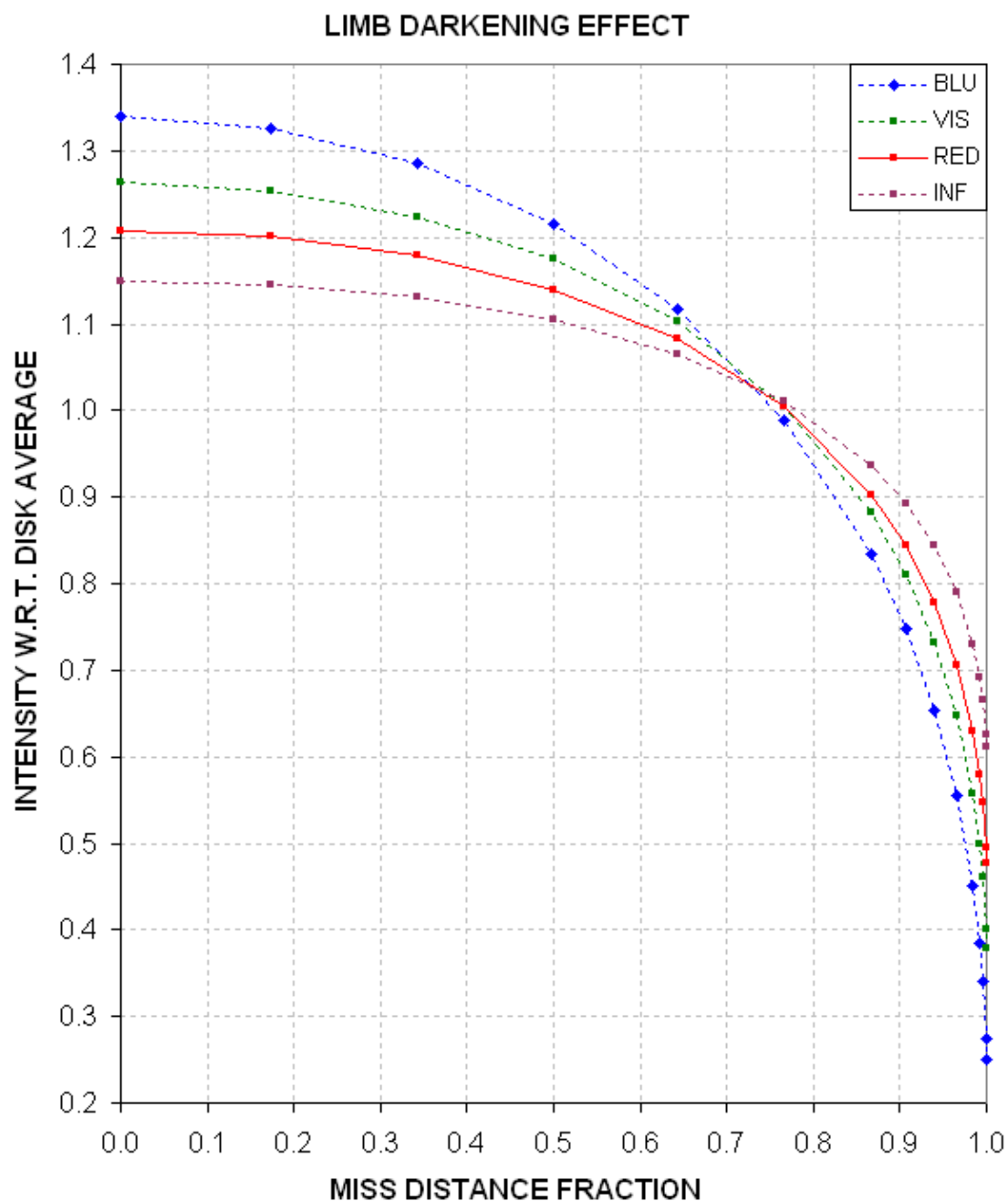


Figure D.19. *Limb darkening effect, LDe , versus transit miss distance (impact parameter) and filter band.*

This completes the summary of what is done to assess a transit LC to determine if it's due to an exoplanet or EB, and if it's an exoplanet to determine its size. The purpose of this appendix has been to demonstrate that a simple procedure can be used to guide the choice of survey candidates for a night's observing in order to avoid spending time on unlikely (EB blend) candidates.

APPENDIX D – PLANET SIZE MODEL

4.0 EXCEL SPREADSHEET

Now that you understand the concepts I can save you time by offering an Excel spreadsheet that does most of what's described in this appendix. The user simply enters light curve depth D , length L , and star color $B-V$ in the appropriate cells and the spreadsheet calculates a 3-iteration solution for R_p/R_j (provided a solution exists). Here's the link for the Excel spreadsheet that does everything described in Section 1: http://brucegary.net/book_EOA/xls.htm

	A	B	C	D	E	F	G	H	I	J	K
1	Planet Size Iteration Model (Bruce L. Gary, v7203)										
2	Enter values in the light-blue cells (B5:B8, etc) & read the result in B10, D10, etc										
3	Object: XO-1										
4	Enter filter band (B, V, R or I)	B	+/- SE	V	+/- SE	R	+/- SE	I	+/- SE	C	+/- SE
5	Depth of transit [mmag]	24.8	0.5	24.0	1.0	23.7	0.4	23.0	1.0	23.7	0.4
6	Length of transit [hr]	2.95	0.03	2.96	0.07	2.97	0.03	2.97	0.05	2.97	0.10
7	Period [days] = interval between transits	3.9415		3.9415		3.9415		3.942		3.9415	
8	Enter B-V	0.66	0.04	0.66	0.04	0.66	0.04	0.66	0.04	0.66	0.04
9											
10	Rp/Rj solution	1.29		1.29		1.31		1.31		1.31	
11	+/-	0.06		0.07		0.06		0.06		0.06	
12											
13	SE due to SE of B-V	0.06		0.06		0.06		0.06		0.06	
14	SE due to SE of D	0.01		0.03		0.01		0.03		0.01	
15	SE due to SE of L	0.00		0.01		0.00		0.00		0.01	

Figure D.20. Example of the Excel spreadsheet with XO-1 entries for several filter bands (B5:C8 for B-band, etc) and the R_p/R_j solution (B10:B11 for B, etc).

The line for SE of " R_p/R_j solution" is based on changes in D , L and $B-V$ using their respective SE. In this example note that the R_p/R_j solutions for all bands are about the same, 1.30. This provides a good "reality check" on data quality as well as the limb darkening model. Rows 13-15 show the SE on R_p/R_j due to the SE on $B-V$, D and L separately. The largest component of uncertainty comes from $B-V$. Even if $B-V$ were known exactly there's an uncertainty in converting it to star radius and mass, given that the "main sequence" of the HR diagram consists of a spread of star locations and there's a corresponding spread in the relationship between radius versus $B-V$ and mass versus $B-V$.

A future version of this spreadsheet will include a section for the user to enter a transit shape parameter value, F_p , and an answer cell will show the likelihood of S/D being associated with an exoplanet versus an EB. I also plan on expanding the limb darkening model to take into account limb darkening dependence on star color.

APPENDIX E – Measuring CCD Linearity

The maximum ADU counts that can be read out of a 16-bit CCD is 65,535. It is commonly understood that you shouldn't trust readings greater than about half this value, ~35,000 counts, due to something called "non-linearity." Whereas you can trust ratios of star fluxes when none of them have maximum counts, C_x , greater than 35,000, when one of them has a $C_x > 35,000$ it's measured flux is probably smaller than it should be. Only for a hypothetical CCD that is linear all the way to 65,535 counts can you trust star fluxes with C_x values in the range ~35,000 to 65,534 counts.

Don't believe this! I was pleasantly surprised with a measurement showing that my CCD is linear all the way to ~59,000 counts! The implications for knowing this are significant. If it's true that you can safely use the longer exposure times corresponding to C_x as high as ~59,000 counts, for example, then your observing will be more efficient (less time spent downloading images), your scintillation and Poisson noise will be lower (by up to ~40% for each image), and the importance of readout noise will be less.

I'll review the cautious reasoning that continues to lead CCD users to be wary of high C_x . Then I'll illustrate how to measure your CCD's linearity safety zone.

Cautious Conventional Wisdom

Each pixel is capable of "holding" an approximate total number of photoelectrons. The term "full well capacity" is used loosely to refer to that number. However, we must make a distinction between "full well capacity" and "linear full well capacity."

A user's manual may state that your model of CCD has a "full well capacity" of 100,000 electrons, for example. That's what the SBIG manual states for my ST-8. The manual also states that my CCD's "gain" is set so that each count represents 2.3 electrons. According to these two numbers "the well is full" at ~43,500 counts (100,000 electrons / 2.3 electrons per count). Since my CCD can produce higher counts I assume that SBIG's term "full well capacity" was a conservative way of saying that a pixel fills at a linear rate up to 100,000 electrons then becomes non-linear as it continues to fill further. In other words, I assumed the manual meant to say that my CCD's "**linear** full well capacity" was ~100,000 electrons. This would imply that my CCD might be linear up to ~43,500 counts, but I remained cautious for a long time by keeping exposures short enough that stars to be used photometrically had C_x less than ~35,000 counts. The fact that stars would produce C_x all the way up to digital saturation (65,535 counts) means that my CCD's silicon crystal pixels must be capable of holding at least 150,000 electrons at readout time ($65,535 \times 2.3$).

For a long time I neglected to measure my CCD's linearity thinking that all the specifications in the manual were compatible with the common wisdom of keeping C_x below about half scale in order to avoid non-linearity problems. I also postponed measuring linearity in the belief that it would be difficult. It isn't, and it can be fun, especially if you learn good things about your CCD.

The following methods are presented in a way that hopefully illustrates properties of CCDs and ways to explore these properties from special observations and analysis. Once this understanding has been accomplished subsequent measurements of linearity will be almost effortless.

Twilight Sky Flats Method

The simplest way to determine how high C_x can be while still being within the linear region is to expose a series of twilight sky flats using exposure times that produce maximum counts, C_x , that span the entire region of interest: 30 to 65 kct (kct = kilo-counts = 1000 counts). Any filter will work, but you'll have a "stronger" result by using the filter that has the *worst* vignetting. For me, the I-band filter is slightly worse than the others, with a faintest area to brightest area ratio = 0.79. It's not necessary to do this for other filters since one photoelectron is the same as another from the standpoint of silicon crystals in the CCD.

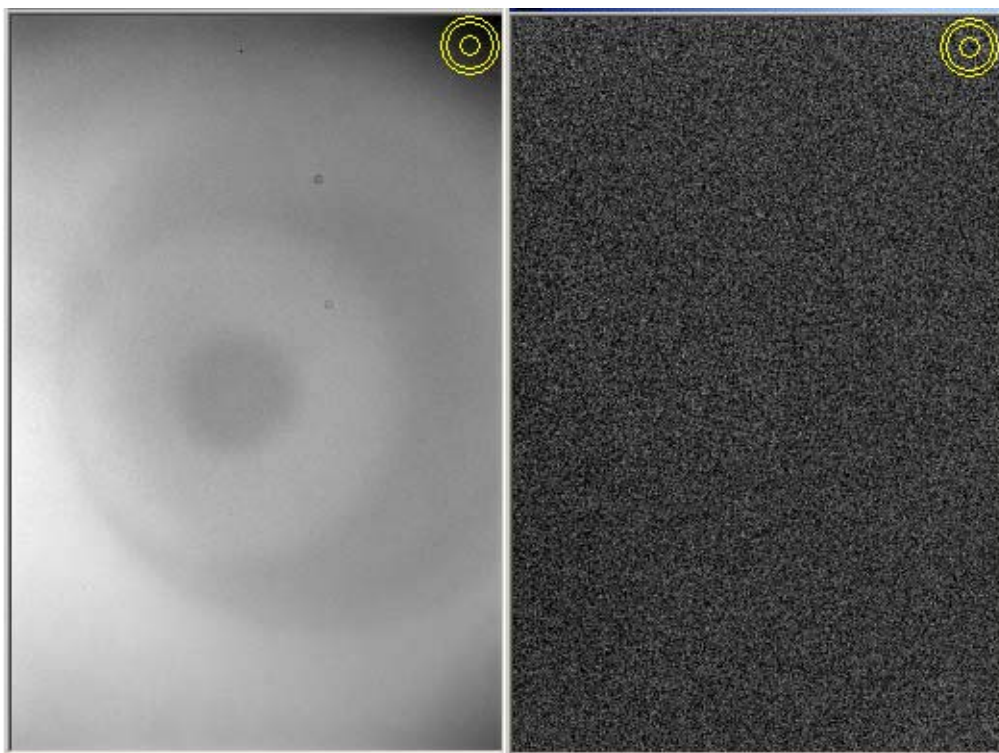


Figure E.01. *I-band flat field with $C_x = 62$ kct before and after calibration using a 34 kct C_x flat frame. The faintest area (upper-right) to brightest have a "vignette range" of 21% and 0.2%, implying that the flat field response was reduced 100-fold, to acceptable levels. The CCD appears to be "linear" even for ADU values as high as 62 kct!*

Average the images with C_x between 25 and 35 kct, which everyone will accept as being free of linearity problems. Call this a master flat for use with the brighter flat fields. Let's define "vignette range" to be a percentage version of the faintest to brightest area of the linear master flat. For example, my I-band "vignette range" is 21 % (i.e., faintest to brightest counts = 0.79).

Next, divide a bright flat by the master flat. This can be done by treating the bright flat as a light frame that must be calibrated using the master flat field. (I'm assuming all flats were made using a dark frame at the time of exposure.)

APPENDIX E – CCD LINEARITY

After calibrating all bright flat fields using the ~30 kct master flat you are ready to evaluate linearity for each. Measure the average counts for the same regions that were faintest and brightest and express their ratio as a percentage. For example, after calibrating my I-band flat that had $C_x = 62$ kct I measured the same areas that were faintest and brightest in the master flat (also the same areas that were faintest and brightest in the $C_x = 62$ kct before calibration), and got a “vignette range” of 0.21%. In other words, the “vignette range” went from 21% to 0.21% simply by calibrating using the master flat field. That’s a 100-fold improvement, and any flat with residual errors of 0.2% is good! Flat field errors may be present in both flat fields, so it cannot be concluded that both flats are good to 0.2%. The result we’re after, however, is that a flat field with counts as high as 62,000 has the same brightness distribution as the ones having a maximum count of ~35,000 counts. This can be interpreted to mean that **my CCD is linear all the way up to ~62,000 counts!**

I performed the same analyses using 4 other filters, and they all gave the same result. The only problem encountered with flats having $C_x > 55$ kct was the appearance of hot pixels at three locations (with cold pixels nearby).

Star Flux Ratio versus Maximum Counts Method

This method will involve more analysis, but it will provide more information about how your CCD responds to too much light.

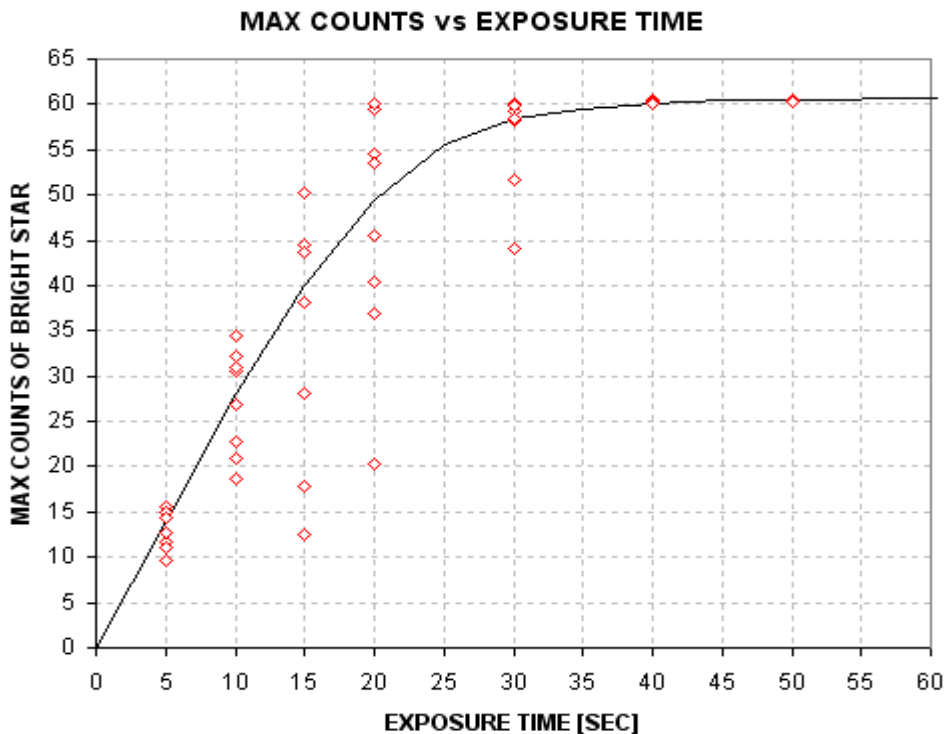


Figure E.02. Maximum counts versus exposure time for the brighter of two stars.

APPENDIX E – CCD LINEARITY

The method involves taking images of two stars in the same FOV with several exposure times. The two stars should have a flux ratio of about 2:1 (magnitude difference ~ 0.75). Be sure the stars are near zenith; otherwise you'll have to correct for extinction.

The shortest exposure time should be whatever produces $C_x \sim 10$ to 20 kct for the brightest star. I'll illustrate this method using a pair of stars near NGC 5371 with V-magnitudes ~ 9.0 and 9.7. My exposure sequence ranged from 5 to 40 seconds.

Figure E.02 is a plot of C_x versus exposure time for the brightest star. There are two things to notice about Fig. E.02. First, typical C_x flux values increase with exposure time until a "saturation" value of ~ 60 kct is reached. Second, for each exposure time below "saturation" C_x flux values have a large scatter. The scatter is produced by Poisson noise, scintillation and changes in seeing (or auto-guiding quality). This will be described later.

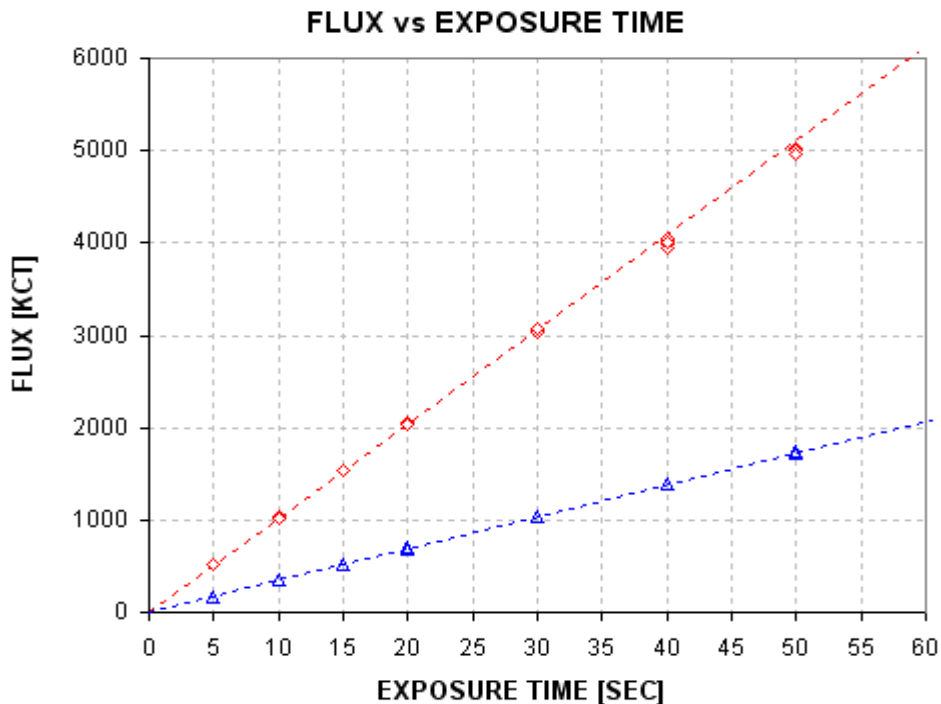


Figure E.03. Flux versus exposure time for two stars.

Figure E.03 plots star flux versus exposure time for both stars. The brighter star shows evidence of "falling below" the fitted line for exposure times 40 and 50 seconds. The fainter star agrees with its fit for all exposures. The reasons for this will become apparent shortly.

The ratio of the two star fluxes is plotted in Fig. E.04.

APPENDIX E – CCD LINEARITY

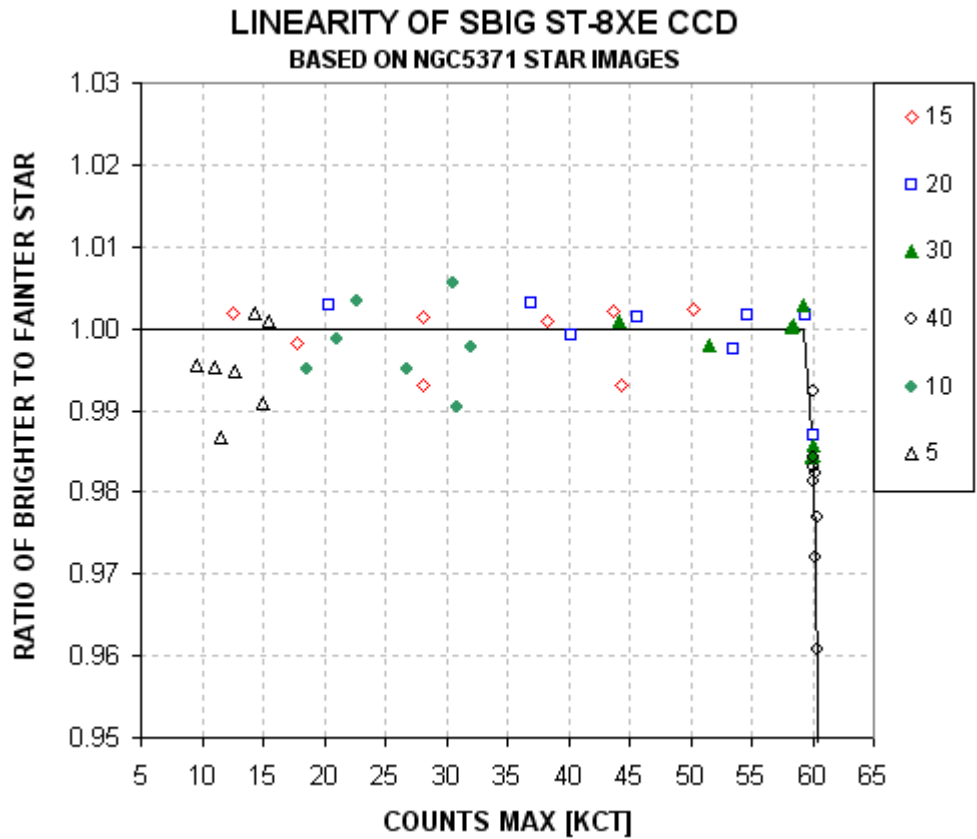


Figure E.04. Ratio of star fluxes (bright divided by faint) versus C_x . The ratio is normalized so that the average unsaturated value is 1.00. The legend shows the association of plotted symbols with exposure time.

When C_x for the bright star exceeds ~59 kct it becomes fainter than would be expected from images having lower C_x values. This suggests that photoelectrons may be “lost” when a pixel accumulates more electrons than a saturation value corresponding to 59 kct for this CCD. This result is what we’re after:

The CCD is linear for stars having $C_x < 59$ kct!

This conclusion is based on star ratios. Let’s see if we can come to the same conclusion using fluxes from just one star. Figure E.05 plots flux rate versus C_s ; “flux rate” is defined as flux divided by exposure time. As before, “flux rate” versus C_x (in Fig. E.05) suggests that the CCD is linear for $C_x < 59$ kct. The RMS scatter for most of the unsaturated data is ~1/3 %.

Figure E.03 suggests that the faint star is never “saturated” for the images under consideration. Therefore, the FWHM ratio for all images should reveal anomalous behavior for just the bright star. Figure E.06 is a plot of FWHM for the bright star divided by FWHM for the faint star.

APPENDIX E – CCD LINEARITY

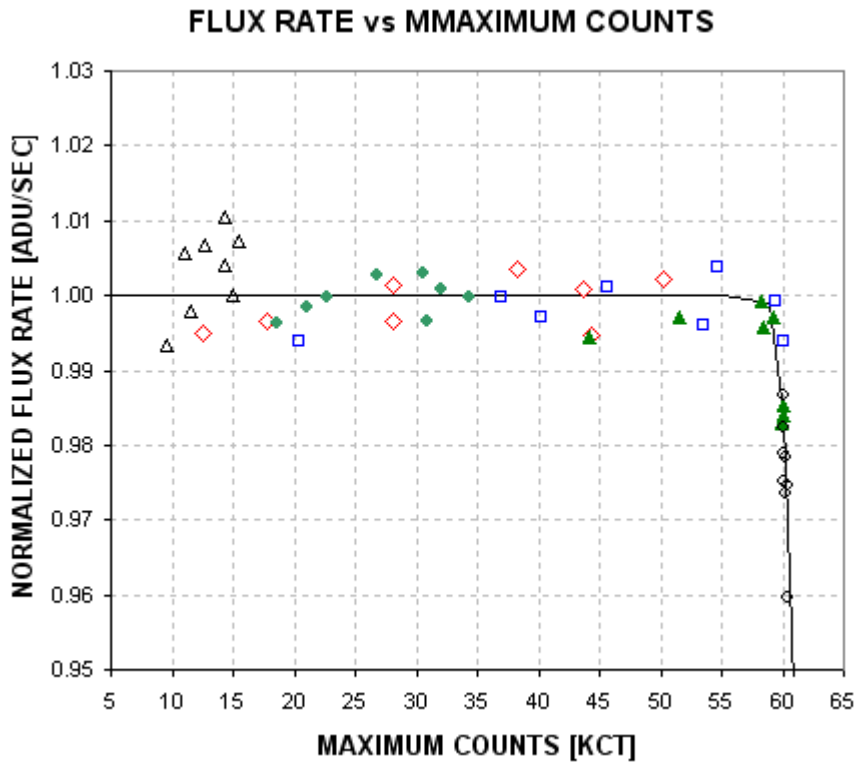


Figure E.05. Flux rate (normalized to 1.00 for unsaturated values) versus C_x , using the brighter star.

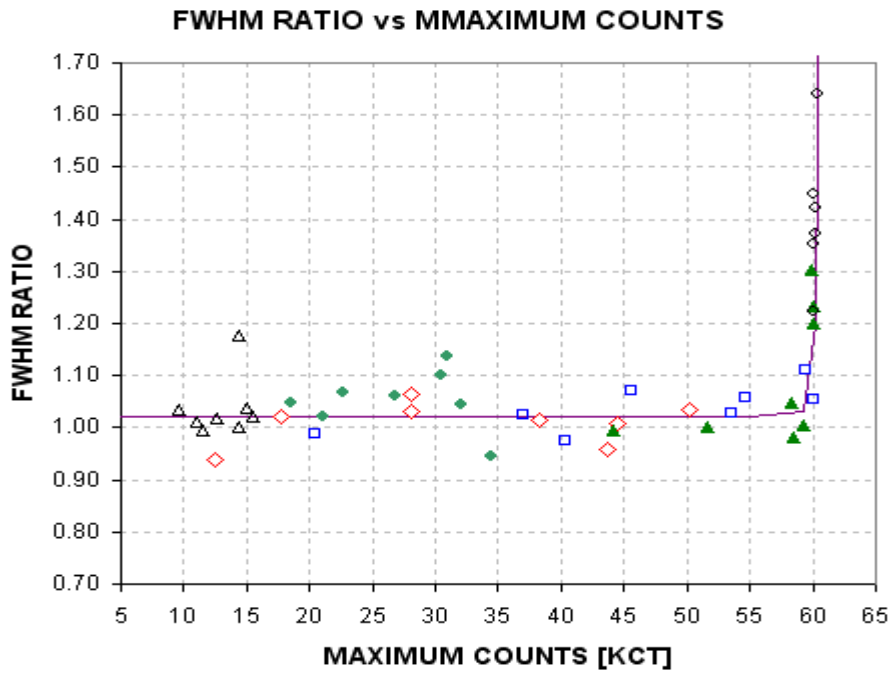


Figure E.06. FWHM for bright star divided by FWHM for faint star, versus C_x for the bright star.

APPENDIX E – CCD LINEARITY

When the bright star saturates its FWHM increases. This is what would be expected if the Gaussian shaped point-spread-function becomes “flat topped” when saturation occurs. Another way of showing this is to plot FWHM for the bright star versus FWHM for the faint star, which is shown as Fig. E.07. When both stars are unsaturated the two FWHM values are within the “box” area. Within this box both FWHM variations are correlated, suggesting that either “seeing” or autoguiding varied and affected both stars in a similar way.

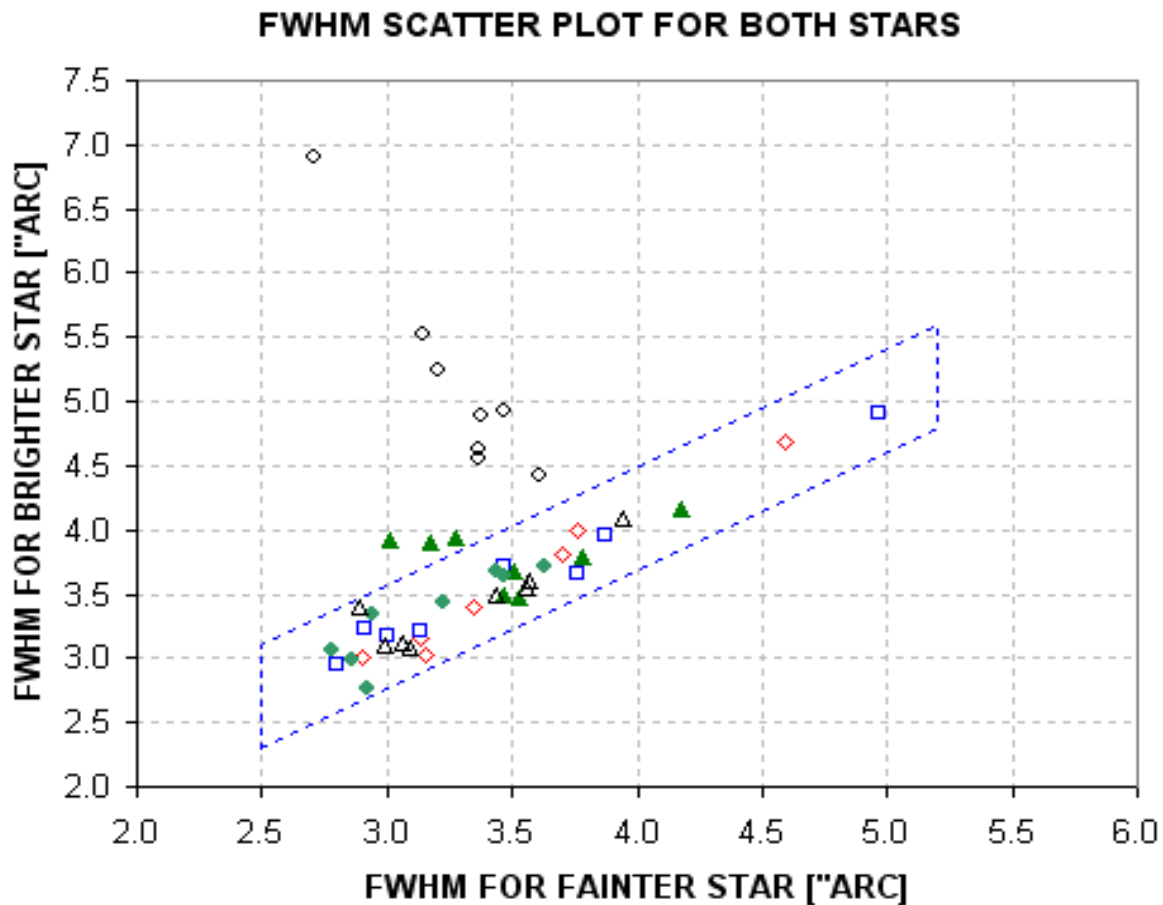


Figure E.07. *FWHM for bright star versus FWHM for faint star. The box identifies the situation of unsaturated stars.*

Whenever a star is unsaturated, established here by the condition $C_x < 59$ kct, the following simple relationship should exist: $C_x = \text{const} / \text{FWHM}^2$. As FWHM decreases C_x will increase in order for flux to remain the same. The next figure shows agreement with this theoretical relation; it also shows how C_x saturates when FWHM decreases below a specific value (different for each exposure time).

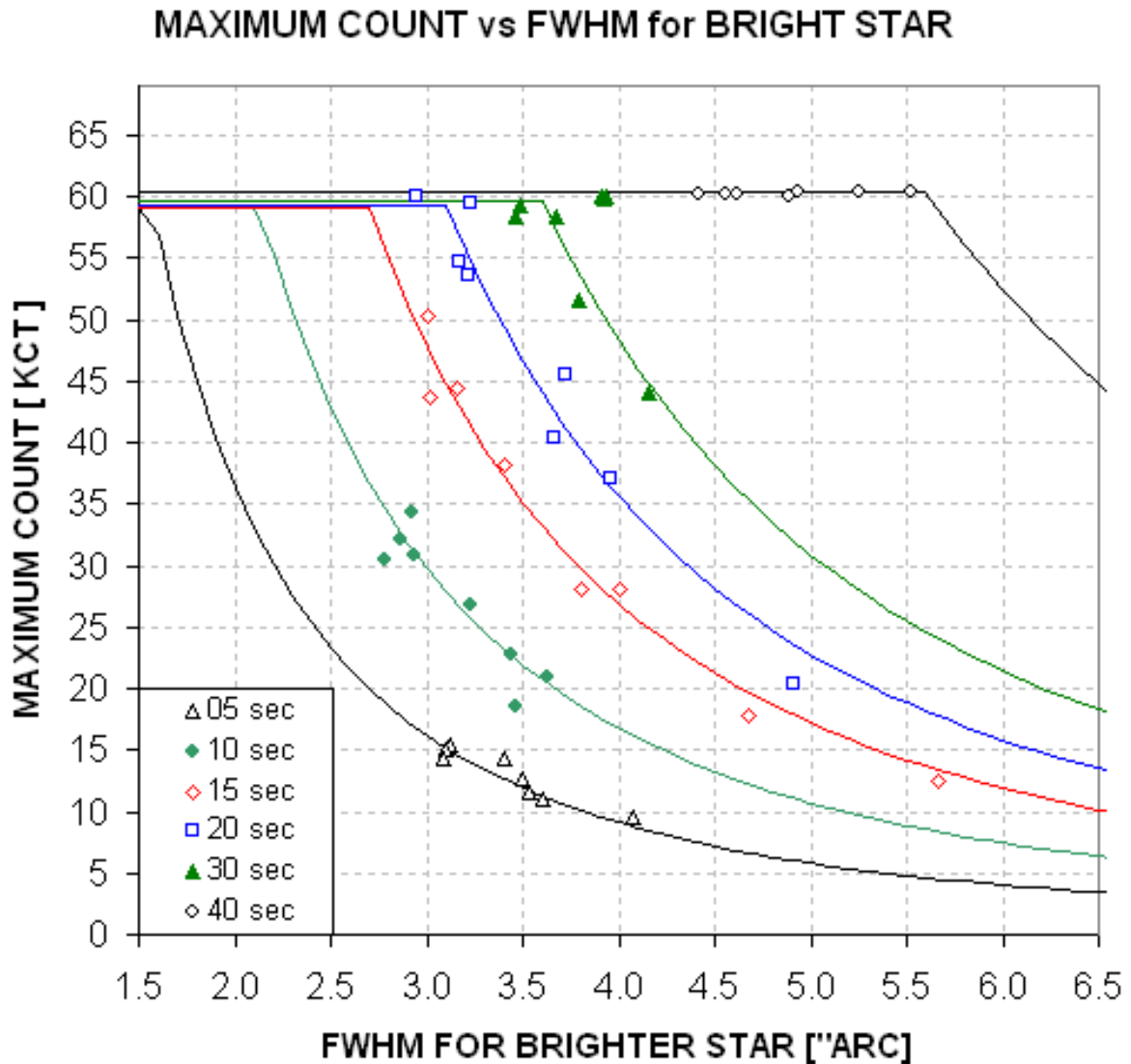


Figure E.08. *C_x versus FWHM for the bright star for a selection of exposure times (color coded with exposure times given by the legend). Model fits are explained in the text.*

This plot demonstrates that the brightest pixel for a star will increase until the pixel’s “well is full.” For this CCD “fullness” occurs when 159,300 electrons have accumulated ($59,000 \times 2.7$ electrons per ADU, where 2.7 electrons per ADU is the “gain” I measured from the same images). But what happens to photoelectrons that are added after the pixel’s well is full? In theory these additional electrons could simply migrate to nearby pixels and still be counted when the photometry measurement is made. To investigate this we need to see how flux ratio varies with exposure time.

APPENDIX E – CCD LINEARITY

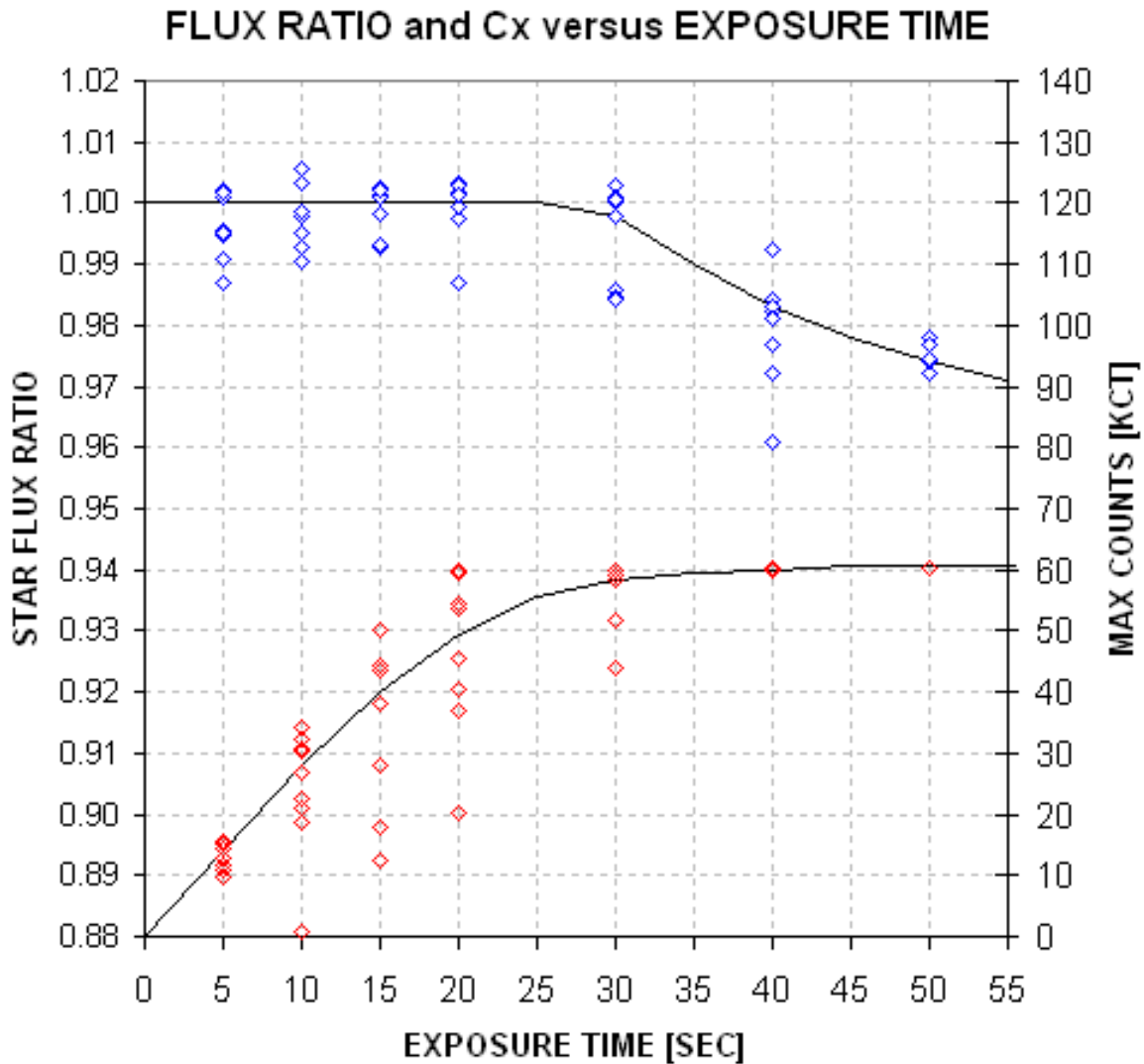


Figure E.09. Star flux ratio (blue) and bright star’s Cx (red) versus exposure time.

When exposure time is 50 seconds the bright star is “saturated” in every image; nevertheless, the ratio of fluxes is affected only slightly! This means that after a pixel’s well fills additional electrons migrate to nearby pixels, and only a small percentage are “lost.” If linearity is defined as <2% departure from linear then this CCD is linear even for conditions associated with the longest exposure images of this analysis. Figure E.10 is a point-spread-function cross-section of the bright star that is saturated in a 50-second exposure. Even this star’s image produces a flux that is low by only 2%.

The statement that the CCD is linear whenever Cx <59 kct is conservative, since saturation above this value may depart from linear by only a small amount.

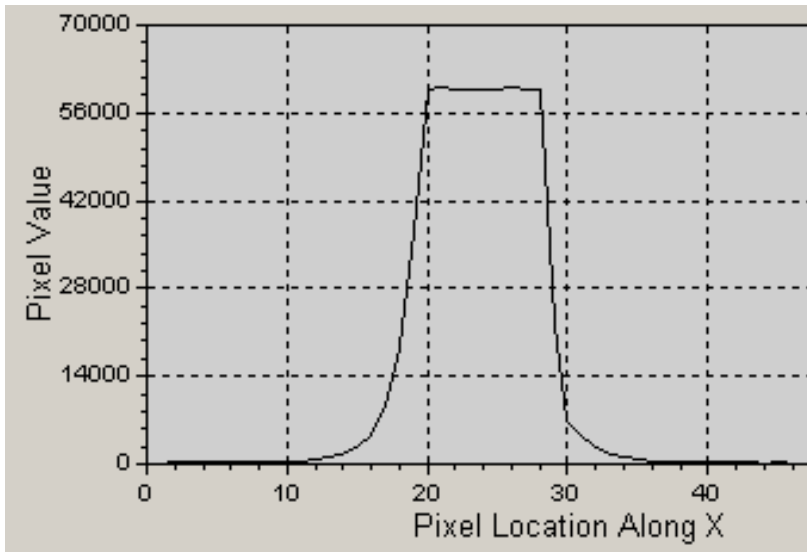


Figure E.10. PSF of a saturated star (the bright star) with $C_x = 60.3$ in a 50-second exposure. The flux of this star is only ~2% low compared with an extrapolation of what it should be based on measurements with the CCD in the linear region.

Conclusion

I conclude that flux measurements with this CCD are “linear” to ~1/3 % for all C_x up to 59,000 counts. For a CCD gain of 2.7 electrons/ADU, the 59,000 counts correspond to ~159,000 electrons. The measurements reported here therefore show that my CCD has a “linear full well capacity” of ~159,000 electrons. This is more than the “full well capacity” of 100,000 electrons listed in the manual, which shows that SBIG was being conservative in describing this CCD model.

The various methods for assessing non-linearity can be summarized:

- | | |
|---------------------------------|----------------|
| 1. Flat field method | safe to 62 kct |
| 2. Two Star flux ratio vs C_x | safe to 59 kct |
| 3. Star flux rate vs C_x | safe to 59 kct |

In no instance is there evidence to support the “common wisdom” that to avoid non-linearity effects it is necessary to keep $C_x < 35$ kct.

Each observer will want to measure their CCD linearity in ways that reveal safe C_x limits. The payoffs are significant. By adopting higher C_x limits longer exposures are permissible, and this reduces scintillation per image, it reduces Poisson noise per image, it reduces the importance of read noise and it improves “information rate” (due to smaller losses to image download time).

APPENDIX F – Measuring CCD Gain

Steve Howell's book *Handbook of CCD Astronomy* (2000) presents a way to measure CCD gain using only bias frames and flat frames. I'll embellish his description in ways that could be helpful for typical amateur hardware.

I suggest making 3 pairs of bias frames, and 3 pairs of flat frames in quick succession. (Only one pair of each is needed to get one gain measurement, but 3 pairs allows for a way to estimate the accuracy of the result.) Crop all of them the same way to preserve the flattest part of the flat field. Cropping may also be influenced by the desire to avoid known bad pixels.

Sum and difference each pair, calling the sums Bs and Fs and calling the differences Bd and Fd (where B denotes bias frames and F denotes flat field frames). In performing a difference be sure to specify that the image processing program adds a fixed amount of counts to all pixels (such as 100 counts); if you don't do this about half the pixels will be zero and this will ruin the SE calculation. In performing a difference between flats subtract the lower value flat from the higher value flat (to assure that all pixel values are above zero). Check the "minimum" value to be sure it's not zero; if it is, then repeat the image subtraction with the specification that a fixed level be added to all pixels. Read the standard deviation of the difference images and call them SEb and SEf. With this nomenclature, each pair can be used to calculate CCD gain according to the following formula:

$$G = (Fs - Bs) / (SEf^2 - SEb^2)$$

Where (repeating) Fs is the average level of the sum of two flat fields, Bs is the average level of the sum of two bias frames, SEf is the SE of the difference between the same two flat fields and SEb is the SE of the difference between two bias frames.

As a bonus "read noise" can be calculated from:

$$\text{Read Noise} = G \times SEb / \text{sqrt}(2)$$

Maybe you'd like some values to compare with. When I did this for my 5-year old SBIG ST-8XE, using cropped versions of the middle ~50% area, I get the following:

Fs avg = 85328, 89173, 95628
Bs avg = 213, 209, 213
Fd SE = 177.43, 181.35, 185.49
Bd SE = 9.80, 9.79, 9.77

The first group gives $G = (85328 - 213) / (177.43^2 - 9.80^2) = 2.71$ electrons/ADU. Groups 2 and 3 give $G = 2.71$ and 2.78 electrons/ADU. The average of these 3 determinations is 2.73 ± 0.03 electron/ADU, which is the best estimate of gain with this simple pairing. For greater accuracy other pair combinations can be used, and other flat field and bias field images can be added to the analysis.

APPENDIX F – CCD GAIN

Calculating read noise:

$$\text{Read Noise} = 2.73 \times 9.80 / \text{sqrt}(2) = 18.9 \text{ electrons for the first group.}$$

The other two groups give 18.8 and 19.2, for a best estimate Read Noise = 18.9 ± 0.2 electrons. The SBIG manual states that read noise is approximately 15 electrons. It's possible my CCD has "aged." But read noise is usually not an important contributor to total error so the 19 electrons versus 15 electrons read noise won't matter. This accuracy is more than adequate for error budget calculations.

APPENDIX G – Plotting Light Curve Data

This appendix has two parts. The first part is about combining noisy data and a warning about plotting “running averages.” The second part is a “rant” about error bars.

Combining Noisy Data

When you have a data set of, let's say 45 images, and they have noise greater than the signal you're looking for, it is perfectly good practice to divide the individual measurements into groups for either averaging or median combining (MC) for larger symbol over-plotting. For example, with 45 measurements you could group them into 5 groups, consisting of 9 individual data values in each group, and perform the average (or MC) on each of these groups. The new set of data is an alternative representation of the original group of noisy data, provided the only signal present is not under-sampled by use of the group data version (i.e., provided the signal changes slowly compared with the group sampled data). Each of the 5 new data points is independent of the others, in the sense that an individual datum from the original 45 contributes to only one of the 5 new data points. The new data will exhibit an RMS that is 1/3 of the original 45-data RMS. In terms of "information theory" this is equivalent to a hypothetical observation in which the exposure time for each observation was 9 times longer (during the same observing interval only 5 of these longer exposures are acquired).

Everything in the previous paragraph should be obvious. I include the paragraph because occasionally I encounter a scientist who believes that it's dishonest to display only group averages. Even when the measurements are so short that their SE uncertainty is huge in comparison with the searched-for signal, the individual data points are plotted with a ridiculous wealth of points that show absolutely nothing of interest. For such a situation it is perfectly honest to plot only group averages! The group average size should strive to be large enough to reveal the signal, while being shorter than any expected real changes in the thing being measured. If there is reason to expect “outliers” a median combine should be used for the groups instead of average, and something should be stated about how the outlier rejection threshold was chosen.

Now, consider a running average representation of the same 45 data points. This is usually accomplished by averaging an odd number of original data values at each data location. For example, doing it this way would produce almost as many running average data points as there are individual data points. If a 3-point group average is used for each of the 45 running average points then there will be 43 such running average points. If a 9-group running average is used the new data will exhibit an RMS that is 1/3 of the original 45-data RMS. However, the new set of 45 points is not equivalent to 45 measurements with 9-times longer exposure, since each of the original measurements contributes to 9 of the new group average data. Information theory states that there is no additional "information" in this more densely plotted representation of averages compared to the non-overlapping group averages of the previous paragraph. The "eye" perceives the two group average representations differently. The running average representation gives a false impression of good precision since each data point is close to its neighbor. Too much credibility is given to variations that have their origin in a single noisy datum. Plotting a running average with symbols is therefore misleading. For these reasons the only correct way to plot a running average is with a trace - either a solid line trace or a dotted or dashed line trace. This removes the false impression of good precision that is not present. Only the non-overlapping group averages should be plotted with symbols!

APPENDIX G – PLOTTING LC DATA

Error Bars

When I was a young scientist (some 40 years ago) it was common to plot error bars as “probable error” (PE). This provided a convenient way to assess a model trace’s compatibility with the data because a compatible model trace should intercept about half of the PE bars.

Gradually I noticed that papers were being published with standard error (SE) bars. This meant that to assess model compatibility with data you had to see if the model trace intercepted ~68% of the SE bars. It became customary to count the number of SE bars that weren’t intercepted by the model trace and compare this with the total number of data points. Because 32% is smaller than 50% there were fewer cases for testing compatibility (using this quick and simple method) than if PE bars were used. At the time this didn’t bother me much because there are some fundamental properties of SE bars that made them useful for other purposes.

A few years later I noticed something totally unexpected and disturbing: error bars were displayed in plots that were twice the SE! This is when I began to wonder why. It quickly became apparent to me that the observer was trying to hide poor quality data by pretending to be cautious! The culture in astronomy at that time was to never overstate how good you were; which translated to intentionally understating how good your data was. The incentive for understating data quality was especially strong when in fact data quality was poor by hiding that fact from a casual reader.

That’s when I began to lament the time when PE was king!

Summary of Rant

I could give examples of the embarrassing use of $2xSE$ bars, as well as the misuse of running averages and the ridiculous reluctance to average data, but I don’t want to embarrass my colleagues. You can find these examples on one of my web page if you search enough.

This little appendix is an appeal to please don’t misuse data by plotting running averages as points, and please don’t plot very noisy data when it should be averaged down to something approximating the size of the signal, and please don’t use non-standard error bars such as twice SE! Thanks for considering this.

APPENDIX H – Filter Playoff Observations

Summary of Results

Observations were made of CoRoT-3 on 2009.09.14 using filters CBB, NIR, V, Rc and i' rotated into place in alternation. Exposure times were set in a way that led to similar total flux (and SNR) for the target for each filter. A standard procedure was used for image processing and spreadsheet light curve optimization for each filter. Since for this 5-hour observing session there was no transit the data were fitted using a simple model with three free parameters (offset, slope and air mass curvature). RMS departure from the best model fit was used to assess measurement quality. Since exposure times ranged from 5 seconds to 32 seconds a "figure of merit" was calculated that endeavors to predict the RMS quality of what would have been measured if each filter were used exclusively during the observing session. The figure of merit is proportional to "information rate" (proportional to the inverse square-root of the predicted RMS off a model light curve) using exposure times of 48 seconds and download and settle times totaling 12 seconds (which are typical observing settings for amateur telescopes observing typical exoplanet stars). Such a figure of merit can be described as the speed with which a specific precision can be achieved. The results of these calculations show the following "speed for reaching a precision goal", presented in order of the fastest (and normalized to the slowest filter): CBB (6.3), Rc (2.9), NIR (1.7), i' (1.3) and V (1.0). For this observing situation the CBB filter was about 6 times better than the V-band filter. Since CoRoT-3 is fainter than the typical exoplanet star the same set of 500 images was re-processed with a brighter star assigned to the role of exoplanet. For a "make believe" exoplanet star with $V = 11.7$ (similar to the median for the list of 46 BTEs) the following figure of merits were determined: CBB (8.1), NIR (5.4), Rc (5.1), I' (4.6) and V (1.0). When an even brighter star was assigned the exoplanet star role ($V = 10.2$) the results were essentially the same: i' (8.1), NIR (6.8), CBB (6.2), Rc (5.4) and V (1.0).

Introduction

The observations reported here were designed to determine which filter produces the best quality light curves for typical exoplanet observing conditions using amateur hardware and software. I use my Celestron 11-inch (CPC 1100) telescope with a focal reducer placed in front of the CFW/CCD. The CCD is a SBIG ST-8XE (KAF 1602E chip). Autoguiding is performed using the second CCD chip. The CFW contains the following filters, all of which are used in this evaluation: CBB, NIR, V, Rc and i' (where CBB is a clear filter with blue blocking at ~ 480 nm, NIR is a long pass filter with turn-on at 710 nm, V is Johnson V-band, Rc is a Cousins R-band and i' is SDSS i-band). Although additional observing sessions may be used to verify the results reported here the following description of the first observing session, on 2009.09.14, shall serve to illustrate the protocol and analysis procedures for all of them.

Observation Protocol

The observing session was 4 hours long (after which the dome's low-elevation opening obstructed observations). Observations started at air mass 1.2 and data for air mass > 4.5 were not used. CoRoT-3 was observed under out-of-transit conditions. This enabled the measured magnitudes to be fitted using a simple light curve (LC) model with only three free parameters (offset, slope and air mass curvature). It was decided to employ exposure times that produced approximately the same flux for the target star (CoRoT-3) for each filter (Arne's suggestion). This led to greatly different exposure

APPENDIX H – FILTER PLAYOFF

times due to the large range of filter throughputs. Filter throughputs for all the filters I use are listed in the following table, and the exposure times used for this “filter playoff” observing session. For the chosen exposure times the star fluxes for the target were approximately the same and so were the SNR’s (although SNRs should differ slightly because sky background levels differ with wavelength).

Filter Throughput (at airmass 1.2) and Exposure Times

CLR	100%	
CBB	92%	5 sec
NIR	37%	16 sec
B	6%	
V	19%	32 sec
R	36%	14 sec
I	22%	
g'	26%	
r'	48%	
i'	37%	16 sec
z'	9%	

Images were made in the following sequence: NIR, V, Rc, i' and CBB. Exactly 100 cycles of this sequence were made (prior to the dome obstruction problem), so there are 100 images with each of these 5 filters. Autoguiding was used to maintain the star field fixed to the CCD pixel field (although some wander did occur). Master flats were made on the same night of these observations for each filter using the twilight sky (and a diffuser over the telescope aperture). A master dark frame was made at the end of the target observations (at the same CCD temperature as the target observations). A bias frame was used from a previous observing session. Focus settings were automatically adjusted to compensate for telescope tube temperature changes. Measures were taken so that all images had the same sharpness (FWHM typically 4.5 pixels). All observing was controlled by MaxIm DL (MDL).

MDL was also used for image calibration and measurement. Calibration consisted of bias, dark and flat field corrections. Hot pixels were removed from each image (25% was determined to be “safe” because it didn’t change a star’s maximum count for many tests of sharp images). Star alignment was made for all images for a filter group. MDL was then used to perform photometric measurements of the target star (CoRoT-3), the artificial star (flux the same for all images) and 27 nearby bright (unsaturated) stars. CSV files were recorded for measurements made with a selection of photometry aperture radii. It is well known that the optimum aperture size depends on SNR. Faint asteroids provide the best rotation LCs for a photometry aperture radius, r , of about 1.4 x FWHM. Bright stars produce the best LCs for r about 3 x FWHM. CoRoT-3 is of intermediate brightness for the present choice of exposure times (SNR \sim 40) so the range of photometry apertures employed was from \sim 1.8 to 3 x FWHM.

A spreadsheet was used for the rest of the analysis. Star magnitudes were converted to flux, and these were added for all 27 non-target stars in order to solve for atmospheric extinction. It was found that extinction ranged from 0.065 mag/airmass (NIR) to 0.160 mag/airmass (V-band). A search was made for which subset of the 27 stars provided the lowest RMS noise for the target. This RMS noise was calculated by comparing each target star magnitude with the median of its 8 closest neighbors, and a standard deviation of all such differences (with a small correction for the fact that 8 isn’t infinity) was used to establish an RMS for the filter of interest and for the entire observing session. The next step was to model-fit the target magnitudes using as a criterion the lowest RMS deviation from the model,

APPENDIX H – FILTER PLAYOFF

called RMSmodel. When a good model fit was found a search was made of reference star sub-sets that produced the lowest RMS deviation from the model. This step usually did not lead to many changes in reference star selection (a change would occur if systematic effects differed among the 27 candidate reference stars). If a large improvement in fitting the model was achieved by changing the reference star sub-set then another iteration was performed: model fit for minimum RMSmodel, search for a better reference star subset (that reduces RMSmodel). It is rare to have to iterate like this more than once. I view the final model and reference star subset to be a “global minimum” solution.

Observational Results

The next figure is a “solution” for CBB.

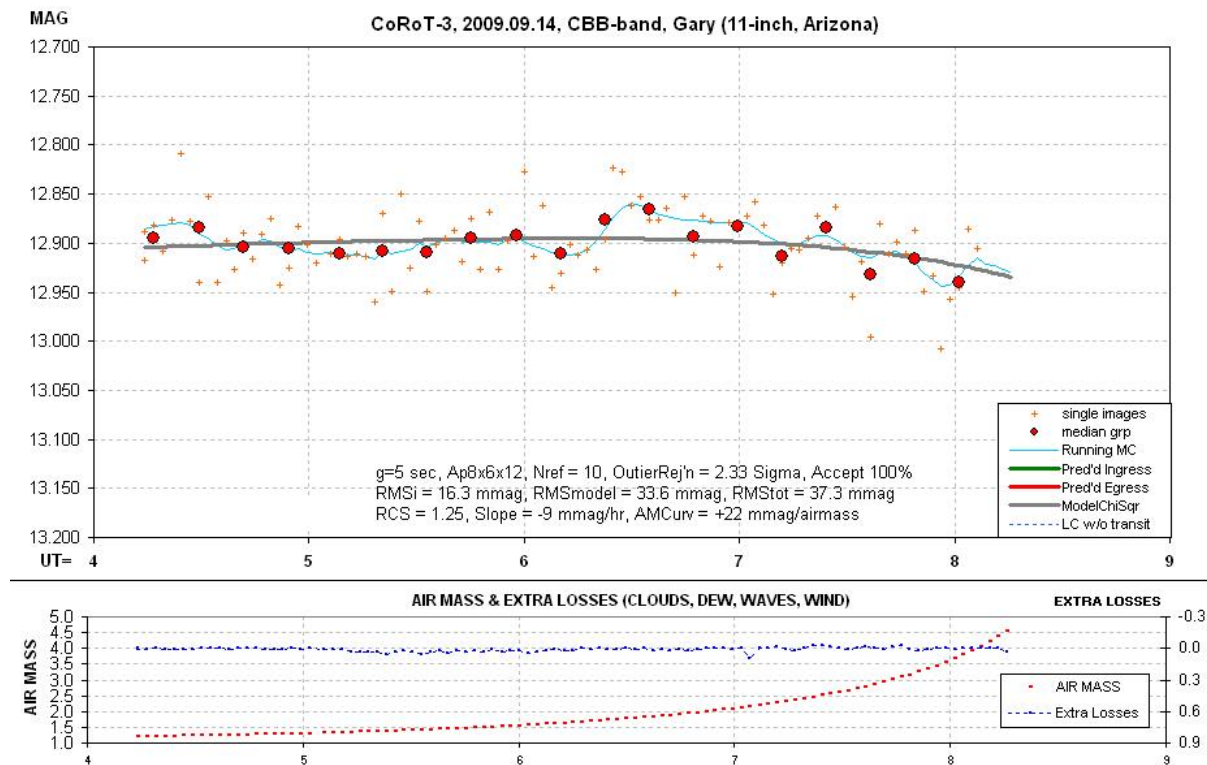


Figure H.01. Example of a LC solution. The filter is CBB and exposures were 5 seconds.

The other filters produced similar looking light curves. The target is bluer than average ($B-V = +0.91$), so most of the references stars must be redder. Notice that air mass exceeds 3.0 during the last 40 minutes, and this, combined with the difference in color of the target and references stars, must cause the model fit to require an “air mass curvature” component.

The next table summarizes the measurements for each filter image set. The first row (below filter names) is “throughput” – or percentage of light from a typical star that reaches the CCD when a filter that is in the optical path compared to the amount of light reaching the CCD when no filter is in place. The second row is the median FWHM of the images. The third row shows the photometry aperture radius that produced the best result. By best result is meant the smallest RMS departure from the LC

APPENDIX H – FILTER PLAYOFF

model fit (where all of the following parameters were optimized: sub-set of candidate reference stars used for reference, model offset, slope and airmass curvature). The next row shows atmospheric extinction. The next row shows RMS_i, which is the RMS of measurements with respect to the median of the 8 nearest neighbors. This noise is for a short timescale, and if systematics vary slowly they will not affect RMS_i. Next is RMS_{model}, which is the RMS deviation of differences with the best fitting model LC. This RMS can be thought of as the orthogonal sum of RMS_i and RMS_{sys} (systematics). Therefore, by orthogonally subtracting RMS_i from RMS_{model} we arrive at RMS_{sys}, shown in the next row. Exposure time, *g*, is shown in the next row. Info/image is “information per image”, calculated from the inverse square of RMS_{model}. The next row converts RMS_{model} and exposure time to “Precision per minute of observing time” under the assumption that one exposure is made each minute with an exposure time of 48 seconds (which allows 8 seconds for download and 4 seconds for autoguider re-acquisition). This row is calculated by multiplying RMS_{model} by the square-root of *g*/48. Finally, a Figure of Merit is calculated by multiplying a constant by the inverse square of the previous row. The constant is chosen so that the V-band filter has a Figure of Merit equal to one. This Figure of Merit can be viewed as the speed with which a specific precision can be achieved. For example, if a precision of 27.6 mmag per minute of observing time is chosen as the goal, then using the V-band filter this level of precision can be achieved in 1 minute. If the Rc-band filter were used this level of precision could be achieved 2.93 times faster (or 20 seconds, neglecting for now that short exposure times incur a duty cycle penalty). When the CBB filter is used specific level of precision can be achieved 6.3 times faster than if the V-band filter were used.

Star V = 13.3	CBB	NIR	VIS	RED	i'	Data of 20090914
Throughput	92	37	19	36	37	%
FWHM	3.8	4.3	4.4	5.1	4.3	pixels
PhotApRadius	8	8	10	8	10	pixels
K'	90	65	160	115	75	mmag/airmass
RMS _i	16.7	19.5	17.6	15.2	21.7	mmag per image
RMS _{model}	34.1	36.9	33.8	29.8	42.5	mmag per image
RMS _{sys}	29.7	31.3	28.9	25.6	36.5	mmag per image
<i>g</i>	5	16	32	14	16	sec
Info/image	1.13	1.02	1.20	1.52	0.75	Arbitrary units
Precision/Minute	11.0	21.3	27.6	16.1	24.5	mmag (per minute)
Figure of Merit	6.27	1.67	1.00	2.93	1.26	Speed reaching a goal

Figure H.02. Summary of filter playoff results for the CoRoT-3 (*V* = 13.3).

There are some instructive things to notice about this table. The values of RMS_i should decrease with increasing exposure time, according to $1/\sqrt{g}$, if we're in the “faint star” domain – where stochastic noise (thermal, sky background, etc) is dominant. The values for RMS_{sys}, however, should not change with exposure time since they are a component of systematics that presumably varies slowly with time (as the star field slowly moves over the CCD field, for example) and some components of systematics will be approximately the same for each filter.

RMS_i consists of two major components: Poisson noise and scintillation noise. It is always interesting to keep track of the importance of scintillation noise in order to know how to fine-tune observing strategy. Although the level of scintillation can change greatly from night to night, or even on hour timescales, it's worth asking what a typical scintillation level should be for the observing conditions of this case study. According to Dravins et al (1998):

APPENDIX H – FILTER PLAYOFF

$$\sigma \approx 0.09 \times D^{-2/3} \times \sec(Z)^{1.75} \times \exp(-h/h_0)/(2g)^{1/2}$$

where sigma is RMS fluctuation (fractional intensity), D is telescope diameter (cm), sec(Z) is air mass, h is observing site altitude (meters) and g is exposure time (seconds). All observations reported here have the same D and h, so this equation becomes:

$$\text{Sigma [mmag]} = 5.8 * \text{AirMass}^{1.75} / \text{sqrt}(g)$$

The highest scintillation level is predicted for CBB-band near the end of the observing session; during the last 40 minutes the scintillation level is predicted to be ~ 23 mmag. Inspection of the RMSi(t) plot shows an increase at this time, being ~38 mmag (instead of 32 mmag before then). These two RMSi values are consistent with the predicted scintillation increase. For the other filters and exposure times predicted scintillation was never significant.

It is interesting to note the relation between “Precision per Minute” and filter throughput.

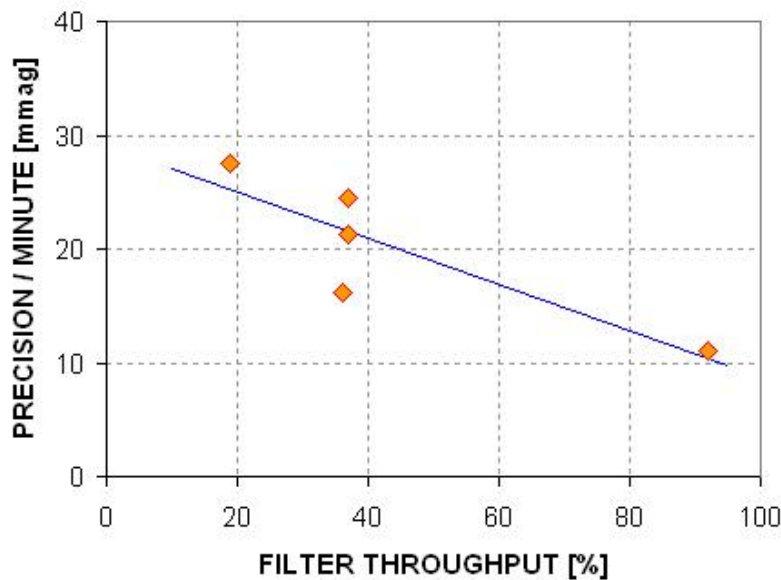


Figure H.03. Precision/Minute versus filter throughput (13.3 magnitude star and 11-inch aperture).

The message of this plot is “The greater the filter throughput the better the precision!” This may simply be a consequence of observing a faint target (SNR ~ 40 for all filters). This result suggests that optimum filter choice may depend on target brightness, and the results so far are what we can expect for the faint regime. It is therefore not surprising that for this example the Figure of Merit is correlated with filter throughput. Just because the CBB filter is optimum for faint exoplanet stars doesn’t mean it will be optimum for bright exoplanet stars.

APPENDIX H – FILTER PLAYOFF

Fortunately, the set of images used in the analysis so far can be used to evaluate Figure of Merit for a brighter star. This can be done by simply selecting a brighter star for treatment as the “target.” That’s the goal of the next section of this appendix.

Average BTE Brightness Target Star Analysis

The following figure shows two other stars that can serve as surrogate exoplanet stars in OOT mode available for use to evaluate Figure of Merit versus star brightness.

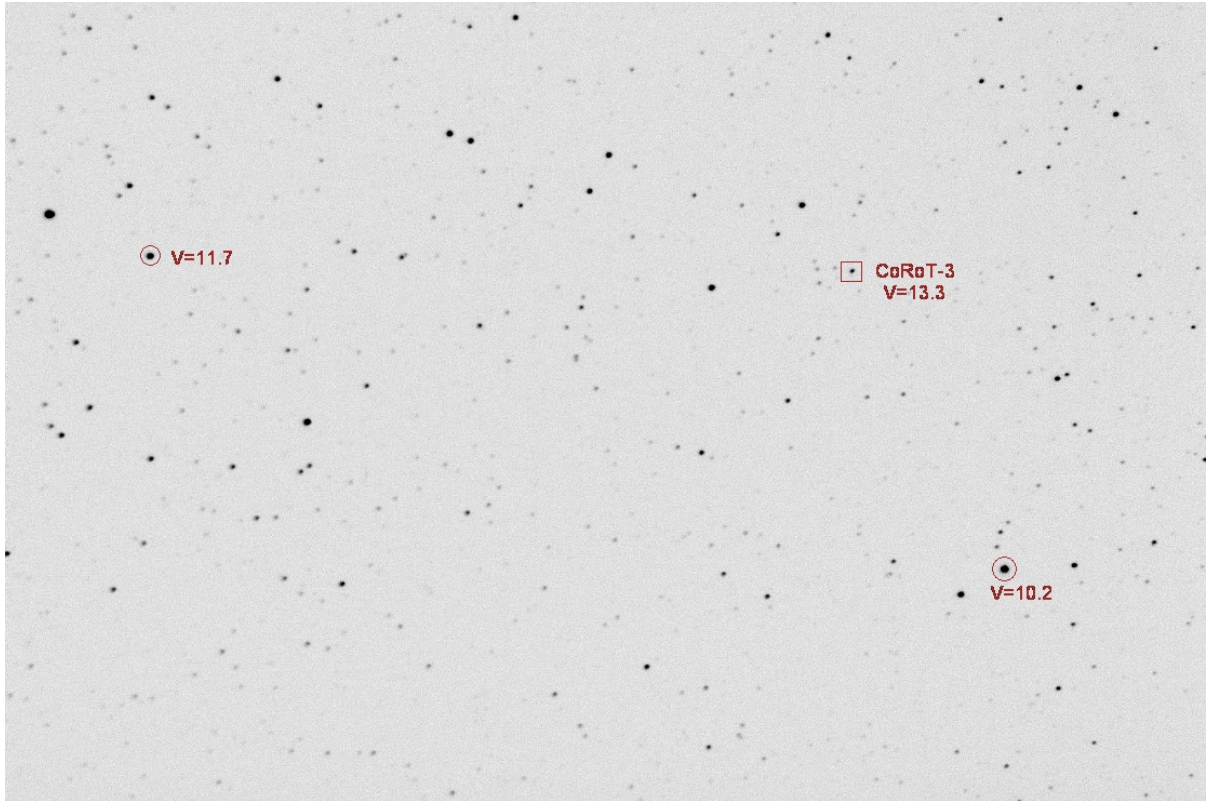


Figure H.04. *CoRoT-3 FOV, 22x14 ‘arc, showing two stars brighter than CoRoT-3.*

The star labeled V=11.7 is 1.6 magnitudes brighter than CoRoT-3 and is also close to the median brightness of the list of 46 known BTEs. It will be used to determine filter performance in a way analogous to what was done in the previous section.

The same procedure used for CoRoT-3 was used with the V-mag = 11.7 star. As expected the LC quality for this brighter star is better than for the 13.3 magnitude exoplanet star. The next figure is the LC using the NIR filter.

APPENDIX H – FILTER PLAYOFF

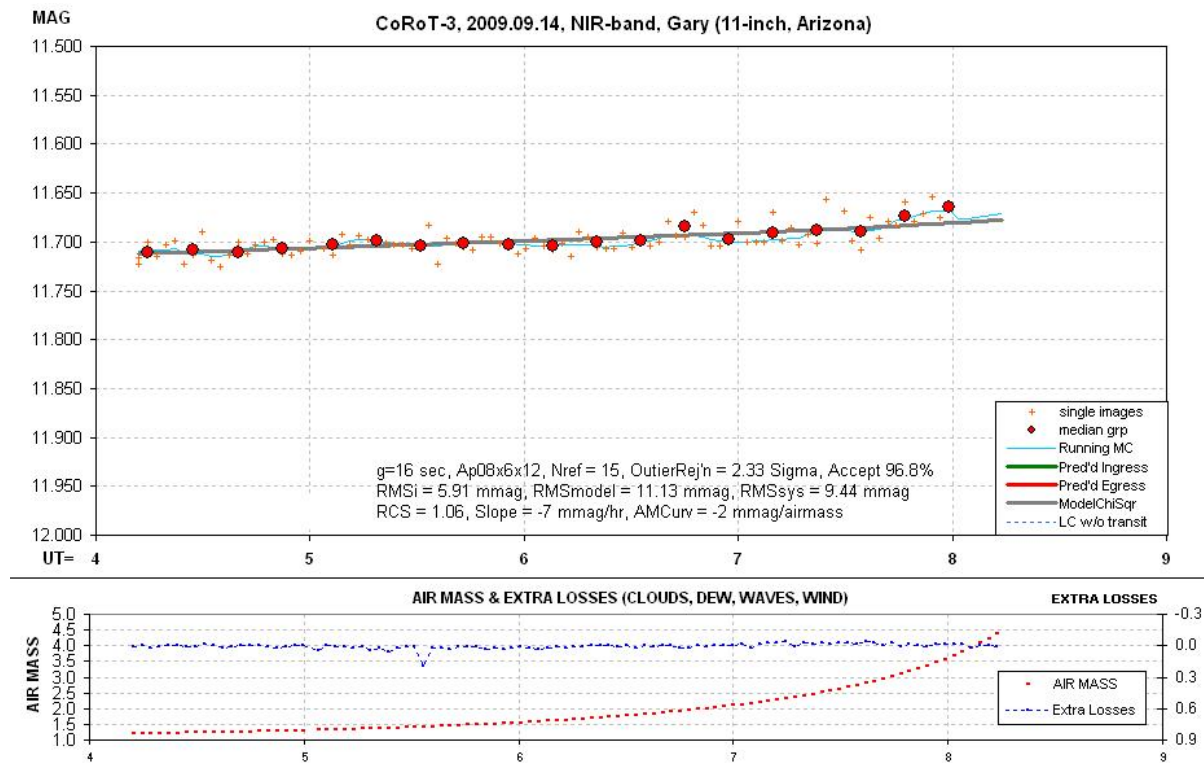


Figure H.05. NIR filter LC for the V-mag 11.7 star.

The following figure summarizes results for this star for the 5 filters.

Star V = 11.7	CBB	NIR	VIS	RED	i'	Data of 20090914
Throughput	92	37	19	36	37	%
FWHM	3.8	4.3	4.4	5.1	4.3	pixels
PhotApRadius	8	8	10	8	10	pixels
K'	90	65	160	115	75	mmag/airmass
RMSi	8.15	5.91	14.7	5.86	5.86	mmag per image
RMSmodel	16.33	11.13	18.4	12.3	12.05	mmag per image
RMSsys	14.2	9.4	11.1	10.8	10.5	mmag per image
g	5	16	32	14	16	sec
Info/image	3.75	8.07	2.95	6.61	6.89	Arbitrary units
Precision/Minute	5.3	6.4	15.0	6.6	7.0	mmag (per minute)
Figure of Merit	8.10	5.45	1.00	5.10	4.65	Speed reaching a goal

Figure H.06. Summary of observations of a star with V = 11.7, similar to typical BTE.

The highest Figure of Merit is obtained using the CBB filter, but the NIR, Rc and i' filters are all a close second. The V-band filter is the slowest choice for achieving useable LCs.

Precision per Minute is not as strongly correlated with filter throughput as it is for the fainter star, as the next figure shows.

APPENDIX H – FILTER PLAYOFF

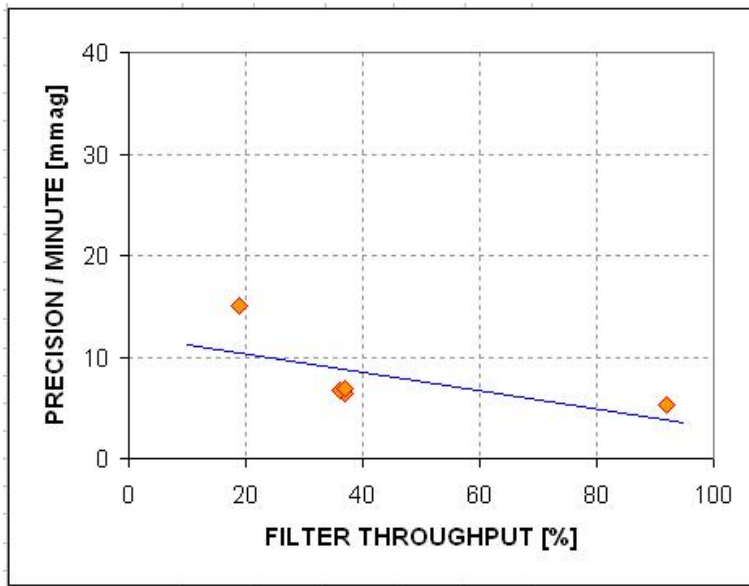


Figure H.07. Precision performance versus filter throughput for the $V = 11.7$ star.

Scintillation is predicted to be more important for the brighter star simply because other stochastic noise levels are lower (whereas scintillation level is the same for all stars, regardless of their brightness.) The scintillation levels for each filter will be the same as calculated above, for fainter CORoT-3. As stated above, the highest scintillation is expected for the CBB images, with a low of 3.6 mmag for the first few hours and an average of ~ 23 mmag during the last 40 minutes. A plot of $RMS_i(t)$ shows a rise from ~ 12 mmag during the first few hours to ~ 25 mmag near the end of the observing session. This could be explained if scintillation near the end was ~ 22 mmag, which is close to what is expected from the Dravins et al (1998) scintillation model. Scintillation levels for V-band ranged from 1.4 mmag to 9.2 mmag, and these are small enough to have only small effects on the observing session averages.

For given levels of noise and scintillation, if we ignore the effect of duty cycle on exposure time, longer exposure times don't reduce the effect of scintillation when considering "information rate" – or Precision per Minute of observing time. In other words, the average of 10 short exposures will have the same level of scintillation noise as one exposure 10 times as long. This concept is commonly understood for other stochastic noise levels (such as thermal noise, sky background noise, etc), but when the issue is scintillation there is a tendency to forget the concept and mistakenly recommend long exposures to reduce scintillation.

Brighter Than Average BTE Target Star Analysis

Finally, let's consider a star brighter than most exoplanets to see if CBB continues to outperform the other filters. The $V = 10.2$ star, shown in Fig. A.04, has been processed using the same procedure used for the two fainter stars. The LC performances for the i' and V filters are shown in the next two figures.

APPENDIX H – FILTER PLAYOFF

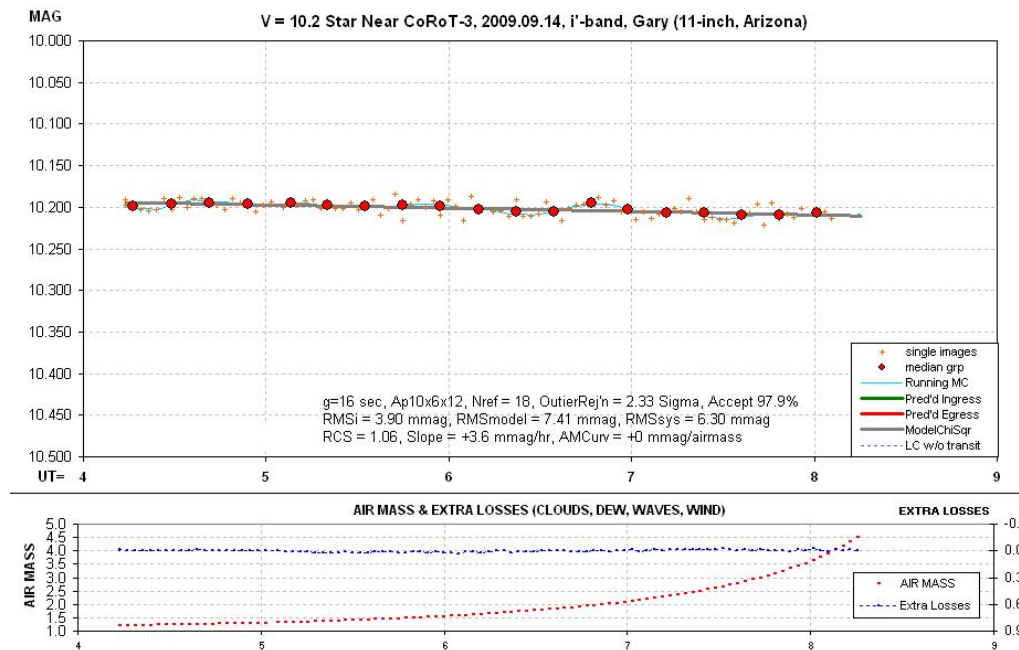


Figure H.08. *i'*-band light curve for the $V = 10.2$ star.

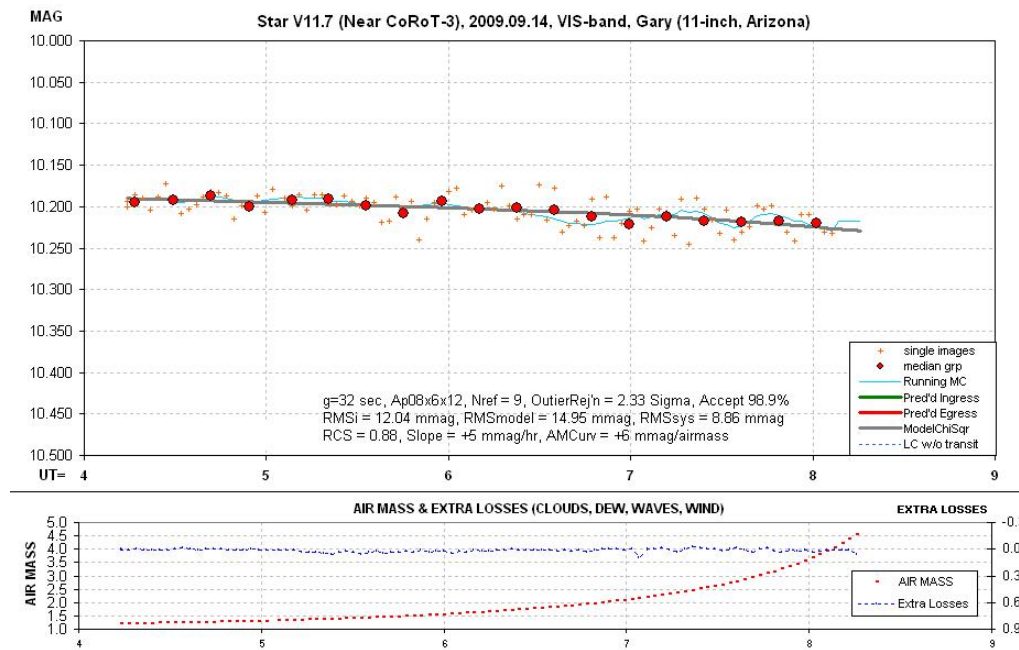


Figure H.08. *V*-band light curve for the $V = 10.2$ star.

It's apparent from visual inspection that the *i'*-band light curve is a better quality one than the *V*-band light curve. This is also borne out by the quantitative measurements, shown in Fig. A.09.

APPENDIX H – FILTER PLAYOFF

Star V = 10.2	CBB	NIR	VIS	RED	i'	Data of 20090914
Throughput	92	37	19	36	37	%
FWHM	3.8	4.3	4.4	5.1	4.3	pixels
PhotApRadius	8	8	10	8	10	pixels
K'	90	65	160	115	75	mmag/airmass
RMSi	8.43	3.68	12.04	5.08	3.9	mmag per image
RMSmodel	15.24	8.09	14.95	9.75	7.41	mmag per image
RMSsys	12.7	7.2	8.9	8.3	6.3	mmag per image
g	5	16	32	14	16	sec
Info/image	4.31	15.28	4.47	10.52	18.21	Arbitrary units
Precision/Minute	4.9	4.7	12.2	5.3	4.3	mmag (per minute)
Figure of Merit	6.16	6.83	1.00	5.37	8.14	Speed reaching a goal

Figure H.09. Summary of observations of a star with $V = 10.2$, brighter than a typical BTE star.

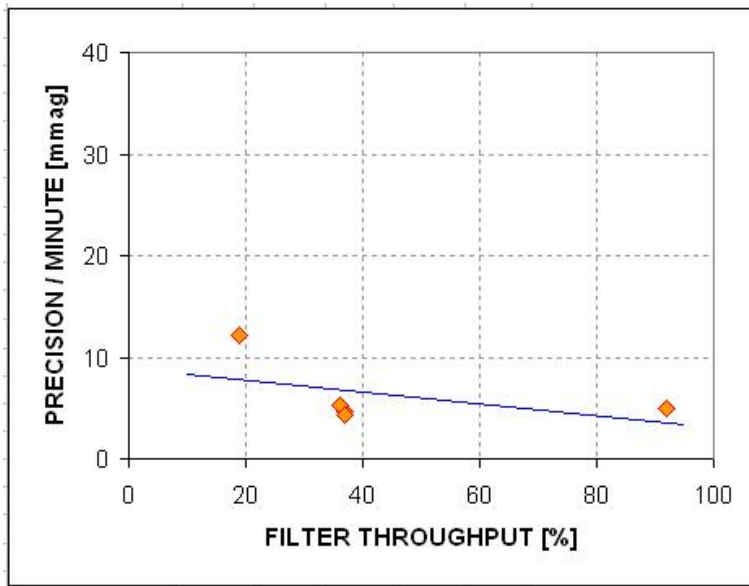


Figure H.10. Precision performance versus filter throughput for the $V = 10.2$ star.

For stars near the bright end of those in the BTE list the best filter for light curves is the i' -band filter. It is 8 times faster than the V-band filter in achieving a specific RMS level of precision. The NIR filter is almost as good, and the CBB and RED filters are close behind.

Concluding Remarks

The results reported here suggest that the best overall filter choice for exoplanet light curve observing is the CBB filter. Brighter exoplanet stars might be observed with greater precision using an i' -band filter, or maybe the NIR filter. For star ranging in brightness from brighter than typical to the faintest, the worst-performing filter was found to be V-band.

Most of the superior performance of the CBB filter can be attributed to its large throughput. That being the case, why not use a clear filter? As explained in the Chapter about “Star Colors” (Chapter

APPENDIX H – FILTER PLAYOFF

19), a clear filter should be avoided for exoplanet light curve observations because it has different effective atmospheric extinction values for red and blue stars (0.132 and 0.191 mmag/airmass), whereas with a CBB filter the two extinction coefficients are almost the same (0.116 and 0.124 mmag/airmass). In other words, the extinction difference between red and blue stars is 59 mmag/airmass for a clear filter and only 8 mmag/airmass for a CBB filter. That's a 7-fold improvement, which means there should be a 7-fold reduction in the size of the “air mass curvature” systematic error component when using a CBB filter instead of a clear filter. For a typical star the CBB filter passes ~92% of the light passed by the clear filter. This 8% loss is a small penalty for a 7-fold reduction in the “air mass curvature” component of systematic error.

To my knowledge this is the first report of results from an observing session designed specifically to identify optimum filter choices for exoplanet light curve observing. There may be flaws in my procedure, and I am open to comments on an improved observing protocol or an improved image analysis protocol. I welcome others to conduct their own “filter playoff” observations, and share them with the community of amateur exoplanet observers. Until others confirm what I have found it is fair to characterize my results as merely “suggestive.” The suggestion, to be explicit, is that the overall best filter choice is CBB-band.

APPENDIX I – Transit Model and Fitting Procedure

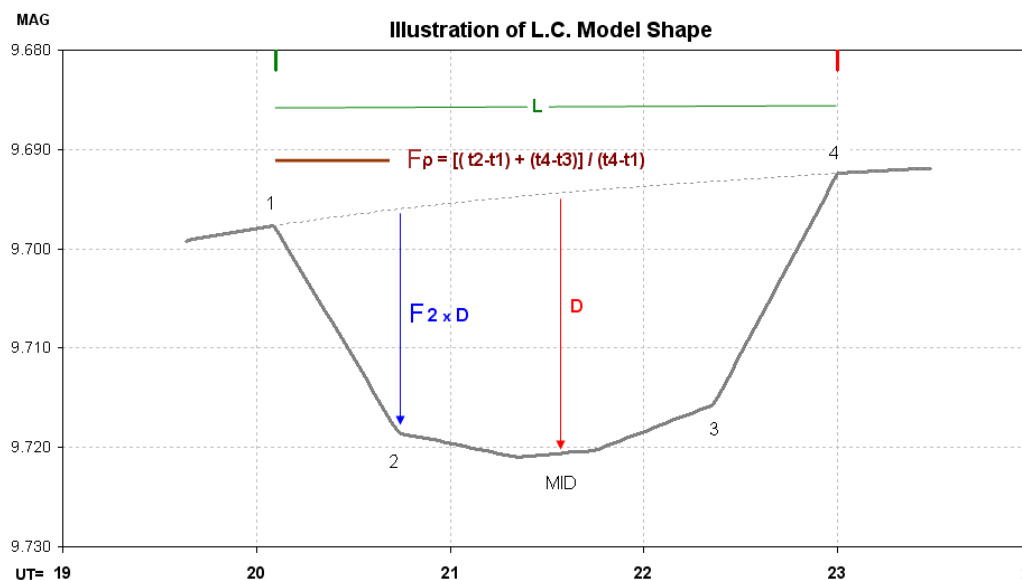
This appendix was originally prepared for the Amateur Exoplanet Archive (AXA) web site. It explained how a priori information was made use of by an auto-fitting program used for data files submitted to the AXA. The auto-fit program was designed to implement the same algorithm used by the spreadsheets described in Chapters 17 and 18.

Introduction

Amateur light curve (LC) data is almost always "noisier" than professional data. Often the level of noise does not permit a solution to be sought for some of the subtle aspects of LC shape. I use a procedure that allows for these limitations without sacrificing the ability to extract mid-transit time from noisy data.

Another difference between amateur and professional LC data is the size of systematic errors. There are two main systematics: 1) temporal trends (produced by polar axis mis-alignment that cause image rotation, which in turn produces LC trends as the star field moves across an imperfect flat field), and 2) "air mass curvature" (produced differences in star color between the target star and reference stars). The first effect is usually greater for amateurs because our polar axis alignment is rarely as good as at professional observatories, and our flat fields are probably not as good. The second effect is usually greater for amateurs because our observing sites are at lower altitudes, where extinction is greater, and where the effect of star color differences is greater. Note that each star's extinction coefficient is slightly different depending on its color.

Because the two main systematic effects on LCs are greater for amateurs there's a greater need to address them and remove their effect when processing amateur data. In order for the AXA viewer to see how much systematics may be affecting the final LC I have decided to include two LC versions with each observer's data submission: 1) including systematics, and 2) with systematics removed.



Figure

I.01. LC model used in fitting AXA submitted transit data. Trend and air mass curvature systematics are present. First contact occurs at t1, etc. Descriptions are in the text.

APPENDIX I – TRANSIT MODEL

Model Description

I use the term "model" reluctantly because my model is primitive compared with the models used by professionals. Figure I.01 illustrates what I'm calling a "model."

This "model" includes 7 parameters (plus an offset), listed here:

- 1) ingress time, t_1
- 2) egress time, t_4
- 3) depth at mid-transit, D [mmag]
- 4) fraction of transit that's partial, $F_p = [(t_2 - t_1) + (t_4 - t_3)] / (t_4 - t_1)$
- 5) relative depth at contact 2, F_2 (depth at contact 2 divided by depth at mid-transit),
- 6) temporal trend [mmag/hour], and
- 7) air mass curvature [mmag/airmass].

In this "model" mid-transit is "flattened" for a time interval given by $(t_3 - t_2)/4$.

Including an "air mass curvature" term requires that *air mass versus time* be represented by an equation including terms for powers of "t-to." I use a 4th power expansion, and **to** is set equal to the mid-point of observations.

The interval t_1 to t_2 and t_3 to t_4 are "partial transit." The parameter "Fp" is the fraction of the total transit time that's partial. When a transit is "central" (impact parameter $b = 0$) F_p can be used to estimate the size of the transiting exoplanet (or brown dwarf star) compared with the size of the star being obscured.

The parameter "F2" is used to specify the amount of this limb darkening effect.

The interval t_2 to t_3 is not flat, but rounded due to stellar "limb darkening."

Depth at mid-transit, D [mmag], can be used to estimate the size of the transiting exoplanet (or brown dwarf).

Least-Squares Fitting Procedure

Many steps are needed to perform a least-squares (LS) fit of a model to data. Sorry for the detail in what follows, but some readers may want to know.

Deriving SE versus time

Every measurement has an associated uncertainty. If a region of data share the same SE (standard error) uncertainty, it is possible to deduce the value for SE by comparing a measured value with the average of its neighbors. This assumes that the thing being measured changes slowly compared with the time spanned by the neighbor values being averaged. Let's clarify this: the average of neighbors will be a good representation of the true value being measured provided the second derivative of the thing being measured is small (I won't belabor this since if you know about second derivatives you'll know what I'm getting at). I like using the 4 preceding neighbors and the 4 following neighbors, and I also prefer using their median instead of average (to be less affected by outliers). The median of 8 neighbors will itself have an uncertainty, but it will be much smaller than that for the measurement under consideration. Using the median of 8 neighbors leads to a SE on the 8 neighbors of $\sim SE_i$

APPENDIX I – TRANSIT MODEL

$\times 1.15 \times \sqrt{1/7}$, where SE_i is the SE per individual measurement (the 1.15 accounts for use of median instead of average, and “7” comes from 8 measurements minus one degree of freedom). When a measurement is compared with this slightly uncertain version of "truth" the difference is slightly more uncertain than the measurement's actual SE. The histogram of many such differences will have a spread that is larger than SE_i by 9% ($\sqrt{1+(1.15 \times \sqrt{1/7})^2}-1$). My procedure for calculating SE_i versus time during the observing session is to calculate the standard deviation of the "neighbor differences" data at each time step, then divide the entire sequence by 1.09.

This description left out one data quality checking step. The "neighbor differences" data can be used to identify outliers. When the absolute value of a measurement's neighbor difference exceeds a user-specified rejection criterion the measurement is rejected! Although the rejection criterion should depend on the total number of measurements, and should be set to a multiple of the SE_i determined to exist at the time of the measurement under question, I prefer to set the criterion to about 2.5 times the typical SE_i for the observing session. This usually leads to a rejection of about 2% of the data (it would be 1.2% if only Gaussian noise were present). There's one other data quality checking step that is applied to some submitted data. When check stars (or even just one check star) are included in the submission it's possible to assess the amount of loss due to cirrus clouds, or dew on the corrector plate, or PSF spreading outside the aperture circle (due to seeing changes or focus drift), etc. I usually reject all data that has losses exceeding ~ 0.1 magnitude.

Solving for Model Parameter Values

Minimizing chi-square is a subset of least squares. Both assume that a measurement is actually a probability function having width given by SE_i . The goal is to adjust model parameters to maximize the combined probability that the model "belongs" to the data. I suppose the word "belongs" should be explained.

For a single measurement with SE_i specified there is just one parameter that can be adjusted for assessing "belong." The key concept is that every parameter value under consideration has a probability of "belonging" to the measurement, and this probability is simply the value of the Gaussian function at the parameter value's location. With two measured values the combined probability is the product of each probability. Since the Gaussian probability function is proportional to the inverse square of the difference, divided by SE_i , the maximum combined probability will be achieved by a model that also minimizes the sum of squares of "model minus measurement divided by SE_i ." Chi-squared analysis involves finding a set of parameter values that minimize this sum, and it is equivalent to maximizing probability products. ("Probability products" is a Bayesian technique, and it lends itself to the case when probability functions are not Gaussian.)

There's one more feature available when minimizing chi-squared (or maximizing probability products). Outside information about likely values for model parameters can be explicitly made use of by treating them in a way similar to the way measurements are treated. If a model parameter has a known *a priori* probability function it can be included in the analysis. For example, if a Bayesian approach (product of probabilities) is used then whenever a model parameter is being evaluated the *a priori* probability that the value under consideration can be included in the set of probability products. If it is assumed that all probability functions are Gaussian, then the chi-squared procedure can be used and a model parameter's difference from it's most likely value can be included in the sum of chi-squares. Although most of the terms in the probability product come from comparing measurements with model predicted values 7 terms are from the model. For each model parameter the additional

APPENDIX I – TRANSIT MODEL

term to include in the chi-square sum is "model parameter value minus most likely value divided by SE for the parameter." The effect of including this term is to reward model parameter values that agree with expectations, and punish model parameter values that stray too far from what is expected. For want of a better term I'll say that my auto-fit procedure minimizes "Super Chi-Squared" where:

$$SuperChiSquare = \sum \left(\frac{(O_i - C_i)}{SE_i} \right)^2 + \sum \left(\frac{P_i - P_m}{SE_p} \right)^2$$

where measured magnitudes O_i and model computed magnitudes C_i are differenced and divided by measured magnitude SE_i , then squared and summed for all measurements; followed by a set of model terms consisting of model parameter value P_i differenced with an *a priori* (most likely) value for the parameter P_m (based on a history of fitted light curves for the exoplanet in question) and divided by an *a priori* uncertainty of this parameter SE_p , which are also squared.

Of course there is a potential danger in assigning *a priori* SE for model parameter values and punishing solutions that involve parameters that stray too far from what's expected. When an exoplanet transit has never been observed there is little information besides some basic physics for bounding parameter values (e.g., depth can't exceed 100% would be one example). There are occasions when using *a priori* SE for model parameters is appropriate. Consider the following most common one for exoplanet transits. XO-1 has been observed on a few occasions with high precision, so the shape and depth and length of the LC are well established. For example, $F_p = 0.26 \pm 0.02$, $F_2 = 0.83 \pm 0.05$, $D = 23.8 \pm 0.5$ mmag (for R-band) and $L = 2.91 \pm 0.03$ hours. Whenever a new high-precision complete transit observation is being fitted it is not necessary to make use of this *a priori* information since the new LC data can be used to solve for all parameters. However, when a low precision LC data set is to be fitted, or when only an ingress (or egress) was observed, it is not possible to solve for F_p and F_2 , and sometimes it is also not possible to solve for L or D with an expectation of reasonable results. Should this noisy or partial transit data set be rejected? No. If we constrain the parameters for which we have confidence, then solve for the parameter(s) that may be changing, such as mid-transit time, we will be making legitimate use of prior knowledge as we try to learn about something for which we do not have prior knowledge. In the case of XO-1, for example, this permits us to make use of noisy LC data, or partial transit data, to solve for mid-transit time - a parameter that can be useful in a search for transit timing variations (TTV) produced by another exoplanet in a resonant orbit.

Professional LC data is usually very precise, for several reasons: large apertures have higher SNR and lower scintillation effects, professional observatories are at high altitude where extinction is less and image rotation is non-existent because polar axes are well aligned. Professional LCs therefore should have small temporal trends, small air mass curvatures and should never need to have model parameters constrained by *a priori* information. We poor amateurs, on the other hand, must work harder to overcome all the handicaps of not benefitting from the above list. This section is long because I need to explain the many procedures for overcoming amateur LC limitations.

I have decided to present two versions of every amateur LC so that the severity of systematics and my success at removing them can be assessed. My graphical presentation of LC fits on the AXA web

APPENDIX I – TRANSIT MODEL

pages has one version with systematics removed (which is what the professionals do) and immediately below it is another LC without systematics removed.

The next figure is an example of a LC with systematics present.

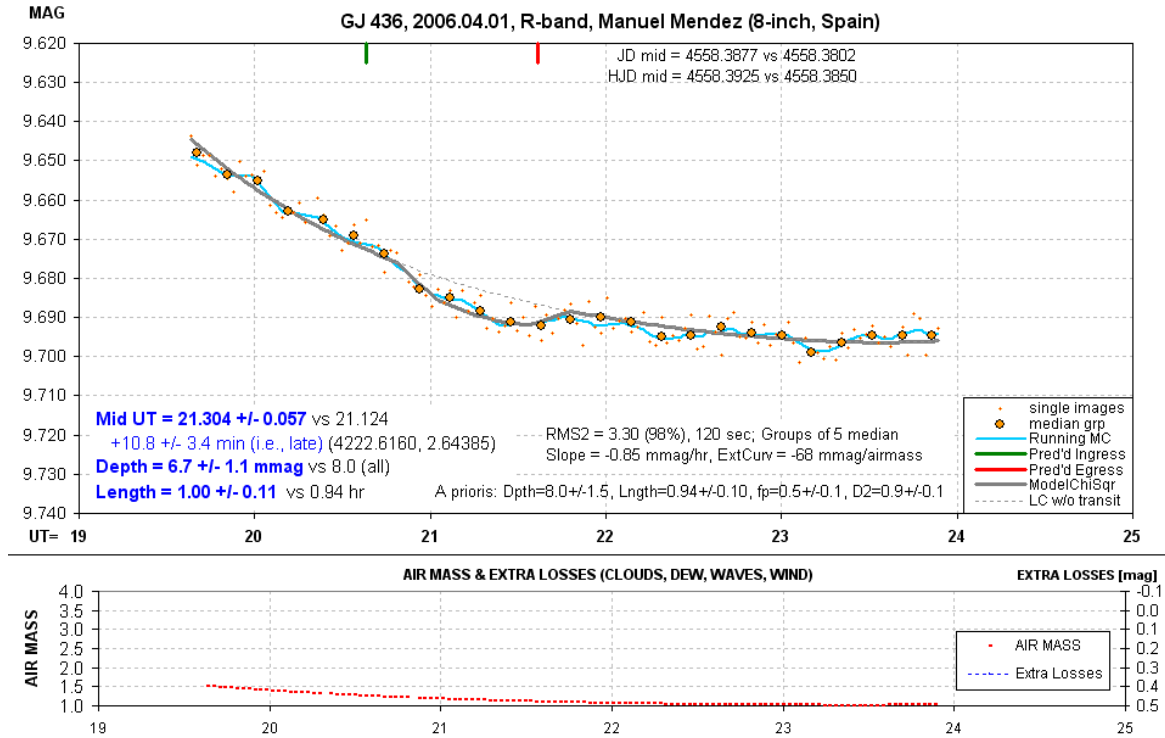


Figure I.02. Amateur LC with a chi-square fit that includes a priori values for model parameters F_p , F_2 , D and L . Other details are described in the text. (f_p is the same as F_p , f_2 is the same as F_2 .)

Magnitudes from individual images are shown by small orange dots. Groups of 5 non-overlapping individual measurements are shown with large orange symbols. A running average of the individual measurements is shown by a wavy light blue trace. The thick gray trace is a model fit. The gray dotted trace during the transit portion shows how the model would plot if the transit depth were zero.

GJ 436 is a very red star, and no reference stars are available that are equally red (and are bright enough for use as reference). Therefore it is common for LCs of this object to exhibit "air mass curvature" (since the target star and reference stars will have slightly different extinction coefficients). In addition to the air mass curvature this LC plot exhibits a temporal trend (usually due to imperfect polar axis alignment that produces image rotation). As noted near the lower-right corner the solved-for temporal trend coefficient (labeled "Slope") is -0.85 mmag/hour. The air mass curvature is also presented as -68 mmag/airmass (labeled "ExtCurv"). The same text box gives the single-image SE (also referred to as RMS_i elsewhere in this book) to be 3.30 mmag for a neighbor noise rejection criterion that leaves 98% of the data as accepted. The exposure time is 120 seconds. At the bottom center is an information box listing *a priori* model parameter assumptions: $D = 8.0 \pm 1.5$ mmag, $L = 0.94 \pm 0.10$, etc. My choice of SE for these parameters is twice their established SE from previous high-precision LCs.

APPENDIX I – TRANSIT MODEL

The lower-left corner shows solved-for parameters whose solution was subject to the *a priori* constraints. The SE value for each parameter is obtained by adjusting the parameter value until chi-square increases by 2. Normally a chi-square increase of 1 is required, but this assumes that either all parameters are "orthogonal" (do not mimic each others effects) or when a parameter is adjusted all other parameters are free to find their minimum chi-square solution. Since neither condition is met, I have adopted the custom, provisionally, of using a chi-square increase criterion of 2 instead of 1. The ingress and egress times call for a mid-transit time that is 10.8 ± 3.4 minutes later than the ephemeris used for predicting the transit. (It is known that the published ephemeris has a period that is too short, and LCs like this one are helping to establish a new period.)

The lower panel shows air mass. If reference stars had been included in the submission another curve would show "extra losses" due to cirrus clouds, etc.

The next figure shows the same data with the two systematic components removed.

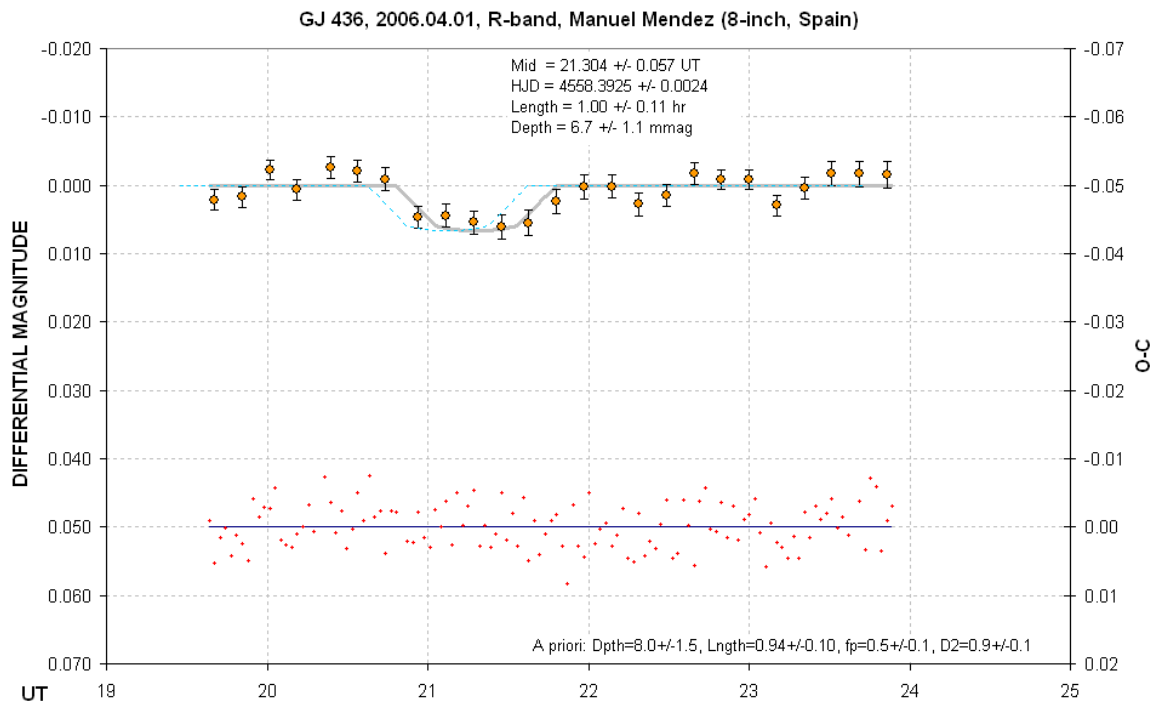


Figure I.03. Systematics removed version of an amateur LC. Description is given below. (*fp* is the same as *Fp*, *f2* is the same as *F2*.)

The dashed blue trace is an offset LC shape showing when the transit was expected. The same 5 non-overlapping data averages are shown using the same orange symbols as in the previous plot. These data have SE bars that are based on the SE_i versus UT (not shown) and divided by square-root of 4. The model fit is horizontal outside of transit, by definition. The small red crosses at the bottom are residuals of the individual image measurements with respect to the model. The information boxes are a repeat from the previous figure.

APPENDIX I – TRANSIT MODEL

On the web pages devoted to each exoplanet I present both graphs. Professionals probably don't publish the graph with systematics present because their systematics are small and it is therefore not necessary to assess their importance. Amateur observations, however, should have the systematics illustrated so that anyone considering using the analysis results can be warned about errors that may remain after attempting to remove the systematics.

Plans for Future Automation

If you think this fitting procedure is labor intensive, you're right! I began doing them using a spreadsheet (LCep.xls, which you can download and use in the same way I use it). Eventually I converted everything I did by hand to a program written in QuickBASIC. This program produces an “objective” solution in a fraction of a second.

TTV Strategy

When a well-observed exoplanet is under study for transit timing variations (TTV) there is no need to solve for F_p and F_2 , as this would just add to the uncertainty of the mid-transit time. It is also not necessary to allow length and depth to be free parameters. Length and depth are usually well established but not with perfect accuracy. Therefore, for TTV studies I assign L and D their best estimate SE, and assign F_p and F_2 zero error, and proceed with the Super Chi-Square minimization procedure inspired by Bayesian Estimation Theory to solve for only mid-transit time. SE on mid-transit time is evaluated by manually adjusting it so that Super Chi-Square increases by ~ 1.5 , then finding a best set of parameter values for L and D (and the systematic parameters trend and air mass curvature), and usually Super Chi-Square comes down to ~ 1.0 . If it doesn't, then I adjust mid-transit time again, and solve for the other parameters. This process actually goes quite fast, and the resulting SE for mid-transit time is an objective evaluation that is valid if stochastic uncertainties dominate systematic errors.

APPENDIX J – Amateur Spectroscopy

The first amateur measurement of exoplanet-produced radial velocity variations was made in 2000 and 2004 by a team led by Tom Kaye (Kaye *et al*, 2006). They observed Tau Boo (V-mag = 3.2) with a 16-inch Meade and home-built fiber-fed spectrograph, and measured a peak-to-peak variation of +/- 470 km/s, in agreement with what professionals measured using substantially larger telescopes and more expensive spectrographs. Tom Kaye's team plans on more capable spectroscopy, using a 1.1-meter telescope that Tom ground during the past 8 years (his first mirror grinding project). This project is called SpectraShift and is described at: <http://www.spectrashift.com/team.shtml>

When I learned about SpectraShift I had visions of amateurs becoming self-sufficient in discovering exoplanets. After all, amateurs could build wide field cameras designed for transit searches, and amateurs can also conduct searches using a telescope with any aperture, and amateurs can follow-up with regular size telescopes to show exactly which star was undergoing transits, and by how much. The final step in confirming that an exoplanet has been discovered would be a set of spectroscopic radial velocity measurements showing that the mass of the transiting object has an exoplanet mass, smaller than ~ 1% of the solar mass (to rule out brown dwarfs).

Another role for amateurs doing spectroscopy that I envisioned was to perform follow-up observations on exoplanet candidates derived from professional wide field survey cameras that amateurs had shown produce exoplanet-like transits. We would no longer be helplessly dependent upon professionals to schedule follow-up RV observations on large telescopes that might not be able to observe the target for months due to scheduling commitments. For example, I have observed an XO Project candidate that has a light curve that looks just like it is produced by an exoplanet, but it is frustrating that no RV follow-up has been scheduled with a professional telescope (such as HET). All we need to know for this candidate star is whether the RV amplitude is large (produced by another star) or small (produced by an exoplanet). It's not necessary to measure RV amplitude accurately to make this distinction. An upper limit to the RV amplitude would be sufficient. If the RV peak-to-peak variation is less than 20 km/s, for example, then the secondary object must have a mass less than that for a red dwarf (assuming a solar mass primary). Just knowing that the secondary is either a brown dwarf or an exoplanet, and not an EB (red dwarf or greater mass) is an important distinction to make.

There's just one problem with these visions. All amateur spectrographs, to date, are incapable of measuring radial velocities to the required accuracy for stars fainter than ~ 9th or 10th magnitude. The only stars remaining to be discovered as undergoing exoplanet transits are going to be fainter than V-mag ~ 12.5. That's about a 3-magnitude discrepancy, so current amateur spectroscopes are ~ 6% of the way to meeting these needs. Combined interferometer spectrographs might yield a 2.5 magnitude improvement, but when these are available for amateur use the 12.5 magnitude threshold for what's needed may have moved to 13.0 or 13.5 magnitude because of more thorough wide field camera surveys by professionals. There may be non-transiting exoplanet systems whose stars are in the 8 to 10 magnitude range, and maybe these should be what amateur spectroscopists should be trying to discover.

I have concluded that in the near-future amateurs with spectroscopes are probably not going to contribute to the discovery of an exoplanet.

ABBREVIATIONS

- AAVSO (American Association of Variable Star Observers) (p-10)
ACDSee (computer option) (men. p-88)
A/D (Analog to Digital) (men. p-65)
ADU (Analog to Digital Unit) (p-221)
am (morning)
AS (Artificial Star) (p-106 to 116, p-221 and index p-236)
ASC-II (computer format) (men. p-73 and p-96)
AXA (Amateur Exoplanet Archive) (p-1)
- b (impact parameter) (p-28)
B-band (* filter) (p-172)
Bd (Bias difference) (p-198)
Bs (Bias sum) (p-198)
BTE (Bright Transiting Exoplanet) (p-1 and index p-237)
B-V (Blue minus Visual, color index) (p-124, p-228)
BVR (Blue Visual Red, Landolt colors) (p-159)
BVRcIc (* filter)
- C (Celsius temperature scale)
C (programming language)
CBB (Clear with Blue Blocking) (* Filter) (p-1, pass-band p-49, default p-50, index p-237)
CCD (Charge Coupled Device, digital camera) (men. p-4..., index p-237)
CFW (Color Filter Wheel) (photo p-19 and index p-237)
CoRoT (Co-nvection Ro-tation and planetary Transit. French Space Program also a BTE name) (p-28)
CSV (Comma Separated Variables) (p-73)
CV (filter residual magnitude) (p-61)
CR (filter residual magnitude) (p-61)
Cs (flux rate) (p-192)
Cx (Count max, for digital camera) (p-140)
- D (Depth at mid-transit) (p-213 and p-214)
dM (delta Magnitude) (men. p-225)
Dec (Declination) (p-28)
DSLR (Digital Single Lens Reflex, camera) (p-14)
- EB (Eclipsing Binary) (p-84, index p-238)
EFL (Effective Focal Length) (index p-238)
ET (Extended Team. XO project) (p-5)
ETD (Exoplanet Transit Database) (p-1 and index p-238)
ExoPTF (ExoPlanet Task Force) (p-149)
- Fd (Flat-field difference) (p-198)
Fs (Flat-field sum) (p-198)
f-ratio (index p-239)
FM (Frequency Modulation, radio & TV sound) (men. p-21)
Fp (Fraction partial, of light curve) (p-103 and index p-239)
FOV (Field Of View) (p-4 and index p-239)
FR (Focal Reducer) (photo p-19)

ABBREVIATIONS

FTE (Faint Transiting Exoplanet) (p-23)
FWHM (Full-Width at Half-Max) (p-224 and index p-239)

g (exposure time) (p-68, p-205)
g'-band (* filter)
G (equation p-198)
Gb (Gigi-byte, computer memory term) (men. p-86)
GEM (German Equatorial Mount) (p-14)
GJ (BTE name) (p-28)
GMST (Greenwich Mean Sidereal Time) (men. p-166)
GPS (Global Positioning System) (men. p-17)
GRB (Gamma Ray Burst) (men. p-21)

H (* filter)
H-alpha (first Hydrogen spectral line) (men. p-51)
HAO (Harvard Astronomical Observatory) (not men.)
HAT (Hungarian Automated Telescope. BTE name.) (p-28)
HD (Henry Draper spectral catalog number. BTE name) (p-28)
HET (Hobby Eberly Telescope. Spectroscopic fixed 9.2-meter. Un. Texas) (men. p-220)
HJD (Heliocentric JD) (p-225)
HJDo (Heliocentric JD at mid-transit) (p-28)
HST (Hubble Space Telescope) (p-147)
Hz (Hertz = frequency in cycles per second) (men. p-224)

i'-band (* filter)
Ic-band (* filter)
IPAC (Infrared Processing Analysis Center) (p-1)
IR (Infra-Red) (p-55)

J (* filter)
JD (Julian Day) (p-225)
J-K (J minus K filter, color index) (* filter) (p-228)
JPL (Jet Propulsion Laboratory) (p-5 and index p-240)
JWST (James Webb Space Telescope, planned launch 2014?) (p-147)

K (* filter)
K (International temperature scale with zero at absolute zero)
KBO (Kuiper Belt Object)
kct (kilo-counts) (p-189)
KELT (Kilo-degree Extremely Little Telescope) (men. p-122)
Kepler telescope (men. p-145)
KST (Kepler Space Telescope) (men. p-145)

LAN (computer connection) (men. p-21)
LC (Light Curve) (p-225)
LHA (Local Hour Angle) (men. p-166)
LN2 (CCD cooling hardware) (p-128)
LS (Least Squares) (p-214)
LST (Local Sidereal Time) (men. p-166)

Mb (Mega-byte, computer memory) (men. p-86)

ABBREVIATIONS

MD (Mid Depth of transit) (fig. p-103)
MDL (software) (p-10 and index p-241)
MC (Median Combining) (p-200)
mmag (milli-magnitude = 1/1000 astronomical magnitude) (p-226)

NASA (National Aeronautics and Space Administration) (men. p-3)
Ni (Noise information without stars) (p-128)
NIR (Near Infra-Red) (* filter) (p-50 and index p-241)
Np (Noise, Poisson) (p-130 and index “Poisson noise” p-242)
NSF (National Science Foundation. And Nearby Star Flux) (men. p-3)
NSTED (NASA Star and Exoplanet Database) (p-1)
NTE (Non-Transiting Exoplanet) (p-23)

OBAFGKMRNS (star spectral sequence)
OGLE (Optical Gravitational Lensing Experiment)
OOT (Out-Of-Transit) (p-25 and index p-242)

PE (Probable Error) (p-201)
pm (afternoon)
PS (Plate Scale) (p-226)
PSF (Point Spread Function) (p-69 and index p-242)

QE (Quantum Efficiency) (p-40)

r'-band (* filter)
R (signal aperture Radius) (p-141 and 142)
RA (Right Ascension) (p-28)
RAM (Random Access Memory) (men. p-86)
R-band (filter) (p-172)
Rc-band (* filter)
RGB (Red Green Blue color model) (men. p-54)
RMS (Root Mean Square) (men. p-113... and index p-243)
Rp/Rj (Ratio of: Radius of exoplanet to Radius of Jupiter) (p-168 to p-170)

SBIG (Santa Barbara Instrument Group) (p-231)
SDSS (Sloan Digital Sky Survey) (p-49)
SE (Standard Error) (p-214 and index p-243)
SEb (Standard Error due to bias) (p-198)
SEf (Standard Error due to flat-field) (p-198)
SEi (Standard Error per individual measurement) (p-215)
SETI (Search for Extra-Terrestrial Intelligence) (men. p-152)
sigma (RMS fluctuations or fractional intensity) (p-206)
SNR (Signal to Noise Ratio) (p-228 and index p-244)
SQR (Square Root)
SRO (Sliding Roof Observatory) (p-17)
STScI (Space Telescope Science Institute) (p-5)
SupperWASP (WASP for the Southern Hemisphere) (p-29)

t1, t2, t3, t4 (four special times during transit) (p-214)
TDV (Transit Duration Variations) (p-26)
TrES (Trans-Atlantic Exoplanet Survey. BTE name.) (p-28)

ABBREVIATIONS

TTV (Transit Timing Variations) (p-26 and index p-245)

UBV (Johnson filters, 1950s on. 1P21 photomultiplier tube)

URL (Uniform Resource Locator. <click> for web access)

USB (Universal System Bus, computer port for mouse, printer, keyboard ..., etc.)

UT (Universal Time) (men. p-20)

UV (Ultra-Violet) (men. p-55)

V-band (Visual-band) (* filter)

V-mag (Visual magnitude) (p-28)

V-R (Visual minus Red. Color index) (p-228)

WASP (Wide Angle Sky Patrol. BTE name) (p-28 and p-29)

WF (Wireless Focuser) (photo p-19)

WWV (radio standard time signals)

WWVB (radio standard time signals) (men. p-20)

XO (BTE name and exoplanet project) (p-5. p-28)

z'-band (* filter)

2MASS (2 Micron All Sky Survey) (p-221)

1420 GHz (Hydrogen-alpha radio wavelength) (p-152)

* Footnote: Filter pass-band graphs:

p-41 B, V, Rc, Ic

p-42 B, CBB, V, Rc, Ic

p-45 B, V, Rc, Ic

p-48 B, V, Rc, Ic, g', r', i', z'

p-49 B, CBB, Rc, Ic, NIR

p-122 B, V, Rc, Ic, CBB, J, H, K

GLOSSARY

2MASS: Two Micron All-Sky Survey; a catalog of point sources (stars) and extended sources (galaxies) covering the entire sky using filters J, H and K. Of the 2.1 billion sources, more than 500 million are stars. J and K magnitudes can be converted to B, V, Rc and Ic magnitudes for most sources. Therefore, J-K star colors can be converted to B-V and V-R star colors, which is useful since all stars that amateurs will want to use for reference are in the 2MASS catalog.

air mass: Ratio of number of molecules of air intercepted by a unit column traversing the atmosphere at a specified elevation angle compared with a zenith traverse. An approximate formula for air mass is secant (zenith angle), or $1 / \sin(\text{elevation angle})$. Because of the Earth's "curvature" the maximum air mass for dry air is ~ 29 (tabulations are available). To the extent that dust and water vapor contribute to line-of-sight extinction the above formulae are a better approximation than air mass tables, since the scale height for dust and water vapor is much smaller in relation to the Earth's radius than the scale height for dry air.

all-sky photometry: Use of a telescope system for transferring standard star magnitudes (such as Landolt stars) to stars in another region of the sky with allowance for differences in atmospheric extinction. c.f. photometry

ADU: Analog-to-digital unit, also called a "data number" and "count," is a number read from each pixel of a CCD camera (using an analog-to-digital converter) that is proportional to the number of electrons freed by photons (photoelectrons) at that pixel location. The ADU count is the number of photoelectrons divided by a constant of the CCD called "gain" (which is inversely proportional to an amplifier's gain).

artificial star: Replacement of a pixel box (upper-left corner) with values that appear to be a star that has a specific peak count (65,535) and Gaussian FWHM (such as 4.77 pixels). The artificial star can be used with a set of images to monitor changes in cloud losses, dew accumulation losses, as well as unwanted photometry losses produced by image quality degradation.

aspect ratio: Ratio of a PSF's widest dimension to its narrowest, usually expressed as a percentage. Anything below 10% is good (i.e., close to circular).

atmospheric seeing: Apparent width (FWHM) of a star recorded on a CCD exposure using a telescope with good optics and collimation and short exposures (0.1 to 1 second). "Seeing" (as it is often referred to) will depend on exposure time and elevation angle. Seeing FWHM increases approximately as a constant plus \sqrt{g} , where g is exposure time. Seeing FWHM also increases with air mass as approximately $\text{airmass}^{1/3}$. Amateurs using CCDs usually say the seeing is good when $\text{FWHM} < 3.0$ "arc. Professionals would say the seeing is good when $\text{FWHM} < 1.0$ "arc. Seeing degradation is due mostly to ground-level temperature inhomogeneities caused by wind-driven turbulence. The scale height for this component of seeing degradation is ~ 7 meters. Other components of seeing are at the top of the "planetary boundary layer" (~ 5000 feet), and tropopause (25,000 to 55,000 feet).

GLOSSARY

binning: Combining of groups of pixels, either 2x2 or 3x3, during the readout phase of collecting electrons from pixels to an output register for the purpose of achieving faster image downloads that have less readout noise, used when the loss of spatial resolution is acceptable.

blackbody spectrum: Plot of power (energy per unit time) radiated by a 100% emissive material (such as an opaque gas) per unit wavelength, versus wavelength. A version also exists using “power per unit frequency.” A star’s atmosphere is 100% emissive (no reflections) and radiates with an approximate blackbody spectrum. Narrow absorption lines are produced by atoms and molecules at higher altitudes and cooler temperatures; they absorb and re-emit at their cooler temperatures (in accordance with a blackbody spectrum determined by their cooler temperature). c.f. Fig. 14.05.

blue-blocking filter: See “Clear with blue blocking filter”

brown dwarf: Star with insufficient mass for fusing hydrogen to helium and releasing energy that would make the star bright. Their mass range is ~ 1 to 8 % of the sun’s mass, and their size is slightly smaller than Jupiter. With only photometry information a dwarf eclipsing binary can be easily confused with a transiting exoplanet.

CBB filter: See “Clear with blue blocking filter”

CFW: Color filter wheel.

check star: Another star in the same set of images as the target star which is processed using the same reference stars (reference stars are sometimes called “comparison” stars for out-of-date reasons). Precision exoplanet photometry usually does not make use of check stars because at the mmag level of precision every star will have a unique dependence on air mass due to its color difference with the reference stars. A check star can provide a false sense of security that systematic errors are not present, or a false sense of alarm that systematics are present. The use of check stars is left-over from variable star work, where mmag systematics are unimportant.

clear filter: A filter that passes most of the light within the wavelength region where CCD chips are sensitive. A clear filter is used instead of no filter (unfiltered) in order to achieve “parfocality” with the other filters (two filters are parfocal when they require the same focus setting).

Clear with blue-blocking filter: A filter that passes photons with wavelengths longer than ~490 nm. A CBB-filter passes ~90% of a typical star’s light and during moonlight it blocks most of the sky background light coming from Rayleigh scattered moon light. With amateur hardware the best light curves are those produced using the CBB filter.

confusion: A technical term referring to the presence of a background of faint stars (or radio sources) that alter the measured brightness of an object. The only way to reduce confusion is to improve spatial resolution. Wide-field exoplanet survey cameras have a high level of confusion, leading to the need for amateurs to detect EB blending situations.

counts: a CCD readout for a pixel corresponding to the number of photoelectrons produced by absorbed photons within that pixel divided by the CCD’s “gain.” Counts is also referred to as ADU, for “analog digital unit.”

CSV-file: Comma-separated-values file, in ASCII (text) format.

dark frame: CCD exposure taken with the shutter closed. A “master dark frame” is a median combine of several dark frames made with the same exposure and same temperature. (Master darks taken at different temperatures and exposure times can be used for pretty picture and variable star work.)

depth (transit depth): decrease in brightness of a star at the mid-point of an exoplanet transit, measured either as a magnitude change or a star flux ratio. When star flux ratio is r the millimagnitude (mmag) change is given as $-2500 \times \text{LOG}_{10}(r)$. For example, $r = 0.99$ corresponds to 10.9 mmag.

differential photometry: Comparison of flux of a target star to the flux of another star, called reference star, expressed as a magnitude. “Ensemble differential photometry” is when more than one reference star is used (either averaged, or median combined, or flux summed).

dust donut: Shadow pattern of a speck of dust on either the CCD chip’s cover plate (small dust donuts) or a filter surface (larger annular shadows). Flat frames correct for the loss of sensitivity at dust donut locations at fixed locations on the CCD pixel field.

eclipsing binary, EB, EB blend: EB means eclipsing binary. EB blend is when an EB is close to a brighter star that is mistaken by a wide-field survey camera for undergoing a possible exoplanet transit because the fade amount is a much smaller fraction of the light from the blend of stars in the survey camera’s aperture.

egress: Transit interval when the smaller object is moving off the star and only part of the smaller object’s projected solid angle is obscuring star light. Contact 3 to 4.

ensemble photometry: Use of 2 or more reference stars in an image for determining a target star’s magnitude

exomoon: A satellite (moon) orbiting an exoplanet

exoplanet: Planet orbiting another star. Also referred to as an extra-solar planet.

extinction, zenith extinction, atmospheric extinction: Loss of light due to the sum of Rayleigh and Mie scattering plus narrow line absorption; usually expressed in terms of “magnitude per air mass.” An extinction curve is a plot of the logarithm of measured star fluxes versus air mass (usually magnitude, a base-10 logarithm times 2.5, versus air mass). A straight line fit to these data has a slope corresponding to zenith extinction.

extra losses: Reductions of a star’s flux level that are not accounted for by atmospheric extinction. The most common origins for “extra losses” are clouds, dew accumulation on the corrector lens, wind-driven telescope vibrations (smearing the PSF for the affected images) and loss of focus (causing the signal aperture to capture a smaller percentage of the entire star’s flux in the poorly focused images).

GLOSSARY

filter bands: Wavelength interval with associated response function for the following commonly-used standards: B-band, V-band, Rc-band, Ic-band, CBB-band, J-band, H-band and K-band. CV-magnitude begins with observations using a clear filter but with corrections designed to produce a V-band equivalent (usually with star color corrections). CR-magnitude is like CV except the goal is an R-band magnitude. CBB-magnitude uses a “clear with blue-blocking” filter (CBB-filter) and is adjusted to simulate R-band magnitude.

flat frame: CCD exposure made of a spatially uniform light source, such as the dawn or dusk sky, often with a diffuser covering the aperture. Flat frames can be made of an illuminated white board, or made pointed at the inside of a dome (“dome flat”). Several flat frame exposures are combined to produce a “master flat.” A master flat is used to correct for vignetting, dust donuts and small pixel-specific differences in bias and sensitivity (QE).

flux: Star flux is defined to be the sum of all counts that can be attributed to a star based on differences with a sky background level that is calculated from the counts in a sky reference annulus.

FOV: Field-of-view

FWHM: Full-width at half-maximum, describing the angular size of the distribution of light on a CCD produced by a point source, i.e., star. c.f. aspect ratio.

gain: For a CCD the term “gain” is the number of photoelectrons required to produce a change of one ADU. Gain can be measured by noting RMS for a subframe of two flat fields subtracted (similar levels) and RMS for the same subframe of two bias frames subtracted. $\text{Gain} = (\text{Sum of median counts for the flats} - \text{sum of median counts for the bias frames}) / (\text{RMS for flats}^2 + \text{RMS for bias}^2)$. c.f. Appendix F.

information rate: Reciprocal of the time it takes to achieve a specified SNR for a specified target star. Alternative observing strategies, as well as alternative telescope configurations (or different telescopes), can be judged using “information rate” as a figure of merit.

ingress: Transit interval when the smaller object appears to move onto the star and only part of the smaller object’s projected solid angle is obscuring star light. Contact 1 to 2.

image rotation: Rotation of the star field with respect to the pixel field during a single observing session; caused by an error in the mount’s polar alignment. The “center” for image rotation will be the star used for autoguiding.

image stabilizer: Mirror assembly that tips and tilts under motor control at a fast rate (typically 5 to 10 Hz) using an autoguide star. It is used to minimize atmospheric seeing movements of a star field. When the star field drifts close to the mirror motion limit a command is issued to the telescope mount motors to nudge the star field back to within the mirror’s range. SBIG makes a good image stabilizer, the AO-7 for regular size CCD chips and the AO-L for large format CCD chips.

impact parameter: “Distance from star center to the transit chord” divided by the star’s radius. An impact parameter of zero is a central transit.

JD and HJD: Julian Date and Heliocentric Julian Date. JD is the time of an event as recorded at the Earth (center). HJD is the time of an event if it were recorded at the center of the solar system. The two vary throughout the year depending on RA/Dec and time of year, but the difference is always < 8.4 minutes.

length of transit: Interval between contact 1 and contact 4. Survey camera lengths may resemble something intermediate between this and the time between contact 2 and 3, due to insufficient SNR.

LC: See Light Curve

light curve: Plot of brightness of a star versus time during a single observing session. Abbreviated LC, it is usually representing brightness in terms of magnitude, with increasing magnitude plotted in a downward direction. LCs may be embellished with marks for predicted ingress and egress, or model fits meant to guide the eye to what the observer believes the measurements should convey.

limb darkening: Stellar brightness distribution for a specific wavelength (filter band) expressed as 1.00 at the star center and decreasing toward the edge (caused by star light close to the limb being emitted from higher and cooler altitudes of the stellar atmosphere). An alternative representation is to normalize to the disk average brightness. Two or three constants are sufficient to represent these shapes. Limb darkening functions vary with spectral type.

linearity: The property of a CCD's readout (ADU counts) being proportional to the accumulated number of photoelectrons in a pixel. A CCD may be linear for readings from zero to ~90% of the maximum reading possible (i.e., $\sim 0.90 \times 65,535 = \sim 59,000$ counts). Linearity and saturation have different meanings but are commonly used interchangeably.

magnitude: Ratio of star fluxes converted to a logarithm. Magnitude differences are calculated using the formula: $dM = 2.5 \times \text{LOG}_{10}(S_i / S_o)$, where S_i is the flux of star "i" and S_o is the flux of star "o". Flux ratio can be calculated from magnitude differences using the following: $S_i / S_o = 2.512^{dM}$. A mmag = milli-magnitude = magnitude / 1000.

median combine: Finding the middle value in a set of values arranged by value. The median combine process is relatively unaffected by an occasional outlier value whereas averaging is vulnerable to outlier corruption. The standard error uncertainty of a median combine is ~15% greater than the SE of an average, provided all data are belong to a Gaussian distribution (i.e., outliers are not present). A median combine can be performed on a group of images as well as single set of values, since a group of images is just a set of values for each pixel location.

MDL: MaxIm DL, Diffraction Limited's program for control of telescope, CCD, image stabilizer, focuser, and also image processing with photometry analysis.

Mie scattering: Aerosols (airborne dust) with a circumference greater than the wavelength of light produces Mie scattering. Mie scattering theory actually encompasses all wavelength to circumference ratios, but in common parlance Mie scattering refers to the situation where the wavelength is slightly longer than the circumference. Much longer wavelengths are trivial to treat as mere blocking of light.

GLOSSARY

Rayleigh scattering is a subset of Mie scattering theory reserved for the case of wavelength much smaller than aerosol (or molecule) circumference.

mmag: Milli-magnitude, $1/1000^{\text{th}}$ of a magnitude. A transit depth of 1 mmag is equivalent to a brightness ratio given by $2.512^{-1.0 \text{ mmag} / 1000}$, or 0.999079 (i.e., 0.0921% fade).

NIR filter: Near infra-red filter, passing light with wavelengths longer than ~ 720 nm.

non-linearity: The property of a CCD's readouts (ADU counts) failing to be proportional to the accumulated number of photoelectrons within a pixel when the number of photoelectrons exceeds a "linear full well capacity." See also "linearity."

occultation: Orbital motion of a larger object in front of a smaller one, obscuring some of the light from the smaller object. c.f. transit.

OOT: Out-of-transit portions of a light curve. OOT data can be used to assess the presence and magnitude of systematic errors produced by image rotation and color differences between the target star and reference stars.

photoelectron: Electron released from a CCD's silicon crystal by absorption of a photon. One photon releases exactly one electron.

photometric sky: Weather conditions that are cloudless and calm (no more than a very light breeze), and no discernible haze due to dust.

photometry: Art of measuring the brightness of one star in relation to either another one or a standard set of stars (photometric standards, such as the Landolt stars). Brightness is often loosely defined, but in this case it can be thought of as meaning the rate of energy flow through a unit surface, normal to the direction to the star, caused by a flow of photons incident upon a telescope aperture. c.f. all-sky photometry.

photometry aperture and circles: A circular "signal aperture" within which a star to be measured is placed, specified by a radius [pixels], surrounded by a gap with a specified pixel width, surrounded by a sky background annulus. An aperture configuration is specified by 3 numbers (the 3 radii). Some photometry programs do not have a gap capability.

plate scale: Also referred to as "image scale," is the conversion constant for pixels to "arc on the sky." $\text{PS [}^{\circ}\text{arc/pixel]} = 206.265 \times \text{pixel width [nm]} / \text{EFL [mm]}$

point-spread-function, PSF: Shape of light intensity versus projected location on sky (or location on the CCD chip) by a point source (star), with widths described by FWHM and aspect ratio.

Poisson noise: Subset of stochastic noise pertaining to the case in which a discrete number of "random" events occur during a specified time originating from a "source" that is assumed to be at a constant level of activity during the measurement interval. The "Poisson process" is a mathematical treatment whose most relevant statement for photometry is that when a large number of events are measured, n , the SE uncertainty on the measured number is \sqrt{n} . cf. stochastic noise

precision: The internal consistency among measurements in an observing session. All such measurements may share systematic errors, which are unimportant for the task of detecting transit features. Precision is affected almost entirely by stochastic processes. Accuracy is different from precision; accuracy is the orthogonal sum of precision and estimated systematic errors.

Rayleigh scattering: Atmospheric molecular interactions with light waves that bend the path of the wave front and therefore change the direction of travel of the associated “photon.” This is what makes the sky blue. c.f. Mie scattering

read noise: The RMS noise produced by the process of reading a pixel’s accumulation of photoelectrons at completion of an exposure. Read noise [counts] = $\text{RMS}' / \sqrt{2}$, where RMS’ is the counts “standard deviation” for an image produced by subtracting two bias frames. Read noise for modern CCDs is so small that it can usually be neglected when assessing error budgets. c.f. Appendix F.

red dwarf: Star with sufficient mass for fusing hydrogen to helium in it’s core, thus releasing energy sufficient to make it shine at visible wavelengths, but smaller, fainter and redder (i.e., cooler) than all other stars. Red dwarfs are transitional between “brown dwarfs” and “normal” stars; they have masses of ~ 8 to 40 % of the sun’s mass, and radii between 10 and 50 % of the sun’s radius. With only photometry information a small red dwarf eclipsing binary can be easily confused with a transiting exoplanet.

reference star: A star in the same image as the target star and check stars whose flux is used to form ratios with the target and check stars for determining magnitude differences. The purpose can be detection of image to image changes or simply an average difference between a calibrated star and an uncalibrated or variable star. This is called differential photometry when the reference star is another star. When several reference stars are used it is called “ensemble photometry.” When the reference star is an artificial star it is a special case of differential photometry (without a name, as far as I know). The term “comparison star(s)” is sometimes confused with reference star(s); this is a term left over from the days when visual observers of variable stars used stars of similar magnitude to “compare” with the target star.

residual image: When photoelectrons remain in the silicon CCD elements after a read-out they may be included in the next exposure’s read-out and can produce a faint residual “ghost image” from the earlier image. This is more likely to occur after a long exposure when bright stars are present that saturate some CCD elements, causing photoelectrons to become more firmly attached to silicon impurities than other electrons. The problem is most noticeable when the following image is a dark frame; the problem is worse when the CCD is very cold.

saturation: Saturation can refer to a pixel’s output exceeding it’s “linear full well capacity” with an associated loss of proportionality between incident flux and CCD counts. The ADU counts where this proportionality is lost is the linearity limit (typically ~40,000 to 60,000 counts). Saturation can also refer to the accumulation of so many photoelectrons that the analog-to-digital converter (A/D converter) exceeds its capacity for representing an output value. For a 16-bit A/D converter this version of saturation produces an ADU count of 65,535.

GLOSSARY

SBIG: Santa Barbara Instruments Group, located in Goleta, CA (west of Santa Barbara; formerly located in up-scale Montecito, east of Santa Barbara; and never located in Santa Barbara).

scintillation: Intensity fluctuations of stars observed from the ground (caused by atmospheric temperature inhomogeneities at the tropopause). Scintillation can vary by large amounts on hour time scales (doubling), but time-average fluctuation levels are fairly predictable using dependencies on air mass, site altitude, telescope aperture, wavelength and exposure time.

sky background level: Average counts within the sky background annulus. Dark current is one contributor to background level, and it increases with CCD temperature, doubling every ~4 degrees Centigrade. Sky brightness is another contributor. A full moon will raise sky brightness from ~21 magnitude per square "arc to 17 or 18 magnitude square "arc. The increase is more than 3 or 4 magnitudes in B-band, which is the motivation for using a CBB-filter when moon light is present.

SNR: signal-to-noise ratio, the ratio of measured "flux" to SE uncertainty of that flux. For bright stars SNR is affected by Poisson noise and scintillation, whereas for faint ones the dominant components are thermal noise generated by the CCD silicon crystals ("dark current"), electronic readout noise and sky background brightness. $SNR [mmag] = 1086 * SNR$.

star color: Difference in magnitude between a wavelength band and a longer one, such as B-V, V-R, or J-K. They are correlated with each other for most stars.

stochastic error: Uncertainty due to the measurement of something that is the result of physical events that are too numerous and impractical to calculate (thermal noise) or beyond present knowledge too understand because the physics of it hasn't been discovered (radioactive emissions), which nevertheless obey mathematical laws describing the distribution of events per unit time. These mathematical laws allow for the calculation of noise levels, or uncertainty for a specific measurement. c.f. Poisson noise. Stochastic errors are different from systematic errors in that stochastic SE can be reduced by taking more measurements with the expectation that after N measurements $SE = SE_i / \sqrt{N}$ (where SE_i is the SE of an individual measurement). Systematic errors are unaffected by more measurements.

stray light: Light that does not follow the designed (desired) optical path, as happens with reflection of light from nearby bright stars (or moonlight) off internal structures, which is registered by the CCD. Light that leaks through a housing joint (CCD, or CFW, or AO-7, etc) and is reflected onto the CCD is stray light.

sub-frame: Rectangular area of CCD, specified by the user, that is downloaded when fast downloads of a smaller FOV are desired.

TheSky/Six: A good sky map program (also referred to as a "planetarium program") showing star locations for any site location, any date and time, and any orientation (zenith up, north up, etc). J, H and K magnitudes are shown for virtually every star shown (plus V-magnitude estimates). Limiting magnitude is ~16 (V-mag). User objects and telescope FOVs can be added to the catalog.

transit: Orbital motion of a smaller object in front of a star that is larger, obscuring some of the light from the star. c.f. occultation.

GLOSSARY

transit depth: Magnitude difference between the measured value at mid-transit and a model-predicted value at the same time. In the absence of systematic errors affecting the shape of the light curve (which often have a component of curvature correlated with air mass and a trend correlated with time) the transit depth is simply the difference between the average of the out-of-transit magnitudes and the mid-transit value, which is what most observers do even when systematic effects are present (unfortunately).

transit timing analysis: Search for patterns in a plot of mid-transit time minus predicted transit time versus date using a fixed period (interval between transits). Anomalies that persist for months before changing sign, with sign reversal periods of many months, are predicted to occur if an Earth-mass exoplanet is present in an orbit whose period is in a simple resonance with the transiting exoplanet's period (such as 2:1).

Astronomy Hardware Company

Contact Information

Summary of Basic Equipment Needed for Exoplanet Observing

Telescope (such as Celestron CPC 800 or Meade LX200, both 8-inch)
Equatorial wedge for above
CCD camera (such as SBIG's ST-7XE or Starlight Express SXVR-H9)
Color filter wheel with CBB filter (such as Adirondack's XOP-BB or CBB filter)
Software for control of telescope and CCD, and image analysis (such as Maxim DL)

Adirondack Astronomy (no longer in business)

AstroDon

Dr. Don S. Goldman
Astrodon Imaging
9224 Mott Court
Orangevale, CA 95662
916.712.2559
www.astrodon.com
don@astrodon.com
Photometric and Imaging Filters

Celestron

Celestron Customer Service Department, 2835 Columbia Street, Torrance, CA 90503. ...
Phone: 310-803-5955
Email: Support Contact Form
Telescopes & Mounts

Custom Scientific, Inc.

3852 North 15th Avenue
Phoenix, Arizona 85015 USA
Phone: 602-200-9200
Fax: 602-200-9206
<http://www.customscientific.com/>
optics@CustomScientific.com
CBB Filters, Photometric Filters & more

Diffraction Limited

100 Craig Henry Drive, Unit 202
Ottawa, Ontario
K2G 5W3
Canada
Telephone (613) 225-2732; fax: (613) 225-9688
<http://www.cyanogen.com>
Maxim DL / CCD Software

ASTRONOMY HARDWARE COMPANIES

Explora Dome

by Polydome
62824 250th Street
Litchfield, MN 55355
Phone: 320-693-8370
Phone: 320-693-9323
Toll Free: 800-328-7659, Fax: 320-693-2434
Email: Dan@PolyDome.com
URL: ExploraDome.us
[http://www.exploradome.us/
backyard observatories](http://www.exploradome.us/backyard_observatories)

Meade Instruments Corporation

27 Hubble
Irvine, CA 92618
(800) 626-3233 (U.S.A. Only)
telescopes & mounts

OPTEC Inc.

199 Smith Street · Lowell, Michigan 49331 · U.S.A.
Toll free: 888-488-0381 · Office: 616-897-9351 · Fax: 616-897-8229
<http://www.optecinc.com/>
focal reducers, filter wheels

Santa Barbara Instrument Group

147-A Castilian Drive
Santa Barbara, CA 93117
www.sbig.com
Phone: (805) 571-7244 Fax: (805) 571-1147
CCD cameras, filter wheels , adaptive optics& accessories

Software Bisque

www.bisque.com
Sales (USA & Canada only): +1 800 843 7599
International: +1 303 278 4478
Fax: +1 303 278 0045
TheSky/Six Planetarium Software, and Image Processing Software

Starizona (sale of hard copy of this book)

<http://starizona.com/acb/>
5757 N. Oracle Rd., Suite 103 · Tucson, Arizona 85704
520 292-5010

ASTRONOMY HARDWARE COMPANIES

Starlight Xpress Ltd.

Postal address

The Office, Foxley Green Farm, Ascot Road, Holyport, Berks., UK. SL6 3LA

Telephone +44 (0)1628 777126; fax: +44 (0)1628 580411

<http://www.starlight-xpress.co.uk/>

General Information: info@starlight-xpress.co.uk

CCD Cameras, Filter Wheels, Adaptive Optics

Willmann Bell

P.O. Box 35025, Richmond, Virginia 23235 USA

Voice: (804) 320-7016 and 1-800-825-STAR (7827); fax: (804) 272-5920

<http://www.willbell.com/Default.htm>

AIP Software

ACKNOWLEDGEMENTS

An excellent discussion of CCD hardware can be found in the book *Handbook of CCD Astronomy* (2000) by Steve B. Howell. Some of the material in this book is based on Howell's book.

I am grateful to the Society for Astronomical Sciences for permission to use figures in this book that were presented on my behalf at the society's 2007 annual meeting at Big Bear, CA and published in the meeting proceedings.

Thanks are due to Cindy Foote for allowing me to reproduce (in Appendix D) her amazing light curves of a transit of an exoplanet candidate made with three filters on the same night.

I also want to acknowledge the help of John Watson, a manuscript reviewer for Springer book publishing company, who gave me several ideas that I incorporated in the book and who succeeded in persuading Springer to agree to publishing it. (After waiting 5 weeks for a book contract that required only 3 signatures I became concerned about Springer's responsiveness during the editing phase, so I checked with some authors who had used Springer and eventually decided to self-publish.)

REFERENCES

- Algol E, Steffen J, Sari R et al (2005) *MNRAS*, 359, p 567.
- Barnes JW and Fortney JJ (2004) "Transit Detectability of Ring Systems around Extrasolar Giant Planets" *Astrophys. J.*, 616, 1193-1203.
- Bissiner RB (2004) "Detection of Possible Anomalies in the Transit Lightcurves of Exoplanet TrES-1b Using a Distributed Observer Network"
- Caldwell JAR, Cousins AWJ, Ahlers CC et al (1993) "Statistical Relationships Between the Photometric Colours of Common Types of Stars in the UBVRcIc, JHK and uvby Systems," South African Astronomical Observatory Circular #15.
- Charbonneau D, Brown T, Latham D et al (2000) "Detection of Planetary Transits Across a Sun-like Star," *Astrophys. J.*, 529, pp L45-48.
- Charbonneau D (2004) "Hubble's View of Transiting Planets" *eprint arXiv:astro-ph/0410674*
- Cox A, Editor (2000) *Allen's Astrophysical Quantities*, Fourth Edition, Springer-Verlag, New York.
- Dravins D, Lennart L, Mezey E et al (1998) "Atmospheric Intensity Scintillation of Stars. III. Effects for Different Telescope Apertures," *PASP*, 110, pp 610-633.
- Gillion M, Pont F, Demory B, et al (2007) "Detection of transits of the nearby hot Neptune GJ 436 b", *arXiv:0705.2219v2*
- Holman MJ, and Murray NW (2005) *Science*, 307, p 1288.
- Howell SB (2000) *Handbook of CCD Astronomy*, Cambridge University Press, Cambridge, UK.
- Howell S (2002) *The Planetary Report*, XXII, Nr. 4, July/August.
- Kaye T, Vanaverbeke S and Innis J, "High-precision radial-velocity measurements with a small telescope: Detection of the Tau Bootis exoplanet" (2006), *J. Br. Astron. Assoc.*, 116, 2.
- Landolt AU (1992) *Astronom. J.*, 104, p 340.
- Mandushev G, Guillermo T, Latham D et al (2005) "The Challenge of Wide-Field Transit Surveys: The Case of GSC 01944-02289," *Astroph. J.*, 621, pp 1061-1071.
- Massey, P., C. Gronwall and C. A. Pilachowski (1990), "The Spectrum of the Kitt Peak Night Sky," *PASP*, **102**, 1046-1051
- McCullough PR, Stys JE, Valenti JA et al (2006) "A Transiting Planet of a Sun-like Star", *Astrophys. J.*, 648, 2, pp 1228-1238.

REFERENCES

Steffen J (2006) "Detecting New Planets in Transiting Systems," Doctoral Thesis, University of Washington.

Steffen JH and Agol E, (2005) "An Analysis of the Transit Times of TrES-1b," *MNRAS*, 364, L96.

Toon B and Pollack J (1976) *J. Appl. Met.*, 15.

Warner B and Harris A (2007) "Asteroid Light Curve Work at The Palmer Divide Observatory," *Minor Planet Bulletin*, 34-4.

INDEX

A

AAVSO 1-2, 10, 13-14, 96, 137, 139-140, 144, 151
absorption 40-1, 46, 226
accuracy 123, 137, 139-40, 143, 167, 198-9, 226
ADU 60, 130, 195, 221, 224-5, 227
aerosols (and aerosol scattering) 41, 43-4, 46, 225
air mass, airmass, AirMass viii, 31, 38, 43, 46, 53, 66, 75, 83-4, 100, 103, 106-7, 109-10, 118-120,
132-3, 138, 160, 202-203, 206, 221-3, 227-8
air mass curvature 50, 103, 114-16, 123, 202, 212-14, 216-17, 219
all-sky photometry 61, 123, 138, 156, 158, 160, 221
amateur astronomers 4, 7, 13, 16, 68
amateur data submissions 1, 97, 145
Amateur Exoplanet Archive 1, 28-9, 51, 84, 86, 91, 97, 137, 144, 151, 213
amateur exoplanet observers 16, 27, 34, 150, 212
amateur hardware 7-8, 15, 130, 198, 202, 222, 235
amateur light curves 25, 88, 147, 163, 213
amateur observatories 4, 7, 149
amateur spectroscopy viii, 27, 220
anomalies viii, 9, 26, 53, 144-8, 228, 235
AO-7 image stabilizer 57, 62, 75
aperture pixel noise 126, 128-31, 133, 135-6, 162
aperture sizes (radius) 69, 75, 79-80, 82-3, 88, 134-5, 142
aperture (telescope) 12, 15, 50-1, 53
artificial star vii, 73, 75, 86, 88-91, 94, 96, 100, 106-16, 203, 221, 227
Astrodon 49
atmosphere 41-7
atmospheric composition 4, 23-4
atmospheric extinction 40-3, 45, 49-50, 52, 55, 65-6, 83, 89, 94, 117, 203, 205, 221, 223, 233
atmospheric seeing 12, 17, 38, 69, 72, 77, 132-5, 140, 142, 149, 152, 191, 194, 215, 221, 233
autoguider chip 76-7, 141
autoguider star 77, 141
autoguiding vii, 12, 18, 35, 53, 63, 76-7, 141, 156, 194, 202-3, 224
average, running 102, 200-1, 217
AXA 1-2, 29-30, 51-2, 54, 86, 91, 94-5, 97, 106, 114-15, 144-5, 151, 153, 213
AXA auto-fit program 93-4, 114-15
AXA format 92

B

B-band 43, 58-59, 66, 76, 118-20, 123, 156, 169, 172, 187, 223, 228
background level 60, 128, 227
bandpasses 37, 46, 53, 117
BB-filter 223, 228
bias frames 64, 198, 203, 224, 227

binning 18, 38, 59-60, 222, 233
 blue-blocking filter 42, 50, 119, 222-3, 233
 clear with 1, 50, 122
 brightening 25, 71-2, 74, 147
 BTE list 29-32
 BTEs (bright transiting exoplanets) 1, 4, 23, 25-6, 28-31, 34, 37, 50-3, 68, 84, 145, 148, 202, 208, 235
 BTEs (known) 24-5, 27, 29, 34, 51, 207
 BVRcIc 45-6, 51-2

C

calibration, pointing 8, 75
 Caltech 1, 5, 97, 144-5
 candidate references stars 106
 CBB-band 1, 37, 42, 50, 58, 123, 206, 212
 CBB-band filter 38-9, 49, 135, 230
 CBB filter 35, 42, 49-53, 55, 63, 68, 76, 122-3, 202, 205-6, 208, 211-12, 222
 CCD cameras 4, 12, 16, 57, 76, 149-50, 152, 221
 CCD chip 43, 62, 155, 202, 222-3, 226
 CCD linearity 189-97
 CCD pixel field 15, 147, 156, 160, 203, 223
 CCD Transformation Equations 138-9
 Celestron CPC-1100 17-19
 CFW (color filter wheel) 12, 18-19, 50, 55, 202, 222, 228
 check stars 73, 84, 90-1, 96, 215, 222, 227, 233
 chi-square 104, 111, 215, 218
 reduced 111, 114
 chip's FOV, main 35-6, 77
 cirrus clouds 74-5, 77, 89, 109, 215, 218
 clear filter 1, 35, 42, 49-51, 53-5, 59, 123, 157, 202, 211-12, 222-3, 233
 clear with blue blocking filter 222
 Cmax 65-6, 69, 130
 collaborations, professional/amateur 3, 6, 144
 color filter wheel *see* CFW
 comp (star) 1, 84-6, 88, 91, 96, 138-9
 comp/check vii, 86, 88-9, 91, 96, 98-9, 104-6, 115
 confusion 222
 control room 17, 20-1, 77
 converting star color 170-1
 correction, hot pixel 87
 cosmic ray defects 60, 64, 67
 CSV-file 73, 88-92, 146, 222
 Cx 140, 188-97
 Czech Republic's Exoplanet Transit Database (see ETD)

INDEX

D

dark frames vii, 13, 60-1, 64, 87, 189, 223, 227, 233
data
 archiving amateur exoplanet 1
 noisy 200-1, 213
data file 86, 91-2, 94, 96-9, 106, 114-15, 144-5, 213
data quality 187, 201, 215
defocus 68-70
defocusing vii, 1, 51, 65, 69-70
differential photometry 7, 84, 89, 94, 137, 223, 227, 233
diffuser 33, 56, 61, 203, 223
Dravins 132, 134, 205, 209, 231
dust donut 41, 43-4, 221, 223, 226
duty cycle 52, 64, 67-9, 209
dwarfs, brown and red 27, 214, 220, 222, 227

E

EB (eclipsing binary) 5, 84, 104, 163, 167, 172-3, 181-4, 186-7, 220, 222-3, 227, 233
EB blend 165, 182, 186, 223
EFL (effective focal length) 149-50, 226
egress 25, 29-31, 34-5, 53, 55, 67, 110, 113, 120, 147, 150, 153-4, 216, 223, 225, 233
electrons/ADU 197-8
elevation angle 53, 221
elevations 29-30, 34-5, 49, 55, 66, 75
ensemble vii, 84, 86, 89, 91, 95, 104, 106, 115, 136-7, 161
ensemble photometry 92, 96, 104, 126, 129-30, 136, 223, 227, 233
ensemble SE for target 129-30
error bars 200-1
ETD (Exoplanet Transit Database) 1, 29, 86, 97, 114-15, 145, 151
evaluating flat fields 156-62
Excel spreadsheet 167, 170, 183, 187
exoplanet candidates 5, 22, 33, 73-4, 163, 165, 220, 230
exoplanet discoveries v, 3-4, 6, 27, 144
exoplanet image's FOV 84
exoplanet monitoring 14, 57
exoplanet observer's goal 141
exoplanet projects vii, 23-7, 31
exoplanet star fields 84, 137
Exoplanet Transit Database *see* ETD
exoplanet transit models 164
exoplanet transit observers 51, 125, 146
exoplanet transits 1-2, 4-6, 9-12, 15, 27, 33, 49-51, 53, 67, 77, 83, 85, 139, 163-4, 173, 216
exoplanets, non-transiting 23
exoplanet's star color 22
experience 7-8, 13-14, 42, 55, 119, 122, 137, 143, 152

exposure time 36, 59-60, 64-8, 87, 100, 132-4, 136, 138, 140, 160, 190-2, 194-6, 200, 205-6, 209, 221
 exposures, short 51-2, 59, 66-8, 133-4, 209, 221
 extinction 40-4, 46-7, 50, 55, 89, 110, 117, 131, 191, 203, 213, 216, 223, 233
 total 44, 46
 extra losses 73, 77, 106-7, 109-10, 113-15, 147, 218, 223, 233

F

f-ratio 56, 149-50
 faint exoplanet stars 206
 faint transiting exoplanets 23
 fields, perfect flat 57, 61
 filter band 27, 46, 56, 62, 66, 117, 138-9, 167, 171, 182-3, 186-7, 223, 225
 filter choices vii, 37, 48-9, 55, 97, 122, 211
 filter playoff 203-12
 filter throughput 203, 206, 208-9, 211
 filters vi, 1, 26, 33-5, 42-3, 46-56, 58-9, 61-2, 64, 122-3, 138, 155-6, 189-90, 202-6, 208-9, 221-2
 standard 51-2, 55, 68, 138
 flat field calibration 141
 flat field corrections 15, 56-7, 61, 157-8, 160, 203
 flat field errors 63, 141, 156-7, 160, 162, 190
 flat field exposures 58-9
 flat frames 21, 33, 56-7, 59-62, 64, 77, 87, 110, 155-6, 189-90, 198, 223-4, 233
 flux, missing 142
 flux ratios 66, 79, 89, 161-2, 191, 195, 225
 focal reducer lens (FR) 8, 17-19, 55-6, 62, 149, 155, 202
 focus 5, 7-8, 17, 64-5, 71-5, 140-1, 203, 223
 focus drift vii, 71-5, 80, 215
 FOV 4, 18, 35-7, 57, 61, 66-8, 96-7, 118, 123-4, 134, 141, 149-50, 156, 159-60, 191, 224
 autoguider's 35, 76
 Fp 103, 168, 174-8, 180-1, 183, 187, 214, 216-19
 full moon 50, 52, 123, 227
 full well capacity 188, 197
 linear 188, 197, 225, 227
 FWHM 18, 38, 64, 66, 69, 78-82, 87-9, 127-8, 130, 133-4, 140, 142-3, 149, 192-5, 203, 221

G

gain (CCD gain), 130, 197-198
 German equatorial mount (GEM) 14, 150

H

Harris 123-4
 header lines 91-2, 96, 98, 106, 114
 hot pixel removal 87

INDEX

Hubble Space Telescope 147

I

Ic-band 35, 43, 46, 50-1, 53, 58-9, 169, 189-90
image analysis 84, 137, 143
image analysis programs 78, 90
image measurements 137, 218
image processing vii, 1, 4, 10, 12-13, 57, 86-90, 139, 202, 225
image processing program 64, 86, 88, 91, 137, 198
image quality degradations 73, 221
image rotation 83, 87, 110, 162, 213, 216-17, 224, 226, 233, 235
image scale 69, 130, 140, 150, 226
image sharpness 66, 80, 149
image stabilizer 8, 12, 76, 224-5, 233
images, sharpest 12, 55
impact parameter 25-6, 28, 103, 167, 169, 171, 176, 186, 214, 224, 233
information rate 65-7, 197, 202, 209, 224, 233
Information window 78-9, 128
ingress 25, 29, 31, 34-5, 38, 53, 55, 67, 110-11, 113, 120, 147, 150, 216, 218, 224
intensity 78-9, 130, 138, 171, 174
IPAC computer 144

J

J-K 22, 35-37, 123-125, 163-164, 168, 183, 221, 228
JD and HJD 23, 91, 96, 98, 114, 146, 166, 224
JPL (Jet Propulsion Laboratory) 4-5, 144, 152

K

L

Landolt magnitudes 159-60
Landolt stars (fields) 61, 124, 158-9, 161-2, 221, 226
LCas.xls (spreadsheet) 106-8, 114-16
LCep.xls (spreadsheet) 97-101, 105-7, 115, 219
least-squares (LS) 160, 214
limb darkening vi, 53, 103, 169, 183, 214, 225, 233
limb darkening corrections 169-70
limb darkening model 187
linearity (of CCD) 188, 190, 196, 225, 233-4
LS (least-squares) 160, 214

M

mag-mag scatter plots 157-8

magnitude precision 89, 140-1
 magnitude scale, standard 85, 137-9
 main sequence 170-1, 178, 182, 187
 main sequence stars 164, 167
 mass 5, 23, 27, 146, 164, 168, 170, 183, 185, 187, 220, 227
 master dark 64, 87, 223
 master flats 56-7, 60, 203, 224
 MaxIm DL *see* MDL
 McCullough, Peter 5-6, 152-3, 157
 MDL (MaxIm DL) 10, 12, 19, 72, 75-6, 78, 80, 82, 86-92, 94, 128, 136, 138, 203, 225, 233
 median 12, 38, 53, 56, 60, 64, 88, 109, 124, 147, 162, 200, 202-3, 205, 214-15, 223-5
 median combining (MC) 56, 60, 64, 147, 200
 merit, figure of 34, 202, 205-7
 mid-transit 29-31, 35, 55, 103, 110, 120, 146, 153, 174, 214, 228
 mid-transit time 1, 31, 67, 84, 88, 97, 139, 216, 218-19
 mid-transit timings 26, 145-7, 150
 Mie scattering 41, 43-4, 223, 225-6, 233
 milli-magnitude 5, 23, 131, 225
 miss distance (impact parameter) 169, 172, 176-81, 183
 model fit vi, 43, 91, 102, 109, 111-12, 160-1, 204-5, 217-18
 model fitting 27, 67, 101-2, 104, 107, 114, 122
 model parameter values 215-16
 model parameters 111, 215-16
 moons 4, 16, 26, 49, 55, 57, 122-3, 133, 146-7

N

NASA/IPAC/NEExSci Star and Exoplanet Database 1, 97
 neighbor differences 215
 Ni 128-30, 136
 NIR filter 48, 45, 49-55, 58, 202-3, 207-8, 211, 225
 noise
 measured 135
 stochastic 7, 126, 205, 226
 noise levels 42, 64, 79, 104, 106, 133, 162, 164, 213, 228
 stochastic 80, 84, 209
 thermal 64
 noise sources 128, 162
 non-linearity (of CCD), *see* linearity (of CCD)
 NStED 1, 144
 NTE exoplanets 26-7

O

Observatory Tour vii, 17-22, 77
 observing log 8, 20, 33, 38, 75, 77
 observing site 27, 29-31, 33-4, 41, 43-5, 53, 66, 83, 128, 133, 150, 213

INDEX

observing site altitudes 43-4, 66, 132, 206
OOT 25, 31-2, 34, 53, 110, 122, 147, 226, 233
optical tube assembly (OTA) 150
optimum filter choices 206, 212
optimum observatory viii, 148-51
orbit 25, 145-8, 163, 173, 229
 exoplanet's 23, 26, 147
orbital period 25, 28, 164, 167-8
outliers 67, 81, 200, 214-15, 225

P

parameter F_p 174, 177, 179-82, 184
parameter values 161, 187, 215, 218-19
parameters 103-4, 110, 114, 118, 132, 164, 167-8, 174-5, 178, 183, 205, 214-19
photoelectrons 126, 130, 188-9, 192, 195, 221, 224-7
photometry 13, 57, 65, 78, 90-1, 96, 106, 126, 136, 146, 153-4, 221, 226
photometry aperture circles 78-9, 81, 149
photometry aperture radius 130, 203-4
photometry aperture size vii, 78-82, 88-90
photometry apertures 73-4, 80, 83, 128, 134, 136, 141, 150, 167, 203, 226, 233
photometry pitfalls vii, 83-5
photometry tool 87-90
 image processor's 91, 106
pixel errors 69
pixel noise, mmag Aperture 135
pixel width 226
pixels, hot 87, 190, 203
planet radius 167, 169
planet size model viii, 167-87
planning vii, 27, 29, 33-9, 63, 96, 145, 164-5
plate scale 18, 38, 140, 149-50, 226, 233
point-spread-function *see* PSF
Poisson noise 65, 68, 126, 128, 130-1, 133, 136, 141, 149, 162, 188, 191, 197, 205, 226, 228, 233
polar axis alignment 63, 141, 213
precision 80, 83, 117, 137, 139, 143, 202, 205-6, 208-9, 211, 222, 226, 235
precision exoplanet transit 64
probabilities, combined 215
probability functions 215
probability products 215
professional astronomers 1, 3-5, 7, 15, 23, 27, 33, 42, 50, 52, 68, 70, 83, 97, 102, 137-8, 144-5,
 151, 170, 219-21
programs, auto-fit 91, 97, 114, 144, 213
PSF (point-spread-function) 66, 69, 73-4, 79-80, 87, 140, 142, 194, 197, 215, 223, 226

R

Rc-band filter 1, 34, 37, 41, 49-51, 52, 58-9, 75-6, 119, 135, 156, 169, 172, 216

radius
 orbital 25, 164
 stellar 170

Rayleigh scattering 40, 42-6, 222-3, 225-6, 233

readout noise 38, 141, 188, 198-9, 222

red dwarfs 220, 227

reference star color 118, 120-1, 150

reference star subset 204

reference stars 35, 37, 71, 73-5, 80, 84, 88-92, 96-7, 110-13, 116-17, 129-32, 135-7, 139-41, 217-18, 222-3, 226-7
 average of 129, 136
 candidate 81, 108, 124, 158, 204-5
 color 120, 122-3
 ensemble 89
 ensemble SE for 129
 red 120
 same color 40
 selecting 110
 single 96, 136

reference stars SE 129

RGB images 54

rings 57, 146-7

RMS scatter 61, 104, 110, 113, 128, 134-5, 160, 192, 200, 203, 205, 224, 226

RMSi 205-6, 209, 217

RMSmodel 204-5

RMSsys 205

Rp/Rj solutions 187

Rstr/Rsun 177-8

S

Santa Barbara Instrument Group *see* SBIG

saturation (see also linearity and non-linearity) 36, 43, 60, 65, 68, 70, 130, 135, 140, 194, 196, 225, 227, 234

SBIG (Santa Barbara Instrument Group) 12, 60, 76, 150, 197, 224, 227

SBIG AO-7 tip/tilt image stabilizer 18, 76

scintillation 37, 51, 65, 68-70, 84, 94, 104, 126, 132-3, 135-6, 139-40, 162, 188, 191, 209, 227-8
 amplitude of 135, 139
 target star's 132, 140

scintillation noise 37, 68-9, 126, 131, 133, 136, 140, 149, 162, 205-6, 209

SDSS filter set 49

SE (standard error) 111, 114, 128-31, 136, 162, 170, 187, 198, 201, 214-17, 219, 225, 228

SE bars (proper use of) 201, 218

secondary size 167-8, 173-4, 176-7, 183

INDEX

seeing , see atmospheric seeing
seeing noise 126, 133, 135-6
SEi 214-15, 218, 228
selecting target viii, 163-5
sequence stars 84, 96
SETI projects 150, 152
sharpness 65, 133-4, 203
shutter 58-9, 223
signal aperture 67, 73, 78-80, 90, 128-30, 136, 141-2, 149, 223, 226
signal aperture radius 79-82, 90
size of star images 83, 140
sky background annulus 78-9, 81, 87, 128, 226-7
sky background level 41-2, 122-3, 128, 203, 224, 227, 234
sky brightness 40, 42, 58, 60, 227
slide bars 98, 111
sliding roof observatory (SRO) 17-19, 56, 60, 67, 150, 152
slopes (of light curves) 53, 111, 117, 123, 138, 202, 205, 217, 223
SNR 49-50, 52, 54-5, 61, 67, 69, 75, 78-80, 83, 123, 128, 140-1, 143, 173, 202-3, 228
spatial resolution 5, 163, 222
spatial structures 162
spreadsheet processing vii, 96, 106
SRO *see* sliding roof observatory
star color extinction effects 37
star colors vii, 22, 36, 52, 57, 61, 84, 117-25, 127, 138, 156, 160, 163-4, 167-8, 187, 221
star flux ratio 190, 196-7
stars
 brown dwarf 103, 214
 candidate 150, 183, 220
 comp 1, 88-9
 interfering 82, 150
 red dwarf 220, 227
 references 89, 96, 134, 204
star's flux 57, 73, 79-80, 89, 131, 136, 138, 223
starspots 24, 147
Steffen 145, 231-2
stochastic noise (error budget) 7, 80, 84, 113, 126, 128, 130, 143, 205, 209, 219, 226, 228
stray light 57, 228, 234
sunset 33, 35, 38, 58-61, 63
survey cameras, wide-field 3, 5, 223
systematics 53, 113-14, 116, 205, 213, 216-19, 222

T

T-shirt diffuser, double 58-9
telescope
 space-based 145, 147
 survey 173

telescope aperture 1, 7, 12, 56, 58, 103, 132, 135, 173, 203, 226-7, 231, 235
 telescope drive motors 12, 20, 76
 telescope system, exoplanet optimum 150
 telescope tubes 83, 235
 temperature 19-20, 23-4, 60, 70, 75, 87, 117, 132, 140, 223
 thermal noise 60, 209, 228
 TheSky/Six 19, 35, 38, 55, 123, 163, 228, 234
 timing (transit timing variations) *see* TTV
 total flux 42, 69, 74-5, 79-80, 131-2, 134, 142, 202
 transit chord 28, 52, 164, 224
 transit depth 23, 52-3, 84, 88, 97, 117, 120, 122, 139, 164, 167-8, 172-3, 177, 180, 183, 228
 transit interval 223-4
 transit length vi, 1, 26, 29, 35, 51, 67, 97, 115, 139, 148, 163-4, 168-9, 183, 224, 233
 transit light curve 14, 51, 90, 167-8, 173, 182
 transit model 86, 106, 110, 144, 214-19
 transit model and fitting procedure viii, 213
 transit timing variations *see* TTV
 transiting exoplanet systems 34, 145
 transitions, sharp 53
 transits
 central 163, 169, 172, 174-5, 184, 224
 consecutive 30-1
 trim (spreadsheet rows) 100, 104
 Trojan (exoplanets) 25-26, 31-32, 34
 TTV (transit timing variations) 16, 26-7, 53, 67, 120-122, 145-148, 150-151, 216, 218-219
 twinkling 132, 139

U

unfiltered observations 53, 119, 123

V

V-band filter 10, 35, 37, 41-2, 49-51, 52, 54-5, 58-9, 68-9, 122, 134, 156, 159-60, 169, 202-3, 205,
 208-9, 211, 223
 V-filter fluxes to V-magnitudes 61
 V-mag vi, 1, 23, 35, 52-3, 68, 76, 123, 160, 207-8, 220, 228

 variable stars viii, 5-6, 10, 13, 83, 85, 117, 137-43, 227, 235
 variations, transit timing 26, 216, 219

W

Warner 123-4
 water vapor 41, 46, 221
 web site 2, 27, 29, 33, 70, 89, 97, 106, 124, 213
 white boards 56

INDEX

winds 12, 19-20, 34, 56, 67, 132, 149
wireless focuser (WF) 18-19
working memory 86-90

X

XO-1 11, 34-8, 55, 63, 135, 146, 154, 170, 178-81, 216
XO-3 126-7, 129-30, 135
XO-3 star field 126-7, 135
XO Project 3-6, 27, 144, 152, 154, 163
XOP-BB 49, 230

Numbers

2MASS, 122-123, 221